Hydraulics Research
Wallingford

DESIGNING CIRCULATION CHAMBER SEDIMENT EXTRACTOR

T C Paul
Research Officer, Hydraulics Division No 1
Irrigation & Power Research Insitute
Punjab, Amritsar, India

Report No OD 91
January 1988

Registered Office: Hydraulics Research Limited, Wallingford, Oxfordshire OX10 8BA.
Telephone: 0491 35381. Telex: 848552

ABSTRACT

To aid an economical and efficient design of circulation chamber sediment extractor this report presents rational guidelines based on elaborate experimentation over the years. It has been shown that in the region bounded by circulation chamber wall and the edge of orifice, the tangential velocity does not vary inversely with the distance from the orifice centre but remains constant over a distance equal to the width of the inlet channel from the chamber periphery and attains a maximum value (V_{to}) at the edge of the orifice. This maximum value is independent of the provision or otherwise of a deflector in the chamber. The tangential velocity at the chamber periphery is 0.256 V_{to} or about 0.85 times the inlet channel velocity. It has been shown that optimum chamber size is five times the inlet channel width. Reliable criteria has been suggested for the evaluation of various design elements, eg size of flushing pipe, length of spill weir, susceptibility to air core formation, etc. Pitfalls to be avoided have been identified and substantiated with experimental evidence. The suggested predictor for evaluation of trapping efficiency has a discrepancy ratio of 1.06 with standard deviation of 0.34. Need has been stressed for evaluation of limit radial velocity of coarse sediment particles when these will stop moving radially towards the orifice to be flushed but instead start revolving in the chamber in circular paths around the orifice.

CONTENTS

CONTENTS CONTINUED

FIGURES CONTINUED

CONTENTS CONTINUED

FIGURES CONTINUED

APPENDIX

LIST OF SYMBOLS

B	Bed width of inlet or parent channel
b	Mean thickness of the jet so that $V_r = Q_{cc}/2\Pi rb$
C	Constant of swirl or free vortex; sediment concentration by volume
CD_0	No deflector in the circulation chamber
CD_1	Deflector of width, B, covering only the cross-section of spill weir
CD_2	Deflector of width, B, starts from entrance of inlet channel and covers half circumference of the chamber including spillweir
CD_3	Deflector of width, B, covering entire periphery of circulation chamber
$\bar{C}_b$	Mean concentration of bed load
C_d	Discharge coefficient for orifice or flushing pipe
$\bar{C}_s$	Mean concentration of suspended load
Cfs	Cubic feet per second
D_s	Sediment particle diameter or size, ie D_{50} is medium grain diameter
DR	Discrepancy ratio (= mean of predicted/measured)
d	Diameter of circulation chamber (=2R)
d_0	Diameter of orifice or flushing pipe (= $2r_0$)
F	Froude number (= $4Q_0/\Pi d_0^2 \sqrt{gd_0}$)
f/s	Feet per second
g	Acceleration due to gravity; gram
H	Height of circulation chamber
h_0	Depth of water in circulation chamber over the orifice
h_1	Height of diaphragm in inlet channel above the bed
h_2	Depth of circulation chamber periphery from inlet channel bed
h^*	Vertical distance from the chamber bed
h_0^*	Depth of water at the periphery of the chamber
k_1	Mobility number of sediment (= V_s/V_*)
k_2	Coefficient of settling (= $V_s d/V_0 h_0$)
l	Litre
m	Metre
N_τ	Circulation number (= $\tau d_0/Q_0$)
P	Sediment trapping efficiency
p	Pressure
Q_c	Parent of inlet channel discharge
Q_{cc}	Discharge entering the circulation chamber
Q_d	Design discharge

Q_0 Flushing discharge or discharge through orifice

Q_s Discharge spilling from circulation chamber into downstream channel

R Radius of circulation chamber (= d/2); hydraulic radius

R_e Reynolds number

r Distance from centre of chamber or orifice

r_c Distance from centre of orifice where free and forced vortices intersect

r_0 Radius of orifice or flushing pipe (= $d_0/2$)

S Slope of channel bed or water surface or energy gradient line

S_c Chamber bed slope

SD Standard deviation

s Second

t Detention time

U_c Mean critical velocity for resuspension of deposited sediment particles

U_* Shear velocity (= $\sqrt{\tau_0/\rho_f}$) = $\sqrt{gRS}$

u Radial velocity; tangential velocity

V_c Mean velocity in inlet or parent channel

V_{cc} Water volume in circulation chamber

V_0 Mean velocity in circulation chamber

V_r Radial velocity

V_s Settling velocity (in quiet water) of sediment particle

V_t Tangential velocity

V_{to} Tangential velocity at r = r_0 or edge of orifice

V_{tR} Tangential velocity at the periphery of chamber or at r = R

Vz Axial velocity

W Upward velocity in circulation chamber

Z Slope (Z horizontal to 1 vertical)

γ_f Specific weight of fluid

γ_s Specific weight of sediment

δ Thickness of radial velocity region

E Diffusion coefficient

λ Model scale

μ Kinematic viscosity of fluid

ρ_f mass density of fluid

ρ_s Mass density of sediment

τ Circulation (= $2\Pi r V_t$); time

τ_0 Total bed shear stress

ω Angular velocity

1 INTRODUCTION

The circulation chamber sediment extractor (CCSE) is a device for the removal of excess sediments from irrigation or power canals. To trap or to eject the sediments, the CCSE utilizes the secondary flow generated by the circulatory flow induced in a circular chamber. Maximisation of the strength of circulation warrants that the inlet to the chamber be tangential. The axial outlet pipe provided at the centre of circular chamber flushes the settled sediments out into the waste or escape channel. Figure 1 depicts the principle of operation of the CCSE which incorporates a major deviation from the designs proposed by Cecen and Bayazit (1975), Cecen (1977), Curi et al (1975), Salakhov (1975), and Ogihara and Sakaguchi (1984) relying on leading the full discharge of the parent or inlet channel into the chamber. For comparison, the designs as proposed by Curi et al (1975), Salakhov (1975) and Ogihara and Sakaguchi (1984) are shown in Figures 2, 3 and 4 respectively. With a view to minimise the size of the circulation chamber, only the lower layers of the parent channel flow transporting high sediment loads are led into the CCSE whilst the upper layers are by-passed into the downstream channel - a technique also made use of in the case of conventional tunnel type sediment extractors. The most attractive feature of the CCSE is that it yields the same, if not higher, sediment removal efficiency as expected of the conventional tunnel type or vortex tube sediment extractors but with water abstraction of only 5 to 10% compared to 15 to 25% in the case of the conventional types. This report presents criteria for the design of CCSE.

1.1 Design philosophy

Like other sediment extraction devices, the overall philosophy governing the design of CCSE is to maximise sediment extraction with minimum water abstraction. The abstracted water should, however, be capable of transporting the extracted sediment to the waste or escape channel or a natural drain. The basic principle of the CCSE design could probably be traced to the model studies conducted by Smisson (1967) which led him to the installation of two prototype structures at The White Ladies Road in Bristol (UK) for the removal of solids from the combined sanitary sewage and storm water flows. However, much earlier Walton and Key (1939) had examined the performance of circular chambers with:

(i) Tangential inlet, and

(ii) A vertically placed rectangular inlet port extending from the floor of the chambers upwards,

in an attempt to design clarifiers for waterworks for the City of Alexandria (Egypt), as shown in Figure 5.

Although at the commencement of model tests, the tangential inlet arrangement (Fig 5(a)) gave a certain amount of promise, but on continuing the experiments this proved to be illusory due to the updraught and lifting of sludge from the floor of the chamber in the neighbourhood of the central draw-off. However, these experiments revealed that:

(i) A slight increase in transparency occurred, and

(ii) The kinetic energy of the effluent, in spite of its very low velocity, was sufficient to cause a

noticeable rotation of the water already in the chamber - a somewhat "surprising" and encouraging result.

In these experiments the inlet velocity was limited to 0.0508m/s. With the finally adopted arrangement, as shown in Figure 5(b), it has been possible to remove silt to the extent of 2.243 tonnes per annum during the years 1935 to 38.

The use of circular chambers, as advocated by Walton and Key (1939), has also been examined by Vokes and Jenkins (1943) to whom the opportunity offered itself at Birmingham. They altered quite cheaply one of three upward-flow tanks working in parallel for the separation of activated sludge. The tanks were 13.4m (44ft) in diameter, with central inlet and peripheral discharge. From one of these tanks the centre feed arrangements were removed and a silting chamber was created in the peripheral wall, from which the flow entered the tank horizontally, at an angle such as to cause the contents to rotate about the vertical axis. A wall was constructed on the existing weir, thus causing the flow to pass two-thirds of the periphery before coming to the submerged outlet weir occupying the last third. The experiments run at different rates of flow and over a considerable time proved conclusively that, for separating activated sludge under these conditions, the performance of the altered tank was inferior to that of the unaltered tanks, the original design proving decidedly superior. A personal communication from Rea (Quentin, Babtie Shaw & Morton, Consulting Engineers, Calthorpe House, 30 Hagley Road, Birmingham B16 8QY, England), however, indicates that a clarifier, similar to the one for waterworks for The City of Alexandria, in place at York Water Treatment Works is fairly successful at

removing sediments from diverted river water but cannot be used for sludge removal.

Nevertheless, the experience gained from the two vortex regulator prototypes, designed by Smisson (1967), was subsequently made use of by the American Public Works Association (APWA) for the development of design of swirl concentrator, Sullivan (1972).

1.2 Design elements

The problem could be enunciated as under:

A channel with bed width, B, depth of flow, h, side slopes as Z hor to 1 vert and bed slope, S, carries full supply discharge, Q_c, with sediment concentration of x ppm as per size grading curve supplied. Design a CCSE which will flush sediment with size D_s, with an efficiency of P%. A solution of such a problem will entail the following elements of design:

(i) Chamber diameter, d . The chamber size can be specified in relation to:

  (a) Channel bed width, B,
  (b) Size of sediment to be flushed/extracted, D_s.

(ii) Orifice diameter or size of flushing pipe, d_o.

(iii) Flushing discharge, Q_o.

(iv) Discharge coefficient for orifice, C_d.

(v) Depth of flow in chamber over the orifice, h_o.

(vi) Chamber bed slope S_c, if any.

(vii) Height of diaphragm, h_1, in inlet channel from its

bed, if the total channel discharge, Q_c, is not to be led in to the circulation chamber,

(viii) Peripheral length of circulation chamber, C_1, for spillage of discharge into the downstream canal or channel.

(ix) Discharge coefficient, C_{d1}, for the peripheral spillweir.

(x) Effect of deflector in the circulation chamber, and the economical and efficient type (or design) for maximum trapping efficiency.

(xi) Conditions critical to air core or air-entraining vortex formation.

(xii) Modelling criteria.

(xiii) Chamber depth at the periphery, h_2.

The symbols used for various parameters have also been explained in Figure 6. Before discussing and quantifying the role of various elements enlisted above for the design of CCSE, a review of the available literature is presented so as to have a picture of the state of the art in this field of hydraulic engineering.

2 LITERATURE OVERVIEW

2.1 Vortex regulator

Model studies conducted by Smisson (1967) for the removal of unwanted materials from the waste water flows using vortex flows led him to the design and development of two prototype units, as shown in Figure 7, since in operation at the White Ladies Road

in Bristol (England). Longitudinal flows of combined sanitary sewage and storm water tend either to hold solids admixed with the liquid phase (due to scouring velocities, or agitation), or to allow solids to settle out or stratify in the liquid flows. The removal of the heavier grit in grit-separation units, and the eventual removal of the lighter solid fractions in settling chambers utilize the gravity solids - clarification for the removal of materials.

The removal processes are dependent on:

(i) The settling characteristics of solid particles, and

(ii) The time to reach the degree of removal required.

In the design of such solids - removal facilities, the time element is of great importance as it influences the size of the chambers to provide adequate volume for the lowering of velocities and the deposition of solids. The requisites of this device may be summarised as:

(i) Removal of waste-water solids by means of force other than gravity,

(ii) Relatively short periods of time for removal,

(iii) Relatively small (volumetric) size,

(iv) Absence of any moving mechanical parts in the chamber,

(v) Its self-cleansing of deposited solids by using flow patterns created by the device itself, and,

(vi) Cost.

2.2 Combined overflow regulator

The basic design features of the Bristol device and the experience gained from the two field installations were subsequently made use of by the APWA for the development of the swirl concentrator as a Combined Overflow Regulator Facility for the City of Lancaster, Pennsylvania, as shown in Figure 8, after Sullivan (1972). The suggested criteria for the design of the swirl concentrator as a combined sewer overflow regulator is based both on physical and mathematical models.

In the physical model, similitude of the transport of sediment was achieved by equalizing the scale of the settling velocity of the sediment grains to the scale of the flow velocity (Ref Sumer (1970) and Cecen et al (1969)) and utilizing an undistorted model.

2.2.1 Mathematical model

The mathematical model was devised to predict variations in performance of the swirl concentrator under conditions of variable design criteria to help arrive at an optimum configuration for the unit. As a first step, the liquid flow field within the swirl concentrator (neglecting the presence of particles) was calculated using a relaxation procedure to solve numerically the equations for turbulent axisymmetric flow. To relate the local turbulent Reynolds' stresses to the gradients of the mean flow properties, a three-dimensional eddy-viscosity model was used. For the computation of particle flow through the liquid, at each mesh point (where liquid flow had been calculated) the three particle momentum equations (involving turbulent diffusion terms, virtual mass

effects, gravity forces, and drag), and the equation for continuity were solved to determine the particle velocities and concentrations. These equations were solved with a time-dependent scheme, integrating forward in time till a steady state was achieved. The axi-symmetric model appeared to be quite satisfactory in its mathematical form as it approximated the average behaviour of the flow at most radial locations. Particle settling rates and the scale factor diagram are shown in Figures 9 and 10 respectively. Design examples from the mathematical model appear in Table 1. It will be seen that for design discharge, Q_d, of 4.672m^3/s and 90% removal efficiency of settleable solids with size greater than 1.0mm, the mathematical model yields chamber diameter, d, of 14.63m as compared to 11.08m yielded by the physical (hydraulic) model (which is obtained from storm discharge versus chamber diameter curve in Figure 11 or from the corrolation

$$d = 3.0\ (Q_d/0.322)^{0.4}$$

where

d is in ft; Q_d is in cusec.

The dimension of the square inlet, B, is obtained from Figure 12. The curve for removal of solids as related to inflow (storm) discharge is shown in Figure 13.

Design criteria

Since the model separation chamber used had a diameter of 0.914 (3ft), and was operated according to Froude's Law, thus the prototype discharge is proportional to 2.5 λ where λ is the scale of prototype to model. Therefore, for the design peak discharge used on the model as 0.009118m^3/s (0.322 cusec), the scale of

relation between chamber diameter, d, and the peak discharge is

$$d = 0.9144 \ (Q_d/0.00912)^{0.4}$$

where

d is in m; Q_d is in m^3/s.

$$d = 3.0 \times (Q_d/0.322)^{0.4}$$

where

d is in ft; Q_d is in cusec.

The curve in Figure 11 is based on this equation and is used as a design curve to determine chamber sizes. The procedure for the design is as under;

(i) Carry out a hydrological study to establish a storm hydrograph giving the possibility of run-off from various sized storms.

(ii) Adopt either the peak discharge from the hydrograph established in (i) above or determine from an economic study the flow which can economically be considered, say a two, five or ten year storm, and consider it as the design storm discharge, Q_d.

(iii) Using Q_d, read from Figure 11 the corresponding chamber diameter, d.

(iv) With this d, go to Figure 8, first to find B, then to compute the dimensions of the chamber elements.

(v) The dry weather sanitary flow was taken as 2% of Q_d in the model study. The same value was maintained as the foul or flushing outflow during storm operation. In practical design, 2% of Q_d should be retained, and the main gutter designed to carry it through the chamber to the foul outlet during dry weather.

Figure 8 enlists the dimensions for the various internal elements of the separation chamber. Doubtless the chamber diameter, d, is the basic dimension taken off the design curve on Figure 11, advantage has been taken of the ratio d/B = 6, and this has been selected as the unit dimension. The resulting symbolic relations given on Figure 8 are:

B = inlet dimension = unit

d = diamneter of chamber = 6B

D_3= diameter of scum ring = 4B

D_4= diameter of the over-flow weir = $\frac{10}{3}$ B

h_4= height of overflow weir = 0.5B

h_3= height of scum ring = 0.33B

b_1= distance between scum ring and overflow weir = 0.33B

b_2= offset distance to determine locations of gutter = $\frac{1}{6}$ B

d_1= depth from weir plate = 1.5B

h_2= distance from inlet invert to bottom of chamber = $\frac{5}{6}$ B

The chief limitations of the mathematical model were:

(i) It failed to reproduce the non-axisymmetric behaviour, such as local vortices observed in the physical model, and

(ii) Non-reproduction exactly of the main effect of the baffle plate, (defector) at the inlet to

raise the tangential velcity which necessitated the adjustment of free constants associated with eddy-viscosity and the wall shear.

The experience gained on the model study of the swirl concentrator chamber strongly supported the validity of the basic principles of its operation. These are summarized as below:

(i) The flow inside the chamber must not be allowed to accelerate to the point where vortex forces take control of the particle movements.

(ii) The particles must be allowed to settle either through the water along the perimeter wall on to the chamber floor and be drawn along by the swirl or the gutters towards the foul outlet.

(iii) The flow must be introduced tangentially.

(iv) Inlet invert should come in on the floor of the chamber so that solids tend to stay down and are not picked up by the swirl.

(v) Greater chamber depths give only marginally better removal, and this is not always consistent.

(vi) Though chamber diameter was not varied yet extrapolation of the depth studies indicated that greater diameters should give more efficient solids separation.

(vii) Although the aim should be to avoid any auxiliary appurtenances in the chamber, a defector was found necessary. In the absence of

a deflector the rotational velocity builds up and reduces solids separation.

(viii) Flat floors in the chamber perform perfectly acceptably when flows are constant, however, a slope toward the centre helps to clear floating material.

(ix) The chamber diameter, d, is kept equal to 6B where B is the dimension of the square inlet.

2.3 Grit separator

The effectiveness of the swirl concentrator principle at removing particles of various grain sizes and specific gravity combinations from flows prompted the APWA to use the same principle for the development of a grit separator device, as shown in Figure 14 (Ref Sullivan et al (1974)). The swirl concentrator principle involves the development of a flow chamber utilizing circular long path kinetic energy to induce separation of solids from liquid and settling of the particles. The settling is achieved by ensuring optimum hydraulic conditions and the removal of solids without the use of mechanical accessories. The hydraulic model study led to the following conclusions:

(i) A flat floor is inadequate over wide ranges of discharge. At lower flows deposits are likely to be a serious problem.

(ii) A conical (cone surface at an angle of 60° with the horizontal) floor was found to be satisfactorily adaptable over a wide range of sizes. The ratio of height or depth to chamber diameter can be varied from 0.167 to 0.32.

2.4 Developments in pollution control, irrigation and hydro-power sectors

Curri et al (1975) investigated the use of a vortex as a separation device as one of the possible solutions to the problem of high-velocity solid-liquid separation. According to them, if in a cylindrical tank having an orifice at its centre, a relatively high-velocity flow in introduced tangentially to its centre, the resulting flow will be a combination of free and forced vortices, Vallentine (1950).

Cecen and Akmandor (1973) and Cecen and Bayazit (1977) had also examined the use of a circular settling basin having a bath-tub type vortex motion due to flow through an orifice in the centre of the basin. It was observed that sediment particles entering such a tank begin to settle due to gravity and also rotate with the fluid until caught by the vortex flow and ejected through the orifice. It may be remarked that the experimental layout adopted by Curi et al (1975) is essentially the same as adopted in reports emanating from the Technical University of Istanbul (Turkey).

2.4.1 Design Practice in Turkey

According to Cecen and Bayazit (1975), in the case of a circular settling basin (with a horizontal bed and an entrance canal joining the basin at its periphery near the bottom) the kinetic energy of flow produces a forced vortex with tangential velocity $V_t = \omega r$ near the periphery, whereas a potential vortex with $V_t = \frac{\tau}{2\pi r} = \frac{C}{r}$ occurs near the centre. Here, ω is the

angular velocity of the forced vortex, r is the radial distance from the centre of vortex or circular tank, V_t is the tangential velocity of the fluid, τ is the circualtion, and C is the swirl or free vortex constant. It may be remarked that contrary to the assertion of Cecen and Bayazit (1975) that a forced vortex forms in the outer region (near the chamber periphery) and a potential or free vortex occurs near the centre, Knauss (1972), Julien (1986), Sanmuganathan (1985), Odgaard (1986), and Anwar (1969) have shown that the Rankine combined vortex is composed of a forced vortex core near the axis of rotation in the inner region surrounded by a free vortex in the outer region. However, Dr Cecen (1985) in a private communication stated that "In our experiments with the circular basin, forced vortex occurred near the periphery, and free vortex near the centre". The intersection of these potential and forced vortices is at a distance, r_c, related to C and ω as:

$$r_c = \sqrt{C/\omega} \qquad (1)$$

According to Rott (1958),

$$r_{c\ Rott} = \sqrt{2\ \nu/a}, \text{ where } a = 1.93\ (g/h_o)^{0.5} \qquad (2)$$

According to Odgaard (1986),

$$r_{c\ Odgaard} = \sqrt{2.5\ \nu/a} \qquad (3)$$

However, Anwar (1967) has, both from theory and experiments, shown that

$$r_{c\ Anwar} \simeq r_o \text{ or } do/2 \qquad (4)$$

Sediment particles are removed through the hole at the centre by the potential vortex action, and the air nucleus at the centre of the hole reduces the flushing discharge considerably (to the extent of 5 to 6% of the parent channel discharge, Q_c). In the model experiments, ω of the forced vortex is obtained from the following non-dimensional form:

$$\omega\, h_o^{0.5}\, d^{2.5}/Q_{cc} = 55.64 \qquad (5)$$

where h_o is the depth of flow in vortex tank (ie at the orifice), d is the diameter of the vortex tank, and Q_{cc} is the discharge entering the vortex tank or circulation chamber. The constant C of the free vortex is obtained as a function of d/do, where do is the diameter of the orifice or the central hole, as shown in Figure 15:

$$C\, h_o^{0.5}\, d^{0.5}/Q_{cc} = F\,(d/do) \qquad (6)$$

The trapping efficiency, P, of the circular basin could be expressed as :

$$P = \phi\,(V_s/U_*,\ V_s\, d/V_o h_o) \qquad (7)$$

where V_s is the settling velocity of particle, U_* is the shear velocity ($= \sqrt{\tau_o/\ell_f}$ or $\sqrt{gRS}$ where τ_o is the total bed shear stress in the chamber, ℓ_f is the density of water and, R is the hydraulic radius), and V_o is the velocity (tangential) of the fluid in vortex motion at the outer periphery of the basin (Ref Cecen (1985)). This sediment-removal or trapping efficiency function for a vortex type settling basin or circulation chamber is shown in Figure 16. For the sake of comparison, the sediment removal function as applicable to classical settling basins after Rouse (1950) is also reproduced in Figure 17. Suprisingly,

for a given mobility number, as the coefficient of settling increases, the trapping efficiency increases according to Figure 17 (Rouse 1950) but it decreases as in Figure 16 (Cecen & Bayazit (1975)), ie increased coefficient of settling produced negative effect on settling.

Dimensions of the basin which maximise the efficiency of settling are given by the following correlations :

$$d = 5.224\ (U_*/V_o)^{0.25}(k_1k_2)^{0.5}(Q_{cc}/V_s)^{0.5} \qquad (8)$$

and

$$h_o = k_1\ U_*d/k_2\ V_o \qquad (9)$$

where k_1 is the mobility number of the sediment V_s/U_* and k_2 is the coefficient of settling = V_sd/V_oh_o. As to how U_* in circular basin has been determined has not been clarified. The model of vortex solid liquid separator employed by Curi et al (1975) in their studies comprised a cylindrical tank d = 90cm with inlet and outlet channels laid tangential to the tank periphery, and an orifice of size d_o = 1.27cm, 2.54cm and 5.08cm located at the centre of the tank. Water supply to the tank was through an enclosed rectangular channel with width B = 18cm reaching the elevation at the bottom of the tank. The outlet channel was also rectangular in cross-section with B = 18cm and at an angle of 120° with the inlet channel. The invert of the outlet channel was placed 5cm above the bottom of the tank. Design details are shown in Figure 2. The design of the vortex separator ensured that:

(i) Suspended particles are prevented from going directly from the inlet to the outlet channel.

(ii) The inflow and suspended solids entered from the bottom of the tank to facilitate removal of particles, and

(iii) The position of the invert of the outlet channel above the bottom of the tank minimized the opportunity for particles to escape from the tank.

Physical properties of the test materials used by Curi et al (1975) and elsewhere are given in Table 2. The test results are reproduced in Table 3. The particle removal efficiency has been defined as the ratio of the concentration (by weight) of the particles removed through the orifice to the concentration of particles in the flow entering the tank. The data in Table 3 have been plotted in Figure 18, and in fact this figure depicts the variation of sediment trapping efficiency with water abstraction ratio, Q_o/Q_{cc}. It is to be noted that Curi et al (1975) added test materials into the tank by sudden batch loads from the inlet channel (thus procedure adopted is invalid for continuous loads) so that their specific gravity resembled the specific gravity of particles actually present in sewage, as their experiments were directed primarily to control pollution. The results (Table 3) were evaluated with the aid of a multiple regression programme and the following correlations obtained:

$$P = 1.74 + \ell n \frac{do^{0.11}(\gamma_s/\gamma_f)^{0.88}}{Q_{cc}^{0.58}} \qquad (10)$$

where d_o is in cm, γ_s and γ_f are the specific weights of sediment and fluid respectively, and Q_{cc} is in ℓ/s.

The correlation coefficient of Equation 10 was 0.93. However, a less complicated equation with a slightly lower correlation coefficient of 0.85 was as under:

$$P = 2.32\ Q_{cc}^{-0.55}\ (\gamma_s/\gamma_f)^{1.34} \qquad (11)$$

The data in Table 3 have also been plotted in Figure 19 in an effort to evaluate the variation of d/do with $h_o^{0.5}\ d^{0.5}/\ Q_{cc}$ after Cecen and Bayazit (1975). In the experiments reported by Curi et al (1975), the detention period was extremely small and varied between 7 and 13 seconds.

According to Curi et al (1975), the trapping efficiency of a vortex type solid liquid separator is proportional to d_o and specific weight of particles and inversely proportional to chamber discharge, Equation 10. However, the plot of their data in Figure 18 indicates that any trapping efficiency varying from 30 to 100% can be achieved with different sediments and Q_o/Q_{cc} of 5%. As Q_o/Q_{cc} increases beyond 5%, the trapping efficiency is independent of size of the orifice or the flushing discharge, Q_o. The fitness test for any correlation for trapping efficiency is that when Q_o, or Q_{cc} is zero, P should be zero. Further, Curi et al (1975) data plotted in Figure 19 after Cecen and Bayazit (1975) do not lend credence to the latter's contention that $(C\ h_o^{0.5}\ d^{0.5})/Q_{cc}$ should decrease with an increase in d/d_o.

2.4.2 Flow regions in circulation chamber

According to Cecen (1977), in a vortex settling basin, settling takes place due to the secondary flow which moves the fluid layers near the bottom towards

the orifice. The sediment particles which are heavier than the liquid and which are concentrated mainly in the lower layers are flushed with only a relatively small amount of water. He has suggested a sub-division of flow in a circular basin into four regions:

(i) Along the periphery of the basin where the flow from the parent channel enters and leaves the settling basin. This region is characterized by highly complex flow conditions which depend to a large extent on the geometry of the entrance and escape.

(ii) Adjacent to this region, a forced vortex is formed in which tangential velocity, V_t, increases with radius, r, ie $V_t \propto r$.

(iii) Near the orifice, the velocity distribution follows that of a free vortex with velocities increasing towards the centre.

(iv) In the middle an air core is present. It is advisable to establish an air core in order to reduce the discharge through the orifice.

The tangential velocities measured (by using a miniature current meter) at various distances from the bottom in four sections of the basin are shown plotted in Figure 20, and exhibit general features of flow. Some non-uniformity is clearly evident among the various sections presumably due to the effect of entrance conditions. The velocity distribution in Figure 20 (after Cecen (1977)) on comparison with the one in a two-dimensional Rankine combined vortex in Figure 21 after Julien (1986) and in Figure 22 after Anwar (1969) were found to be quite contradictory. The tangential velocity distribution in CCSE (Fig 1) after

Paul (1983) is shown in Figure 23 which also does not lend support to the tangential velocity distribution in Figure 20 after Cecen (1977).

Since the original concept of vortex type settling basins were evolved for public health engineering applications where removal of mixed density debris including heavier sediment and lighter floating debris is the objective, it is therefore not suprising, according to Sanmuganathan (1985) that in most applications the abstracted flow was so adjusted as to form an air core at the centre. By this means the floating debris can be extracted in addition to the heavier sediments swept towards the orifice by the secondary currents. When the device is used for extracting heavier sediments only, the question has to be asked as to whether an air core should be allowed to form. Cecen and Bayazit (1975) argue that the presence of air core at the centre of outlet pipe or orifice reduces the flushing discharge considerably. This implies a unique dependence of discharge on flow area. This must be wrong because flow depends on the area and average velocity. It is well known that in cases such as this, an air core does not form at low abstraction rates; a dimple forms on the free surface. It is only when the abstraction rate is increased past a critical value that an aircore forms. To argue that an aircore helps to reduce discharge is to confuse between dependent and independent variables.

In the case of CCSE, the object is to minimise abstraction rates and maximise sediment extraction. If an air core is allowed to form, water from the surface layers will also be abstracted carrying with it little or no sediment. Since the formation of air core can be prevented by reducing abstraction rates, both desirable features, CCSE should be designed for such a condition.

It may turn out that if an air core is prevented from forming, the abstraction rate is too small to sweep out all the sediment that settles on the bed of CCSE. This difficulty, if relevant, could be resolved by sloping the chamber bed down towards the outlet. The slope will depend on the size of the sand grains and the flow geometry.

As such, two questions arise. Firstly, what is the critical abstraction rate above which the air core will form for the chosen geometry? This will yield an upper limit to the abstraction rate. Secondly what is the head difference needed or discharge coefficient of the orifice to induce a selected abstraction rate?

Behaviour of sediment particles.

Inside the rotating fluid, layers near the floor are decelerated by friction. The resulting non-unformity of centrigual forces along a vertical causes the particles near the floor to be moved towards the centre of curvature. A solid particle entering the basin is moved along the helicoidal path towards the centre. Since in such a basin, the settling length of a sediment particle is many times larger than the dimensions of the basin, higher velocities can be allowed in contrast to the classical basins.

The behaviour of coarse gravel in the basin is of interest as these particles do not leave the basin with the flow through the orifice but continue to revolve along a circular path around the centre of the basin. This phenomenon can be explained as follows. For a solid particle to revolve along a circle of radius, r, the centripetal force should be balanced by the force due to pressure gradient, ie:

$$m_s \cdot \frac{V_{ts}^2}{r} = C \frac{\Delta p}{\Delta r} \cdot A \cdot D_s \qquad (12)$$

where m_s is the mass of the sediment particle, V_{ts} its tangential velocity, D_s is its size, and A is its projectional area on a vertical plane. The pressure gradient is related to V_{tf}, the average tangential velocity of the fluid along the vertical at radius, r:

$$\frac{\Delta p}{\Delta r} = \ell_f \frac{(V_{tf})^2}{r} \qquad (13)$$

where

ℓ_f is the density of the fluid. Combining the Equations 12 and 13,

$$\frac{\ell_s \cdot D_s^3 V_{ts}^2}{r} = c_1 \frac{\ell_f (V_{tf})^2 D_s^3}{r} \qquad (14)$$

where

c_1 is a shape coefficient. Therefore

$$(Vt_s / Vt_f)^2 = c_1 (\ell_f / \ell_s) \qquad (15)$$

V_{ts} is very much smaller than V_{tf} because the solid particle is moving near the bed where the local fluid velocity is low and as it also lags behind the flow. From experiments with spheres of various densities, it was observed (Cecen, 1977) that particles with equal weight to diameter ratio revolved along the same path and their periods of revolution were inversely proportional to their densities:

$$m_{s_1}/D_{s_1} = m_{s_2}/D_{s_2}; \quad V_{ts_1}/V_{ts_2} = D_{s_1}/D_{s_2} \qquad (16)$$

Experimental set up and variants

The experimental set up utilized by Cecen (1977) comprised the simplest possible geometry, viz a circular basin with diameter d = 200 cm placed tangentially to the main channel with flow entering the circular basin near the floor tagentially and escaping near the surface above a step on the floor, after rotating through one complete revolution. Heavy particles in the lower layers were moved towards the centre during the rotation and thus, could not leave the basin through the exit channel. These were eventually flushed through the orifice in the centre and only very fine particles reached the channel by being raised towards the water surface by turbulence. The following three options were examined:

ALTERNATIVE No	SPECIFICATIONS
(i)	Basin floor horizontal; water escaping tangentially.
(ii)	Basin floor sloping radially towards the centre on a slope of 10 hor to 1 vert; water escaping tangentially.
(iii)	Water leaving the basin not tangentially but by spilling over a weir along the periphery.

In his experiments d_o varied from 4 to 12cm or d/d_o from 17 to 50. The axis of the air core made a small angle with the vertical and was slightly displaced in respect to the geometrical centre of the basin (about 17° as reported by Chrysostomou (1983). It was observed that the water abstraction ratio, Q_o/Q_{cc}, was 3 to 10%; higher ratios being obtained in the case of a sloping floor. The flushing discharge, Q_o, was roughly proportional to flushing pipe diameter, d_o as

the air core was affected by the orifice size. The water surface profile along a section through the centre of the basin is also shown in Figure 20, along with the piozometric line. Piezometric readings indicated pressures below the hydrostatic near the aircore, as would be expected, due to curvature of streamlines.

Source of radial flow

Injection of dye at various points and various levels indicated that the dye injected near the water surface in the forced and free vortex regions rotated along circular paths for a fairly long time with negligible diffusion. This clearly demonstrated that the radial flow through the orifice is mainly supplied by the fluid layers near the floor of the basin. However, it was not possible to measure radial velocities accurately.

The motion of sand particles in the basin was modelled by lightweight plastic grains (specific gravity of 1.03 to 1.50) and those particles which entered the basin near the floor were moved towards the centre along a helicoidal path, and were totally flushed by the flow through the orifice in all the experiments where the exit was tangential. However, in the basin with peripheral spilling (Alt iii), the diffusion of heavy particles in the radial direction was more intense, and some of them left the basin with the spilling water and thus entered the outlet channel.

The behaviour of coarse gravel (size 16 to 32mm), as already brought out above, in the basin was of interest as these particles did not leave the basin with the flow through the orifice but continued to revolve along a circular path around the centre of the basin. Lewis (1981) has, however, reported the

development of the use of an inverted hydro-cyclone which successfully clarifies gravel in the size range 2mm to 6mm. This device also makes use of vortex type flow.

Effect of chamber bottom slope

From a comparison of the circular basin with horizontal floor and with a sloping floor, it was inferred that:

(i) Radial slope of the floor helps the coarser material to be flushed more easily.

(ii) Discharge wasted is some what more when the floor is sloping due to greater depths near the orifice.

(iii) Flow through the orifice can be returned to the channel more easily when the floor is horizontal, and

(iv) Basin with horizontal floor is easier to construct. Circular settling basin with the tangential exit seems to be better than the basin with peripheral spilling.

Merits of circulation chamber device

The experimental results presented above indicate the following merits and demerits of the vortex type basin over the classical types of continuously flushing settling basins.

(i) Vortex type basin functions as a continuously flushing device that effectively removes the suspended particles.

(ii) It affords an economical means to separate the solid particles as its dimensions are small and the amount of water wasted in flushing the sediments is small.

(iii) Solid particles enter the system near the bottom by a suitable design of entrance.

(iv) Although the presence of the air core reduces the water discharge yet a small part of the entrance discharge is lost continuously through the orifice. This can, however, be prevented during the low water season by by-passing the flow directly into the channel downstream. There is little risk of the orifice being choked as the orifice is large.

2.4.3 Prototype installations

Cecen (1977) cites an example of prototype installation of the device "vortex-type settling basin" on the upstream of a classical settling basin where it serves as a preliminary flashing device for the part of the sediment grains (particularly the relatively coarser grains) which are removed beforehand from the flow at Sizir (Kayseri) plant. This plant is located on a stream having an inflow rate of $5.25 m^3/s$ and high sediment transport occurs only during the flood periods. In this device, the width of the inlet channel, B, is 1.75m and the bottom slope is 2%. Water enters from the lower half-depth of the 15m diameter circular basin ($d = 8.57$ B) and is guided by a horizontal plate in such a way that it cannot migrate upwards and has a circular motion. At the centre of this circular basin there is a 0.6m diameter hole ($d/d_o = 25$) for continuous flushing of the deposited sediment. It has been claimed that a considerable amount of sediment is removed by this

preliminary flushing device with water abstraction of only 3%.

2.5 Studies at IPRI

At the Hydraulics Research Station, Malakpore of the Irrigation and Power Research Institute, Punjab, Amristar, India (IPRI), the design of vortex type circular basin has been investigated on the following two Froudian scale models.

Model I It is to a scale of 1:10 and represents the concrete lined Upper Bari Doab Hydel Channel (UBD Hydel).

Model II It is to a scale of 1:25 and simulates the combined channel (downstream the confluence of the Kansal and Suketri flashy streams) feeding Sukhua lake at Chandigarh (India). The bed material in the combined channel comprises sand and coarse gravel.

The relevant prototype and model parameters are as under:

PARAMETER	PROTOTYPE	MODEL
(a) UBD Hydel Channel	Model I	Scale 1:10
Bed width, B	9.144m	0.914m
FS Depth, h	4.206m	0.421m
Side Slope, Z	1.5 Hor to 1 Vert	1.5 Hor to 1 Vert
FS discharge, Q_c	125.7 cumec	0.397 cumec

(In study 4_I, B in the approach to the vortex tank was increased to 14.960m (1.496m on model) and side slopes of the channel and the tank made vertical.)

(b) Combined Channel Model II Scale 1:25

Bedwidth, B	38.1m	1.524m
FS Depth, h	2.332m	0.093m
Side Slope, Z	1.5 Hor to 1 Vert	1.5 Hor to 1 Vert
FS Discharge, Q_c	283.2 cumec	0.0906 cumec

The description of the various tests conducted on Models I and II is given below:

Test No	Basin dia d(m)	Orifice dia d_o(m)	Radial slope S_c	Q_o/Q_c (%)	h_o (m)	d/d_o	P (%)
Description of various dimensions, trapping efficiency, etc, are model values							
1_I	5B=4.572	B/6=0.152	10	5.5	0.535	30	67
2_I	5B=4.572	B/6=0.152	10	5.5	0.535	30	62
3_I	4B=3.658	B/6=0.152	10	3.5	0.512	24	49
4_I	4B=5.984	B/9.82= 0.152	0	2.2	0.533	39	49
1_{II}	4B=6.096	B/24=0.063	10	4.1	0.246	96	23
2_{II}	4B=6.096	B/20=0.076	10	4.5	0.246	80	33
3_{II}	4B=6.096	B/15=0.100	10	7.5	0.246	60	36
4_{II}	4B=6.096	B/15=0.100	10	7.5	0.246	60	40
5_{II}	3B=4.572	B/15=0.100	10	7.5	0.212	45	41

The physical properties of test materials are given in Table 2. The experimental data pertaining to variants and the resultant trapping efficiency of the CCSE are shown plotted in Figures 18 and 19. In these experiments tangential and radial velocities at various depths and a number of verticals along radial lines through the centre of circulation chamber or orifice to the periphery of the circulation chamber were measured using a Prandtl pitot tube. (However, Rea (1984) considers the results of radial velocity measurements as unreliable since use was made of a Prandtl pitot tube which according to him is

unsuitable for such small currents and are also likely to be affected by the tangential velocity. In order to make the record straight it may be mentioned that for the measurement of radial velocities due to a chamber discharge of $0.0011m^3/s$, Levi (1983) also used a pitot tube whereas the discharge in Model I at IPRI was $0.397m^3/s$, ie about 361 times more.)

Non-uniformity in the tangential velocity distribution has been attributed to the entrance conditions and the sloping peripheral wall of the circulation chamber (in all the test runs excepting 4_I). Mean tangential and radial velocities for test runs 3_I and 4_I are shown in Figure 24 (where in r is the distance from the centre of the orifice and V_c is the mean velocity of flow in the parent channel). In the test run 3_I, sand with D_{50} size of 0.217mm was injected at the upstream end of the inlet channel and the distribution of concentration of sediments in suspension and along the bed in the circulation chamber was examined by siphoning water samples with nozzles of appropriate sizes (ensuring the velocity of flow through the nozzles was approximately the same as the circulation chamber flow velocity). The data are shown plotted in Figure 25 wherein C_b and C_s are the mean concentrations of bed load and suspended load respectively.

2.6 Contributions from HRL

Since The Collaborative Research Programme between HRL and IPRI signed in May 1981 included the research theme 'Sediment Control' as well so it was decided to conduct a study for the formulation of a mathematical model or a manual to facilitate the design of circulation chamber or vortex type sediment extractor - a device which holds promise on account of its water conservation capability (water abstraction ratio is the least), minimum detention time, simplicity of the constructional features, lower costs involved, etc.

However, with the background of the available literature and limited controversial experimental observations and data - particularly the basic issues whether in a Rankine combined vortex free vortex is located in the outer or inner region, influence of the air core on reduction in abstracted discharge, inconsistencies in the formulations for the trapping efficiency, etc - it was decided to examine the features of vortex flow in CCSE. Accordingly, a pilot physical model, as shown in Figure 1, was fabricated (Ref Paul (1983)).

Model details

The inlet and outlet channels, measuring 15cm wide x 14.5cm deep, and the circulation chamber with d = 55cm are in perspex. The flow enters and leaves the chamber tangentially. The chamber bed slope, S_c, is 10.7. The chamber bed at its periphery can be adjusted at any distance, h_2, between 0 to 6cm below the bed of the inlet channel. The bed width, B, of the inlet channel can be varied by inserting appropriate sized fillets (width 4cm and 8cm) giving d/B ratio of 3.67, 5.00 and 7.86. To regulate the water levels in the outlet channel, a tilting gate has been provided at its downstream end. The orifice (of 5cm diameter) located at the centre of the circulation chamber discharges into a flashing pipe with its diameter, d_o, as 1.90cm so that $d/d_o = 28.95$. The flushing pipe is kept fully open in the tests.

A right-angled V notch weir is used to measure water discharges through the outlet channel. Since the abstracted or flushing flow is small, it is measured volumetrically using a graduated cylinder and stop watch, and is also checked with a flow meter. The water supply is through a recirculatory system. The circulation chamber, on its outer periphery, has a

perspex jacket filled with water to facilitate visualization of flow and trajectories of sediment particles with the aid of a powerful light source.

The entire discharge of the inlet channel, Q_c, is not introduced into the circulation chamber, as also explained earlier/above. In order to lead the sediment-laden bottom layers of flow from the inlet channel into the chamber, a horizontal diaphragm has been positioned at h_1 equal to 5cm above the bed or at $^1/_3$ the design full supply depth of flow in the inlet channel. In the tests the elevation of the diaphragm is not possible to be altered, however, the ratio of h_2/h_1 can be varied between 0 and 1.2.

In the circulation chamber, if no horizontal plate (henceforth referred to as a 'deflector') is provided, the pressure flow (jet) entering the chamber tangentially will undergo an abrupt expansion in a comparatively large rotating mass of water, thus some sediment particles in the influent may be prevented from settling by upward flow velocity. However, if a deflector, along the inner periphery of the chamber and level with the diaphragm in the inlet channel, is introduced, the sediment particles are shielded from upward forces and settlement is encouraged. The alternative geometries of the deflector are:

(i) No deflector in the chamber, CD_o

(ii) Deflector covering only the exit section of the spill weir, CD_1

(iii) Deflector extending from the entrance of the inlet channel to cover half the circumference of the chamber (including the spill weir section), CD_2 and

(iv) Deflector extending all along the inner periphery of the chamber, CD_3

The width of the deflector, B, is kept constant at about 11cm (approximately equal to the bed width of the inlet channel). In the experimental studies the possible variants are: Q_c, Q_{cc}, h, h_o, B, d/B (from 3.67 to 7.86), h_2/h_1 (from 0 to 1.2), geometry of deflector, etc. It is not possible to vary d/d_o (= 28.95). Tangential velocities in the circulation chamber are measured by using a miniature propeller current meter fabricated and calibrated at HRL.

2.6.1

Paul (1983) was the first researcher to work on this pilot model at HRL (Fig 1). From an analysis of the available data, results of the tests conducted on the pilot model of the CCSE, and the preliminary analytical considerations for the formulation of a mathematical model, he brought out the following inferences:

(i) Unique region of flow

In the circulation chamber there is a characteristic region of flow located at a distance of $(\frac{d}{2} - B)$ from the geometric centre and extending over a width equal to the bed width of the parent or inlet channel, B. The characteristic properties of this region are:

(a) Mean tangential velocity (V_t) or the ratio of mean tangential velocity to mean inlet channel velocity (V_t/V_c) remains constant.

(b) Mean radial velocity, V_r, or ratio of mean

radial velocity to mean inlet channel velocity, V_r/V_c, remains constant; and

(c) Mean concentration of the sediment load at the chamber bed remains constant.

(ii) Source of flushing discharge

Radial diffusion is negligibly small, and the flushing discharge is mainly contributed by the fluid layers in the vicinity of the orifice. From distribution of radial velocities recorded in Model I, test run 3_I, it has been shown that the discharge contributed to the orifice computes to $0.0168 m^3/s$ against actually measured value of $0.0139 m^3/s$, ie excess by about 21%.

(iii) Size of circulation chamber

The preliminary analytical treatment (see Appendix A) suggests that optimum size of circulation chamber has a diameter, d, equal to five times the width of the parent/inlet channel, ie d = 5B. Available experimental data as shown in Figure 26, lend credence to this optimal size (also Ref Paul & Dhillon (1985)).

(iv) Chamber depth

The HRL model envisages introduction of a diaphragm in the inlet channel at a distance of one third of design full supply depth of flow, and with this lay out, the optimum chamber periphery depth below the bed of inlet channel is 0.4 times the height of diaphragm, ie $h_2 = 0.4h_1$ or 0.13h, as shown in Figure 27.

(v) Chamber deflector

Provision of a deflector in the circulation chamber increases the magnitude of the trapping efficiency of CCSE. If no deflector is provided some sediment which is in the process of settling in the circulation chamber may be picked up and get escaped with the spill flow into the outlet channel. In the case of an unlined channel, adoption of the deflector CD_1 is suggested, whilst for lined channels deflector CD_3 should be considered as an alternative to CD_2 after a cost: benefit analysis. When the parent or inlet channel transports fine sediment in suspension, the provision of diaphram in the inlet channel be dispensed with, and deflector CD_3 adopted.

(vi) Design discharge

Since the trapping efficiency of this device reduces when the inlet channel discharge, Q_c, increases beyond the design limit, as shown in Figure 28, great care needs to be exercised in selecting the design discharge. Also refer to Figure 13.

(vii) Optimum water abstraction

For optimum efficiency the flushing discharge appears to be 5% of the inlet channel discharge (when $Q_c = Q_{cc}$), Figure 18.

(viii) Chamber bed slope

A chamber bed slope, S_c, of 10 horizontal to 1 vertical toward the orifice slightly increases the water abstraction but helps keep the bed clear of sediment deposits.

2.6.2

Chrysostomou (1983), was the next researcher to work on the HRL pilot model of CCSE (Fig 1). He concentrated his attention mainly on the measurement of detention time and visualization of flow patterns in the circulation chamber. Detention time, t, is defined as the time a definite quantity of water remains in the circulation chamber. Longer the detention time, longer the sediment particles remain in the circulation chamber to settle to the bottom and eventually flushed thereby yielding higher values of trapping efficiency. He measured the detention time (ie the time taken by certain dye to travel through the chamber) by introducing a colorimeter tube at the boundary between the inlet channel and the deflector. Time was recorded with the aid of a UV oscillograph. Dye was introduced using a hyperdermic needle and a syringe. A typical record of intensity of dye in relation to time is shown in Figure 29.

Visualization of the secondary flow

This is best accomplished by introducing neutrally buoyant particles having a dispersion angle of 90° in the water (as these neither float nor sink but follow the flow or current pattern in the circulation chamber). Since the tangential velocity, V_t, is very much larger than the radial velocity, V_r or V_z, V_t

should not be visible. This is achieved by selecting a radial section in the chamber and observing it at an angle of 90°.

The most suitable particle types are: fragmentated wax, red polystyrene, and alluminium flakes, however, he found 4 micron or 0.04mm fire flakes' silver in colour to be an idealized sediment. Section DD, as shown in Figure 1, 15mm thick was selected as it was located away from the inlet and exit channels. A mercury compact source lamp was positioned in a black box, with a lens at one end to concentrate the light beam through a 15mm slot marked with black tape on the lens and so into the circulation chamber. This arrangement provided a beam of light 15mm wide and 12cm high. To facilitate observation of flow pattern on the photograph, the camera shutter speed has to be appropriate to the flow in the chamber and was 1s for very low flow and thus low velocity.

Tests were conducted using chamber deflector CD_1, CD_2 and CD_3; and chamber depth as its periphery below the bed of the inlet channel, h_2 equal to 4cm and 0cm.

Vortex stability

It was observed that for certain deflector conditions and water depths in the chamber at its periphery, h_o^* the vortex oscillated around the centre of the chamber in an elliptical orbit offset at times by as much as 5cm, ie 18% of chamber radius, R, or 17° with the chamber axis.

Flow disturbances

These were located between the outlet channel to a point inside the chamber. The strength and the length of the disturbances depended on the type of the deflector.

Strong disturbances were observed with the deflector CD_1. However, with deflector CD_2 disturbances were small and with deflector CD_3 these were absent. The overall effect of flow disturbances was to reduce the detention time, t, for certain conditions because the vortex tended to lift water from the bottom and thus sediment with it. This could cause the flow to become unstable and turbulent, thus reduce the trapping efficiency of the device.

Results of detention time studies

The experimental data pertaining to detention time studies have been analysed using the following dimensionless forms:

(i) t^2g/d versus V_c^2/gd for variations of h_o^*/d

(ii) t^2g/d versus V^2/gd for variations of B/d, and

(iii) t^2g/d versus V_c^2/gd for different deflector types.

(a) Effect of peripheral water depth, h_o^* on t and V_c

The data in Figure 30 indicate that the detention time, t, increases with the increase in water depth at the periphery of the circulation chamber, h_o^* but V_c gets reduced simultaneously.

However, t is more sensitive to h_o^* variations than the variations in V_c.

(b) Effect of B on t and V_c

A family of curves, in Figures 31 and 32, for B = 15cm and 11cm and 7cm and various h_o^*/d values when h_2 is 3.2cm and 5.6cm and defletor CD_2 in the chamber; indicate that for a given value of V_c, t increases as d/B increases from 3.67 to 7.86. However, for water depths lower than 0.26, V_c is more sensitive to d/B variations than detention time is. For water depths, h_o^*/d = 0.28 and more, the opposite occurs.

(c) Effect of h_2 on t and V_c

Tests were conducted by varying the chamber depth, h_2, such that h_2/d was 0.10, 0.058 and 0.00 whilst keeping all other variants constant. From the data in Figures 33 and 34 in will be seen that at relatively high inlet channel velocities (V_c^2/gd greater than 0.02) and low peripheral water depths (h_o^*/d less than 0.24), detention time is marginally longer with chamber depths, h_2/d equal to 0.10. However, if the chamber depth is decreased so that h_2/d equals to 0.058, t for certain inlet velocities is longer than that obtainable with h_2/d = 0.10. This chamber depth, ie h_2/d = 0.058, appears to be optimum because any further reduction in chamber depth simply decreases detention time.

(d) Effect of various deflectors on t and V_c

This has been examined using deflectors CD_1, CD_2 and CD_3 and the data are shown plotted in Figures 35, 36 and 37. It can be seen that for a given inlet channel velocity, V_c, detention time, t, is longer with the deflector CD_2 than it is for deflector CD_1, or CD_3. At low values of h_o^*/d, V_c is a little more sensitive to the changes in deflectors than detention time, t. However, at higher values of h_o^*/d and V_c, the opposite occurs.

Comparison of secondary flow patterns

This has been done using deflectors CD_1, CD_2 and CD_3. When the deflector CD_1, is in position, a proportion of the particles (constituting a layer not more than 5cm thick) travel along the bottom and across the chamber into the orifice. The water in the bottom half of the chamber tended to be lifted over a swirl because of the presence of the bottom boundary where the major part of the flow is forced towards the orifice taking the particles with it into the vortex. In the upper half of the depth in the chamber, the opposite happens. The particles are forced down until they are in contact with the particles rising from the bottom, and then a second swirl in the top layer forces them upwards and into the vortex. There appears to be a dead zone in the middle where the particles travel horizontally towards the vortex as caught between the two swirls. This being more distinctive with the greater chamber depths. However, as the chamber depth decreases, more and more particles are forced into the bottom part of the flow depth where they swirl up and enter the vortex region.

With the deflector CD_2 in position, the overall flow pattern is more or less the same except for the flow near the outer periphery and especially in the upper half depth where particles travel towards the bottom faster, ie at a steeper angle than with deflector CD_1, and are then taken through, by the bottom swirl, into the centre of the section. There the majority of the particles are then attracted by the vortex at the bottom for chamber depth equal to 4cm or by the vortex at the top half for h = 0cm.

With the deflector CD_3 in position, the distinctive features are:

(i) A greater number of particles travel directly into the chamber along the bottom surface, and

(ii) Presence of three different swirls: one under the deflector, second on the top of the deflector, and third in the centre of the section between the deflector and the vortex.

It is the exact position of this third swirl which defines the difference in flow between the two different chamber depths, whilst the other two swirls are formed in both cases because of the restricted area between the deflector and the upper and lower surfaces of the flow. When the chamber depth, h_2, is zero, the third swirl is positioned very close to the bottom boundary of the chamber, thus causing shoot up of particles, coming from under the deflector, along the end of the deflector, where they are joined by the particles from the upper swirl. The forced current of the middle swirl guides them into the centre of the section, and so into the vortex. However, when the chamber depth, h_2, is 4cm, the third swirl is located more in the centre of the section. This has the effect, of not forcing the particles in the bottom

half upwards, but taking them round the swirl and then into the bottom layers of the chamber, and so into the vortex. In addition, a portion of the particles from the swirl above the deflector are also drawn downwards along the deflector to follow the current. The rest of the upper particles follow the current of the middle swirl upwards and so they are drawn into the centre and into the vortex.

Inferences

(i) The more the water depth in the chamber, the longer the detention time, t, and therefore, h_o^*/d greater than 0.26 is suggested.

(ii) The optimum peripheral chamber depth, below the inlet channel bed, h_2, has to be 0.6 times h_1, ie $h_2/h_1 = 0.6$ or $h_2/d = 0.058$ when $h_1/d = 0.011$.

(iii) Deflector CD_2 gives the maximum detention time

(iv) Decrease in bed width, B, increases detention time for a given value of inlet channel velocity. With chamber depth, $h_2/h_1 = 0.6$ or $h_2/d = 0.058$, $d/B = 7.86$. Detention time for a given inlet channel velocity is very sensitive to variation in: (a) d/B and h_o^*/d.

Remarks

The finding that the deflector CD_2 ensures the maximum detention time, as reported by Chrysostomou (1983), corraborates the inference drawn by Paul (1983) and APWA practice, Sullivan (1972). A reference to his (Chrysostomou's) data plots in Figures 31 and 32 will indicate that for peripheral water depths, h_o^*/d

greater 0.24, the gain in detention time when the chamber size is increased from d/B = 5 to d/B = 7.86 is not significant to the extent to justify the adoption of d/B = 7.86. The recommendation that the chamber depth at its periphery) be $h_2/h_1 = 0.6$ against $h_2/h_1 = 0.4$ proposed by Paul (1983) is acceptable on the considerations of detention time. His recommendation that chamber peripheral water depth, h_o^*/d should be greater than 0.26 is rather complicated. It is well known that the water level in the CCSE for all practical purposes is the same as in the parent/inlet channel. Therefore, the water depth at the chamber periphery $h_o^* = h + h_2$, where h is the water depth in the inlet channel. With the peripheral chamber depth fixed at $h_2 = 0.6h_1 = 0.2h$ below the inlet channel bed, $h_o^* = 1.2h$. Therefore, the depth of water in CCSE at the periphery gets automatically fixed and cannot be increased, if required unless abstracted discharge is manipulated with a valve provided in the flushing pipe. Such an eventuality can lead to choking of flushing pipe upstream of the valve location because of restriction of flow passage imposed by the partial opening of the valve. As such, for the present this requirement may be enlisted in another form, viz to ensure that the efficiency of CCSE is not impaired, its operation may ensure that $h_o^*/d > 0.26$ (this, however, will be reviewed subsequently).

2.6.3

With a view to gain a better understanding of the nature of flow within the circulation chamber, Rea (1984) undertook a detailed examination of the region of high radial velocities near the bed of the chamber and the pattern of secondary currents again using the

pilot model at HRL. To facilitate visualization of secondary flow or currents, a thin vertical wall of light was directed at the centre of the chamber illuminating one radius. Small neutrally buoyant particles entered the chamber with the flow and could only be seen when they passed the beam of light. By looking at right angles to the beam of light, the secondary flow could be discerned from the motion of the particles. Long exposure photographs of this region showed streaks representing the direction of secondary flow. The effect of tangential velocities was eliminated because the photographs were taken in a tangential direction.

For the measurement of radial velocity, a rotating fan was placed in front of the camera so that instead of streaks, the particle paths showed up as a series of dashes. The fan when appropriately located permits a small dot to appear at one end of each dash and facilitated determination of the flow direction. A powerful slide projector used produced a uniform, 1cm wide beam with clearly defined edges in which the particles showed up brightly.

For the measurement of velocity, a strobe lamp was tried but found to be neither bright enough nor well focusing. However, it proved to be useful at a later stage as a means of setting the rotating fan to the correct speed.

Photographs were taken using a Nikon F2 SLR camera with an 85mm lens. With this lens positioned at a distance of 0.8m from the wall of light, the view was about 10° from the perpendicular at the edge of the photographs. Thus, tangential velocity did produce streaks in these areas. Thus, a particle moving in a purely tangential direction would show up as a streak 1.7mm long as it passed through the 0.1m wide beam.

Further, near to the centre (where the radius of the particles is small compared to the width of the beam) the curvature of particle paths could create a streak even if they had no radial velocity. For example, such a particle rotating at a radius of 10mm would produce a horizontal streak 1.8mm long.

The computation of horizontal length of streaks produced by a particle moving in a purely tangential direction is slightly complicated because each of the effects mentioned above is predominant in more than one region. The horizontal length of a streak produced by a particle moving in a purely tangential direction along with a graphical description of as to why the respective effect is predominant in each region is shown in Figure 38. It can be seen that the error due to above mentioned causes is under 1.7mm for 99.9% of the field view and can, therefore, be safely ignored when analysing the photographs. Vertical streaks could also be produced by tangential motion near to the top and bottom of the photographs but these are a maximum of 0.75mm long. The combined effect produces a maximum streak length of 1.8mm which is yet not large enough to effect the analysis significantly.

Experimental results

Radial flow near to the bed

Near to the bed of the chamber, there is a very distinct region, about 0.01m thick, of high radial velocity. Particles in this region can be seen moving towards the centre. The flow in the near-bed region towards the orifice can be expressed as:

$$Q_r = 2 \pi r \delta \bar{V}_r \qquad (17)$$

where r is the distance from the centre, δ is the thickness of the radial velocity region, and $\bar{V}_r$ is the average radial velocity within the region. Since the thickness of the radial velocity region cannot be precisely defined as such approximations to δ and $\bar{V}_r$ have to be made. Figure 39 shows the distribution of radial velocities, measured in the near-bed region, in the radial direction. It will be seen that radial velocity at any one point can take a number of values, however, the maximum is inversely proportional to the distance from the orifice, r. To the data, the curve defined below, fits the maximum velocities:

$$V_r = 55/r$$

Near to the centre of the circulation chamber, the maximum values do fall below this curve. However, near to the perimeter, a few measured velocity points lie above the curve. Radial velocity at the chamber periphery is zero, it follows that the distribution of maximum radial velocities does not follow the inverse proportionality rule in that region. The most likely maximum radial velocity distribution in the region near to the chamber periphery is shown by the dotted line in Figure 39.

From Equation 18 it follows that V x r is a constant, $55 cm^2/s$ in the present case. If the radial velocity profile in the vertical direction in similar at various radial distances from the chamber centre, then a plot of the V_r x r against the vertical distance from the chamber bed, h*, will provide an indication of its shape, Figure 40. The solid curve in Figure 40 gives the radial velocity distribution for the case of motion near a stationary wall when the fluid at a large distance above it rotates at a constant circular velocity after Schilichting (1962). Scatter though

large yet can be attributed to the random experimental errors. The points manifesting the largest scatter are those which represent conditions near to the chamber periphery. However, it is certain that the shape of the radial velocity distribution is not exactly the same at all radii and at all times, particularly the height of the maximum velocity tends to be larger with larger radial distances or radii. The solid curve in Figure 40 yields thickness of the radial velocity region, δ = 1.85cm (Schlichting (1962)). Now if it is assumed that δ is proportional to the height of maximum velocity, h_m, equal to 0.74cm, that is:

$$\delta = c_1 h_m$$

For δ = 1.85cm, and h_m = 0.74cm, c_1 is approximately 2.5.

Another assumption is then made that at a given radius, the average radial velocity over the region is proportional to maximum radial velocity and that flow is axisymmetric, that is:

$$\bar{V}_r = C_2 V_{r\,max} \qquad (20)$$

The experimental data indicate the value of c_2 as 0.55. Equation 17, therefore, becomes:

$$Q_r \simeq 2 \pi r C_1 h_m c_2 V_{r\,max}$$

or

$$Q_r \simeq 8.64 r h_m V_{r\,max} \qquad (17a)$$

The measured values of h_m and V_r max at various radii, as taken from Film 7, are enlisted below:

r (cm)	$V_r$max (cm/s)	h_m (cm)	Q_r (cm^3/s)
5	9.33	0.50	202
7	6.67	0.50	202
8	6.17	0.50	213
10	5.33	0.50	230
12	4.33	0.55	247
14	4.00	0.55	266
16	3.17	0.60	263
18	3.00	0.55	257
20	2.67	0.60	276
22	2.67	0.65	230
24	2.33	0.60	290
24.5	1.67	0.70	257

The calculated values of Q_r are shown plotted in Figure 41 along with the line of best fit. This line must pass through zero at the periphery and at the centre as no flow passes these points. In the region r = 0 to 2.5cm, the radial flow decreases rapidly as it enters the orifice. Further out, from r = 2.5 to 19cm, the flow in the near-bed region decreases gradually towards the centre showing that water is rising into the zone above which will affect the settlement of the sediment particles. Near to the perimeter, from r = 22.5 to 27.5cm, the amount of radial flow increases rapidly and there is a sizeable downward flow. This is the region where all the near-bed flow originates and also where most of the sediment particles must enter the radial flow region. The most interesting part of the curve is between r = 19cm and r = 22.5cm; water leaves the radial flow zone rapidly and, therefore, is likely to take sediment away with it. The rapid decrease in radial flow arises from a decrease in $V_r \times r$ as well as a decrease in δ. This ejection process can be clearly seen in Figure 42.

Almost all researchers agree that the flow in the region $r > r_o$ of the circulation chamber is similar to a free vortex, ie $V_t \times r$ constant. It has also been shown above that near to the bed $V_{r\ max} \times r$ is a

constant. Therefore:

$$[V_t \times r / V_{r\,max} \times r] = \text{constant}$$

or

$$\tan\left[\frac{V_t}{V_{r\,max}}\right] = \text{constant} \qquad (21)$$

This implies that the flow tends to approach the orifice at a constant angle in the maximum radial flow margin.

Further, from Figure 41 it can be seen that the total radial flow at the edge of the orifice is approximately $170 cm^3/s$ or about 2.5 times the measured value of $70.3 cm^3/s$.

Inferences

(i) Photographic analysis of the flow pattern in the CCSE indicated that there are two distinct regions of flow in the chamber: (a) near to bed, there is a rapid radial flow towards the orifice, and (b) in the rest of the chamber, the flow is slower and much more complicated.

(ii) Radial velocity measurements in the near bed region of the CCSE indicate that $V_{r\,max} \times r$ is a constant. Since in the free vortex region $V_t \times r$ is also constant, this implies that the flow approaches the orifice at a constant angle ($= \tan^{-1} V_t / V_{r\,max}$). The vertical distribution of radial velocity is similar to the theoretical distribution of radial velocity for the motion near a stationary wall when the fluid at large distance above it rotates at a constant angular velocity.

(iii) From measured distribution of radial velocity, the estimated radial distribution of the total flow towards the orifice in the near bed region indicates that the total radial flow increases from the periphery down to a distance equal to 0.8R. There is then a rapid ejection of fluid from the near-bed region. The flow then decreases more gradually towards the centre.

(iv) The most important finding concerning the secondary flow patterns in the bulk of the fluid is that they are of a non-steady, periodic nature. The time period of the cycles corresponds to the period of revolution of the fluid at 0.7R.

Remarks

(i) In the estimation of the discharge contributed to the orifice by the radial flow in the near-bed region, Rea (1984) is in error on the following two accounts:

(a) Since in the region 4cm < r < 5cm, Figure 39 indicated that there is only one measured radial velocity as such it is not judicious to pass the total near-bed flow curve in Figure 41 through this point, viz $202cm^3/s$, and

(b) Since the diameter of the flushing pipe is 1.9cm or the radius of the effective orifice is 0.95cm, therefore, the total near-bed flow curve in Figure 41, should pass through 0.95cm point.

When these two points are attended to, the dotted curve shall be obtained. This yields the

orifice discharge very nearly equal to 70.3cm^3/s - the measured value. This lends confidence in the technique adopted for the measurement of radial velocity.

(ii) The curve in Figure 41 indicates that the vertical flow near to the bed changes direction at 0.8R distance from the centre of the chamber or the orifice whilst the photographs indicate that this distance varies from 0.6R to 0.8R. Since the curve in Figure 41 is based on only one measurement so it will be more realistic to suggest that the vertical flow changes direction at 0.6R distance as shown from analytical considerations by Paul (1983) or Appendix 'A'.

2.7

Salakhov (1975) has reported on water intake structures with circulation chamber. The type of water intake, as shown in Figure 3(a), belongs to the category of side water intake structures whose main element is a circulation chamber which is built on the bank behind a side weir with a sill. The water intake structure essentially comprises a pocket provided with a flushing gate, gated-openings, curvi-linear directing sill and an earth-lined bund.

In case the discharge diverted is comparatively high and one circulation chamber is not sufficient, a series of circulation chambers is provided, as shown in Figure 3(b). The function of the circulation chamber is to control bed and near-bed sediment load. It is useful both with and without water intake dams.

The chamber (Fig 3(a)) is essentially a round basin with a vertical wall to which water is supplied through a closed pipe tangentially to its circumference. The clarified water is escaped through

a circular open trough running outside, around the periphery of the chamber in its upper part. A flushing pipe is connected to a port in the centre of the chamber floor to remove the sediment to the downstream.

On entering the chamber, water is set in rotational motion in respect to vertical axis passing through the centre of the orifice. The velocity of the movement increases towards the centre of the chamber. The movement results in a break of the stream continuity in the centre of the chamber and an air funnel is formed over the bottom port of the orifice so that a comparatively small water flow is achieved through the orifice.

The bulk of the water overflows the chamber edge along its entire periphery, arrives at the circular trough and flows to the main canal of the irrigation system.

Sediments entering the chamber travel along a spiral trajectory in the chamber bottom towards the orifice from where they are discharged through the flushing pipe to the downstream. The transport of the sediment from the periphery towards the centre of the chamber is caused by bottom (secondary) flows which are formed due to rotary movement of the stream in the chamber and are intensified by the flushing opening.

The CCSE effectively operates where the following relationships between its dimensions are observed:

$$H' > 0.33R > 0.17d \qquad (22)$$

$$h = 0.4 \text{ to } 0.6H \qquad (23)$$

$$\text{and} \quad S_c > 0.02 \qquad (24)$$

The relation in Equation 22, viz H/d > 0.17 could be compared with h_o^*/d 0.26 after Chrysostomou (1983) discussed above under Inference (i), paragraph 2.6.2. Here H is the height of the circulation chamber.

Hydraulics of flow in circulation chamber

(a) In all cases where the flushing discharge escapes to the atmosphere, ie exit end of flushing pipe is not submerged, irrespective of the chamber discharges, Q_{cc} an air funnel (air core) is formed over the orifice piercing the entire flow depth and causing the water to release through the orifice having a comparatively small cross-section, as shown in Figure 3(c).

(b) When the exit end of the flushing pipe is submerged the air funnel in the chamber becomes less deep and 'lifted' resembling Rankines' composite vortex. The funnel cavity, approximately to the depth of circumference, is filled with water whose motion is different from that of the main stream and is governed by the statistical rotation.

(c) A circular boundary line is observed on the free surface of the stream. Floats entering the area inside this line are carried over the funnel cavity and into the orifice while those outside this are diverted towards the edge of the chamber and further to the diversion channel.

(d) The greater the velocity of water entering the chamber, the greater the size of the funnel.

(e) Flushing discharge is relatively very small compared to the total chamber discharge Q_{cc},

depending on the orifice opening diameter. Generally Q_o is 5 to 8% of Q_{cc}.

(f) When a one-sided inlet to the chamber is employed, the air funnel axis does not coincide with the axis of the orifice/chamber; it tends to shift towards the bisector of the third quarter of the circle in the direction of the flow movement, the magnitude of the shift being dependent on the stream circulation intensity in the chamber.

(g) The streamflow in the circulation chamber is asymmetrical.

(h) The peripheral velocities are uniformly distributed in depth of the stream; the stream flow in horizontal planes of the chamber can be considered as a two-dimensional problem while the entire flow in the chamber as a potential flow.

(i) Peripheral velocity, changing along the radius of the chamber, is not governed by the law of areas- it is conditioned by a simultaneous action of the laws of dynamic and static rotation. The peripheral velocity along the orifice radius, irrespective of change along the chamber radius has an almost constant (maximum) value, as shown in Figure 3(d).

The peripheral velocity variation along the chamber radius is given by:

$$V = V_d \, (R/r)^{\alpha} + V_s \, (r/R)^{1/\alpha} \qquad (25)$$

where V_d and V_s are the initial velocities of dynamic and static rotation respectively. The exponent, α varies from 0.792 to 0.948, and the

values of V_d and V_s are obtained from the following relationships:

$$\left.\begin{aligned} V_d/V_s &= \frac{1}{\alpha^2}\,(r_p/R)^{\alpha+1/\alpha} \\ V_d + V_s &= d/(R - r_p)^{h_o} \end{aligned}\right\} \qquad (26)$$

where r_p and h_o are the radius and height respectively of the circulation chamber branch.

(j) Sediment fractions with $D_s > 0.5$ to 1mm tend to settle in the circulation chamber with diameter, d, given by the relationship:

$$d^2 = 2\,Q_{cc}/V_s \qquad (27)$$

where

V_s is the fall velocity of the sediment fraction.

Examples of prototype installations

According to Salakhov (1975), since 1957 to 59, two circulation chamber intakes designed for 2.2 to 2.5m^3/s discharge have been operted on the rivers Kudialchai and Akara in the Azerbaijan SSR. Field investigations spread over a number of years have indicated a high effectiveness of circulation chambers for the control of both bed and near-bed sediment loads.

2.8

Ogihara and Sakaguchi (1984) have reported investigations which lead to the development of new systems to separate the sediments from the water flow by using the rotating flow, as shown in Figure 4. According to them, when the flow rotates horizontally

in a cylindrical tank, the secondary flow, such as vertical rotating flow, is generated. This secondary flow consists of the vertical upward flow in the centre of the tank and downward flow near by the inside part of the tank wall. As such, the water at the surface flows from centre to outside and that at the bottom goes from outside to the centre. This secondary flow transports the deposits on the bottom of the tank from outside to the centre part of the tank.

This method for separating the sand, silt and other deposits from the water by secondary flow has many advantages, eg:

(i) Rotating flow is made automatically by the energy of inlet flow.

(ii) The secondary flow is generated automatically by the rotating flow.

(iii) The sediments are transported by this secondary flow to the bottom of the tank and collected to the centre. And

(iv) The sand and silts at the bottom of the tank are flushed out through the outlet pipe at the bottom of the tank.

Theoretical analysis assumes that the main flow in the tank is a horizontal rotating flow and its velocity distribution is given by:

$$u = R\,\omega \tag{28}$$

And that the pressure distribution (from Euler's equation) is given by:

$$p = \frac{\ell\ \omega^2\ r^2}{2} + \ell\ g(H-z) \qquad (29)$$

Equations 28 and 29 give the main flow characteristics. Assuming that the velocity of the secondary flow at the bottom of the tank is given by:

$$u_b = u.E \qquad (30)$$

E is the coefficient of reduction ratio of velocity due to the friction effect of the bottom wall. Since the velocity of secondary flow is smaller than that of main flow, so the square term of the velocity of secondary flow can be neglected as compared to the other terms in Navier-Stokes equation in cylindrical co-ordinate system. Then the basic equation of motion is:

$$\frac{\omega^2 r(1-E^2)}{\nu} = \frac{1}{r}\frac{\delta}{\delta r}(r\frac{\delta v}{\delta r}) + \frac{\delta^2 v}{\delta z} - \frac{v}{r^2}$$

$$\frac{1}{r}\frac{\delta}{\delta r}(r\frac{\delta w}{\delta r}) + \frac{\delta^2 w}{\delta z^2} = 0 \qquad (31)$$

If the velocity of secondary flow is given by:

$$v = v(r) + v'(r, z),\ \omega = \omega'(r,z) \qquad (32)$$

These equations and the equation of continuity yield the following four equations:

$$\frac{\omega^2 r(1-E^2)}{\nu} = \frac{1}{r}\frac{\delta}{\delta r}(r\frac{\delta v}{\delta r}) - \frac{v}{r^2}$$

$$\frac{1}{r}\frac{\delta}{\delta r}(r\frac{\delta v^1}{\delta r}) + \frac{\delta^2 v'}{\delta z^2} - \frac{v'}{r^2} = 0$$

$$\frac{1}{r}\frac{\delta}{\delta r}(r\frac{\delta \omega'}{\delta r}) + \frac{\delta^2 w'}{\delta z^2} = 0, \text{ and}$$

$$\frac{1}{r}\frac{\delta}{\delta r}(vr) + \frac{1}{r}\frac{\delta}{\delta r}(v'r) + \frac{\delta w'}{\delta z} = 0 \qquad (33)$$

Boundary conditions for the secondary flow are:

$r = 0$ and $r = R$, $v = 0$, $z = 0$, $w' = 0$

The solution of Equation 33 which satisfies the boundary conditions is:

$$v = \frac{\omega^2(1-E^2)}{8\nu} r(r^2-R^2) + AJ_1(\lambda r)\text{Sinh } \lambda z$$

$$w = -\frac{\omega^2(1-E^2)}{8\nu}(4r^2-2R^2)z - AJ_0(\lambda r)(\text{Cosh } \lambda z-1)$$

$$A = \frac{2R^2h}{\cosh\lambda H-1} \frac{\omega^2(1-E^2)}{8\nu} \tag{34}$$

Equation 34 can be rewritten in a non-dimensional form as:

$$\frac{v}{8R_e\beta} = -\frac{r}{R}\left[\left(\frac{r}{R}\right)^2-1\right] + 2\frac{h}{R}\frac{\text{Sinh } \lambda z}{\text{Cosh } \lambda H-1} J_1(\lambda r)$$

$$\frac{w}{8R_e\beta} = \frac{H}{R}\left[\frac{z}{h}\left(4\frac{r^2}{R^2}-1\right) - 2J_0(\lambda r)\frac{\text{Cosh } \lambda z-1}{\text{Cosh } \lambda H-1}\right] \tag{35}$$

$$v = \frac{v+v'}{\omega R}; \quad w = \frac{w'}{\omega R}; \quad R_e = \frac{\omega R.R}{\nu}; \quad \beta = 1 - E^2 \text{ and } \lambda = \lambda'/R \tag{36}$$

Here $J_0()$ and $J_1()$ are Bessel functions and λ_1 is a root of Bessel functin of the first order and ν is the kinematic viscosity. The upward velocity in the centre of the tank becomes larger in the case the ratio H/R is larger.

Relationship between the inlet velocity and the velocity of rotating flow

Since the rotating flow is made continuously, the best method is to use the energy of inlet flow. Such a relation is important for the design of the sediment tank.

Energy of inlet flow

The inlet flow is supplied from inlet port of rectangular cross-section of area, A_c. When the discharge Q_c is supplied to the tank, the energy supplied is:

$$E_{i\cdot} = \frac{1}{2}(\ell\ A_c\ v_c)v_c^2 = \frac{1}{2}\ell\ A_c\ v_c^3 = \frac{1}{2}\ell\ Q_c\ v_c^2 = \frac{\ell}{2}\frac{Q_c^3}{A_c^2} \quad (37)$$

Energy of flow spilling into the downstream channel

If the area is A_s, velocity is v_s and discharge is Q_s, then:

$$E_s = \frac{1}{2}\ \ell\ Q_s\ v_s^2 = \frac{1}{2}\ \ell\ Q_s^3/A_s^2 \quad (38)$$

Kinematic energy of rotating flow

The energy of rotating flow with velocity distribution as in Equation 28 is given by:

$$E_r = \frac{\ell RH'}{8}(R\omega)^3 \quad (39)$$

Energy loss due to internal friction

Loss of energy with the velocity distribution as in Equation 28 is given as dissipation function in unit volume:

$$\Phi = \frac{8}{3}\mu\ \omega^2 \quad (40)$$

Total loss of energy due to internal friction is given by:

$$E_{if} = \frac{8\pi}{3}\ell\ \nu(R\omega)^2\ H' \quad (41)$$

Energy loss at wall due to friction

Since the friction force, $\tau_0 = c_f \frac{\ell u^2}{2}$ (42)

where the coefficient c_f is a function of Reynolds number.

Energy loss at side wall, $E_{sw} = \ell \Pi R H c_f (R\omega)^2$ (43)

Energy loss at tank bottom, $E_{tb} = \frac{\ell \Pi}{5} c_f (R\omega)^3 R^2$ (44)

Energy balance in the tank

Energy balance in the tank can be written as:

$$E_i = E_s + E_r + E_{if} + E_{sw} + E_{tb}$$

This equation in view of the above equations, yields the following relationships:

$$(\frac{v_s}{R\omega})^3 = \frac{RH' \quad 2\pi}{A_c[1-(A_c/A_s)^3]} \times (\frac{1}{8\pi} + \frac{16\Pi}{3R_e} + c_f + \frac{c_f}{5}.\frac{R}{H}) \quad (45)$$

where

$$R_e = \frac{2\Pi R}{\nu}.R\omega \quad (46)$$

$$c_f = 1.328/R_e^{0.5} \text{ (for laminer flow)} \quad (47)$$

and

$$c_f = 0.074\ R_e^{-0.2} \text{ (for turbulent flow)} \quad (48)$$

Next the right hand side term in Equation 45 as shown by last parenthesis is related to the Reynolds number and aspect ratio, H/R. Denoting this part as C, the relation of velocities of inlet and spill flow is given as:

$$C = F(R_e, \frac{R}{H}) = \left[(\frac{v_c}{R\omega})^3 \frac{A_c}{2\Pi RH}(1- \frac{A_c}{A_s})^3 \right] \qquad (49)$$

Experimental results

Experiments were conducted using first small tank with d = 43cm and H = 50cm (Case 1), then using large tank of diameter of 200cm and depth as 200cm. The area, A_c, of the inlet channel in Case 3 was half that in Case 2, as below:

	CASE	A_c	R	H	$A_s = 2\Pi RH$
Tank	1	20	21.5	40	169.6
Dimensions	2	1900	100	150	4084
	3	950	100	150	1084
		(cm^2)	(cm)	(cm)	(cm^2)

To obtain relationship between inlet velocity and rotating velocity, inlet velocity is obtained by diving the discharge entering the tank by the inlet channel area, and the rotating velocity at the side wall is measured by a velocity meter. The relation between these two is shown in Figure 43. It can be seen that the two velocities have proportional relations but the coefficient of proportion is different in each case. Now to make these three lines to collapse into a single one, Equation 49 is made use of and the following parameters are introduced:

$$p_1 = (\frac{A_c}{2\Pi RH})^{1/3}$$

$$p_2 = \left[1-(A_c/A_s)^3\right]^{1/3} \qquad (50)$$

This yields the following values for the three cases:

CASE	P_1	P_2
1	0.1584	0.9993
2	0.2725	0.9651
3	0.2159	0.9956

The relationship between rotating velocity and the modified inlet velocity which is calculated by multiplying the inlet velocity and these parameters, is shown in Figure 44. The constant, C, is obtained from the slope of this line and its value varies from 0.0181 to 0.1940 or to account for the scatter in the data the value may be taken as 0.015 to 0.020.

Separation of sediment from water flow

Separation of sediments from the inlet flow is determined by the relationship between the fall velocity of the sediment particles and the vertical upward velocity at the centre of the tank. The particles which have larger settling velocity as compared to this upward velocity, go to the bottom of the tank.

When the discharge, Q_{cc}, is larger, the upward velocity is controlled by the flows at the outlet portion of surface intake structures as shown in Figure 4 instead of the secondary rotating flow. The results of observations as to how the sediment separate between upward flow and downward flow are shown in Figure 45. In this figure, curves, V_3', correspond to the upward velocity which is calculated from:

$$Q_{cc} / \frac{\pi d^2}{4}$$

Lower curve, V_3', corresponds to the case where flushing discharge is released to flush out the sediment deposits. So the upward velocity gets

decreased by the magnitude of the flushing discharge. The curve, W, indicates the velocity of upward flow at the water surface which is calculated by numerical solution of Laplace equation for stream function. These curves are very similar especially in the range of large values of rate of discharge.

This velocity is related to the ratio Q_0/Q_{cc}. These relationships are shown in Figure 46. Curve (a) represents the case of float sink in which water flows over the circular disk, and Curve (b) represents the case of point sink. These curves show the maximum and minimum velocity at the same level of the disk. In Figure 45, black points show the settling velocity of sediments from the orifice and white points show that of the sediments transported by over flow. The sediments used are powders of coal with specific gravity of 1.55.

The mean settling velocity of black points is 3.75cm/s and that of white points varies with the inflow discharge, Q_{cc}. These values become the same at $Q_{cc} = 70\ell/s$. This point gives the limit condition to separate the sediment of this coal powder from the inflow in the tank.

The efficiency of separation of sediments from the inflow is determined by the velocity of upward flow at the sink point of outflow. This result is better only in the case of large rate of inflow and large settling velocity of sediment. When the sediments settle with small falling velocity less than 1cm/s, the upward velocity is calculated by the analysis of secondary flow in the tank.

2.9

Sanmuganathan (1985) questions the concept of considerable reduction in flushing discharge by the presence of air core, as advocated by Salakhov (1975),

Cecen (1977) and others, because this implies a unique dependence of discharge on flow area. Accordingly, models for:

(i) Conditions critical to air core formation, and
(ii) Discharge coefficient, c_d, for orifice or flushing pipe

have been proposed by Sanmuganathan (1986) and Sanmuganathan (1985) respectively. The practicability of these two models has been examined next.

2.9.1 Air core formation

Identification of parameters critical to air core formation or yielding critical (relative) submergence being relevant to the design of different types of intakes or outlets has attracted considerable attention. Chang (1976), Knauss (1983), Hecker (1981) and others have presented comprehensive literature reviews. Paul and Dhillon (1987) examine the reliability of various analytical models for vortex characteristics in vertical gravity intakes. His model, based on sound logic and theoretical considerations, relies on the estimation of two non-dimensional parameters:

$$\beta = \tau^2/gh_0t^2 \text{ (ie circulation)} \qquad (51)$$

$$\alpha = [Q_0{}^2/\delta\Pi^2 gh_0{}^5)^{1/5} \text{ (ie discharge)} \qquad (52)$$

where

τ is the circulation; h_0 is the submergence of the intake; 2t is the diameter of the forced vortex; and using this pair with $\delta = d_0/2h_0$, is:

$$f(\alpha, \beta, \delta) = 0 \qquad (53)$$

where

d_0 is the diameter of orifice or flushing outlet pipe.

Equation 53 represents a family of curves each for a constant value of δ defined in the α, β plane that presents critical conditions, as shown in Figure 47. The region bounded by the α and β axes and the line $\alpha = 0.5$ is the one where no air core forms. The non-dimensional parameters α and β represent two separate causes responsible for air core formation indepentently and should not be combined (as in the Kolf number) advised Sanmuganathan (1986).

From a regression analysis of Anwar and Amphlett data, reproduced in Sanmuganathan (1985) and also in Table 4, comprising 258 sets of h_0/d_0, $N_\tau = \tau d_0/Q_0$, and $c_d = 4Q_0/\Pi d^2\sqrt{2gh_0}$ describing critcal conditions for air core formation in vertcial gravity intakes, consiting of three groups each of 86 sets corresponding to a single value of r/d_0 (where r is a large radius) as 2.0, 2.5 and 3.0. Sanmuganathan (1986) deduces the relation describing the diameter of forced vortex as:

$$d_0/2t = 0.527e^{0.0116\ h_o/d_o} \qquad (54)$$

The correlation coefficient of Equation 54 is 0.623.

For reliability test of the model in Equation 53, the predictions of circulation number are compared by him with 258 experimental observations and the model is adjudged to perform well as the mean of the ratio of predicted to observed (ie discrepancy ratio, DR) critical circulation number (N_τ) turns out as 1.05 with a standard deviation (SD) of 0.31, Sanmuganathan (1986).

Discussion of air core model

(i) Since by definition:

$$Q_0 = c_d \frac{\Pi d_0^2}{4} \sqrt{2gh_0}$$

therefore, Equation 52 yields:

$$\alpha = c_d^{2/5} / [64^{1/5} . (h_0/d_0)^{4/5}] \qquad (55)$$

From Figure 47 it is seen that for critical conditions, $\alpha = 0.5$. With this value of α, Equation 55 yields.

$$C_d = \sqrt{2}\ (h_0/d_0)^2 \qquad (56)$$

That is an answer which is unrealistic because discharge coefficient cannot be a function of h_0/d_0 alone and that too with exponent as 2.

(ii) A perusal of Figure 47 indicates that on the Y-axis the maximum value of β is 1.0. However, β can be greater than one when:

$$\tau^2 > gh_0 t^2 \text{ or } \tau > g^{1/2} h_0^{1/2} t \qquad (57)$$

To ascertain this, use was made of Anwar and Amphlett data (86 sets of data for $r/d_0 = 2.0$) to compute τ. The corresponding values of t were computed from Sanmuganathan's (1986) correlation in Equation 54. It was observed that in 47 sets air core forms because β values lie beyond the region bounded by α and β axes and δ curves. This is contrary to the stipulation that Anwar and Amphlett data describe the critical conditions for air core formation. For more details readers may refer to Paul and Sayal (1988). An analysis of 86

sets of Anwar and Amphlett data for $r/d_0 = 2.0$, indicates that the best fit correlation yielding relative critical submergence or critical condition for air core formation is:

$$h_0/d_0 = 12.77\ N_\tau^{0.664}\ F^{1.31}/R_e^{0.065} \qquad (58)$$

where

F is the Froude number = $(Q_0/\frac{\Pi d_0^2}{4})/\sqrt{gd_0}$

R_e is the Reynolds number defined as $Q_0/\nu d_0$.

This correlation gives DR as 1.04 with SD of 0.29. However, when all the 258 data sets are considered, DR becomes 1.048 with SD of 0.294 (Paul & Dhillon (X)).

The inference is that the empirical correlatin for air core formation in Equation 58 decidedly yields the same, if not higher, reliability as Sanmuganathan's (1986) model does.

(iii) Though Harleman et al (1959), from investigation of incipient drawdown of the lighter fluid in a cylindrical container with two immiscible liquids - a case analogous to air core formation, suggest that for the drawdown to occur:

$$h_0/d_0 = 0.75\ F^{0.4} \qquad (59)$$

and it is heartening to note that this yields $\alpha = 0.50$ but not consoling because literature is impregnated with the correlations of the form:

$$h_0/d_0 = AF^B \qquad (60)$$

for vertical gravity intakes where the exponent B is 0.4, 0.5, 1.0 and 2.0, and all such correlations are supported by experimental evidence.

2.9.2 Discharge coefficient

According to Sanmuganathan (1985), the height, h_0, as shown in Figure 48, along with the other relevant parameters influences two events:

(a) It determines whether air core forms or not; and
(b) It determines the magnitude of Q_0.

It has been argued that though h_0 is an independent variable but whether Q_0 is an independent variable or not depends on other factors. Both Q_0 and h_0 can be considered independent parameters only when H^* (ie the head difference between the water levels in CCSE and the waste or escape channel) is not equal to zero, and in such situations Q_0 replaces H^* as an independent parameter. The discharge through the outlet can be stated as:

$$Q_0 = f(H^*, \tau, d_0, t) \qquad (61)$$

Referring to the situation A in Figure 48, the applied head is $H^* - H_L$, where H_L is the friction loss in the outlet pipe. Part of this applied head is dissipated as swirling velocity. Taking the swirling velocity at $r = d_{0/2}$ as the basis, the energy lost in swirling flow computes to $2\tau^2/gd_0^2$ yielding effective head as $H^* - H_L' - (2\tau^2/gd_0^2)$. This yields discharge coefficient:

$$C_d = 4Q_0/\Pi d_0^2 \sqrt{2g} \left[H^* - H_L - (2\tau^2/gd_0^2)\right]^{1/2} \qquad (62)$$

The inference is that C_d will depend on t which is a function of h_0/d_0 (see Equation 54) or $c_d = c_d(h_0/d_0)$ in addition to other parameters like R, etc.

If the vortex is not of a forced vortex type, the flow situation would be as in (B), Figure 48. Herein the fluid loses energy before entering the outlet. It has been shown that the effective head in this case is

$$H^* - H_L - \frac{\tau^2}{gd_0^2}\left[(16t^2/d_0^2)-1\right]$$

or discharge coefficient:

$$c_d = 4Q_0/\Pi d_0^2\sqrt{2g}\left[H^* - H_L - \frac{\tau^2}{gd_0^2}\left(\frac{16t^2}{d_0^2} - 1\right)\right]^{1/2} \quad (63)$$

which is similar to Equation 62 but with a much higher value - of the order of 0.6. The variation of c_d with h_0/d_0, if any, is required to be determined experimentally.

Discussion of discharge coefficient model(s)

Unfortunately no data are available in published literature to determine the reliability of the models in Equations 62 and 63. Nevertheless, if an assumption is made in Anwar and Amphlett experiments, that the outlet discharged freely to the atmosphere, it becomes possible to evaluate the Equations 62 and 63 as these then reduce to:

$$C_d = 4Q_0/\Pi d_0^2\sqrt{2g}\left[h_0 - (2\tau^2/gd_0^2)\right]^{1/2} \quad (62a)$$

and

$$C_d = 4Q_0/\Pi d_0^2\sqrt{2g}\left[h_0 - (\tau^2/gd_0^2)\left(\frac{16t^2}{d_0^2} - 1\right)\right]^{1/2} \quad (63a)$$

(i) Application of Equation 62 or 62(a) necessitates that 2t should be smaller than d_0 or $d_0/2t$ should be greater than one, situation A in Figure 48. Equation 54 indicates that for such eventualities, h_0/d_0 should be greater than about 55 - a condition highly improbable in CCSE. A review of Anwar and Amphlett data (Table 4) comprising 86 sets for $r/d_0 = 2.0$ indicates that $h_0/d_0 > 55$ only in nine cases - two for $d_0 = 0.016$m and seven for d = 0.0096m. Further, the values of c_d as predicted from Equation 62(a) are shown plotted against h_0/d_0 in Figure 49. It will be seen that c_d varies from 0.52 to 0.89. Similar values from the other two sets for $r/d_0 = 2.5$ and $r/d_0 = 3.0$ are also shown plotted against h_0/d_0 in Figure 49. The inferences are:

(a) There is no trend for the variation of C_d with h_0/d_0;

(b) All the values are higher than expected; and

(c) If the effective head is to account for the water level in the waste channel and the outlet pipe losses, apprehension is that C_d will further increase. However, a comparison of 27 predicted (from Equation 62(a)) with the corresponding C_d observed values yields DR of 1.34 with SD of 0.35.

(ii) The flow situation (B) in Figure 48 necessitates the use of Equation 63(a). Anwar and Amplett data for $r/d_0 = 2.0$ and $d_0 = 0.1528$m yield t varying from 0.1318m to 0.1373m; τ varying between 0.3608 and 0.4706 or

$(16t^2/d_0^2 - 1)$ varying between 10.904 and 11.919 with mean as 9.02m against the value of h_0 varying from 0.7163 to 1.2512m yielding effective head with negative value or imaginary or unrealistic value of C_d.

The inference if that Equation 63 cannot be used to compute C_d.

(iii) On the other hand, an analysis of 258 sets of Anwar and Amphlett data yields:

$$C_d = 0.22\ R_e^{0.075}\ N_\tau^{0.054}\ F^{0.965}/(h_0/d_0)^{0.375} \qquad (64)$$

having DR of 1.009 with SD of 0.058 (Paul & Dhillon (X)).

(iv) Reliability of correlation for C_d, Equation 64

It must be made clear that Anwar and Amphlett data used for arriving at the correleation for discharge coefficient, c_d, in Equation 64 pertain to experiments conducted under idealized conditions, viz the outlet discharge, Q_0, was always equal to the chamber discharge, Q_{cc}, as discharge spilling into the downstream channel was nil or $Q_0 = Q_{cc} = Q_c$. Equation 64 indicates that the circulation directly affects the discharge coefficient of the outlet pipe. Anwar (1967) has shown (from theory and experiments) that the maximum tangential velocity occurs at $r \simeq r_0 = d_0/2$ or the edge of the orifice and it is related to the head on the orifice, h_0, as:

$$V_{to} = \sqrt{2gh_0/3.45} \qquad (65)$$

and that the tangential velocity at any distance r in the free vortex region can be obtained from V_{to} as:

V_t at a distance r from the centre of orifice
$= V_{to} \times r_0/r$ (66)

Thus the circulation, τ, at a large radius is given by.

$$\tau = 2\Pi r\ V_t = 2\Pi r\ V_{to}\ r_0/r = \Pi d_0 \sqrt{\frac{2gh_0}{3.45}} \quad (67)$$

and the circulation number, $N_\tau = \tau d_0/Q_0$ as:

$$N_\tau = \frac{\Pi d_0^2}{Q_0} \sqrt{\frac{2gh_0}{3.45}} \quad (68)$$

Since, Froude number, $F = \dfrac{4Q_0}{\Pi d_0^2 \sqrt{gd_0}}$

and Reynolds number, $R_e = Q_0/\nu d_0$

it means that if for CCSE, orfice diameter and head on it and discharge escaping are known, the predicted values of C_d from Equation 64 can be compared with the observed values of:

$$C_d = \frac{4Q_0}{\Pi d_0^2 \sqrt{2gh_0}}$$

This has been done utilizing Curi et al (1975) data for d_0 = 0.0254m and 0.0508m (Table 3); HRL data (Paul (1983)) pertaining to runs 1_{III} to 10_{III}, that is a total of 19 points where presumably air core was allowed to form; and fresh data from Hydraulics Research Station, Malak Pore (IPRI) given in Table 5 for a model of CCSE similar to HRL pilot model but

with inlet channel 0.60m wide x 1.0m deep; $h_2/h_1 = 0.4$, $S_c = 10$ hor to 1 vert, $d = 5B$, and $d_0 = 0.09m$, 0.10m and 0.15m, a total of 30 points, where air core was not allowed to form. For the data range:

$5.45 < h_0/d_0 < 10.28$; $5.77 < N_\tau < 10.17$; $0.70 < F < 1.62$; $6.9 \times 10^4 < R_e < 1.7 \times 10^5$ - no air core, and

$1.63 < h_0/d_0 < 9.70$; $2.09 < N_\tau < 9.54$; $0.51 < F$ 4.35; $1.17 \times 10^4 < R_e < 4.81 \times 10^4$ - air core.

The variation of C_d predicted with C_d observed is shown in Figure 50. It will be seen that:

DR = 0.87 with SD = 0.22 for air core forming
DR = 1.071 with SD = 0.016 for no air core
DR = 0.97 with SD = 0.15 overall

This comparison provides confidence in the prediction ability of correlation Equation 64 for dicharge coefficient of orifice. Also the inference is that the circulation, for its effect on discharge coefficient of pipe outlet, does not depend on:

(a) chamber discharge; and
(b) chamber diameter.

2.10

Levi (1983) has reported on the development of a fluidic device which transforms a radial motion in a rotatory motion and finds application to water treament processes, such as: mixing, aeration, clarification, etc. The radial motion is generated by a submerged water jet, discharged along the floor of a cylindrical tank by a set of vertical nozzles at the

centre of tank and directed downwards, as shown in Figure 51. The existence of a set of fixed, equally distributed oblique vanes, helps create a stable vortex above. The water level is kept steady by equipping the tank with an outlet controlled by a weir, valve or gate. The vanes are usually fastened to two supporting annular plates, forming a stabilizer coaxial with the nozzle, sufficiently separated from the floor to allow the jet to pass below freely, hit the vessel and be reflected toward the vanes at an upper level. The inner diameter of the tank is found to have practically no influence on the performance of the device, in so far as the distance between the stabilizer and the wall is not less than about 10% of the stabilizer radius.

Since the radial jet, raised and deflected inwards by the wall, acquires a tangential V_t component as soon as it enters the stabilizer, so d the diameter of the stabilizer can be assumed to represent the diameter of the vortext produced inside the stabilizer. Nozzle discharge, Q_{cc}, is a function of the nozzle diameter, d_0, and its height, h_0, above the floor. Experiments show that the Reynolds number, $4Qh_o/\Pi d_0^2\nu$, is related to h_0/d_0 as:

$$4Q_{cc}h_0/\Pi d_0^2\nu = (73.3\ h_0/d_0 - 2.87) \times 10^3 \qquad (69)$$

The distribution of radial velocity is given by:

$$V_r/V_{ro} = 2^{-(y/y_c)^{2.8}} \qquad (70)$$

where

V_{ro} is the radial velocity close to the floor and y_c is the elevation at which $V_r = V_{ro}/2$. Consider that the vortex circulation, $\tau = 2\Pi r\ V_t$ and τ_0 is its value

far away from the vortex axis. The two Reynolds numbers associated with the jet-vortex motion, viz:

$$R_{ej} = Q_{cc}/\nu \sqrt{h_0 d_0} \text{ and } R_{ev} = \frac{\tau_0}{\nu} \sqrt{\frac{h_0^*}{d}}$$

where

h_0^* is the liquid depth in the tank, are correlated as.

$$R_{ev} = 1.314\ R_{ej} \tag{71}$$

The jet-vortex correlation coefficient

$$\lambda = R_{ev}/R_{ej} = \frac{\tau_0}{Q_{cc}} \cdot \sqrt{\frac{h_0 h_0^* d_0}{d}}$$

appears to be related to the momentum transfer from the jet to the vortex. The tangential velocity at the outer opening of the stabilizer (r = d/2) is given by:

$$V_{td} = \tau_0/\Pi d \tag{72}$$

The efficiency of the vortex as a part of the jet-vortex system, η_v, is given by:

$$\eta_v = \frac{b^2\ h_0^*}{2\Pi}\left(\frac{\tau_0}{Q_{cc}}\right)^3 \left(\ell_n \frac{\sqrt{2gh_0^*}}{V_{td}} - \tfrac{1}{2}\right) \tag{73}$$

where

$$\tau_0/Q_{cc} = \lambda \sqrt{\frac{d}{h_0 h_0^* d_0}},\ V_{td} = \frac{\lambda Q_{ec}}{\Pi \sqrt{h_0 h_0^* d d_0}}, \text{ and}$$

b is the mean thickness of the jet so that $V_r = Q_{cc}/2\Pi rb$. It is expedient to that η_v can be

greater than one becuase the fluid enters the stabilizer with some power, inherited from the jet.

Clarification

The mechanics of a clarificatin process usually involves the following steps: mixing the inflowing fluid with chemicals inside a fast mixer, stirring the mixture in a flocculator and sedimentation of the flocs in a settling basin. The fluidic vortex device described above allows nearly all the prcesses to be carried out within a single vessel. One such facility is as shown in Figure 52. Since laboratory water was clear, colloidal particles were injected using an aqueous suspension of bentonite. Aluminium sulphate was added for coagulating and lime for making the flocs heavier. Through jar tests, the most convenient proportion was found to be 200mg/l bentonite, 60mg/l alum and 80mg/l lime. Solid content of the samples of the liquid before it entered the tank and it had left the tank was determined by gravimetric tests. The settling percentage, p, has been computed from $p = [(S_1 - S_2)/S_1]$ x 100, where S_1 and S_2 are the solid contents before and after the process. Figure 53 shows p as a function of the gap, h_0, and the discharge, Q_{cc}, the critical role of both of them being evident. The maximum settling rate of 83%, was attained with h_0 = 10mm and Q_{cc} = 1.25l/s. With such a high rate of sludge sedimentation inside the reactor no further residence in a settling basin should normally be needed before the filtering process.

2.11

Julien (1986) determines from theory concentration profiles of very fine silts in a steady two-dimensional horizontal vortex and compares with those obtained experimentally. According to him, as opposed to the flow in homogeneous fluids, the flow

characteristics of a water-sediment mixture are obscured by the presence of solid particles. It is intuitively recognised that particles in a vortex tend to separate from the fluid by centrifugal action. Full understanding of this problem is as yet incomplete considering the interaction of viscous, gravitational and inertia forces and the unsteady nature of eddies in turbulent flows. The fluid mixture investaged is composed of very fine cohesionless sediment particles in distilled water. With very small particles, the analysis is simplified since the viscous forces exerted on the particles are dominant compared to their weight and inertia. Analysis considers the motion of a small spherical particle of diameter, D_s, specific mass, ℓ_s, and mass, $\Pi\ell_s D_s^3/6$ located at a distance, r, from the centre of the vortex. Small particles refer to cohesionless particle sizes very much smaller than the vortex core radius, r_0; and the velocity of the particle is very close to the fluid rendering Coriolis acceleration negligible compared to the centrifugal acceleration. The radial acceleration of the particle, a_r, is given by:

$$a_r = \frac{V_{ts}^2}{r} - \frac{\ell_f}{\ell_s}\frac{V_t^2}{r} - 18\,\frac{\ell_f \nu}{\ell_s}\,\frac{V_{rs}}{D_s{}^2} \qquad (74)$$

The tangential acceleration, a_t, is given by:

$$a_t = -\,18\,\frac{\ell_f \nu}{\ell_s}\,(V_{ts} - V_t)/D^2{}_s \qquad (75)$$

Equation 75 indicates that as the ratio ν/D_s^2 becomes very large, the tangential acceleration term prevails until the tangential velocity of the particles, V_{ts}, reaches the velocity of the fluid, V_t. Therefore, the

tangential velocity of small particles should always remain close to the fluid velocity. Equilibrium condition in the radial direction for $V_{ts} = V_t$ occurs when the acceleration component, a_r, from Equation 74 vanishes. The limit velocity, V'_e, of the particles in the radial direction is:

$$V_e' = \frac{1}{18}\left(\frac{\ell_s}{\ell_f} - 1\right)\frac{V_t^2}{r\nu} D_s^2 \qquad (76)$$

Equation 76 can be rewritten in a dimensionless form as a function of the Reynolds number, $R_e = V_t D_s/\nu$, as:

$$V'_e/V_t = \left[\frac{1}{18}\left(\frac{\ell_s}{\rho_f} - 1\right)\frac{D_s}{r}\right]R_e \qquad (77)$$

Thus the limit radial velocity of the particle is proportional to ℓ_s/ℓ_f, D_s and V_t and decreases as the viscosity, ν, and the radius, r, increase.

In a viscous fluid, small sediment particles reach the fluid velocity very rapidly and particles heavier than the fluid are moved outside the vortex core. Therefore the concentration of the particles decreases toward the centre, thereby creating a concnetration gradient across the vortex. A diffusion flux proportional to this gradient induces the transport of solid particles toward the regions of lower concentration. Equilibrium conditions are reached when the flux of sediment particles due to centrifugal force is balanced by diffusion flux in the opposite direction. This equilibrium condition implies that the radius of curvature of the particles is r, and can be described as under:

$$\frac{dC}{C} = \frac{V'_e}{E}\, dr \qquad (78)$$

in which C is the sediment concentration by volume and E is the diffusion coefficient. An assumption is then made that the diffusion coefficient, E, remains independent of r, regardless whether laminar or turbulent diffusion is involved. Substituting for V'_e from Equation 76 into Equation 78, the concentration profile is obtained as under:

$$\int\frac{dC}{C} = \frac{1}{18}\int\left(\frac{\ell_s}{e_f} - 1\right)\frac{V_t^2}{r}\frac{D_s^2}{\nu E}\,dr \qquad (79)$$

With the boundary condition at infinity, $C = C_\infty$, the integration of Equation 79 yields two expressions for the sediment concentration profile since two velocity relationships are applicable to the free and fixed vortex, as:

$$\frac{C}{C_\infty} = e^{a\left(\frac{r^2}{r_0^2} - 2\right)} \quad \text{when } r \leq r_0 \qquad (80)$$

and

$$C/C_\infty = e^{-a\frac{r_0^2}{r^2}} \quad \text{when } r > r_0 \qquad (81)$$

wherein the dimensionless parameter, a, is defined as:

$$a = \left(\frac{\ell_s}{\ell_f} - 1\right)\frac{\tau^2}{144\Pi^2 E\nu}\left(\frac{D_s}{r_0}\right)^2 \qquad (82)$$

Theoretical concentration profiles in a Rankine combined vortex with various, a, values are shown in Figure 54 as a function of r/r_0. The above analysis leads to the inference that the concentration is constant when a = 0 which corresponds to infinitely

small particles or neutrally buoyant particles, $\ell_s = \ell_f$. The curves for a > 0 indicate a decrease in concentration toward the centre of the vortex whilst the concentration increases toward the centre when $\ell_s < \ell_f$. The boundary conditions at $r = r_0$ and at the centre of the vortex (ie r = 0) are:

$$C_{r_0} = C_\infty e^{-a} \tag{83}$$

$$C_0 = C_\infty e^{-2a} \tag{84}$$

Interestingly the ratio C_{ro}/C_∞ is equal to the square root of C_o/C_∞

Verification

For the verification of sediment concentration profiles deduced above theoretically, laboratory experiments were conducted for the condition a > 0. A water sediment mixture comprising very fine silts ($0.0053mm < D_s < 0.0074mm$) with concentration of 50g/l was used. A steady vortex was induced in three litres of the mixture by rotating a 76mm (3 inch) magnetic stirring bar at the bottom of a fixed cylinderical flask. The nearly horizontal motion of sediment particles indicated that no significant secondary circulation was present in the vortex. The circulation, τ; the angular velocity, ω; and the velocity V_{to} at the ratius of the vortex were obtained from water surface profiles measured with a point gauge. Sediment concentrations were obtained from several 30 ml pipetted samples, dried and weighed ($\pm$ 0.1mg). The parameter V_{to} was calculated from $\ell_f V_{to} = p_\infty - p_o$ and r_o from $\tau = 2\Pi r_o V_{to}$. The coefficients a and C_∞ are then evaluated from the sediment concentration data using Equations 80 and 81 duly linearized as follows:

$$\ln C = \ln C_\infty + a\left[\left(\frac{r}{r_o}\right)^2 - 2\right] \text{ when } r \leq r_o \qquad (85)$$

and

$$\ln C = \ln C_\infty - a\left(\frac{r_o}{r}\right)^2 \text{ when } r \geq r_o \qquad (86)$$

A linearized sediment concentration profile is shown in Figure 55 for the evaluation of C_∞ and a. In Figure 56, two measured sediment concentration profiles are compared with the theoretically derived relationships.

Inferences

(i) The excellent agreement obtained in both the cases leads to the conclusion that when $\rho_s > \rho_f$, the sediment concentration decreases toward the centres of vortex.

(ii) The sediment concentration profile depends on three major factors:

(a) diffusion,
(b) friction and
(c) centrifugal force exerted on small particles.

The diffusion coefficients for the two experiments, shown in Figure 50, were respectively $0.000167 m^2/s$ and $0.000940 m^2/s$ which correspond very likely to turbulent diffusion.

Obviously Equations 80 and 81 cannot be applied to CCSE because of the assumption of very fine silts rapidly acquiring the fluid velocity, absence of the secondary flow, horizontal nature of Rankine combined vortex, etc. Nevertheless for the Test Run 3_I (in

Paul 1983) with:

$D_s = 2.17 \times 10^{-4}$m; $r_o = 0.076$m; $\tau = 1.983 m^2/s$;

$Q_{cc} = 0.397$; $\ell_s/\ell = 2.65$; $E = 1.19 \times 10^{-4} m^2/s$;

$C_\infty = 1.009$ g/l and 'a' computing to 347.5,

measured concentrations and the theoretical sediment concentration profile after Julien (1986) are shown plotted in Figure 57, Paul and Sayal (1988). Though both indicate decreasing concentration toward the centre of vortex or orifice but shapes of profiles are quite different.

2.12 Hydraulic modelling

Most investigators, eg Curi et al (1975), Cecen (1977), Salakhov (1975), APWA (Ref Sullivan (1972)), Ogihara and Sakaguchi (1984), and others have used the settling velocity criterion for simulation of suspended sediment particles in Froudian models, ie the ratio of characteristic fluid velocity to settling velocity of sediment particles should be the same both in model and prototype. However, Molof (1975) (Ref Curi et al (1975)) in his discussion of Curi et al (1975) paper has pointed out that the particle size could be evaluated according to the Froude number,

$$F_r = \frac{4Q_o}{\pi d_o^2 \sqrt{gD_s}}$$

where D_s is the length or diameter of the particle. For a 2.54mm particle with a specific gravity of 1.05 in the inlet of a 11m (36ft) prototype unit could be represented by a 0.865mm particle with the same specific gravity of 1.05 in a nearly 0.9m (3ft) model

unit (ie $\lambda = 12$). From Table 3 it could be seen that more than 50% of the tests had been done with a particle of 2.12mm diameter and specific gravity of 1.05 in a nearly 0.9m (3ft) model unit. The settling velocity a 2.1mm particle being 3.8cm/s, the particle size in the prototype unit could be calculated as:

$(V_s)m/(V_s)p = \sqrt{12}$ or $(V_s)p$ as 13.2cm/s

or particle size as 14mm with specific gravity of 2.65 which is very large when compared to expected particle diameters in actual practice.

In their reply to Molof's discussion, the authors (Curi et al (1975)) submitted as under:

"The authors believe that the settling velocity of suspended particles cannot be a criterion in determining model scale ratios for particle sizes. In this respect, holding the Froude and Reynolds numbers related to particles, ie Shields parameters, the same in the model and prototype, as also suggested by Akmandor (1972) may not yield satisfactory results. This approach would result in the following scale ratios:

$D_{sm}/D_{sp} = \lambda^{\frac{1}{2}} = 12^{\frac{1}{2}}$; and $\partial'm/\partial'p = 0.0241$

Thus if the model particle has 2.12mm diameter and specific gravity 1.05, the prototype particle will have a diameter of 0.61mm and specific gravity of 3.07. As can be noted, the results are not quite comparable.

2.12.1

Alquier et al (1982) have called attention to the APWA hydraulic model study (Ref Sullivan (1972)) of a configuration that should produce a maximum concentration of solids at the orifice of outlet pipe. The results indicated that part of the solids are deposited on the chamber floor, and, thus, can be resuspended. According to their belief, the use of terminal settling velocity of particles in quiet water used may not be the most significant parameter. Secondary flows (created in large part by central spoilers) can greatly affect the deposition and resuspension of particles. In the case of increasing flow, particles deposited during the low flow period can be removed through the spill weir; stated in another way, secondary flows can impair removal efficiency.

Characterisation of efficiency

With the sediment flushing pipe in operation, the efficiency of the device, P, could be defined as the percentage of solids initially injected to the solids discharged through the flushing pipe. This criterion is not sufficient to characterize settling because the flow through the outlet can be varied over a large range. In the particular case when $Q_o = 0$, and Q_{cc} is large enough to suspend the settled particles, all solids can pass over the spillweir. Therefore, efficiency must be defined with some other criterion. The swirl concentrator could be looked upon as a particle transfer system whereby a fluid or a solid particle enters at a time, $t = o$, and leaves at time, $t = \tau$. The distribution function of the transit time, τ, a stochastic variable, can be characterized by its statistical moments; the first moments correspond to the mean transit time, τ_f, for fluid

particles, and τ_s for solid particles. It has been shown that

$$\tau_f = V_{cc}/Q_{cc} \tag{87}$$

where

V_{cc} is the water volume in the chamber and Q_{cc} is the fluid discharge.

The ratio of $\bar{t}_s$ to $\bar{t}_f$ can be considered as a characteristic of decantation capacity of the device. If $\bar{t}_s \rightarrow \infty$, the solid particles are perfectly trapped, so the decantation capacity is excellent; if $\bar{t}_s \rightarrow \bar{t}_f$, the solid particles follow the fluid particles perfectly so the decantation capacity reduces to zero. Thus, a dimensionless number defined below can be used to compare the behaviour of different solid particles for fixed hydraulic conditions:

$$\bar{D} = 1 - \bar{t}_f/\bar{t}_s \tag{88}$$

$\bar{D} \rightarrow 1$ or $\bar{t}_f/\bar{t}_s \rightarrow 0$ indicates that the device has a good decantation ability.

The shape of the transit-time distribution depends on convective diffusion in the chamber; since it is greater than first-order moments, it can give information on the flow structure. For a comparison of different geometric configurations of the chamber, use can be made of the dimensionless number - a characteristic of intensity of convective diffusion - defined below:

$$K = M_2/\bar{t}_f^{\,2} \tag{89}$$

Where M_2 is the centred second-order moment of the transit-time distribution of fluid particle.

Solid particles used

The limit fall velocity, V_s, of solid particles, as used by many investigators, as a characteristic parameter to describe the behaviour of a solid phase in suspension, is not considered the best parameter because it does not represent the resuspension of deposited particles. In view of this argument. Alquier et al (1982), make use of critical velocity, U_c, defined as the mean velocity in a given rectangular channel at which the solid material deposited on bottom goes into suspension. Since U_c depends on the channel geometry (Ref the correlation given below) so was measured in the same conditions for each material class used:

$$U_c/\sqrt{gD_s} = 0.61\ (S_s - 1)^{\frac{1}{2}}\ (D_s/R)^{-0.27}$$

for $0.01 < D_s/R < 0.8$ (90)

where

R is the hydraulic radius (Ref Novak & Nalluri (1975)).

The characteristics of solid particles used are listed below:

SOLID PARTICLES USED

S No	MATERIAL	DENSITY g/cm^3	SHAPE	DIAM (mm)	FALL VEL (cm/s)	CRITICAL VEL (cm/s)
1	Nylon	1.08	Cylindical	3.0	7.0	7.7
2	Polyamid	1.11	Parallelopiped	4.6	7.0	11.1
3	Sand	2.65	Irregular	0.3	7.0	18.0
4	Polyestyrene	1.035	Cylindrical	3.8	4.36	5.6
5	Sand	2.65	Irregular	0.7	9.5	18.5
6	Polyestyrene	1.35	Parellelopiped	4.6	9.5	14.4

In order to compare the behaviour of particles having the same, V_s, but different critical velocity, U_c, materials at serial number 1, 2 and 3 were used for tests with various geometric patterns keeping $Q_o = o$. Results tabulated below show that the efficiency coefficient, $\bar{D}$, is not the same for all particles though V_s is the same for the particles, and it is an increasing function of the critical velocity.

EFFICIENCY COEFFICIENT $\bar{D}$ WITH $Q_o = o$

Weir Height (cm)	Weir diam (cm)	Baffle configuration	Material $\bar{D}$ (%) Material 1	Material 2	Material 3
11.5	20.0	1 ———	36.40	69.60	91.00
		2 — —	91.32	96.40	99.98
	30.0	1 ———	88.12	91.96	99.77
		2 ———	89.92	91.80	99.99
16.5	20.0	1 ———	81.32	88.60	99.81
		2 ———	81.00	85.10	99.88
	30.0	1 ———	97.56	98.83	99.99
		2 ———	85.44	90.72	99.99
32.5	20.0	1 ———	99.96	99.97	-
		2 ———	91.16	95.48	-
	30.0	1 ———	99.98	100.00	-
		2 — —	86.68	92.48	-

Tests with flushing pipe in operation

For an inflow discharge, $Q_{cc} = 7.1 \times 10^{-4} m^3/s$, removal efficiency, P, has been measured for materials 1 and 2, for two different Q_o values of $0.305 \times 10^{-3} m^3/s$ and $0.71 \times 10^{-3} m^3/s$. Results tabulated below again show that the removed efficiency, P, depends on U_c.

REMOVAL EFFICIENCY, P, WITH Q_o

Flushing discharge Q_o (m^3/s)	P (%)	
	Material 1	Material 2
0.305×10^{-4}	71	84
0.71×10^{-3}	80	86
Fall Vel (cm/s)	7.0	7.0
Critical Vel (cm/s)	7.7	11.1

The inference is that behaviour of solid particles is better characterized by the critical velocity because of the resuspension of deposited solids rather than by fall velocity. Since the large eddy structure generated impairs the efficiency of the swirl concentrator, an obstacle in the form of three series of two bars on the chamber bed improves the solid separation efficiency by controlling the generation of large eddy structures.

Discussion

Though it has been shown that the critical velocity of solids as related to their resuspension from deposits is a better characteristic parameter than the fall or settling velocity to describe the behaviour of solids in a swirl concentrator yet the method by which critical velocity is to be determined has not been cited Equation 90 indicates that critical velocity

depends on hydraulic radius which most probably cannot be computed for the flow in a swirl concentrator.

2.13 Estimation of Circulation

An analysis of 86 sets of Anwar and Amphlett data (Table 4) for $r/d_o = 2.0$, indicates that the best correlation for circulation is

$$N_\tau = 4.03\ h_o^{0.35}\ d_o^{2.66} / Q_o^{1.2} \qquad (91)$$

The correlation for N_τ in Equation 91 yields mean value of N_τ/ predicted to N_τ measured or DR as 1.024 with SD of 0.266. A comparison of N_τ predicted with N_τ measured, for 86 sets, is shown in Figure 58. Since $N_\tau = \tau d_o/Q_o$, Equation 91 yields circulation, τ, as:

$$\tau = 4.03\ h_o^{0.35}\ d_o^{1.66} / Q_o^{0.2} \qquad (92)$$

Equation 92 can be compared with Equation 68 (derived from Anwar (1967) correlation, $V_{to} = \sqrt{2\ gho/3.45}$, viz:

$$z\ \tau = \pi d_o \sqrt{2\ gho/3.45} = 7.49\ d_o \sqrt{ho} \qquad (68)$$

2.14

Recaptulating the various elements or parameters involved in the CCSE design (as enlisted in Paragraph 1.2 above) and the detailed review of the state-of-art in this field of hydraulic engineering presented above the know-how can now be summarized as follows:

2.14.1 Chamber diameter

The various practices/suggestions indicate that d = 6B APWA practice (Sullivan (1972)):

$d = 1.4 \sqrt{Q_{cc}/V_s}$ for 0.5 mm < D_s < 1.0 mm
(Salakhov (1975))

$$d = 5.274 \ (U_*/V_o)^{0.25} \ (k_1 k_2)^{0.5} \ (Q_{cc}/V_s)^{0.5}$$

(Cecen & Bayazit (1975)

d = 5B (Paul (1983) and Curi et al (1975).

d = 7.86 B (Chrysostomou (1983))

It will be seen that the last term in parenthesis in Cecen & Bayazit (1975) is the same as in Salakhov (1975); and the constant in Cecen & Bayazit is the same as in Paul (1983). Since it is neither known as to how shear velocity, U_*, in the chamber is to be computed nor the formulation for its evaluation has been reported by Cecen and Bayazit (1975), as such this correlation cannot be made use of. Moreover, in their experiments the locations of free and forced vortices were quite different from those generally observed in a Rankine combined vortex. The APWA practice has a more direct application to Public Health engineering problems in small urban catchments or very low storm discharges so that chamber diameter $d = 0.9144 \ (Q_d/0.00912)^{0.4}$ = 6B and the concentration of settleable solids is also not high, therefore APWA practice cannot be extended to irrigation and power canals. Further, as already argued above, chamber diameter d = 7.86 B, as suggested by Chrysostomou (1983), does not significantly lengthen the detention time as compared to the one with d = 5B which is based

on analytical considerations supported by experimental evidence.

It is therefore recommended that for the sediment particle size in the range 0.5mm < D_s < 1.0mm larger diameter out of d = 5B, and d = $1.4\sqrt{Q_{cc}}/\sqrt{V_s}$ be adopted, and for other particle sizes, d = 5B be adopted.

2.14.2 Flushing discharge

Almost all investigators agree that the flushing discharge of this device be limited to 5 to 10% of inlet channel discharge, i.e water abstraction ratio, Q_o/Q_{cc} = 5 to 10%. It is also evident from Figure 18. Alquier, et al (1982) conclude their studies as "..... it is not always of value to increase foul (ie flushing) outlet discharge. The optimum in about 5 to 10% of inlet discharge (ie Q_c)". In the prototype installation cited by by Cecen (1977), water abstraction is only 3%. It is, therefore, recommended that flushing discharge be limited from 5 to 10% of inlet channel discharge or Q_o/Q_c = 5 to 10%.

2.14.3 Height of diaphragm in inlet channel, h_1

In view of the distribution of sediment concentration and particle sizes, the height of diaphragm, to be provided in inlet channel is suggested as $h_1 = h/3$ where h is the full supply depth or depth of flow for design discharge in inlet channel.

2.14 4 Chamber depth at periphary, h_2

Paul (1983) proposed $h_2 = 0.4h_1$, however, subsequently Chrysostomou (1983) from his studies based on

measurement of detention time suggested $h_2 = 0.6h_1$, though dimension wise not significantly different but improves the detention time. It is, accordingly, recommended that $h_2 = 0.6h_1 = 0.2h$ be adopted.

2.14.5 Chamber bed slope, S_c

Although provision of bed slope radially towards the orifice increases the flushing discharge but it also helps in flushing the coarse material more easily. Moreover, the radial flow approaches the orifice at a constant angle = $\tan^{-1}[V_t/V_r \text{ max}]$, Rea (1984). Therefore, chamber slope, S_c, as 10 horizontal to 1 vertical be adopted.

2.14.6 Depth of flow in chamber or over the orifice, h_o

The different suggestions in this context are:

$h^*_o/d > 0.26$

where

h^*_o is the depth of flow at the chamber periphery.

Since $h_2 = 0.6h_1 = 0.6 \times \frac{h}{3} = 0.2h$,

therefore, $h^*_o = h + 0.2h = 1.2h$.

When the chamber has a bed slope of $S_c = 10$,

therefore, $h_o = h^*_o + \frac{1}{10}\left(\frac{d}{2} - r_o\right)$ and if $\frac{d}{2} >>> r_o$

then $h \simeq h^*_o + 0.05d$ or $h^*_o/d = \frac{ho}{d} - 0.05$.

As such, according to Chrysostomou (1983),

$h^*_o/d > 0.26$ or $h/d > 0.22$ or $h_o/d > 0.31$; and

H/d or $h_o/d > 0.17$, Salakhov (1975).

Since chamber flow depth suggested by Chrysostomou (1983) is based on detention time studies so it is recommended for adoption. However, a caution will not be out of place to be sounded here, that is APWA studies suggest that the flow inside the chamber must not be allowed to accelerate to the point where vortex flows take control of the particle movements; and Sanmungathan (1985, 1986) argues that air core must not form as it impairs the efficiency of the device, as such the depth, h_o, must be checked, with the following correlation, to ensure that air core does not form:

$$h_o/d_o = 12.77\ N_\tau^{0.664}\ F^{1.31}/R_e^{0.065} \qquad (58)$$

where in $N_\tau = \tau d_o/Q_o$, $F = 4Q_o/\pi d_o^2 \sqrt{g d_o}$; $R_e = Q_o/\nu d_o$.

Moreover, increase in h_o will also increase Q_o.

2.14.7 Chamber deflector

Necessity of provision of deflector in the chamber has been very clearly brought out by the studies reported by Paul (1983), Chrysostomou (1983) and Rea (1984). Since the deflector CD_2 gives the maximum detention time, and the swirls forming as a result of secondary flow are minimum, as reported by Chrysostomou (1983), therefore, it is suggested that deflector CD_2 be adopted.

2.14 8 Size of flushing pipe or orifice diameter, d_o

Having fixed the flushing discharge, Q_o, as in 2.14.2 above, and depth of flow in the chamber, h_o, as in 2.14.6 above, if discharge coefficient is known, diameter of the flushing pipe or orifice can be computed. It is recommended that C_d be computed from the following
correlation which has DR = 1.009 with SD = 0.058:

$$C_d = 0.22\ R_e^{0.075}\ N_\tau^{0.054}\ F^{0.965}/(h_o/d_o)^{0.375} \qquad (64)$$

2.14.9 Modelling Criteria

Undoubtedly the models of settling basins must have Froude similarity or Froudsian scale models be used for examining the proposed design(s) of CCSE. According to Cecen (1977), the settling velocity of the grains V_s, must be scaled in the same way as the flow velocity. The settling velocity of sediment particles has also been scaled in the same manner by Cecen & Bayazit (1975), Sullivan (1972), Curi et al (1975), Salakhov (1975), Ogihara and Sakaguchi (1984) and others. However, when questioned by Molof (1975), Curi et al (1975) replied that the settling velocity of particles could not be a criterion for determining model scales; and showed that even holding the Froude and Reynolds numbers related to particles, ie Shields parameters, the same in the model and prototype did not yield satisfactory results and, as such, further studies are necessary to determine the scale ratios.

Alquier et al (1982) have very convincingly shown that the terminal settling velocity of particles in quiet water is not the most significant parameter to describe the behaviour of a solid phase in suspension

and instead have suggested the adoption of critical velocity, U_c (defined as the mean velocity in a given rectangular channel at which the solid material deposited on bottom goes into suspension). But they have not specified as to how U_c is to be determined in the CCSE. To sum up it may be said the Froudian scale models be adopted and the settling velocity of particles scaled in the same way as the flow velocity.

Trapping efficiency has been expressed, by Cecen and Bayazit (1975), as a function, ie

$$P = \phi \ (V_s/U_*, \ V_s d/V_o h_o) \qquad (7)$$

which is an exact replica of the function used in the design of classical settling basins. For the function in Equation 7 to be evaluated or used in the design of CCSE, no methodology has been specified for the computation of shear velocity in the circulation chamber. It is, therefore, considered desirable to drop U_* and to use upward velocity of flow, W, in CCSE as suggested by Ogihara and Sakaguchi (1984).

2.14.10 Dark areas

In the design of CCSE some of the areas which are still dark could now be identified as under:

(i) Evaluation of tangential velocity obtainable at the periphery of CCSE, V_{tR}, in relation to mean inlet channel velocity, V_c, or the relation between V_{tR} and V_c.

(ii) Evaluation of maximum magnitude of tangential velocity obtainable at r = ro (ie at the edge of orifice or flushing pipe), V_{to} and its relation with V_{tR} or V_c.

(iii) Extent to which V_{tR} or V_{to} gets altered when deflector CD_2 is incorporated in the circulation chamber.

(iv) Prediction of trapping efficiency, P, of CCSE with decided configuration. The possible parameters which govern the trapping efficiency are.

$$P = f\ (D_s,\ d,\ d_o,\ h_o,\ h_2/h_1,\ Q_o,\ Q_{cc},\ V_{to},\ V_{tR}) \quad (93)$$

It has already been decided that $h_2/h_1 = 0.6$. The sediment size can best be represented by its fall velocity V_s. The parameters Q_{cc}, Q_o and d can be combined in the upward velocity of water spilling from the chamber into the downstream channel, $Q_s = (Q_{cc} - Q_o)$, W, as:

$$W = Q_s / \frac{\pi d^2}{4} = 4Qs/\pi d^2 = 4\ (Q_{cc} - Q_o)/\pi d^2 \quad (94)$$

Accordingly, Equation 93 can be rewritten as:

$$P = f_1\ (V_s/W \text{ or } Vs\ d^2/(Q_{cc} - Q_o)) \quad (95)$$

$$\text{or } P = f_2\ (V_s/V_{to},\ Q_o/Q_{cc}) \quad (96)$$

$$\text{or } P = f_3\ (V_s/V_{to},\ d/do) \quad (97)$$

In the Equations 96 and 97, the parameter V_{to} could be replaced by V_{tR} but V_{to} has been preferred because this can be easily computed (by using Equation 65 after Anwar (1967)) and is also related to V_{tR}.

(v) Discharge coefficient for the spillweir, $C_{d\ell}$, so that its length, C_ℓ can be fixed correctly. If the length of the spillweir, C_ℓ, is smaller than required, heading up of flow may occur in

CCSE which will increase h_o and consequently Q_o - quite unnecessarily. It is, accordingly, proposed to seek solutions to these dark areas with the aid of some additional experimental studies.

3 EXPERIMENTAL STUDIES

The five dark areas, in the design of CCSE, identified above have been examined on three different models to seek solutions. The design of these three models and the scope of studies are described below:

3.1 Model I

A micro hydel scheme with generation capacity of 200 KW has been in operation since 1938 in the eastwhile princely state of Chamba (now a part of Himachal State, India) and is most popular as Bhuri Songh Power House (BSPH) after the name of the then ruler of the state. In 1985 the generation capacity of BSPH was enhanced to 450 KW by adding one 250 KW unit after remodelling the existing works. BSPH utilizes 4.67 m^3/s discharge diverted (with the aid of a raised crested weir) from the river Sal into the 626m long right bank power canal. The power canal is unlined in its headreach and is lined in the tailreach; and has a bed slope of 1 in 95. Although there exists a small desilting tank and there was a proposal to remodel it by providing a hopper type desilting tank but due to constraints imposed by topography, this proposal did not mature. The design organization now proposes to provide a vortex type desilting tank or CCSE at a location upstream of the existing desilting tank so as to remove all sediments of size down up to 0.75mm. The power canal can carry a discharge more than 5.61m^3/s. The bed material in this power canal largely comprises gravel, boulders/rock outcrops and in the reach of the

desilting tank only the left bank is lined in masonry whilst the other bank is unlined. The D_{50} size of the bed material in the power canal is 46mm. The cross-section of the power canal is approximately rectangular with bed width, B as 3.4m. In consultation with the designers it was decided to adopt circulation chamber diameter, d = 17.0m because:

d = 5B = 5 x 3.4m = 17.0m (Paul (1983)), and

$$d = 1.414 \sqrt{Q_{cc}/V_s} = 1.414 \sqrt{5.61/0.114}\ m = 9.50m$$

(Salakhov (1975))

so larger of the two has been adopted in the first instance. Since no criterion was available to determine the size of flushing pipe to escape $0.94m^3/s$ discharge, pipe diameter as d_o = 0.60m or d/d_o = 28.333 was selected quite arbitrarily. The exit end of flushing pipe is to be 855.60m above MSL ____ the HFL in the river Sal. In order to suggest an economical and efficient design of CCSE to fit the available area and to remove all sediments up to 0.75mm size, it was decided to examine the problem on a physical model to a scale of 1:4. It was also decided to lead the total or entire power canal discharge into the chamber, thereby yielding $Q_c = Q_{cc}$. In view of the sediment sizes constituting the bed material in the power canal, the diaphragm has also been incorporated in the inlet channel. The bed of the power canal has been moulded as rigid bed. At the periphey of the circulation chamber where the flow re-enters the power canal downstream of CCSE, a bed bar 0.10m high has been provided to ensure that sediment particles do not enter the downstream power canal. Discharges of 2.0, 3.52 and $5.14m^3/s$ were selected to examine the performance of CCSE.

Total sediment load transport rates in the power canal were computed in accordance with the procedure specified by Ackers & White (1980), and are as under.

Discharge (m^3/s) Prototype/Model		Total load transport rate (kg of dry weight/hour) on model	Concentration (g/ℓ)
2.0	0.0625	103.4	0.460
3.52	0.110	252.5	0.638
5.14	0.1606	320.3	0.554

The mean diameter of the sediment particles injected in the power canal computed to 7.64mm (ie 27.5mm on prototype) with maximum size as 19.05mm (ie 75mm on prototype). The discharges of 0.0625, 0.110 and $0.1606 m^3/s$ were run for 32, 20 and 10 hours in the model respectively when almost stable conditions appeared to have been attained. After attainment of the stable conditions, these discharges were run for another period of 2 hours, 2 hours and 1 hour, and the materials collected in the trenches (constucted towards the exit end of flushing pipe and the downstream power canal) were removed, dried, weighed and analysed. A specimen of the results obtained is given below:

Discharge (m^3/s)	Weight of sediments coarser than 0.4mm (ie 0.75mm proto) (kg)		Mean size of sediment in model (mm)		Water abstraction ratio Q_o/Q_{cc} (%)	Depth h_o/d_o
	Flushed	Retained	Flushed	Retained		
0.0625	108	27	5.41	3.06	19.04	2.0
0.110	311	80	7.12	2.57	18.01	2.76
0.1606	270	38	7.37	2.29	17.76	3.10

Herein retained means material not flushed out but conveyed to the power channel on the downstream of CCSE. Typical gradation analysis curves of the sediment flushed and retained (in $0.1606 m^3/s$

discharge) are shown in Figures 59 and 60 respectively.

The coefficient of discharge, C_d, for the 0.15m diameter flushing pipe as computed from measurements and as predicted from Equation 64 compare as under (see also Fig 50):

Discharge (m^3/s) $Q_c = Q_{cc}$	Q_o	h_o/d_o	R	N_τ	F	Discharge coefficient		
						Measured	Predicted	Diff %
0.0625	0.0119	2.00	88148	7.759	0.56	0.2776	0.2522	9.2
0.110	0.0198	2.76	146748	5.475	0.92	0 3934	0.3727	5.3
0.1606	0.0285	3.10	211311	4.029	1.33	0.5345	0.5128	4.1

The inference is that the prediction ability of Equation 64 is acceptable.

3.1.1 Sediment trapping efficiency

From the gradation curves of the sediment flushed or removed and retained, weights of sediment in various size ranges were obtained. Sediment trapping efficiency has been computed as the ratio of the weight of the sediment removed, in a particular sediment size range, to the total of sediments removed plus retained in the same sediment range.

Tests were repeated on this model by:

(i) Changing the mean size of the sediment injected to 1.48mm as compared to the earlier used size of 7.64mm,

(ii) Changing the flushing pipe size to 0.80m (prototype) or 0.20m (model) but retaining the mean size of injected sediment as 7.64mm, and

(iii) Changing the flushing pipe diameter to 0.50m (prototype) and 0.40m (prototype) or 0.125m (model) and 0.10m (model), and sediment size as 7.64mm.

The results are shown recorded in Table 6.

3.1.2 Vortex stability

Cecen (1977) has reported that in his experimental set up for CCSE, the axis of the aircore made a small angle with the vertical and was slightly displaced in respect to the geometrical axis of the flushing pipe or orifice or circulation chamber. Salakhov (1975) has observed that when the inlet to the chamber is one-sided, the air core axis does not coincide with the axis of orifice/chamber but it tends to shift, the magnitude of the shift depends on the intensity of circulation in the chamber. Chrysostomou (1983) observed that vortex axis was offset at times by as much as 5cm (when R = 27.5cm) or by 0.18R. In BSPH model (Model I) with R = 212.5cm, d_o = 15cm, and Q_{cc} = 0.1606m^3/s, vortex axis shift has been observed as much as by 28cm or 0.13R. The designer objected to it, and in order to increase the trapping efficiency it was suggested to shift the orifice location by 28cm so that the axes of vortex and orifice coincide. However, when this modification was incorporated and test repeated, the trapping efficiency dropped from 87.7% to 7.8% and Q_o/Q_{cc} from 0.1776 to 0.081 in $Q_c = Q_{cc}$ =0.1606m^3/s discharge.

3.1.3 Tangential velocity distribution

Tangential velocities were measured in the region $r_o < r < R$ in discharges of 0.0625, 0.110 and 0.1606m^3/s with flushing pipe of 0.20m diameter in position. Results are presented in Para 3.2.2.

3.2 Model II

It is the pilot model, fabricated and operated at HRL, in which a diaphragm has been introduced in the inlet channel at a height of $h_1 = h/3$ where h is the design full supply depth of flow in the inlet channel as shown in Figure 1. Chamber depth at its periphery, h_2, has been adjusted to $h_2 = 0.6h$, as suggested by Chrysostomou (1983) from his detention time studies. In the present series of experiments either no deflector (CD_0) or deflector (CD_2) (of width B and covering half the circumference of the circulation chamber from the entrance of inlet channel) has been provided. The height of diaphragm from the bed of inlet channel is 5cm whereas the peripheral depth of the chamber is $h_2 = 0.6 \times 5cm = 3.0cm$. The chamber bed slope, S_c is 10.7. The height of the spill weir from chamber periphery is about 7.8cm and from the bed of outlet or downstream channel it is 5.0cm when CD_2 is not in position. The width, along the direction of flow, of the spill weir is 2.5cm whilst its length, C_ℓ, is 29.8cm. The sizes of flushing pipes and sediment used are give below:

Flushing pipe Diam (m)	Flushing pipe Length (m)	Mean size of sediment, $\overline{D}_s$ (mm)
0.050	3.68	0.175
0.038	3.87	0.175
0.032	3.81	0.175

The discharges escaping through the outlet channel and the flushing pipe have been measured with the aid of

V-notch weirs with angles of 90° and 45° respectively. The discharge through the flushing pipe has also been measured volumetrically. The tests conducted on this model were designed to ascertain

(i) Discharge coefficient for spill weir, and the orifice constituted by the diaphragm and bed of inlet channel designated as 'diaphragm orifice'

(ii) Evaluation of V_{to} and V_{tR} and their relation with V_c, and

(iii) Effect of chamber deflector, CD_2 and chamber diameter on trapping efficiency.

3.2.1 Discharge coefficient for spill weir

In the HRL version of CCSE since entire inlet channel discharge is not led into the chamber and only the flow through the bottom layers (h/3 depth) enters the chamber and the water level in the chamber is almost the same as in the inlet channel, so the inlet channel bed and the diaphragm above it constitute 'diaphragm orifice' which performs always under submerged exit conditions. The discharge entering the chamber, Q_{cc}, is partly flushed out through the flushing pipe, Q_o, and the remaining, ($Q_{cc} - Q_o = Q_s$) spills over the circular weir into the downstream or outlet channel. Since the flushing discharge, Q_o is a small fraction of the inlet channel discharge, Q_c, so the spill weir also functions under drowned conditions.

In order to be facilitate the evaluation of discharge coefficients for spill weir, $C_{d\ell}$, and diaphragm orifice, C_{do}, the part flow from inlet channel which escapes over the diaphragm into the outlet channel was stopped by plugging the inlet channel above the diaphragm plate. Thus, under this condition,

$Q_c = Q_{cc} = Q_s + Q_o$. Under various depths of flow in the inlet channel and the outlet channel, discharges Q_s and Q_o and depth of flow above the chamber periphery, h_0^* were measured. The various measurements ranged as: 60.75mm < h < 129.01mm, 89.62mm < h_0^* < 144.87mm; 18mm < depth in outlet channel < 118mm; 0.000 4076m^3/s < Q_s < 0.001901m^3/s; 0.0003810m^3/s < Q_o < 0.0003636m^3/s; and 0.0007886m^3/s < Q_{cc} or Q_c < 0.0022646m^3/s.

The discharge coefficient for spill weir, $C_{d\ell}$, has been computed from the equation:

$$C_{d\ell} = Q_s / C_\ell \, h_s^{1.5} \qquad (98)$$

where $h_s = h_o^*$ - 78mm or head on the crest of spillweir.

Drowning ratio of the spill weir has been computed to be equal to:

[(water level in outlet channel - crest level)/(water level upstream of weir - crest level)]

Figure 61(a) shows the variation of C_{dl} with drowning ratio whereas Figure 61(b) indicates the variation of C_{dl} withthe head onspill weir whilst Figure 61(c) is the definition sketch.

The discharge coefficient for the diagram orifice has been computed using the equation:

$$C_{do} = Q_{cc} / Bh_1 \sqrt{2g(h-h_1/2)} \qquad (99)$$

where B x h_1 is the area of the diagram orifice, and $h-h_1/2$ is the head acting at the centre or mid-height

of the diaphragm orifice. The variation of C_{do} with the ratio of head on diaphragm orifice to entrance height of diaphram orifice is shown in Fig 61 (d).

3.2.2 Relation of tangential velocity and mean channel velocity

A typical tangential velocity distribution obtainable in CSCE when inlet channel width, B = 11cm, chamber diameter = 5B = 55cm; h_1 = 5cm; $h_2 = 0.6h_1$ = 3.0cm, chamber floor slope, S_c is 10.7; chamber deflector CD_2 in position; depth of flow in inlet channel, h = 11.89cm; water depth in chamber, h_o = 17.17cm, $Q_c = 4314 cm^3/s$; $Q_o = 618 cm^3/s$ or Q_o/Q = 14.33% and inlet channel mean velocity V_c = 33.0cm/s, is shown in Figure 62.

It will be seen that in the region $(R-B) < r < 0.5\ d$ or R, tangential velocity equal to V_{tR} remains constant, that is:

$$V_t = 0.256\ V_{to} = V_{tR} \qquad (100)$$

whether the chamber deflector CD_2 is in position or not. Further towards the orifice, viz in the region $0.29\ R < r < (R-B)$, the tangential velocity distribution is not linear and at r = 0.29R is given by

$$V_t \text{ at } r = 0.29R = 0.467\ V_{to} \qquad (101)$$

However, in the region, $r_o < r < 0.29R$, tangential velocity distribution is linear and it attains the maximum value at the edge of the orifice or at $r = r_o$. At the edge of the orifice, the maximum value of the tangentia velocity, V_{to}, on extrapolation of the curve (a) in Figure 62 measures 1.07m/s. However, according to Anwar (1967), Equation 65:

$V_{to} = \sqrt{2gh_o}/3.45 = \sqrt{2x9.81x0.1717}/3.45 = 0.988$ m/s

That is the measured V_{to} is higher by about 8% and for all practical purposes could be considered equal to Anwar. The distribution of tangential velocity V_{to} according to Anwar (1969), ie V_t x r = constant in the region $r/r_o \geq 1$, is also shown as curve (b) in Figure 62 for comparison.

In Model I with d = 4.25m or R = 2.125m; r_o = 0.075m, B = 0.85m; and no deflector in the chamber, tangential velocities were measured at r = 1.625m when $Q_c = Q_{cc}$ was 0.0625 and 0.100m^3/s corresponding to water depth in the chamber, h_o as 0.30m and 0.414m. Since the vertical on which the tangential velocity has been measured, r = 1.625m, lies within the region of constant tangential velocity as such V_t in this region equals to 0.256 V_{to} (Equation 100). Tangential velocities at r = 1.625m as measured have been compared below with those computed from Equation 100.

Discharge (m^3/s)	Depth h_o(m)	V_{to} (m/s)	V_t (m/s) at r = 1.625m		
			Measured	Computed Eq 100	Diff (1%)
0.0625	0.30	1.306	0.325	0.334	+2.8
0.110	0.414	1.534	0.373	0.393	+5.4

As mentioned in Paragraph 3.1.3 above, tangential velocity distribution was also measured in Model I with flushing pipe of 0.20m in position and neither deflector nor diaphram in position and the values of V_{to} and V_{tR} obtained are tabulated below along with those computed:

Discharge (m^3/s) $Q_c = Q_{cc}$	V_{to} (m/s)		V_{tR} (m/s)	
	measured	computed Eq 65 Anwar (1967)	measured	computed, Eq 100
0.0625	1.284	1.284	0.344	0.329
0.110	1.465	1.516	0.371	0.388
0.1606	1.562	1.609	0.410	0.412

It will be seen that the measured values of V_{to} are at variance by 0, 3.4 and 2.9%, and of V_{tR} by 4.6, 4.4 and 0.5% from the computed values. These comparisons are quite encouraging and provide confidence in the tangential velocity distribution approach outlined above and in Equations 65 and 100. The inferences are:

(i) That the maximum tangential velocity obtainable in CCSE, V_{to}, can be computed from Equation 65, Anwar (1967). And once V_{to} is computed, V_{tR} can be estimated from Equation 100, and

(ii) That the provision of a deflector in the chamber does not alter the magnitude of maximum tangential velocity, V_{to}, as it depends only on the head acting on the orifice.

In order to ascertain as to how the tangential velocity at the chamber periphery, V_{tR}, when deflector CD_2 is incorporated in the chamber in comparison to the situation when no deflector has been provided, a few tests were run in Model II. The results are shown plotted in Figure 63. It will be seen that

$$V_{tR} = 0.90\ V_c, \text{ no deflector} \qquad (102)$$

$$V_{tR} = 0.85\ V_c, \text{ with deflector } CD_2 \qquad (103)$$

The inference is that the provision of deflector CD_2 in the circulation chamber reduces the magnitude of peripheral tangential velocity, V_{tR}, as compared to the situation when there is no deflector in the chamber, however, the reduction is quite marginal about 5%. Further with the tangential velocity distribution as shown in Figure 62, since $V_c = 0.33$m/s so Equation 103 yields $V_{tR} = 0.33 \times 0.85 = 0.281$ m/s against 0.253 m/s yielded by the Equation 100, ie within about 10%.

Velocity measurements in Model I (with $d_o = 0.20$m, and h_2 as zero), indicated the following mean values in the inlet channel and chamber periphery:

Discharge (m^3/s)	V_{tR} (m/s)	V_c (m/s)	V_{tR}/V_c
0.0625	0.344	0.570	0.604
0.110	0.371	0.604	0.614
0.1606	0.410	0.668	0.614

Thus when the circulation chamber has no depth at its periphery, ie $h_2 = 0$, and contains no deflector,

$$V_{tR} = 0.61\ V_c \qquad (104)$$

3.3 Model III

Model III is essentially HRL version of CCSE with inlet channel bed width, B = 1.0m; d = 5B; $h_1 = h/3 = 0.20$m; and $h_2 = 0.4\ h_1$. With flushing pipe of 0.1524m diameter and deflector CD_2 in the chamber, the following tests have been conducted on this model to ascertain:

(i) Discharge coefficient for the spill weir, C_{d1}, and

(ii) Discharge coefficient for diaphragm orifice,

C_{do}.

The experimental data and the values of C_{dl} and C_{do} have been incorporated in Table 7.

4 DISCUSSION OF RESULTS

It will be recalled that in Paragraph 2.14.10 above, five dark areas in the design of CCSE were identified for seeking answers from tests on the Models I, II and III. The results of these tests indicate as under.

4.1 Tangential velocity distribution

When the flow entering circulation chamber tangentially is uniformly distributed all along its periphery or the inlet is not one-sided, it has been shown experimentally (eg Ref Anwar (1969)) that in the region $r > r_o$ of the Rankine combined vortex, tangential velocity, V_t is given by:

$$V_t = \tau/2\pi r \text{ or } V_t \times r = \text{constant} \qquad (105)$$

However, when the inlet is one-sided, a forced vortex forms near the periphery, Cecen and Bayazit (1975), so that:

$$V_t = \omega r \qquad (106)$$

and a free vortex, with tangential velocity distribution as in Equation 105, occurs near the chamber centre. Ogihara and Sakaguchi (1984) have, in their theoretical analysis of flow in circulation chamber, also assumed that the velocity distribution of horizontal rotating flow is given by Equation 106.

According to Anwar (1967), the maximum tangential

velocity, V_{to}, in the free vortex region occurs at the edge of flushing pipe orifice, ie at r = ro (Equation 4) and is given by:

$$V_{to} = (2gh_o/3.45)^{0.5} \qquad (65)$$

However, contrary to the above, numerous experiments on different versions of CCSE as conducted earlier (Paul (1983)) and also reported above have shown that in the case of CCSE with one-sided tangential inlet, the tangential velocity distribution is of the type as shown in Figure 62. It will be seen that:

$$V_t = 0.256\ V_{to} \text{ in the region } (R-B) < r < R \qquad (100)$$

That is from the chamber periphery to a distance equal to the width of the inlet channel toward the camber centre tangential velocity remains constant. Its maximum value occurs at r = ro the magnitude of which can be computed from Anwar's (1967) correlation, Equation 65. Since V_{to} depends on the flow depth, h_o, on the orifice so it is independent of flushing pipe diameter, d_o, and provision or otherwise of any deflector in the chamber.

In the region $0.29R < r < (R-B)$, tangential velocity distribution is not linear but is given by:

$$V_t = 0.467\ V_{to} \quad \text{at } r = 0.29R \qquad (101)$$

However, in the region $r_o < r < 0.29R$, tangential velocity increases rapidly but linearly to attain maximum value of V_{to} at r = ro.

The validity of Equation 100 has been substantiated by measurements as already reported above. It has also been shown that the mean velocity in inlet channel,

V_c, and tangential velocity at chamber periphery, V_{tR} are related as under:

$$V_{tR} = 0.90\ V_c, \text{ no deflector but } h_2 = 0.6h, \quad (102)$$

$$V_{tR} = 0.85\ V_c, \text{ deflector } CD_2 \text{ and } h_2 = 0.6h, \quad (103)$$

and $$V_{tR} = 0.61\ V_c, \text{ no deflector and } h_2 = 0 \quad (104)$$

The relations in Equations 102, 103 and 104 can be compared with those obtained by Ogiharaa and Sakaguchi (1984) using two different tanks and three different inlet channel areas. It can be seen from Figure 43 that the ratio of tangential velocity at chamber periphery to V_c is 0.60, 1.05 and 0.83 or on the average.

$$V_{tR} = 0.82\ V_c \quad (107)$$

quite comparable to Equations 102 and 103.

Thus in the case of CCSE, once V_{to} is computed using Equation 65, V_{tR} can be obtained from Equation 100. The provision or non-provision of a deflector in the chamber dose not alter the magnitude of V_{to} as it depends only on h_o. Equations 102, 103 and 104 indicate that tangential velocity at chamber periphery, V_{tR}, is always less than V_c and rightly so because of energy losses occurring at entracne to and exist from circulation chamber, at its floor and side walls, internal fluid friction, sustaining vortex flow, orifice flushing pipe, etc.

4.2 Discharge coefficients

Discharge coefficients of interest are for: 1) Flushing pipe orifice, C_d, ii) Spill weir, $C_{d\perp}$, and iii) Diaphragm orifice when diaphragm is introduced in the inlet channel.

4.2.1

Discharge coefficient, C_d, is of paramount importance as it helps fixing size or diameter of flushing pipe when flushing discharge, Q_o has been decided for adoption. It has been shown that of the various correlations reported in literature none is more reliable than:

$$C_d = 0.22\ R_e^{0.075}\ N_\tau^{0.054}\ F^{0.965}/(ho/d_o)^{0.375} \qquad (64)$$

as suggested by Paul and Dhillon (x). This yields DR of 1.009 with SD of 0.058 when examined with reference to Anwar and Amphlett data in Table 4. The values of C_d predicted by Equation 64 have been compared in Figure 50 with those computed from actual measurements using Curi et at (1975), HRL (Paul (1983)) and fresh data incorporated in Tables 3 and 5 It will be seen that for the entire data DR is 0.97 with SD of 0.15. Further, from the present data (Table 6) values of C_d as measured have also been compared with the predicted values from Equation 64 in Table 8. It will be seen that the predicted values of C_d are within 5% of measured values with the exception of 3 to 4 situations. The overall indication is that C_d as predicted by the use of Equation 64 can be used with confidence for designing CCSE.

4.2.2

Discharge coefficient, C_{dl}, provides a check whether the length C_l of spill weir has been fixed adequately or not. The requirement is that the length C_l be so fixed as to pass $Q_s = Q_{cc}$ or $Q_c - Q_o$ discharge without any increase in water depth in the chamber beyond h_o. Any increase in h_o will cause unnecessary increase in flushing discharge, Q_o. The values of C_{dl} be adopted from Figure 6 and Table 7.

4.2.3

Discharge coefficient, C_{do}, for the orifice constituted by the diaphragm in the inlet channel and inlet channel bed always performs under submerged or drowned exit conditions. Although it is generally assumed that the diaphragm will divide the inlet channel discharge, Q_c, in the ratio of the depths of flow yet it is always expedient to check such an assumption by using C_{do} values from Figure 61 and Table 7.

4.3 Conditions critical to Air Core Formation

Cecen (1977), Salakhov (1975) and others favour the formation of air core in CCSE as it reduces water abstraction. However, Sanmuganathan (1985, 1986) has most vehemently apposed this design norm because this implies a unique dependence of discharge on flow area and also impairs the trapping efficiency of CCSE. Whatever school of thought ultimately prevails in the design of CCSE, the designer needs to be equipped with some norms by the application of which he is in a position to ascertain whether with the values of h_o, Q_o, and d_o to be adopted air core will form or not.

Literature is abound with models which provide means to determine relative submergence of flushing pipe orifice critical to air core formation. Reliability of most of these models as applicable to vertical gravity intakes has been examined by Paul and Dhillon (1987, x) and Paul and Sayal (1988). Paul and Dhillon (x) have shown that of all the models, the one below in Equation 58 is the most reliable and it yields DR of 1.048 with SD of 0.294:

$$h_o/d_o = 12.77\ N_\tau^{0.664}\ F^{1.31}/R_e^{0.065} \qquad (58)$$

In the present studies use was made of three models of CCSE operating under varying h_o/d_o values. A comparison of critical relative submergence and relative submergence adopted has been made in Table 8. A perusal of the data will reveal that none of the models in any run has been operated to discourage air core formation or stated in another way air core always formed. Sunmuganathan (1985, 1986) has argued that air core should not form and if for this eventuality water abstraction is more the same could be controlled by introducing a valve in the flushing pipeline downstream of its orifice. In this context it will not be out of place to remark that use of a valve in the pipeline may encourage sediment deposition in the pipeline upstream of the valve and a constant vigil will have to be kept on the water level in the inlet channel to ensure matching operation of the control valve. This complicates the performance of CCSE as seen through the eyes of under developed or third-world countries particularly when such structures are to be located at remote locations.

4.4 Chamber Diameter

Studies at HRL (Paul (1983)) both on analytical considerations and physical model and additional tests reported by Paul and Dhillon (1985) indicated that chamber diameter should be five times the width of inlet channel, ie d = 5B. However, subsequent studies by Chrysostomou (1983) based on evaluation of detention time indicated that d = 7.857B From a comparison of detention times with d = 5B and d = 7.857B it was argued that the gain in detention time is not so substantial as to justify about 57% increase in chamber diameter. In an effort to further substantiate this argument, tests were undertaken using 0.175mm mean diameter sand on Model II for the following situations:

(i) d = 5B; no deflector in chamber,
(ii) d = 5B; deflector CD_2, and
(iii) d = 7.857B, deflector CD_2

The trapping efficiency is shown plotted versus water abstraction ratio (Q_o/Q_c) in Figure 65. It will be seen that chamber with diameter d = 5B yields higher efficiency though marginally.

4.5 Trapping efficiency

Data pertinent to trapping efficiency evaluations along with the observed/measured trapping efficiencies are incorporated in Table 6. It will be seen that for removing or flushing all sediment sizes coarser than 0.40mm (model size) from injected sediment of mean size 7.64mm (model size). Flushing pipes of diameter d_o as 0 20m and 0.15m have performed quite satisfactorily. However, when d_o was reduced to 0.125m in Test Run 10_I, 11_I and 12_I; and then to 0.100m in Test Runs 13_I, 14_I and 15_I, the trapping

efficiency, P, never increased beyond 15% even when water abstraction was 17.20%. In the analysis for trapping efficiency predictor data pertaining to Test Runs 7_I and 10_I to 15_I have not been used. As already outlined in Paragraph 2.14.10 (iv), the following correlations were sought:

$$P = f_1 \ (V_s/W \text{ or } V_s d^2/(Q_c - Q_o)) \tag{94}$$

$$P = f_2 \ (V_s/V_{to}, \ Q_o/Q_c) \tag{95}$$

$$P = f_3 \ (V_s/V_{to}, \ d/d_o) \tag{96}$$

Measured trapping efficiency versus V_s/W is shown plotted in Figure 65. The best fit correlation is

$$P = 65.96 \ (V_s/W)^{0.069}, \ DR = 1.09, \ SD = 0.40 \tag{108}$$

Although the upward velocity of flow in CCSE, W, contains all the important parameters such as chamber diameter, chamber discharge and flushing discharge yet when Q_o/Q_c is considered as a separate parameter, and P is examined in relation to settling velocity of particles and the maximum tangential velocity, V_{to}, in CCSE, the following correlation is obtained:

$$P = 160.14 \ (V_s/V_{to})^{0.045} \ (Q_o/Q_c)^{0.322} \tag{109}$$

The values predicted from use of Equation 109 have been compared with the measured trapping efficiencies in Figure 66. It will be seen that correlation Equation 109 yields DR = 1.06 with SD = 0.46. In an effort to examine whether flushing pipe diameters, d_o is related to chamber diameter, d, analysis of the experimental data indicated the following correlation:

$$P = 321.7\ (V_s/V_{to})^{0.056}\ (d/d_o)^{-0.373} \qquad (110)$$

Predicted trapping efficiencies have been compared with the corresponding measured values in Figure 67. The comparison indicates DR = 1.08 with SD = 0.35. Through out the search for an appropriate correlation for trapping efficiency much concern was caused by the sudden drop in P when flushing pipe size was reduced to 0.125m and 0.100m. This adverse feature could probably be attributed to the following causes:

(i) Blockage of flushing pipe by sediment caused drop in trapping efficiency and consequently sediment deposition in circulation chamber and in the power canal both on the upstream and downstream of CCSE, or

(ii) Coarse particles started rotating in circular paths around the orifice thereby causing reduction in trapping efficiency (as these do not move in radial direction towards the orifice) and sediment deposition in the entire system.

Although the cause at (i) above does not seem to be probable because during operations for periods over four hours neither the water abstraction dropped nor the predicted and measured C_d values for the orifice were significant apart yet a correlation was sought between pipe size d_o and sediment size D_s and it turned out to be:

$$P = 184.5\ (Q_o/Q_c)^{0.348}\ \ (d_o/D_s)^{-0.0426} \qquad (111)$$

The predicted and measured values of trapping efficiency have been compared in Figure 68. It will be seen that this correlation yields DR = 1.06 with

SD = 0.34, and incidentally turns out to be the best. However, even this correlation fails to account for the performance of 0.125m and 0.100m diameter flushing pipes.

In order to avoid such pitfalls in the design of CCSE, limits for pipe size and water abstraction in relation to particle size were sought as shown in Figures 69 and 70. It will be seen that these limits are:

Limits

Particle size, D_s (mm)	Q_o/Q_c (%)
>1.0	>15
0.5-1.0	10-15
<0.5	<10

and $20 < d/d_o < 30$.

In the context of the cause (ii) for the poor performance of flushing pipes of 0.125m and 0.100m diameter due to circular motion of coarse particles, altention is invited to Cecen (1977) who has shown that for coarse gravel particles not to be flushed but to rotate in a circular path

$$(V_{ts}/V_{tf})^2 = C_1 (\rho_f/\rho_s) \qquad (15)$$

wherein V_{ts} is the tangential velocity of solid particles, V_{tf} is the tangential velocity of the fluid, C, is a coefficient depending on shape of sediment particle and ρ_f and ρ_s are the mass densities of fluid and sediment. Thus coarse gravel particles with specific gravity of 2.65 and shape coefficient (say) 0.6 will not be flushed when $V_{ts} = 0.476\ V_{tf}$. Since V_{ts} is much smaller than V_{tf} so limit is reached

for these not to be flushed. Alternatively, Julien (1986) has shown (Eq 76) that the limit velocity of sediment particles in the radial direction is proportional to $(V_t)^2$, D_s and ℓ_s/ℓ_f and decreases as viscosity of the fluid and distance, r from the orifice increase. Need is, therefore, felt to determine the radial and tangential velocities of sediment particles in relation to tangential velocity of the fluid for the limit of rotation in circular paths so that optimum size of sediment which will not be flushed can be ascertained.

4.6 Vortex stability

Salakhov (1975) has observed that when the inlet to chamber is one-sided, air core axis does not coincide with the axis of flushing pipe orifice or axis of chamber but it tends to shift and shift is related to the intensity of circulation in the chamber. This aspect has also been corraborated by Cecen (1977). Chrysustomou (1983) indicated that the shift in the axis was 0.18R. In the case of Model I, for $Q_c = 0.1606 m^3/s$ and $d_o = 0.150m$, the shift has been observed of the order of 0.13R. At the instance of design engineers when orifice was shifted by 0.28m so that the axes of orifice and vortex coincided the trapping efficiency dropped from 88 to 8% and Q_o/Q_c from 17.76 to 8.1%! The inference is that in situations where inlet to the chamber is one sided, vortex stability be overlooked as asymmetry in the axis of the chamber and orifice can lead to costly mistakes as the performance gets drastically impaired.

4.7 Estimation of circulation

Since the circulation parameter appears in the suggested correlations for C_d (Equation 64) and relative submergence of orifice critical to air core

formation, h_o/d_o (Equation 58) so its evaluation becomes essential. In Paragraph 2.13 above a question was posed at to whether τ be obtained or estimated using Equation 92 or Equation 68. It may be mentioned that Equation 92 is based on statistical best fit to the Anwar and Amphelett data for vertical gravity intakes and pertaining to critical conditions (Table 4). It is suggested that use be made of Equation 68 which is based on maximum tangential velocity, V_{to} evaluation from Anwar's (1967) correlation Equation 65. The reason for this suggestion is that Equation 92 is based on the consideration of tangential velocity distribution given by Equation 105, ie this distribution of tangential velocity does not obtain in CCSE (see Fig 62).

4.8 Modelling criterion

Cecen and Bayazit (1975) suggested the use of shear velocity parameter but did not provide a method for its computation. Alquier et al (1982) convincingly showed that critical velocity, V_c is a better parameter than fall velocity, V_s but they also failed to provide basis for its computation. It is, therefore, suggested that Froudian scale models be adopted and the settling velocity of sediment particles scaled in the same way as the fluid velocity.

5 CONCLUSIONS

In an effort to provide guidelines for an economical and efficient design of CCSE, important elements or parameters involved in design were outlined (in Para 1.2 above). Subsequently a review of available literature was carried out and dark areas identified (see Para 2.14.10). Answers to these undecided issues

have been sought from experiments conducted on three physical models. Inferences are summarized below.

5.1 Chamber Diameter, d

Compute d from the relations
d = 5B, Curi et al (1975), Paul (1983)
$d = 1.4\ (Q_{cc}/V_s)^{0.5}$ for $0.5mm < D_s < 1.0mm$, Salakhov (1975) and adopt the larger of the two.

5.2 Height of diaphragm

In the inlet channel provide a diaphragm plate at a height $h_1 = h/3$ where h is the design full supply depth of flow in inlet channel. Ensure that inlet to the chamber is tangential.

5.3

To compute discharge entering the circulation chamber, Q_{cc}, use C_{do} values as given in Table 7 and Figure 61.

5.4 Chamber depth at Periphery

The depth of chamber at its periphery, h_2 be set as $h_2 = 0.6\ h_1 = 0.2h$.

5.5 Chamber floor

Provide chamber floor with radial slope, $S_c > 0.02$. This may be adjusted in view of the sediment size to be flushed and water abstraction.

5.6

Decide flushing discharge, Q_o to be used. This may be done in view of the limits set forth in Paragraph 4.5, viz:

Particle size, D_s (mm)	Q_o/Q_c (%)
>1.0	>15
0.5-1.0	10-15
<0.5	<10

5.7 Flushing pipe diameter

Having decided the flushing discharge, and chamber floor slope (which determines the depth h_o over the orifice because water level in the inlet channel and circulation chamber are not significantly different) compute pipe size d_o by trial method using C_d value from Equation 65. Ensure that d_o to be adopted is such that d/d_o lies between 20 to 30. Flushing pipe size can be altered by varying the chamber floor slope, S_c.

5.8 Spill weir

A knowledge of Q_{cc} and Q_o determines the discharge Q_s ($= Q_{cc} - Q_o$) to be spilled. Assume water level in chamber the same as in inlet channel, fix height of spill weir and its length C_l so that no heading up is caused or water level in the chamber remains unaltered. To facilitate these computations, values of C_{dl} have been given in Table 7 and Figure 61.

5.9 Chamber deflector

Adopt chamber deflector CD_2. That is it should be of width B and extend from point of entry into chamber to cover half the circumference towards the spill weir.

5.10

When sediment to be flushed is coarser, the adoption of diaphragm and deflector may be dispensed with.

5.11 Air core formation

Relative critical submergence, h_o/d_o can be computed from Equation 58 and used with confidence to estimate whether the design projected will perform with or without air core formation.

5.12 Trapping efficiency

Trapping efficiency of the designed CCSE is best obtained from Equations 111 and 109, viz:

$P = 184.5\ (Q_o/Q_c)^{0.348}\ (d_o/D_s)^{-0.0426}$, DR = 1.06, SD = 0.34, and

$P = 160.14\ (V_s/V_{to})\ (Q_o/Q_c)$, DR = 1.06, SD = 0.46.

It is expected that CSSE designed with chamber deflector will perform better as the above correlations are based on data without deflector.

5.13 Hydraulic modelling

Wherever possible the performance of the projected design be examined with the aid of a physical model. This has become essential because no prototype data are so far available to provide much needed confidence. Use be made of Froudian models and settling velocity of sediment particles scaled in the same manner as fluid velocity is scaled.

5.14 Pitfalls

It must be borne in mind that so long as entry of flow into the chamber is one-sided, the axes of the vortex and flushing pipe orifice will not coincide, and must

be lived with. Any asymmetry in the axes of the chamber and orifice will impair the performance of CCSE.

5.15 Future research needs

(i) Further research needs to be directed to the evaluation of limit radial velocity of sediment particles of coarse grade when these will stop moving towards the orifice to be flushed but instead will continuously revolve in circular paths around the orifice in the circulation chamber.

(ii) Since in the CCSE tangential velocity does not follow the $V_t$xr constant distribution in the region $r>r_o$ as such the radial flow will not approach the orifice at a constant angle - contrary to Rea's (1984) finding. This issue requires further probe.

(iii) An other requirement is that performance of prototype CCSE's be documented.

6 ACKNOWLEDGEMENTS

The work presented in this report was conducted in the Overseas Development Unit of Hydraulics Research, Wallingford (England) headed by Dr K Sanmuganathan and also under his guidance. The writer is indeed indebted to Dr Sanmuganathan for the many indepth discussions held with him and the time he managed to spare despite heavy responsibilities of his office.

Writer's grateful thanks are due to Mr Philip Lawrence but for whose assistance in model assembly, its operation and generous comments this work would not have been possible. The writer thankfully acknowledges the help rendered by Mr David Richards,

Mr Ian Meadowcroft and Mr Ian Fish in the collection of model data, statistical analysis and compilation of the report.

The writer is grateful to Mr Ranjodh Singh, Director (Design), P & D(C) Unit II, HP State Electricity Board, Sundernagar (India) for having generously funded the tests (Model I).

The writer's thanks are due to Dr G S Dhillon, FIE, Chief Engineer (Research)-cum-Director, IPRI for his keen interest in this study and arranging Research Attachment for the second time.

Work reported essentially constitutes a part of the Research Theme 'Sediment Control' under the Collaborative Research Programme between HR and IPRI approved by Governments of United Kingdom and India. The writer's thanks are due to both the Governments.

7 REFERENCES

1. Ackers P & White W R, 1980. Bed material transport: a theory for total load and its verification. Proc International Symposium on River Sedimentation, 24-29 March, Beijing, China, Vol 1, pp 249-268.

2. Akmandor N, 1972. Private communication to Curi et al, 1975.

3. Alquier M, Delmas D & Pellerej M J, 1982. Improvement of swirl concentrator. Journal of the Environmental Engineering Division, ASCE, Vol 108, No 2, April, pp 379-390.

4. Anwar H' O, 1967. Vortices at low head intakes. Water Power and Dam Construction, Vol 19, No 11, pp 445-457.

5. Anwar H' O, 1969. Turbulent flow in a vortex. Journal of Hydraulic Research, Vol 7, No 1, pp 1-29.

6. Cecen K, 1977. Hydraulic criteria of settling basins for water treatment, hydro-power and irrigation. Proc 17th Congress IAHR, Vol 4, pp 275-294.

7. Cecen K, 1985. Private communication.

8. Cecen K & Akmandor N, 1973. Circular settling basins with horizontal floor. MAG Report No 183, TBTAK, Ankara (in Turkish).

9. Cecen K & Bayazit M, 1975. Some laboratory studies on sediment controlling structures. Proc 19th Congress ICID, Question 30, Report 8.

10. Cecen K & Bayazit M, 1977. Vortex-type settling basins for hydro-power intakes. Istanbul Technical University, Turkey, an unpublished work (March 1971).

11. Cecen K, Bayazit M & Sumer M, 1969. Distribution of suspended matter and similarity criterion in settling basins. Proc 13th Congress IAHR, Vol 4, pp 215-225.

12. Chang E, 1976. Review of literature on drain vortices in cylindrical tanks. BHRA Report No TN 1342, Cranfield, England.

13. Chrysostomou V, 1983. Vortex-type settling basin. Dissertation for MSc (Irrigation Engineering) degree, University of Southampton, Department of Civil Engineering, Southampton, England.

14. Curi K V, Esen I I & Velioglu S G, 1975. Vortex type solid-liquid separator. Progress in Water Technology, Vol 7, No 2, pp 183-190, Pergamon Press, Printed in UK.

15. Hecker G E, 1981. Model-prototype comparison of free-surface vortices. Journal of the Hydraulics Division, ASCE, Vol 110, No 10, pp 1243-1259.

16. Julien P Y, 1986. Concentration of very fine silts in a steady vortex. Journal of Hydraulic Research, Vol 24, No 4, pp 255-264.

17. Knauss J, 1972. Vortices and swirling flow at low head intakes in pumped storage schemes. Proc Symposium on Hydro-electric Pumped Storage Schemes, 6-8 November, Athens, Greece.

18. Knauss J (Co-ordinator), 1983. Swirling flow problems at intakes. IAHR, Hydraulic Structures Design Manual, Monograph No 6, First Draft.

19. Levi Enzo, 1983. A fluidic vortex device for water treatment processes. Journal of Hydraulic Research, Vol 21, No 1, pp 17-31.

20. Lewis N S, 1981. The use of an inverted small diameter hydrocyclone to classify particles of sand and gravel. Group Ordinary, Department of Geology, University of Bristol, Bristol, England.

21. Molof, 1975. Discussion on Curi et al (1975). Vortex type solid-liquid separator. Progress in Water Technology, Vol 7, No 2, pp 183-190, Pergamon Press, Printed in UK.

22. Novak P & Nalluri C, 1975. Sediment transport in smooth fixed bed channels. Journal of the Hydraulics Division, ASCE, Vol 101, No 9, pp 1139-1154.

23. Odgaard A J, 1986. Free-surface air core vortex. Journal of Hydraulic Engineering, ASCE, Vol 112, No 7, pp 610-620.

24. Ogihara K & Sakaguchi S, 1984. New systems to separate the sediments from the water flow by using the rotating flow. Proc 4th Congress Asian and Pacific Division, IAHR, Chiangmai, Thailand, 11-13 September, Vol 1, pp 753-766.

25. Paul T C, 1983. Circulation chamber sediment extractor. Report No OD 58, Hydraulics Research, Wallingford, England.

26. Paul T C & Dhillon G S, 1985. Vortex type sediment extractor. Proc 2nd international Workshop on Alluvial River Problems, University of Roorkee, Roorkee, India, 24-26 October, pp 131-141.

27. Paul T C & Dhillon G S, 1987. Reliability of analytical models for intake vortices. Paper accepted for discussion in Technical Session B, 22nd Congress of IAHR, Lausanne, Switzerland.

28. Paul T C & Dhillon G S, X. Analytical models for free-surface air-core vortex. In press with Indian Journal of Power and River Valley Development.

29. Paul T C & Sayal S K, 1988. Some aspects relating circulation chamber sediment extractor design. Proc Indo-British Workshop on Sediment Measurement and Control, Changigarh, India, 22-24 February, Hydraulics Research, Wallingford, England.

30. Rea Quentin, 1984. Secondary currents within the circulation chamber sediment extractor. Dissertation for MSc (Irrigation Engineering) degree, University of Southampton, Department of Civil Engineering, Southampton, England.

31. Rott N, 1958. on the viscous core of a line vortex. Zeits - Ange - Math Physics, Vol 96, pp 543-553.

32. Rouse H, 1950. Engineering Hydraulics. John Wiley & Sons Inc, New York, USA.

33. Salakhov F S, 1975. Rational designs and methods of hydraulic calculation of load - controlling water intake structures for mountain rivers. Proc 9th Congress, ICID, Question 30, Report No 11.

34. Sanmuganathan K, 1985. A note on the outlet pipe design for circulation chamber silt extractors. Report No OD/TN 13, Hydraulics Research, Wallingford, England.

35. Sanmuganathan K, 1986. Air entry in vertical gravity intakes. Proc 5th Congress of Asian and Pacific Regional Division of International Association for Hydraulic Research, Seoul, Republic of Korea, 18-20 August, pp 245-264.

36. Schlichting H, 1962. Bouncary layer theory. McGraw-Hill Book Company Inc, London, England, pp 176-180.

37. Smisson B S, 1967. Design, construction and performance of vortex overflows. Proc Symposium on Storm Sewage Overflows, Institution of Civil Engineers, London, England, 4 May, p99.

38. Sullivan R H, 1972. The swirl concentrator as a combined sewer overflow regulator facility. US Environmental Agency Report No EPA-R2-72-008, Environmental Protection Technological Services, PB 214 687, Office of Research and Monitoring, USEPA, Washington DC 20460, USA.

39. Sullivan R H, Cohn M M & Parkinson F, 1974. The swirl concentrator as a grit separation device. US Environmental Agency Report No EPA-670/2-74-026, National Environmental Research Centre, Office of Research and Development, US EPA, Cincinnati, Ohio 45268, USA.

40. Sumer M, 1970. Model similarity concerning the transport of suspended matter in a turbulent flow field. Journal of Hydraulic Research, Vol 8, No 3, pp 357-364.

41. Vallentine H R, 1950. Applied Hydrodynamics. Butterworth, London, England.

42. Vokes F C & Jenkins S H, 1943. Experiments with a circular sedimentation tank. Journal Institution of Civil Engineers, London, England, Vol 19, January 1943, p 193.

43. Walton B & Key T D, 1939. Application of experimental methods to the design of clarifiers for waterworks. Journal Insitution of Civil Engineers, London Vol 13, November 1939, pp 21-48.

TABLES.

TABLE 1: Design Examples (from mathematical model data, Sullivan (1972))

EXAMPLE No 1

Design Q = 165cfs (4.672 cumec)
Remove 90% of settleable solids greater than 1.0mm
(0.0394 inches) with specific gravity of 1.2 (to conform with storm discharge vs chamber diameter design
Curve ie $d = 3(Q/0.322)^{0.4}$ where Q is in cfs)
From Figure 9 (Particle Settling Rates)
Enter with particle diameter of 0.039 inches with specific gravity of 1.2
Then $V_s = 0.145$f/s (4.42cm/s)
Then $\Psi = Q/V_s^5 = 2.57 \times 10^6$
From Figure 10, Scale Factor Diagram
Enter with $\Psi = 2.57 \times 10^6$ and
$P = 90\%$
Then $\Theta = 0.16$ and $\phi = 0.036$
$S = (Q/\Theta)^{0.4} = (165/0.16^{0.4} = 16.0$
$S = (V_s/\phi)^2 = (0.145/0.036)^2 = 16.2$
Use S = 16, then d = 16 x 3 = 48f (14.63m)
This compares with 36f (10.973m) as determined from storm discharge V_s chamber diameter curve.

EXAMPLE No 2

For 2.0mm (0.078 inches) size of solids, and Q = 165cfs (4.672 cumec)
Remove 90% of solids greater than 2.0mm with specific gravity of 1.2
From Figure 9, $V_s = 0.28$f/s (8.53cm/s)
Then $\Psi = (Q/V_s)^5 = 9.59 \times 10^4$
From Figure 10, $\Theta = 0.28$, $\phi = 0.078$
$S = (Q/\Theta)^{0.4} = 12.8$, and $S = (V_s/\Theta)^2 = 12.9$
Say S = 13
Then d = 13 x 3 = 39f = 11.887m

TABLE 2: Test materials used and their physical properties

Material	D_{50} (mm)	Specific gravity	Settling velocity V_s (cm/s)	Source
Green lentil	3.40	1.33	17.69	Curi et al (1975)
White polystyrene	2.12	1.05	4.29	Curi et al (1975)
Volcanic tuff	1.75	1.21	8.21	Curi et al (1975)
Red lentil	1.50	1.42	10.53	Curi et al (1975)
Thin Wood Shavings	0.80	0.45	-	Curi et al (1975)
Sand 1_I	0.238	2.65	3.17	IPRI (Ref Paul 1983)
Sand 2_I	0.090	2.65	0.64	IPRI (Ref Paul 1983)
Sand 3_I	0.217	2.65	2.72	IPRI (Ref Paul 1983)
Sand 4_I	0.300	2.65	4.15	IPRI (Ref Paul 1983)
Sand 1_{II}	0.080	2.65	0.52	IPRI (Ref Paul 1983)
Sand 2_{II}	0.085	2.65	0.58	IPRI (Ref Paul 1983)
Sand 3_{II}	0.083	2.65	0.55	IPRI (Ref Paul 1983)
Sand 4_{II}	0.084	2.65	0.57	IPRI (Ref Paul 1983)
Sand 5_{II}	0.084	2.65	0.57	IPRI (Ref Paul 1983)
Sand 1_{III}	0.065	2.65	0.39	IPRI (Ref Paul 1983)

Note: For the sands used at IPRI and HRS were computed from the formula given in Gibbs et al (1971) and is given below:

$$V_s = \frac{-3\eta + \sqrt{(9\eta^2 + g r_s^2 \rho_f(\rho_s - \rho_f)\ (0.0001574 + 0.19841 r_s}}{P_s\ (0.00011607 + 0.14881\ rs}$$

where: V_s = settling velocity (m/s)
η = dynamic viscosity of fluid (Ns/M^2)
g = acceleration due to gravity (m/s^2)
r_s = sediment sphere radius (m) from sieve analysis
ρ_f = fluid density (Kg/m^3)
ρ_s = sediment density (Kg/m^3)

TABLE 3: Test results

Exp No	Material	Sp.gr	D_{50} (mm)	d_0 (cm)	Q_{cc} (l/sec)	Q_0 (l/sec)	h_0 (cm)	P
1	Polystyrene	1.05	2.12	2.54	5.40	0.40	14.68	0.96
2	Polystyrene	1.05	2.12	2.54	7.61	0.45	9.38	0.89
3	Polystyrene	1.05	2.12	2.54	5.92	1.10	22.58	0.97
4	Polystyrene	1.05	2.12	5.08	4.75	0.68	21.08	0.93
5	Polystyrene	1.05	2.12	5.08	7.37	0.78	14.18	0.89
6	Polystyrene	1.05	2.12	5.08	4.46	0.94	8.28	0.98
7	Polystyrene	1.05	2.12	1.27	5.14	0.29	8.68	0.98
8	Polystyrene	1.05	2.12	1.27	4.51	0.30	14.48	1.00
9	Red lentil	1.42	1.50	2.54	9.23	0.57	17.53	1.00
10	Green lentil	1.33	3.40	2.54	9.23	0.57	17.53	1.00
11	Wood-shavings	0.45	0.80	2.54	4.48	0.34	10.48	0.35
12	Wood-shavings	0.45	0.80	2.54	4.76	0.41	14.38	0.35
13	Wood-shavings	0.45	0.80	1.27	4.78	0.22	8.98	0.31
14	Wood-shavings	0.45	0.80	1.27	4.48	0.26	11.28	0.41
15	Volcanic tuff	1.21	1.75	2.54	10.56	0.53	15.38	0.98
16	Volcanic tuff	1.21	1.75	5.08	12.75	0.73	12.98	0.96
17	Volcanic tuff	1.21	1.75	1.27	7.24	0.23	10.48	1.00
18	Polystyrene	1.05	2.12	2.54	12.13	0.57	12.78	0.38
19	Polystyrene	1.05	2.12	2.54	11.50	0.45	12.68	0.56
20	Polystyrene	1.05	2.12	2.54	10.37	0.37	12.18	0.80
21	Polystyrene	1.05	2.12	2.54	8.98	0.36	11.48	0.89
22	Polystyrene	1.05	2.12	2.54	11.98	0.67	17.28	0.52
23	Polystyrene	1.05	2.12	2.54	10.59	0.59	16.58	0.66
24	Polysyrene	1.05	2.12	2.54	7.43	0.47	14.78	0.93

TABLE 4A: Amphlett and Anwar data $r/d_o = 2.0$

Outlet Diameter d_o (mm)	h_o/d_o	Coefficient of discharge C_d	Measured Circulation Number N_τ
152.8	4.6876	0.0664	12.0784
152.8	5.2192	0.0679	12.1248
152.8	5.7017	0.0725	11.3778
152.8	6.1372	0.0731	11.2567
152.8	6.4613	0.0761	10.2768
152.8	6.8232	0.0771	10.5346
152.8	7.1894	0.0801	10.2027
152.8	7.5302	0.0820	9.6665
152.8	7.9391	0.0825	9.2641
152.8	8.1884	0.0842	9.4006
101.7	4.8947	0.0828	11.2200
101.7	5.8515	0.0911	10.0971
101.7	6.8058	0.0855	10.2938
101.7	7.2802	0.0905	9.8105
101.7	7.6922	0.0902	9.9416
101.7	8.0668	0.0917	9.7564
101.7	9.2753	0.0946	9.3842
101.7	10.5162	0.0989	8.9301
101.7	11.7259	0.1013	8.6828
101.7	11.0715	0.1263	6.6208
66.3	7.3544	0.1198	7.2846
66.3	9.3619	0.1211	6.7781
66.3	10.6733	0.1274	6.1404
66.3	12.1751	0.1338	5.6508
66.3	6.5128	0.1273	7.0922
66.3	8.9336	0.1240	7.0191
66.3	10.0986	0.1310	6.4901
66.3	9.3248	0.1499	4.4983
66.3	10.7882	0.1608	5.0622
66.3	14.2745	0.1713	4.4155
66.3	13.6654	0.1857	3.9349

TABLE 4A: Continued

Outlet Diameter d_o (mm)	h_o/d_o	Coefficient of discharge C_d	Measured Circulation Number N_τ
38.3	10.8276	0.1787	4.0701
38.3	12.9973	0.1868	3.9427
38.3	14.8563	0.1927	3.5494
38.3	17.7415	0.1878	4.7341
38.3	22.4412	0.1843	4.6252
38.3	26.6945	0.1884	4.3596
38.3	29.3785	0.1984	4.3953
38.3	11.0751	0.2057	4.2911
38.3	9.8015	0.2287	3.8361
38.3	21.9190	0.1867	4.5695
38.3	12.6005	0.2562	4.8871
38.3	16.4281	0.2489	3.0859
38.3	19.4596	0.0854	4.1852
38.3	27.3968	0.0939	4.8871
38.3	21.9712	0.0997	3.8459
38.3	27.8616	0.1144	4.5939
38.3	27.6945	0.1233	4.2771
38.3	28.5692	0.1300	4.5436
38.3	21.3002	0.1546	4.7945
28.8	13.7395	0.2535	2.5771
28.8	16.7569	0.2780	2.2921
28.8	22.0659	0.2765	2.0418
28.8	37.2708	0.3182	2.0662
28.8	36.9895	0.3161	2.5196
22.2	7.4144	0.4292	1.1636
22.2	16.6576	0.3860	1.3222
22.2	21.2117	0.3870	1.2445
22.2	24.6666	0.3703	1.2691
22.2	27.3243	0.3757	1.3102
22.2	32.7792	0.4355	1.0399
22.2	43.3964	0.4173	1.1789
22.2	48.0090	0.4162	1.1372
22.2	12.2747	0.3011	2.6693
22.2	21.1081	0.3054	2.4198
22.2	39.2117	0.3178	2.4036
22.2	18.1576	0.6701	0.3986
22.2	24.4144	0.6949	0.4000
22.2	31.3378	0.6759	0.5028
22.2	41.1666	0.6757	0.4894
22.2	49.7837	0.6795	0.4950

TABLE 4A: Continued

Outlet Diameter d_o (mm)	h_o/d_o	Coefficient of discharge C_d	Measured Circulation Number N_τ
16.0	25.8312	0.4692	1.0342
16.0	30.8625	0.4454	1.1485
16.0	36.5937	0.4547	1.0825
16.0	56.8312	0.5225	0.9897
16.0	62.3875	0.5202	0.9627
9.6	29.6041	0.7235	0.4504
9.6	54.2916	0.7228	0.3701
9.6	64.2187	0.7063	0.4332
9.6	80.3229	0.7590	0.3898
9.6	104.2500	0.7585	0.4439
9.6	46.5520	0.6576	0.3753
9.6	108.7961	0.4841	0.4857
9.6	114.5416	0.7317	0.3820
9.6	102.8125	0.6173	0.3468
9.6	123.8229	0.6217	0.3070

TABLE 4B: $r/d_o = 2.5$

Outlet Diameter D_o (mm)	h_o/d_o	Coefficient of discharge C_d	Measured Circulation Number N_τ
152.8	4.8289	0.0655	11.8026
152.8	5.3791	0.0669	11.7933
152.8	5.9178	0.0712	11.1866
152.8	6.3234	0.0720	10.9846
152.8	6.6570	0.0750	10.5549
152.8	7.0315	0.0766	10.2540
152.8	7.4138	0.0788	10.2540
152.8	7.7629	0.0808	10.1856
152.8	8.1901	0.0813	9.7399
152.8	8.4661	0.0833	9.5579
152.8	8.4661	0.0833	9.1124
101.7	5.0295	0.0817	11.0109
101.7	6.1307	0.0890	9.9643
101.7	7.0205	0.0842	10.2417
101.7	7.5299	0.0890	9.6538
101.7	7.9419	0.0888	9.6534
101.7	8.3539	0.0900	9.6008
101.7	9.5978	0.0930	9.1106
101.7	10.8643	0.0975	8.8810
101.7	12.0156	0.1000	8.5491
101.7	11.3513	0.1223	6.4696
66.3	7.5626	0.1181	7.1729
66.3	9.6003	0.1196	6.7781
66.3	11.0015	0.1254	6.3024
66.3	12.5505	0.1318	5.8982
66.3	6.6889	0.1256	7.0956
66.3	9.1485	0.1226	6.9890
66.3	10.3362	0.1295	6.6846
66.3	9.5070	0.1481	5.3484
66.3	10.9875	0.1593	5.0749
66.3	14.6117	0.1693	4.4069
66.3	13.9374	0.1840	3.9430

TABLE 4B: Continued

Outlet Diameter D_o (mm)	h_o/d_o	Coefficient of discharge C_d	Measured Circulation Number N_τ
38.3	11.0088	0.1773	4.3229
38.3	13.3963	0.1841	4.2388
38.3	15.2193	0.1905	3.7322
38.3	18.0261	0.1864	4.7130
38.3	22.8537	0.1828	4.7219
38.8	27.2767	0.1864	4.4312
38.3	30.0234	0.1929	4.4336
38.3	11.3342	0.2034	4.5056
38.3	10.0000	0.2265	3.9489
38.3	22.3159	0.1851	4.6619
38.3	12.8668	0.2535	3.3711
38.3	16.7597	0.2464	3.2541
38.3	19.4856	0.0854	4.5982
38.3	27.4438	0.0939	5.2323
38.3	22.0104	0.0996	4.1789
38.3	27.9347	0.1143	4.8734
38.3	27.7597	0.1231	4.5401
38.3	28.6632	0.1298	4.8606
38.3	21.4020	0.1544	5.2318
28.8	13.9687	0.2515	2.6357
28.8	17.0381	0.2757	2.3813
28.8	22.4097	0.2768	2.1161
28.8	37.8263	0.3161	2.1359
28.8	37.5625	0.3136	2.6870
22.2	7.5045	0.4269	1.3204
22.2	16.8648	0.3828	1.3804
22.2	21.4549	0.3850	1.3311
22.2	24.9549	0.3682	1.4028
22.2	27.5855	0.3739	1.3934
22.2	33.1351	0.4333	1.1470
22.2	43.7972	0.4153	1.2762
22.2	48.5135	0.4140	1.2459
22.2	12.5180	0.2983	2.8338
22.2	21.4639	0.3028	2.5436
22.2	39.7027	0.3161	2.5926
22.2	18.2387	0.6686	1.0040
22.2	24.4864	0.6937	0.4101
22.2	31.4414	0.6747	0.5195
22.2	41.2477	0.6744	0.4838
22.2	50.0000	0.6781	0.4854

TABLE 4B: Continued

Outlet Diameter d_o (mm)	h_o/d_o	Coefficient of discharge C_d	Measured Circulation Number N_τ
16.0	26.0687	0.4671	1.0962
16.0	31.1312	0.4434	1.2461
16.0	36.8625	0.4532	1.1568
16.0	57.2937	0.5203	1.0604
16.0	62.8125	0.5185	1.0374
9.6	29.7083	0.7222	0.4359
9.6	54.5000	0.7213	0.4131
9.6	64.5625	0.7045	0.4754
9.6	80.4895	0.7582	0.4291
9.6	104.5625	0.7575	0.4924
9.6	46.7291	0.6563	0.4184
9.6	109.1145	0.4833	0.5489
9.6	114.7500	0.7310	0.3875
9.6	103.0520	0.6165	0.3679
9.6	124.0104	0.6212	0.3349
22.2	48.5135	0.4140	1.2459
22.2	12.5180	0.2983	2.8338
22.2	21.4639	0.3028	2.5436
22.2	39.7027	0.3161	2.5926
22.2	18.2387	0.6686	1.0040
22.2	24.4864	0.6937	0.4101
22.2	31.4414	0.6747	0.5195
22.2	41.2477	0.6744	0.4838
22.2	50.0000	0.6781	0.4854
16.0	26.0867	0.4671	1.0962
16.0	31.1312	0.4434	1.2461
16.0	36.8625	0.4532	1.1568
16.0	57.2937	0.5203	1.0604
16.0	62.8125	0.5185	1.0374
9.6	29.7083	0.7222	0.4359
9.6	54.5000	0.7213	0.4131
9.6	64.5625	0.7045	0.4754
9.6	80 4895	0.7582	0.4291
9.6	104.5625	0.7575	0.4924
9.6	46.7291	0.6563	0.4184
9.6	109.1145	0.4833	0.5489
9.6	114.7500	0.7310	0.3875
9.6	103.0520	0.6165	0.3679
9.6	124.0104	0.6212	0.3349

TABLE 4C: $r/d_o = 3.0$

Outlet Diameter d_o (mm)	h_o/d_o	Coefficient of discharge C_d	Measured Circulation Number N_τ
152.8	4.9154	0.0649	12.0632
152.8	5.4474	0.0665	12.1200
152.8	6.0209	0.0706	11.3735
152.8	6.4132	0.0715	11.2688
152.8	6.7656	0.0745	10.7751
152.8	7.1396	0.0760	10.5454
152.8	7.5020	0.0784	10.2095
152.8	7.8893	0.0802	9.6697
152.8	8.2882	0.0808	9.2704
152.8	8.5858	0.0827	9.3975
101.7	5.1300	0.0809	11.0724
101.7	6.4761	0.0866	9.8723
101.7	7.1355	0.0836	10.1727
101.7	7.6675	0.0882	9.5155
101.7	8.0820	0.0881	9.4229
101.7	8.5166	0.0893	9.3413
101.7	9.8079	0.0920	8.9619
101.7	11.0391	0.0966	8.6942
101.7	12.2080	0.0994	8.4751
101.7	11.5137	0.1240	6.2520
66.3	7.6659	0.1173	7.1643
66.3	9.7501	0.1188	6.7510
66.3	11.1330	0.1243	6.4364
66.3	12.7804	0.1307	6.0954
66.3	6.7887	0.1247	7.1128
66.3	9.2903	0.1216	7.1034
66.3	10.4665	0.1286	6.6778
66.3	9.6620	0.1507	5.3862
66.3	11.1255	0.1582	4.9543
66.3	14.7534	0.1686	4.4137
66.3	14.0983	0.1846	3.9511

TABLE 4C: Continued

Outlet Diameter d_o (mm)	h_o/d_o	Coefficient of discharge C_d	Measured Circulation Number N_τ
38.3	11.2211	0.1756	4.4196
38.3	13.6349	0.1825	4.3700
38.3	15.4647	0.1889	3.8083
38.3	18.1723	0.1857	4.6591
38.3	23.1175	0.1818	4.6671
38.3	27.5300	0.1856	4.4575
38.3	30.3994	0.1916	4.4230
38.3	11.4856	0.2020	4.6149
38.3	10.1201	0.2251	3.9385
38.3	22.5561	0.1842	4.6366
38.3	13.0052	0.2523	3.3667
38.3	16.9582	0.2450	3.2906
38.3	19.4986	0.0854	4.8748
38.3	27.4621	0.0939	5.4951
38.3	22.0365	0.0996	4.4019
38.3	27.9739	0.1142	4.9949
38.3	27.7937	0.1231	4.7691
38.3	28.7232	0.1297	4.9450
38.3	21.4751	0.1541	5.4631
28.8	14.0937	0.2507	2.6438
28.8	17.1979	0.2745	2.4200
28.8	22.6319	0.2754	2.1710
28.8	38.1527	0.3147	2.1446
28.8	37.9236	0.3123	2.7090
22.2	7.5630	0.4250	1.0026
22.2	16.9819	0.3823	1.4176
22.2	21.5900	0.3834	1.3861
22.2	25.1036	0.3671	1.4850
22.2	27.7792	0.3726	1.4509
22.2	33.4684	0.4331	1.2230
22.2	43.9909	0.4139	1.3208
22.2	48.7972	0.4130	1.2942
22.2	12.6756	0.2963	2.6784
22.2	21.6801	0.3014	2.5776
22.2	39.9549	0.3151	2.7038
22.2	18.2927	0.6674	0.4174
22.2	24.5180	0.6931	0.4145
22.2	31.5100	0.6742	0.5200
22.2	41.3693	0.6745	0.4771
22.2	50.1351	0.7423	0.4828

TABLE 4C: Continued

Outlet Diameter d_o (mm)	h_o/d_o	Coefficient of discharge C_d	Measured Circulation Number N_τ
16.0	26.2437	0.4656	1.1292
16.0	31.3562	0.4419	1.3089
16.0	37.0375	0.4519	1.2143
16.0	57.5812	0.5193	1.0904
16.0	63.1375	0.5170	1.0620
9.6	29.7916	0.7207	0.4515
9.6	54.6354	0.7207	0.4560
9.6	64.7708	0.7036	0.5036
9.6	80.6145	0.7577	0.4580
9.6	104.7506	0.7567	0.5181
9.6	46.7812	0.6558	0.4452
9.6	109.2500	0.4831	0.6030
9.6	114.9083	0.7310	0.3966
9.6	103.1875	0.6159	0.3810
9.6	124.1458	0.6209	0.3523

TABLE 5: Observed parameters for computation of discharge coefficient of orifice or flushing pipe

No	Discharge (m^3/s) Inlet channel (Q_c)	Discharge (m^3/s) Orifice (Q_o)	Depth over orifice (h_o) (m)	Orifice diameter (d_o) (m)	Circulation τ_o at $r = r_o$ (m^2/s)	Discharge coefficient Predicted	Discharge coefficient Measured
Curi et al (1975) data; d = 0.90m; B = 0.18m							
1	0.00540	0.00040	0.1468	0.0254	0.0729	0.4292	0.4649
2	0.00761	0.00045	0.0938	0.0254	0.0583	0.5261	0.6543
3	0.00592	0.00110	0.2258	0.0254	0.0904	0.9356	1.0308
4	0.00475	0.00168	0.2108	0.0508	0.1747	0.3626	0.4075
5	0.00737	0.00078	0.1418	0.0508	0.1433	0.1953	0.2307
6	0.00446	0.00094	0.0828	0.0508	0.1095	0.2831	0.3638
7	0.00923	0.00057	0.1753	0.0254	0.0797	0.5343	0.6062
8	0.00923	0.00057	0.1753	0.0254	0.0797	0.5343	0.6062
9	0.00448	0.00034	0.1048	0.0254	0.0616	0.3840	0.4677
10	0.00476	0.00041	0.1438	0.0254	0.0722	0.4137	0.4814
11	0.01056	0.00053	0.1538	0.0254	0.0746	0.5205	0.6018
12	0.01273	0.00073	0.1298	0.0508	0.1371	0.1887	0.2257
13	0.01213	0.00057	0.1278	0.0254	0.0680	0.5964	0.7100
14	0.01150	0.00045	0.1268	0.0254	0.0678	0.4737	0.5627
15	0.01037	0.00030	0.1218	0.0254	0.0664	0.3221	0.3828
16	0.00898	0.00036	0.1148	0.0254	0.0645	0.3936	0.4731
17	0.01197	0.00067	0.1728	0.0254	0.0791	0.6298	0.7177
18	0.01059	0.00059	0.1058	0.0254	0.0619	0.6590	0.8077
19	0.00743	0.00047	0.1478	0.0254	0.0732	0.4688	0.5444
HRL data, Paul (1983); d = 0.55m							
1	0.00432	0.000200	0.1894	0.0190	0.0619	0.3314	0.3654
2	0.00430	0.000202	0.1824	0.0190	0.0608	0.3391	0.3760
3	0.00401	0.000217	0.1764	0.0190	0.0598	0.3682	0.4108
4	0.00420	0.000200	0.1844	0.0190	0.0611	0.3345	0.3703
5	0.00411	0.000209	0.1594	0.0190	0.0568	0.3676	0.4162
6	0.00422	0.000204	0.1654	0.0190	0.0579	0.3543	0.3988
7	0.00413	0.000229	0.1794	0.0190	0.0603	0.3860	0.4298
8	0.00423	0.000227	0.1804	0.0190	0.0605	0.3819	0.4249
9	0.00431	0.000229	0.1624	0.0190	0.0574	0.4001	0.4518
10	0.00413	0.000234	0.1404	0.0190	0.0533	0.4294	0.4965

TABLE 5: Continued

No	Discharge (m^3/s) Inlet channel (Q_c)	Orifice (Q_o)	Depth over orifice (h_o) (m)	Orifice diameter (d_o) (m)	Circulation τ_o at $r = r_o$ (m^2/s)	Discharge coefficient Predicted	Measured
HRS (IPRI) data; d = 5.0m; B = 1.0m							
1	0.36	0.023	0.9204	0.15	1.0781	0.3270	0.3060
2	0.36	0.022	0.9217	0.15	1.0789	0.3128	0.2928
3	0.36	0.019	0.9232	0.15	1.0798	0.2706	0.2526
4	0.36	0.017	0.9203	0.15	1.0781	0.2427	0.2264
5	0.36	0.016	0.9212	0.15	1.0786	0.2286	0.2130
6	0.30	0.023	0.5758	0.15	1.0166	0.3407	0.3248
7	0.30	0.022	0.5743	0.15	1.0156	0.3263	0.3110
8	0.30	0.019	0.5781	0.15	1.0180	0.2819	0.2680
9	0.30	0.016	0.5768	0.15	1.0172	0.2381	0.2258
10	0.30	0.015	0.5763	0.15	1.0169	0.2235	0.2158
11	0.36	0.0120	0.9222	0.10	0.7195	0.3878	0.3592
12	0.36	0.0116	0.9221	0.10	0.7194	0.3751	0.3472
13	0.36	0.0101	0.9231	0.10	0.7198	0.3271	0.3022
14	0.36	0.0092	0.9235	0.10	0.7200	0.2983	0.2752
15	0.36	0.0082	0.9232	0.10	0.7198	0.2663	0.2453
16	0.30	0.0109	0.8130	0.10	0.6755	0.3686	0.3475
17	0.30	0.0105	0.8132	0.10	0.6756	0.3552	0.3347
18	0.30	0.0094	0.8134	0.10	0.6757	0.3185	0.2996
19	0.30	0.0082	0.8150	0.10	0.6106	0.2766	0.2611
20	0.30	0.0076	0.8158	0.10	0.6767	0.2547	0.2419
21	0.36	0.0097	0.9213	0.09	0.6472	0.3869	0.3571
22	0.36	0.0086	0.9219	0.09	0.6474	0.3434	0.3164
23	0.36	0.0080	0.9240	0.09	0.6481	0.3225	0.2968
24	0.36	0.0075	0.9242	0.09	0.6482	0.3012	0.2768
25	0.36	0.0069	0.9255	0.09	0.6487	0.2765	0.2538
26	0.30	0.0095	0.8238	0.09	0.6120	0.3972	0.3730
27	0.30	0.0088	0.8245	0.09	0.6122	0.3660	0.3431
28	0.30	0.0075	0.8232	0.09	0.6118	0.3135	0.2933
29	0.30	0.0063	0.3234	0.09	0.6119	0.2636	0.2460
30	0.30	0.0056	0.8235	0.09	0.6119	0.2342	0.2182

DR = 0.97, SD = 0.15

TABLE 6: Statement of Test Conditions and Experimental Data

Here D_s is the sediment size and $\bar{D}_s$ its mean value; d is the chamber diameter; V_s is the settling velocity of sediment particle; W is the upward velocity of flow in CCSE; d_o is the diameter of orifice or flushing pipe, V_{to} is the maximum tangential velocity in CCSE; Q_o is the flushing discharge; P is the observed sediment trapping efficiency and $\bar{P}$ its mean value; Test No 4_{II} means Run No 4 of Model II and h_o is the head on the orifice.

Test No	D_s (mm)	d (m)	V_s/W	d_o (m)	V_s/V_{to}	d/d_o	Q_o/Q_c (%)	P (%)
1_I	$Q_c = Q_{cc} = 0.160625m^3/s$; $h_o = 0.465m$; $W = 0.009312m/s$; $\bar{D}_s = 7.64mm$ and $\bar{P} = 87.7\%$.							
	0.0815	4.25	0.627	0.15	0.0036	28.33	17.76	58.9
	0.097	4.25	0.852	0.15	0.0049	28.33	17.76	58.7
	0.126	4.25	1.320	0.15	0.0076	28.33	17.76	92.8
	0.162	4.25	1.959	0.15	0.0112	28.33	17.76	67.4
	0.237	4.25	3.379	0.15	0.0194	28.33	17.76	64.7
	0.359	4.25	5.727	0.15	0.0328	28.33	17.76	80.7
	0.460	4.25	7.620	0.15	0.0436	28.33	17.76	63.3
	0.75	4.25	12.676	0.15	0.0726	28.33	17.76	63.2
	1.50	4.25	23.55	0.15	0.1349	28.33	17.76	80.5
	3.375	4.25	43.15	0.15	0.2471	28.33	17.76	92.5
	7.125	4.25	69.47	0.15	0.3978	28.33	17.76	92.1
	11.10	4.25	89.91	0.15	0.5148	28 33	17.76	100
	15.875	4.25	109.72	0.15	0.628	28.33	17.76	100
2_I	$Q_c = Q_{cc} = 0.110m^3/s$; $h_o = 0.414m$; $W = 0.006357m/s$; $\bar{D}_s = 7.64mm$; and $\bar{P} = 79.9\%$.							
	0.079	4.25	0.869	0.15	0.0036	28.33	18.01	80.3
	0.126	4.25	1.934	0.15	0.0080	28.33	18.01	86.6
	0.162	4.25	2.870	0.15	0.0119	28.33	18.01	95.6
	0.237	4.25	4.950	0.15	0.0205	28.33	18.01	73.7
	0.359	4.25	8.39	0.15	0.0348	28.33	18.01	73.1
	0.46	4.25	11.163	0.15	0.0462	28.33	18.01	45.7
	0.75	4.25	18.568	0.15	0.0769	28.33	18.01	64.7
	1.50	4.25	34.50	0.15	0.1429	28.33	18.01	72.3
	3.39	4.25	63.4	0.15	0.2627	28.33	18.01	63.7
	7.16	4.25	102.06	0.15	0.4228	28.33	18.01	93.6
	11.13	4.25	131.9	0.15	0.5465	28.33	18.01	60.5
	15.88	4.25	160.7	0.15	0.6660	28.33	18.01	93.4
3_I	$Q_c = Q_{cc} = 0.0625m^3/s$; $h_o = 0.30m$; $W = 0.003567m/s$; $\bar{D}_s = 7.64mm$; and $\bar{P} = 80.3\%$.							
	0.111	4.25	2.80	0.15	0.0076	28.33	19.04	58.0
	0.162	4.25	5.11	0.15	0.0140	28.33	19.04	56.7
	0.212	4.25	7.57	0.15	0.0207	28.33	19.04	68.1
	0.334	4.25	13.70	0.15	0.0374	28.33	19.04	83.2
	0.460	4.25	19.89	0.15	0.0543	28.33	19.04	83.2

TABLE 6: Continued

Test No	D_s (mm)	d (m)	V_s/W	d_o (m)	V_s/V_{to}	d/d_o	Q_o/Q_c (%)	P (%)
	0.750	4.25	33.09	0.15	0.0904	28.33	19.04	58.5
	1.5	4.25	61.48	0.15	0.1679	28.33	19.04	73.3
	3.38	4.25	112.76	0.15	0.3079	28.33	19.04	91.1
	7.13	4.25	181.42	0 15	0.4954	28.33	19.04	86.5
	11.10	4.25	234.71	0.15	0.6409	28.33	19.04	82.6
	15.88	4.25	286.48	0.15	0.7823	28.33	19.04	100
4_I	$Q_c = Q_{cc} = 0.160625 m^3/s$; $h_o = 0.465m$; $W = 0.009312 m/s$; $\bar{D}_s = 1.48mm$ and $\bar{P} = 94.5\%$.							
	0.111	4.25	1.071	0.15	0.0061	28.33	17.76	92.5
	0.162	4.25	1.959	0.15	0.0112	28.33	17.76	86.1
	0.237	4.25	3.379	0.15	0.0194	28.33	17.76	91.5
	0.359	4.25	5.727	0.15	0.0328	28.33	17.76	92.2
	0.46	4.25	7.620	0.15	0.0436	28.33	17.76	95.4
	0.75	4.25	12.676	0.15	0.0726	28.33	17.76	95.4
	1.69	4.25	25.932	0.15	0.1485	28.33	17.76	96.7
5_I	$Q_c = Q_{cc} = 0.110 m^3/s$; $h_o = 0.414m$; $W = 0.006357 m/s$; $\bar{D}_s = 1.48mm$ and $\bar{P} = 95.0\%$.							
	0.111	4.25	1.57	0.15	0.0065	28.33	18.01	97.5
	0.162	4.25	2.87	0.15	0.0119	28.33	18.01	94.3
	0.237	4.25	4.95	0.15	0.0205	28.33	18.01	90.2
	0.359	4.25	8.39	0.15	0.0348	28.33	18.01	96.7
	0.46	4.25	11.163	0.15	0.0462	28.33	18.01	93.7
	0.75	4.25	18.57	0.15	0.0769	28.33	18.01	94.9
	1.69	4.25	37.99	0.15	0.1574	28.33	18.01	95.0
6_I	$Q_c = Q_{cc} = 0.0625 m^3/s$; $h_o = 0.30m$; $W = 0.003567 m/s$; $\bar{D}_s = 1.48mm$ and $\bar{P} = 93.7\%$.							
	0.094	4.25	2.11	0.15	0.0058	28.33	19.04	97.6
	0.136	4.25	3.90	0.15	0.0106	28.33	19.04	87.8
	0.162	4.25	5.11	0.15	0.0140	28.33	19.04	95.0
	0.237	4.25	8.82	0.15	0.0241	28.33	19.04	96.2
	0.359	4.25	14.95	0.15	0.0408	28.33	19.04	95.1
	0.46	4.25	19.89	0.15	0.0543	28.33	19.04	95.5
	0.75	4.25	33.09	0.15	0.0904	28.33	19.04	87.0
	1.69	4.25	67.70	0.15	0.1849	28.33	19.04	94.3
7_I	$Q_c = Q_{cc} = 0.160625 m^3/s$; $W = 0.010405 m/s$; $\bar{D}_s = 7.64mm$; $\bar{P} = 0.437m$							
	Orifice shifted by 0.28m so as to match vortex axis; after 3 hours of running $\bar{P} = 7.8\%$ as compared to 87.7% in Run 1_I							
	7.64	4.25	64.81	0.15	0.4278	28.33	8.1	7.8
8_I	$Q_c = Q_{cc} = 0.160625 m^3/s$; $h_o = 0.455m$; $W = 0.009058 m/s$; $\bar{D}_s = 7.64mm$; and $\bar{P} = 90.0\%$.							

TABLE 6 Continued

Test No	D_s (mm)	d (m)	V_s/W	d_o (m)	V_s/V_{to}	d/d_o	Q_o/Q_c (%)	P (%)
	0.115	4.25	0.983	0.20	0.0055	21.25	20.0	74.0
	0.151	4.25	1.56	0.20	0.0088	21.25	20.0	25.0
	0.237	4.25	3.13	0.20	0.0176	21.25	20.0	53.2
	0.359	4.25	5.48	0.20	0.0309	21.25	20.0	56.8
	0.46	4.25	7.414	0.20	0.0417	21.25	20.0	82.7
	0.75	4.25	12.62	0.20	0.0711	21.25	20.0	76.9
	1.50	4.25	23.87	0.20	0.1344	21.25	20.0	89.9
	3.38	4.25	44.18	0.20	0.2488	21.25	20.0	94.2
	7.14	4.25	71.38	0.20	0.4019	21.25	20.0	97.5
	11.11	4.25	92.39	0.20	0.5202	21.25	20.0	97.2
	15.88	4.25	112.75	0.20	0.6349	21.25	20.0	100
9_I	$Q_c = Q_{cc} = 0.110 m^3/s$; $W = 0.006048 m/s$; $h_o = 0.404 m$; $\bar{D}_s = 7.64 mm$; and $\bar{P} = 88.8\%$.							
	0.096	4.25	1.07	0.20	1.0675	21.25	22.0	75.3
	0.115	4.25	1.47	0.20	1.4717	21.25	22.0	4.7
	0.151	4.25	2.33	0.20	2.3365	21.25	22.0	38.6
	0.237	4.25	4.69	0.20	4.6850	21.25	22.0	41.0
	0.399	4.25	9.37	0.20	9.3661	21.25	22.0	74.0
	0.75	4.25	18.90	0.20	18.899	21.25	22.0	85.7
	1.50	4.25	35.75	0.20	35.75	21.25	22.0	96.2
	3.38	4.25	66.14	0.20	66.17	21.25	22.0	96.9
	7.13	4.25	106.9	0.20	106.9	21.25	22.0	92.6
	11.10	4.25	138.4	0.20	138.4	21.25	22.0	100
10_I	$Q_c = Q_{cc} = 0.160625 m^3/s$; $h_o = 0.485 m$; $W = 0.009772 m/s$; $\bar{D}_s = 7.64 mm$; $\bar{P} = 14.2\%$.							
	7.64	4.25	69.01	0.125	0.4060	34.0	13.69	14.2
11_I	$Q_c = Q_{cc} = 0.110 m^3/s$; $h_o = 0.42 m$; $W = 0.006556 m/s$; $\bar{D}_s = 7.64 mm$; and $\bar{P} = 15.3\%$.							
	7.64	4.25	102.9	0.125	0.4363	34.0	15.45	15.3
12_I	$Q_c = Q_{cc} = 0.0625 m^3/s$; $h_o = 0.3525 m$; $W = 0.003648 m/s$; and $\bar{D}_s = 7.64 mm$							
	7.64	4.25	184.9	0.125	0.4763	34	17.20	15.0
13_I	$Q_c = Q_{cc} = 0.160625 m^3/s$; $h_o = 0.4825 m$; $W = 0.010274 m/s$; $\bar{D}_s = 7.64 mm$; and $\bar{P} = 12.5\%$.							
	7.64	4.25	65.64	0.10	0.4071	42.5	9.26	12.5
14_I	$Q_c = Q_{cc} = 0.110 m^3/s$; $h_o = 0.4175 m$; $W = 0.006944 m/s$; $\bar{D}_s = 7.64 mm$; and $\bar{P} = 14.9\%$.							
	7.64	4.25	97.11	0.10	0.4376	42.5	10.45	14.9
15_I	$Q_c = Q_{cc} = 0.0625 m^3/s$; $h_o = 0.350 m$; $W = 0.003848 m/s$; and $\bar{D}_s = 7.64 mm$;							
	7.64	4.25	175.2	0.10	0.4781	42.5	12.65	14.5

TABLE 6 Continued

Data for tests 16 to 24 are from page 17 (Ref Paul (1983)).

16	0.234	4.572	1.384	0.152	0.0182	30	5.5	67
17	0.090	4.572	0.279	0.152	0.0037	30	5.5	62
18	0.217	3.658	0.745	0.152	0.0159	24	3.5	49
19	0.300	5.984	3.01	0.152	0.0242	39	2.2	47
20	0.080	6.096	1.74	0.063	0.0044	96	4.1	23
21	0.085	6.096	1.95	0.076	0.0049	80	4.5	33
22	0.083	6.096	1.92	0.100	0.0046	60	7.5	36
23	0.084	6.096	1.99	0.100	0.0048	60	7.5	40
24	0.084	4.572	1.12	0.100	0.0052	45	7.5	41

B = 0.11m; CD_0, Q_c = 0.005; 0.0052; and 0.00517m^3/s respectively

25_{II}	0.175	0.55	1.592	0.038	0.0177	14.47	7.14	42
26_{II}	0.175	0.55	1.604	0.050	0.0177	11.0	8.68	44.5
27_{II}	0.175	0.55	1.535	0.032	0.0176	17.19	5.90	33

B = 0.11m; CD_2; Q_c = 0.00516, 0.00509 and 0.00520m^3/s respectively

28_{II}	0.175	0.55	1.810	0.038	0.0177	14.47	12.21	54
29_{II}	0.175	0.55	1.948	0.050	0.0178	11.0	15.27	59
30_{II}	0.175	0.55	1.766	0.032	0.0176	17.19	10.83	52

B = 0.07m; CD_2; Q_c = 0.00495; 0.00518 and 0.00521m^3/s respectively.

31_{II}	0.175	0.55	1.946	0.038	0.0176	14.47	10.76	48
32_{II}	0.175	0.55	1.908	0.050	0.0178	11.0	12.47	53
33_{II}	0.175	0.55	1.852	0.032	0.0176	17.19	10.89	49

B = 1.0m; CD_0; and Q_c = 0.36m^3/s

34_{III}	0.215	5.00	5.87	0.20	0.0114	25	2.6	57

TABLE 7: Values of discharge coefficient for spill weir, C_{d1} and diaphragm orifice, C_{do} from Model III

(a) Discharge coefficient for spill weir

Weir Height (m)	Head on Weir (m)	Drowning ratio (%)	Discharge coefficient (C_{d1})
0	0.327	98	0.329
0	0.359	99	0.197
0	0.380	99	0.180
0	0.383	99	0.178
0	0.386	99	0.177
0.04	0.251	98	0.258
0.04	0.291	99	0.200
0.04	0.329	99	0.233
0.04	0.331	99	0.232
0.04	0.338	99	0.230
0.09	0.203	97	0.302
0.09	0.242	98	0.243
0.09	0.275	99	0.206
0.09	0.284	98	0.248
0.09	0.291	97	0.306

(b) Discharge coefficient for diaphragm orifice ($h_1 = 0.4h$)

Discharge (m^3/s)	Depth, h (m)	Discharge coefficient (C_{do})
0.1290	0.602	0.206
0.1311	0.589	0.212
0.1311	0.611	0.207
0.1311	0.613	0.207
0.1311	0.619	0.205
0.1321	0.613	0.208
0.1509	0.608	0.239
0.1562	0.618	0.245
0.1579	0.620	0.247
0.1615	0.610	0.255
0.1632	0.627	0.254
0.1686	0.594	0.271
0.1825	0.606	0.290
0.1910	0.607	0.303
0.2084	0.597	0.334
0.2265	0.600	0.362

TABLE 8 Comparison of Critical relative submergence and discharge coefficient of flushing pipe orifice

Test No	Q_o (m^3/s)	R_{e_5} X10^5	N_τ	F	h_o/d_o Pred Eq 58	h_o/d_o Obs	C_d Pred Eq 64	C_d Obs
1_I	0.0285	2.11	4.03	1.33	21.11	3.10	0.512	0.534
2_I	0.0198	1.47	5.47	0.92	16.43	2.76	0.371	0.393
3_I	0.0119	0.88	7.76	0.56	10.98	2.00	0.254	0.278
7_I	0.0130	0.96	8.56	0.61	13.11	2.91	0.243	0.251
8_I	0.0321	1.78	6.29	0.73	13.07	3.03	0.293	0.342
9_I	0.0242	1.34	7.87	0.55	10.66	2.02	0.257	0.274
10_I	0.0220	1.95	3.71	1.62	25.94	3.88	0.564	0.581
11_I	0.0170	1.51	4.46	1.25	21.29	3.36	0.459	0.483
12_I	0.0108	0.96	6.47	0.79	15.39	2.82	0.311	0.335
13_I	0.0149	1.65	3.50	1.91	31.40	4.83	0.600	0.617
14_I	0.0115	1.28	4.21	1.48	25.76	4.18	0.490	0.512
15_I	0.0079	0.88	5.61	1.02	6.22	3.50	0.361	0.384
16	0.0218	1.60	5.80	0.99	18.47	3.52	0.367	0.371
18	0.0139	1.02	8.91	0.63	14.00	3.37	0.239	0.242
19	0.0087	0.64	14.47	0.39	10.83	3.51	0.147	0.148
20	0.0037	0.66	3.97	1.52	10.71	3.90	0.490	0.540
21	0.0041	0.60	5.26	1.04	19.84	3.24	0.367	0.411
22	0.0068	0.76	5.47	0.87	15.93	2.46	0.349	0.394
24	0.0068	0.76	5.08	0.87	15.15	2.12	0.368	0.425
34_{III}	0.0094	0.52	32.33	0.21	8.35	5.10	0.072	0.067

FIGURES.

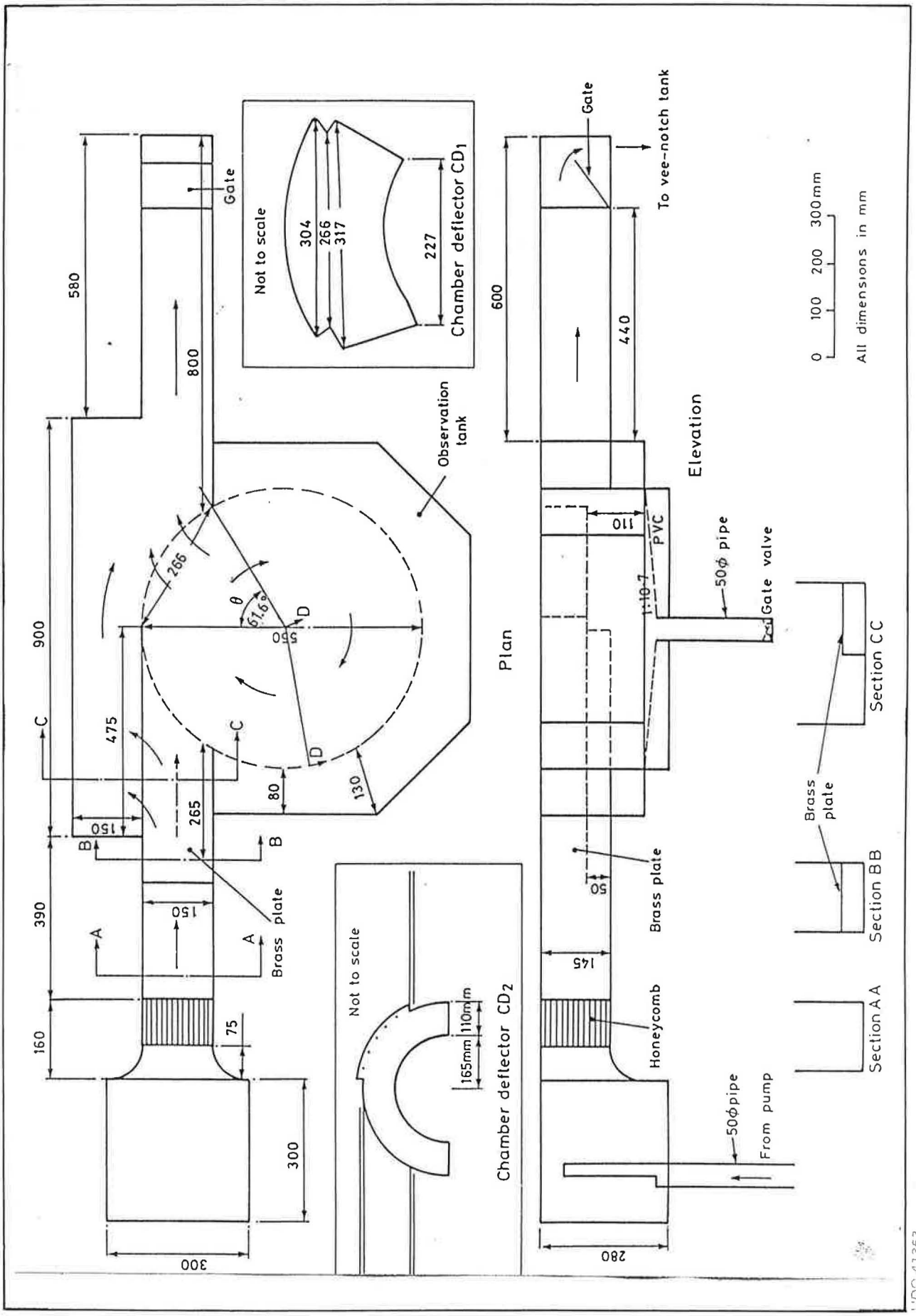

Fig 1 Layout of circulation chamber sediment extractor at HR

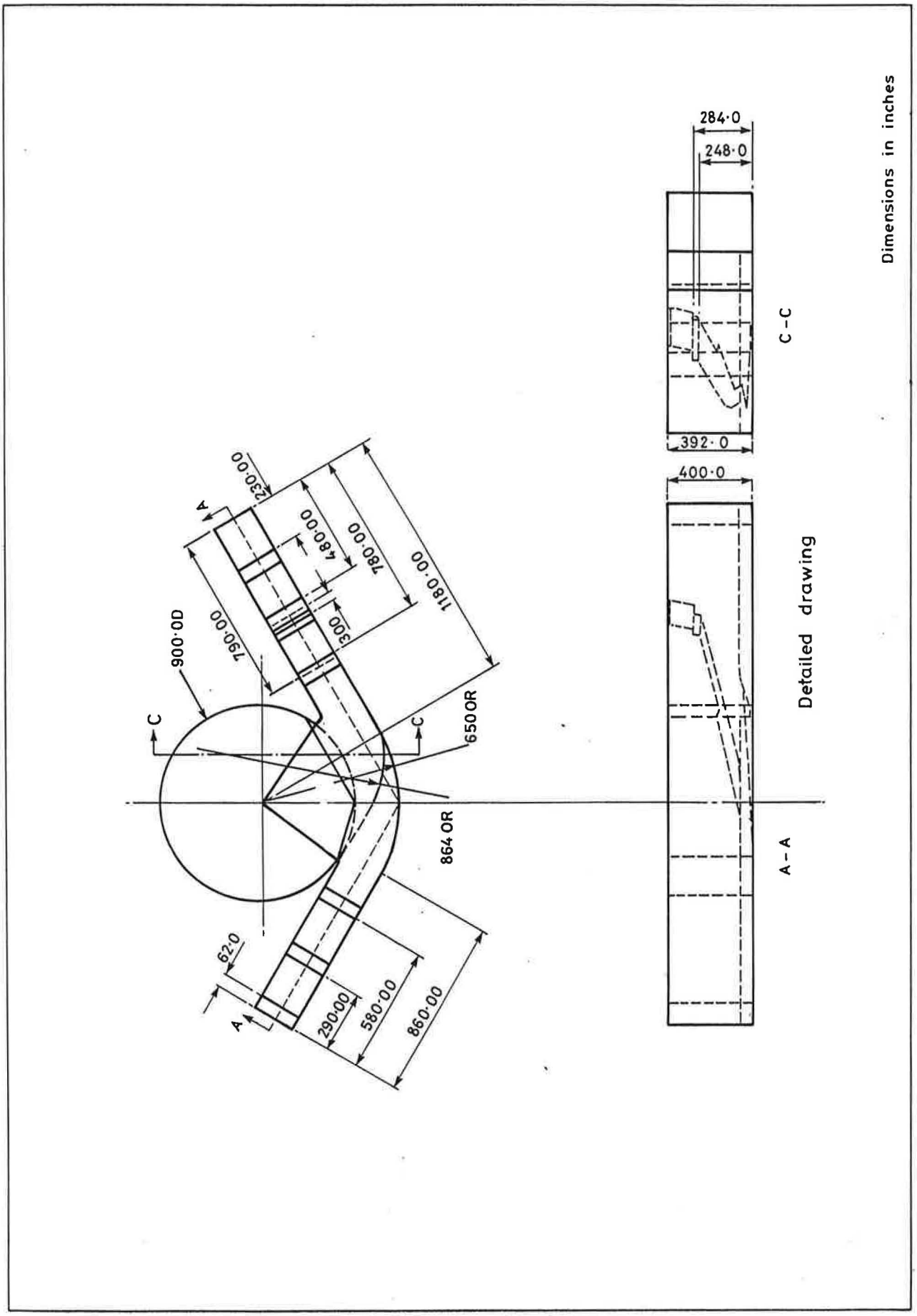

Fig 2 Design details of the vortex separator (Curi et al, 1975)

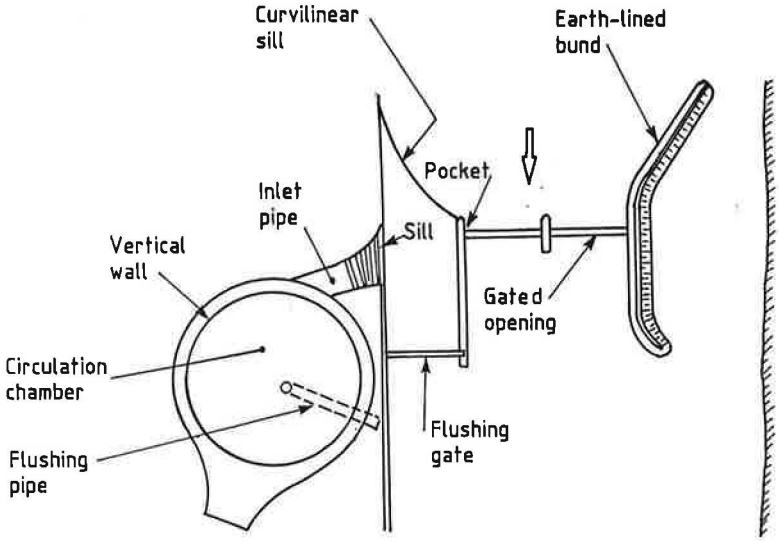

(a) Dam with a circulation water-intake chamber

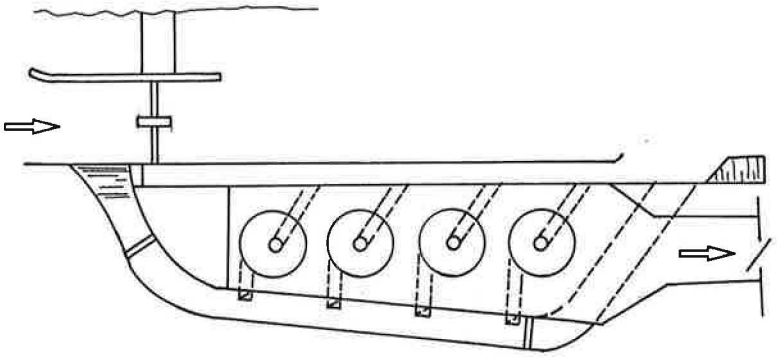

(b) Water intake structure with a series of circulation chambers

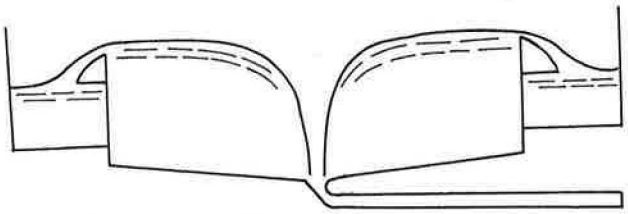

(c) Free surface flow profile in a circulation chamber

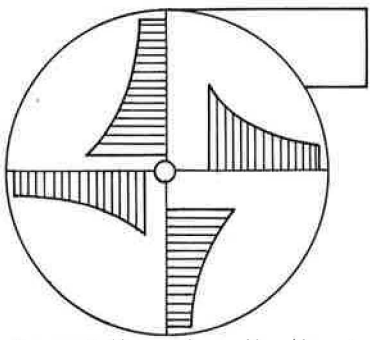

(d) Peripheral velocity variations along the the chamber radius

Fig 3 Design of circulation chamber (s) (Salakhov, 1975)

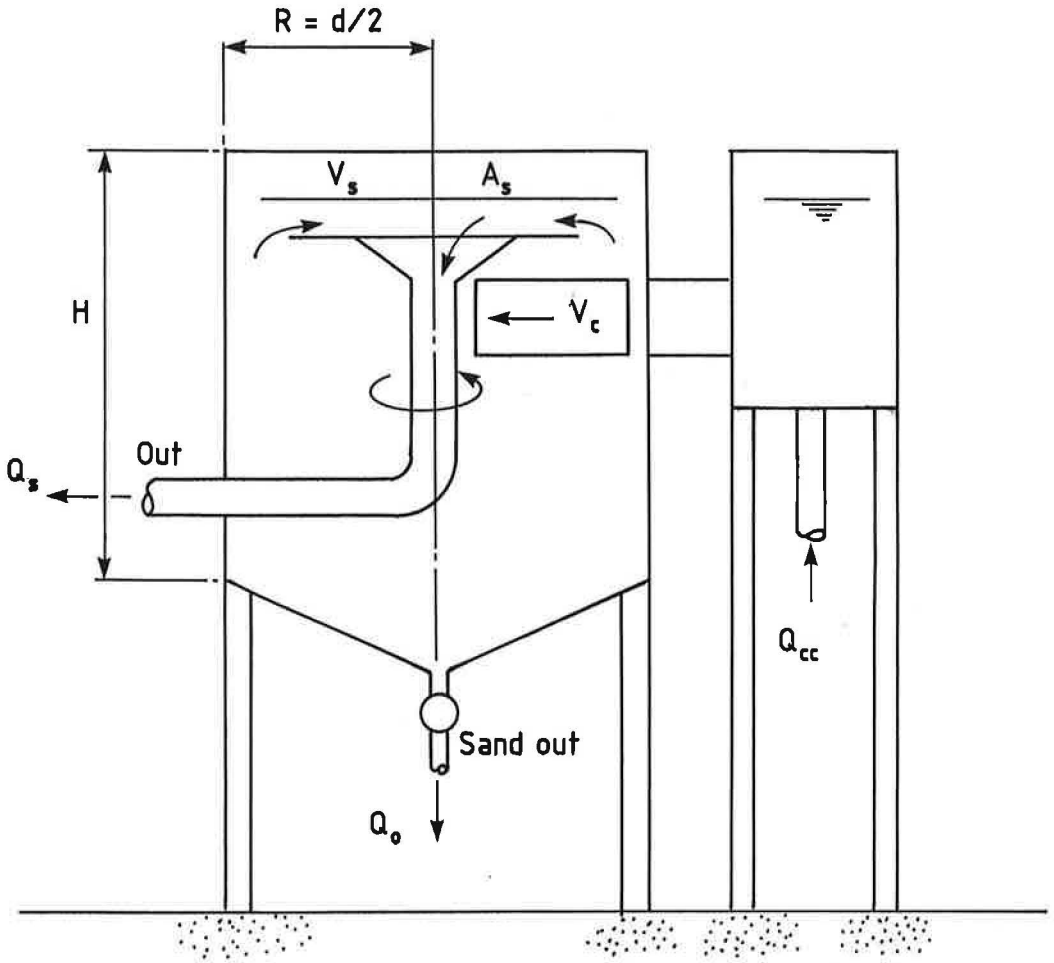

Fig 4 Rotating flow sediment separator
(Ogihara & Sakaguchi, 1984)

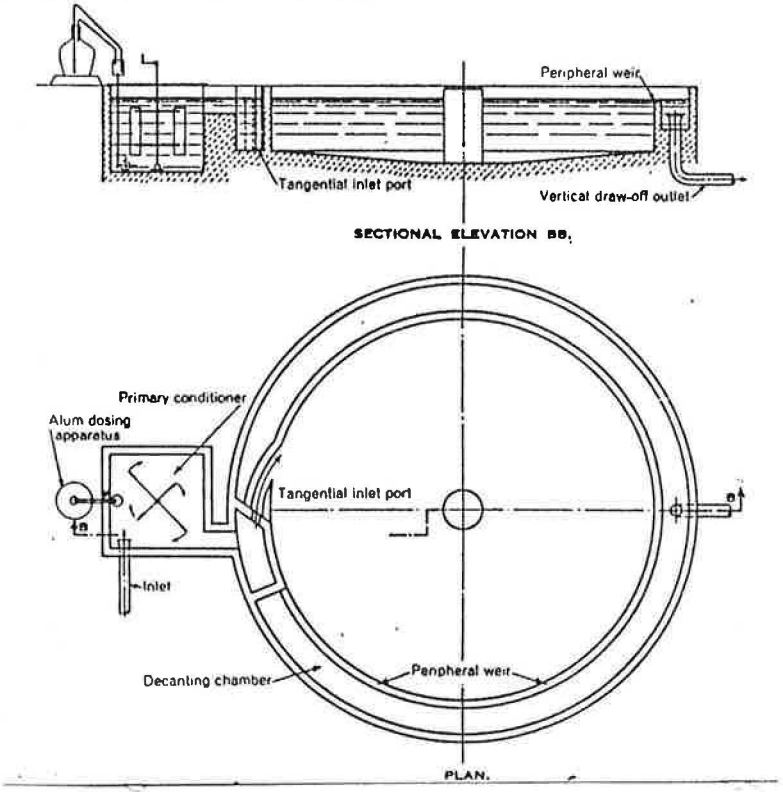

(a) Circular chamber and tangential inlet

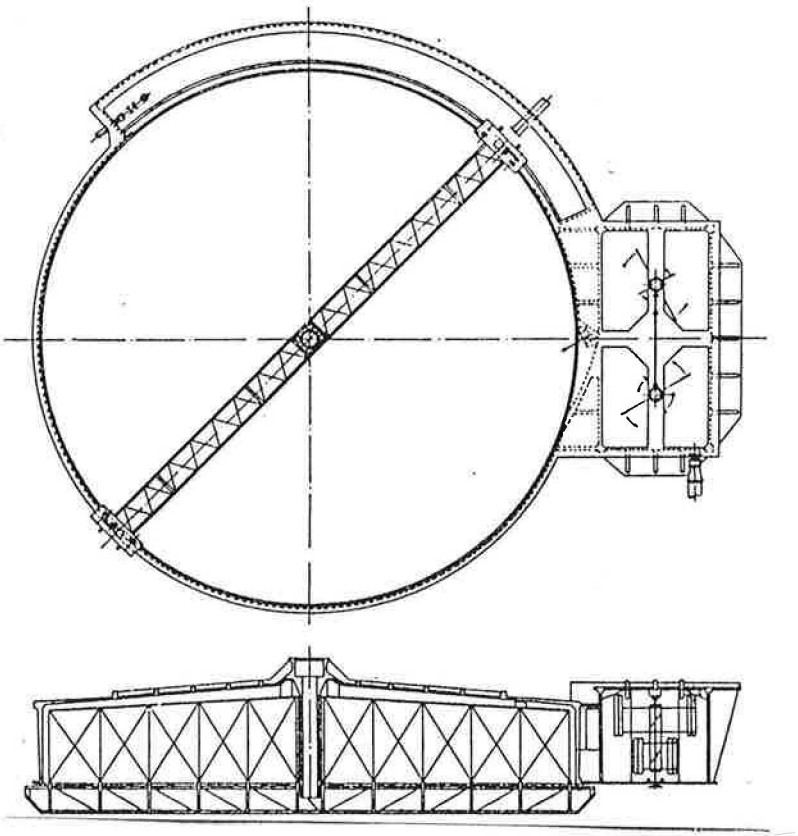

(b) Circular chamber and vertically upward inlet

Fig 5 Design developments for waterworks clarifiers for City of Alexandria (Egypt)

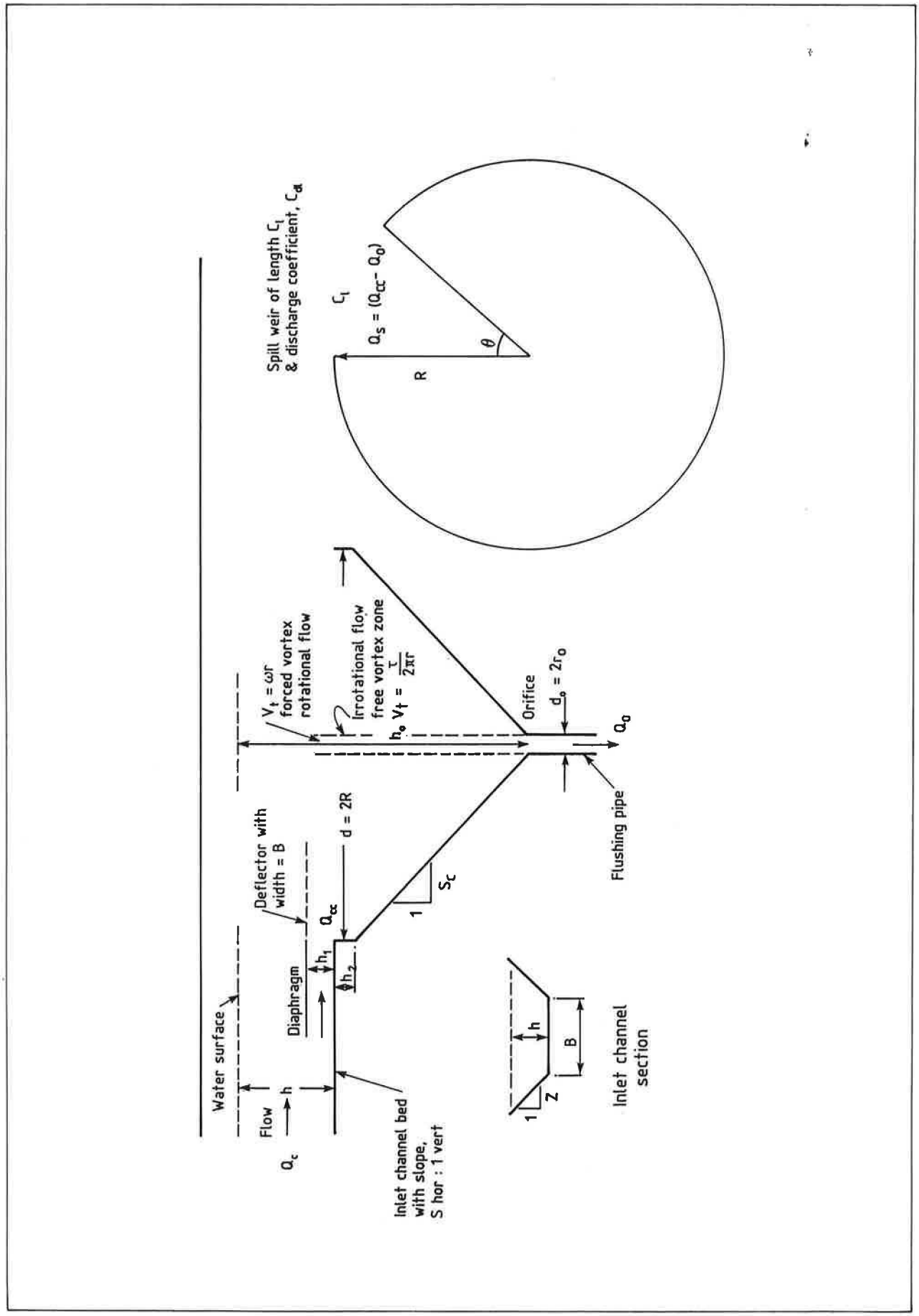

Fig 6 Definition sketch

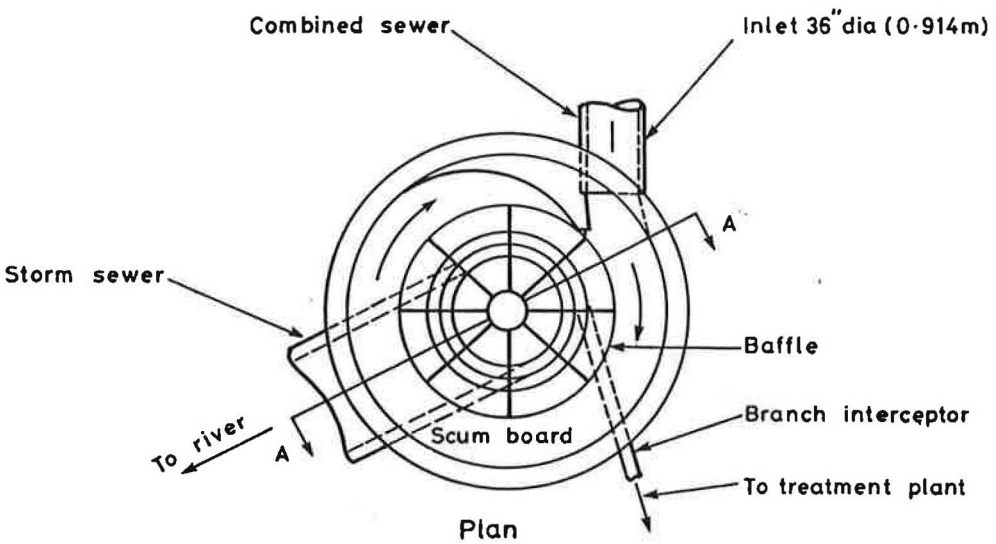

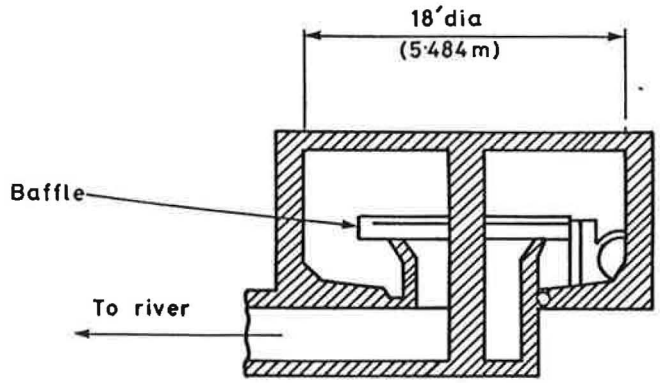

Fig 7 White Ladies Road - vortex regulator

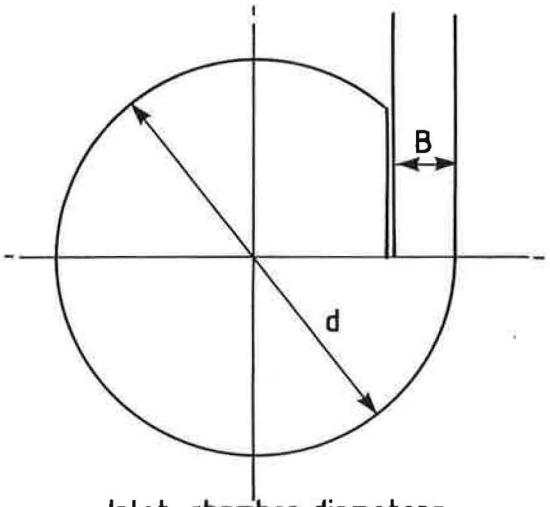

Inlet, chamber diameters

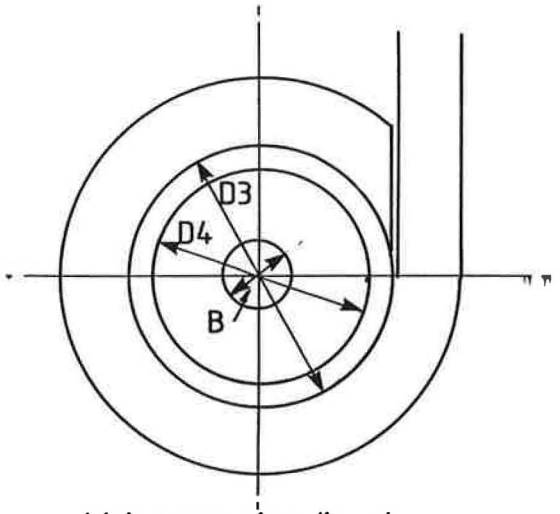

Weir, scum ring diameters

B = unit
h_4 = B/2
h_2 = 5/6B
R_4 = 11/8B
d = 6B
h_3 = D_1/3
R_1 = 7/3B
R_5 = 11/3B

D_3 = 4B
b_1 = B/3
R_2 = 11/2B
b_2 = B/6
D4 = 10/3B
d_1 = 3/2B
R_3 = 5/8B

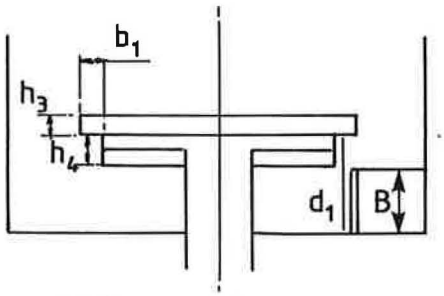

Weir, scum ring details

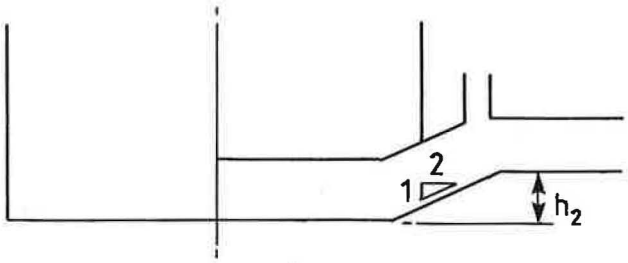

Inlet detail

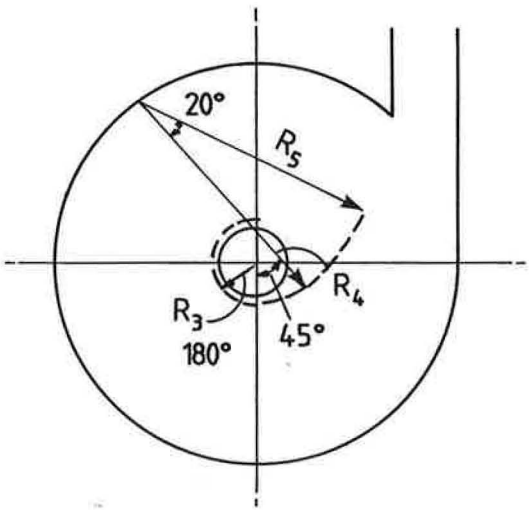

Centreline secondary gutter

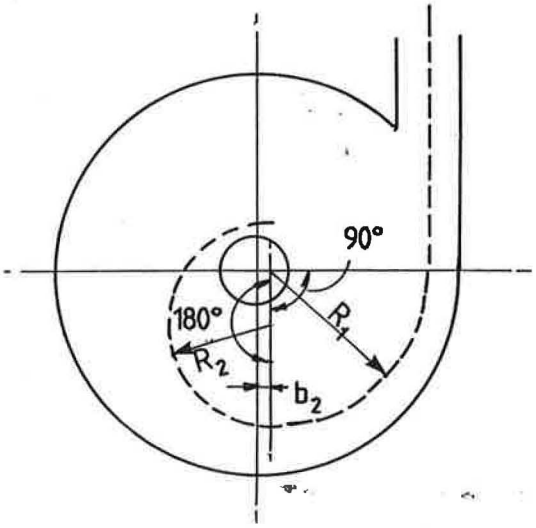

Centreline primary gutter

Fig 8 Design details of Lancaster swirl concentrator as a combined overflow regulator

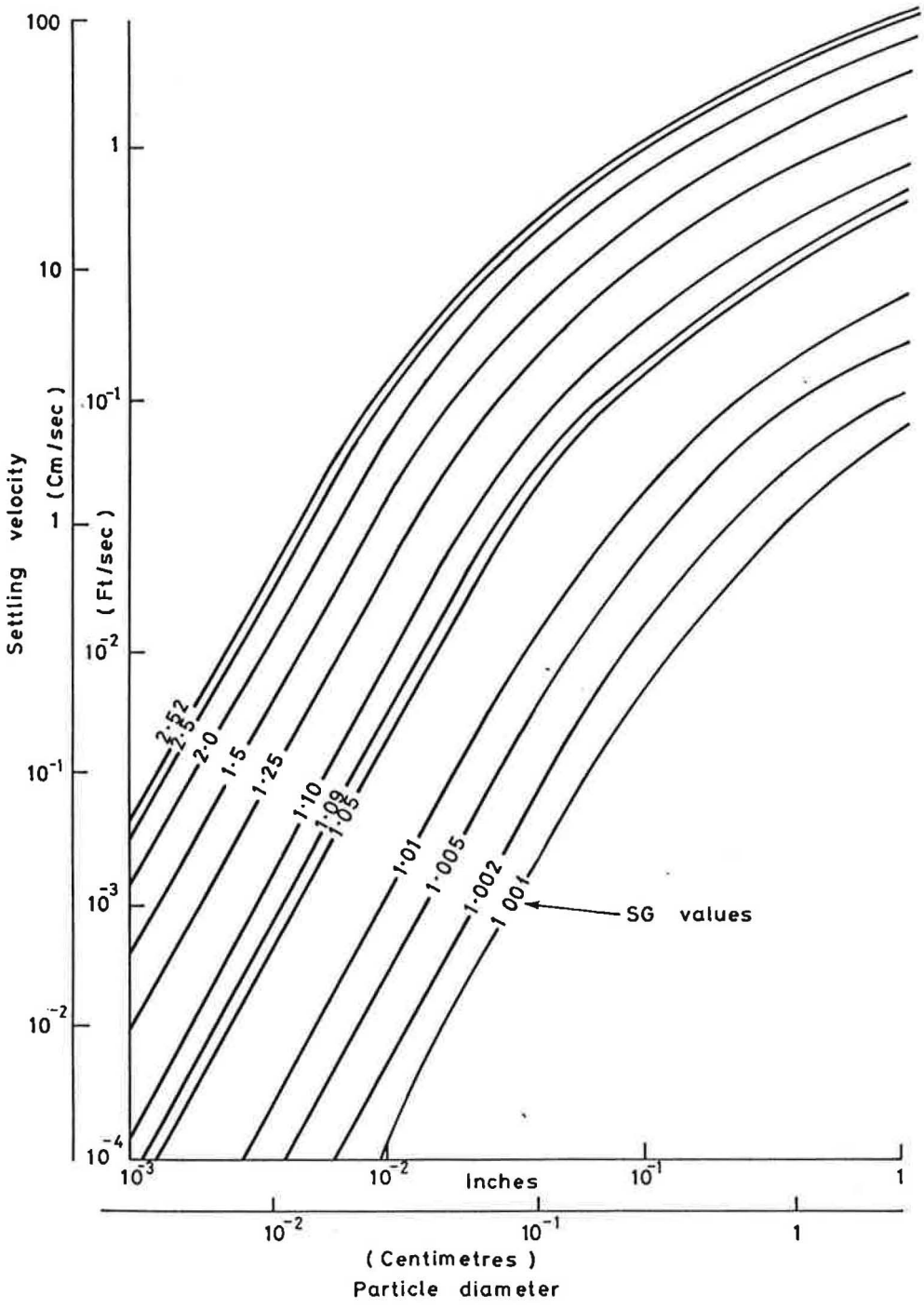

Fig 9 Particle settling rates

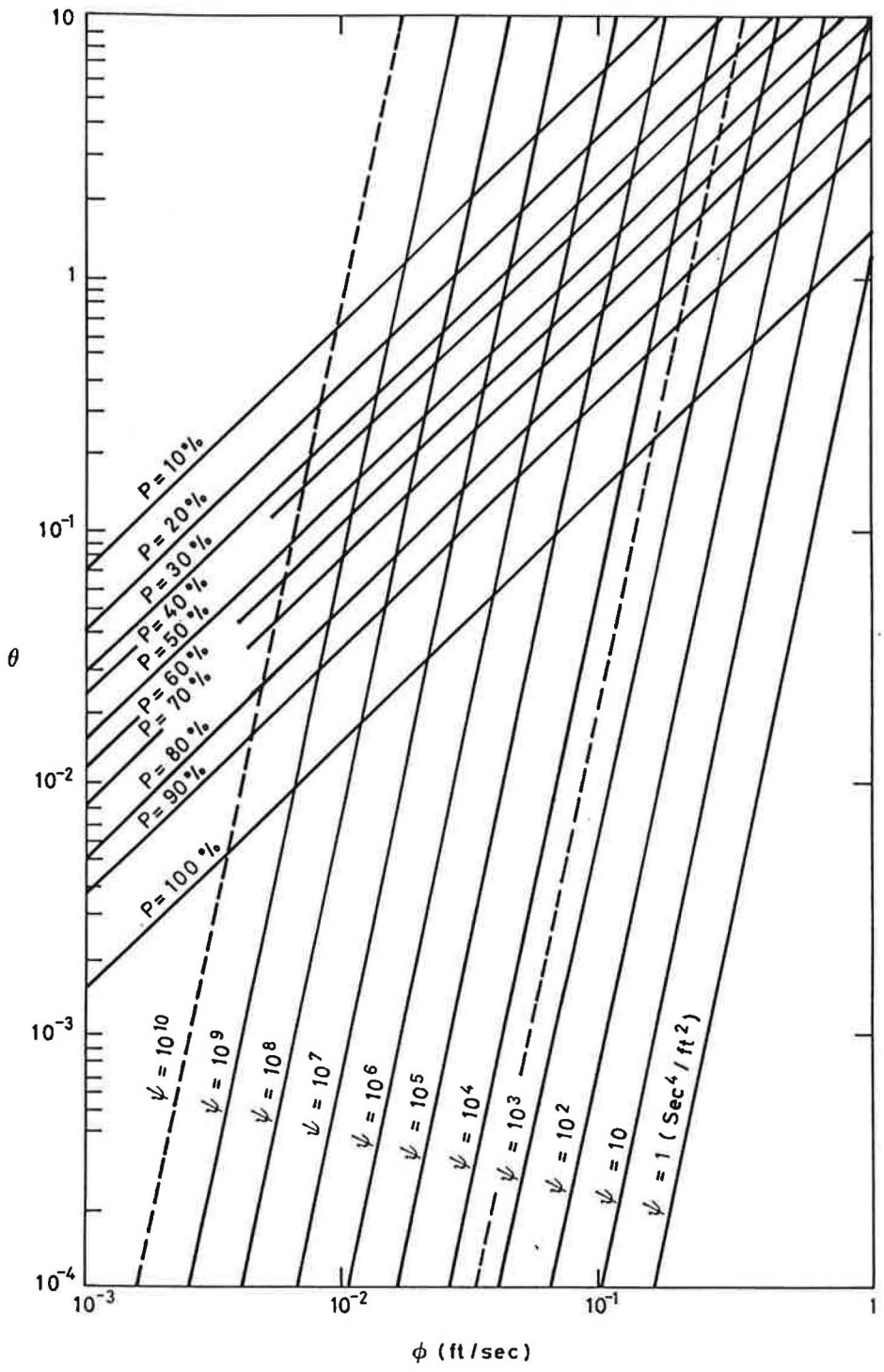

Fig 10 Scale factor diagram

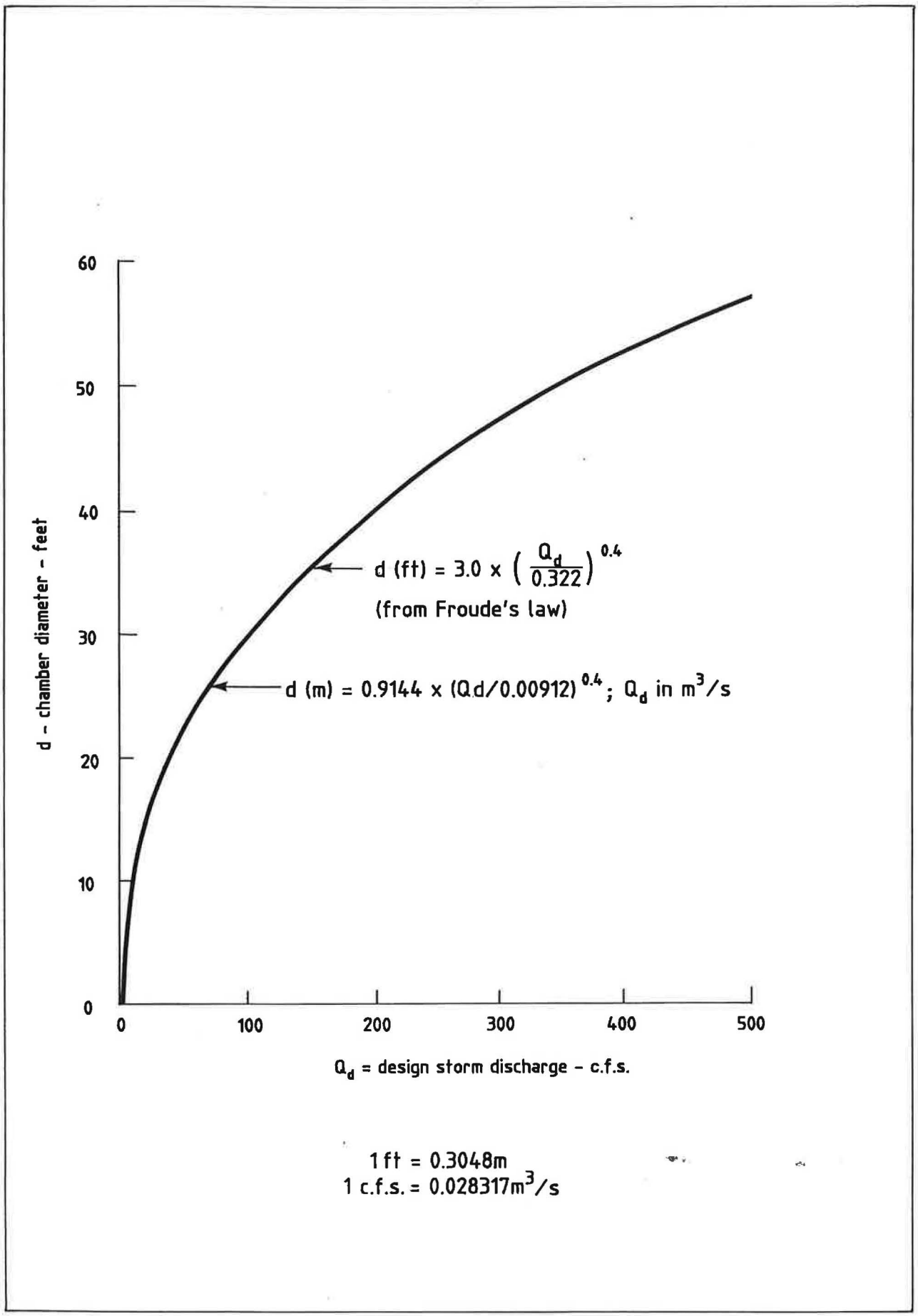

Fig 11 Storm discharge vs chamber diameter

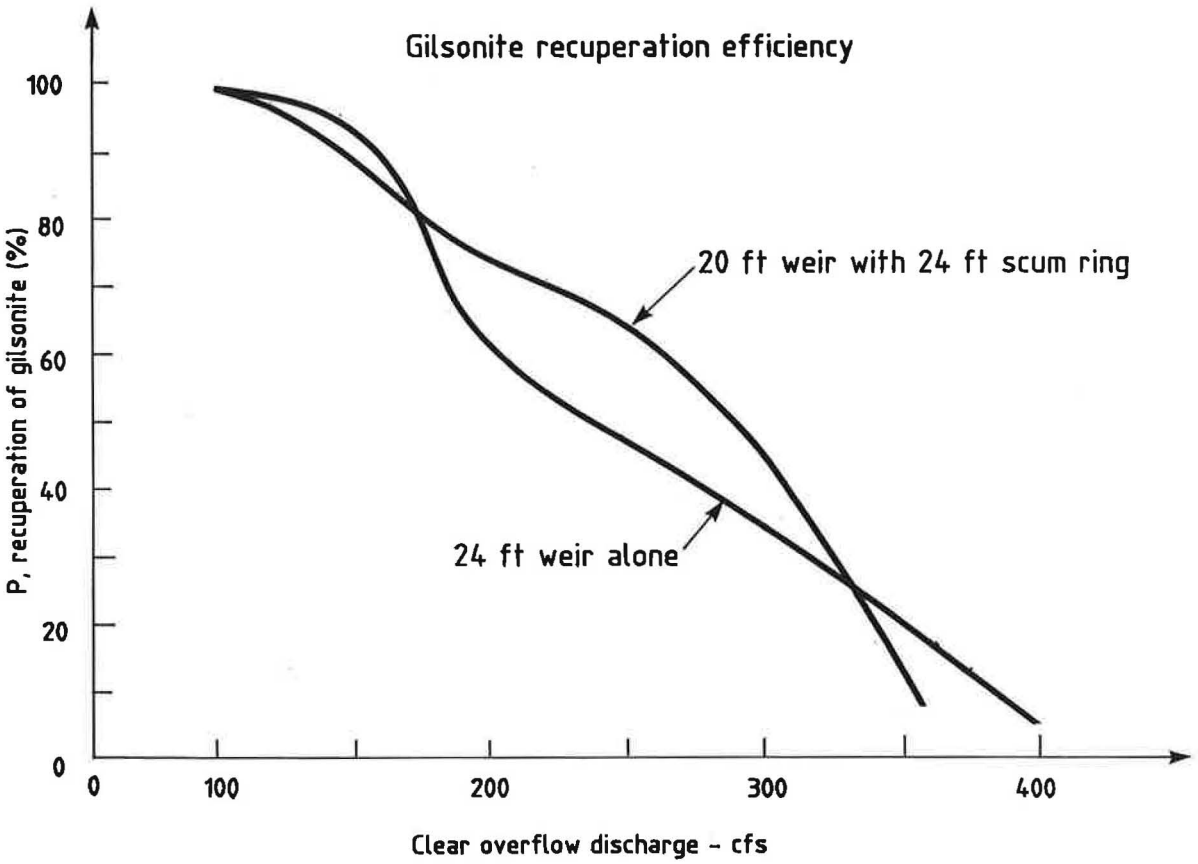

1 ft = 0.3048m
1 c.f.s. = 0.028317m^3/s

Fig 12 Stage discharges and efficiency curves.

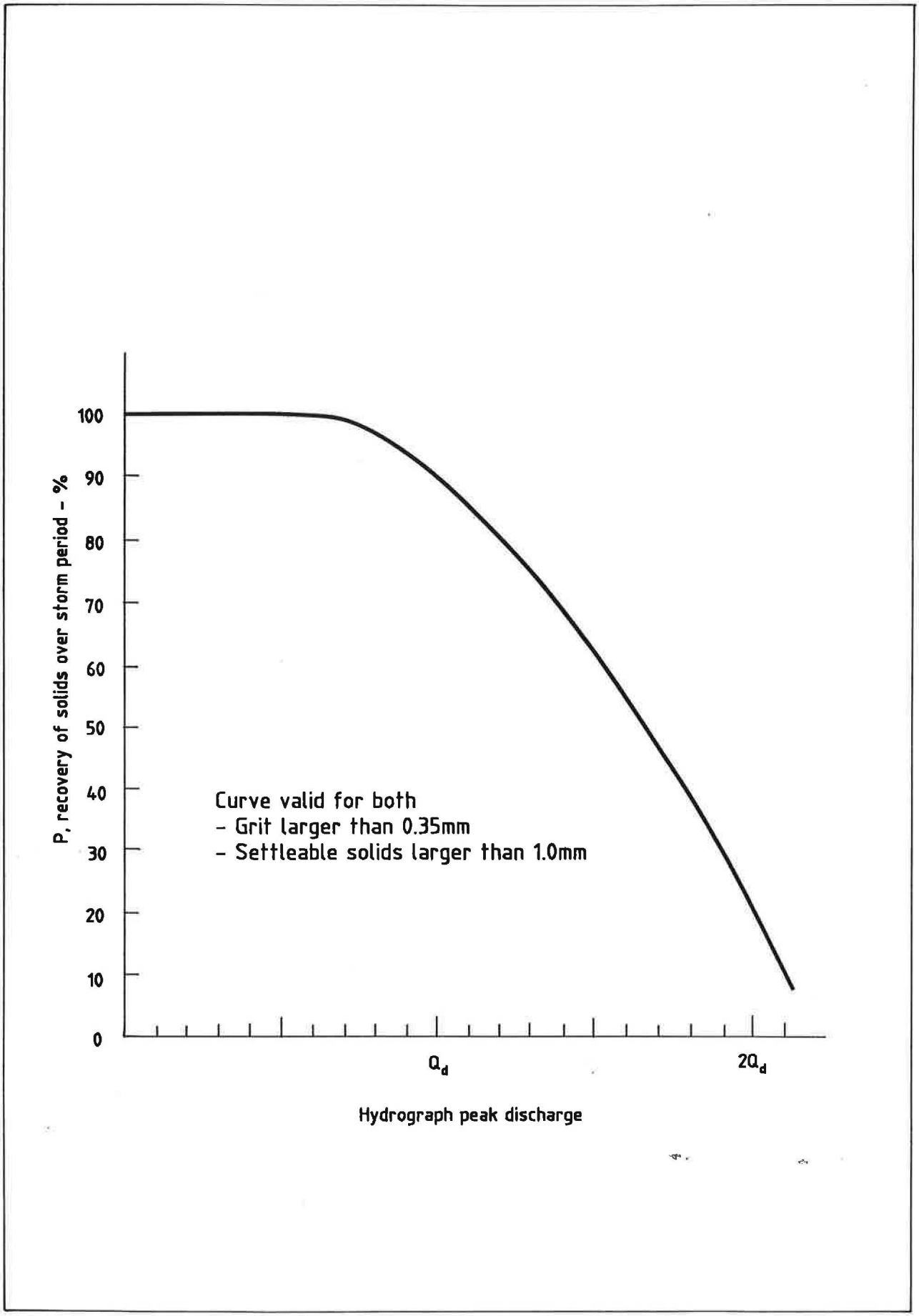

Fig 13 Separation efficiency curve

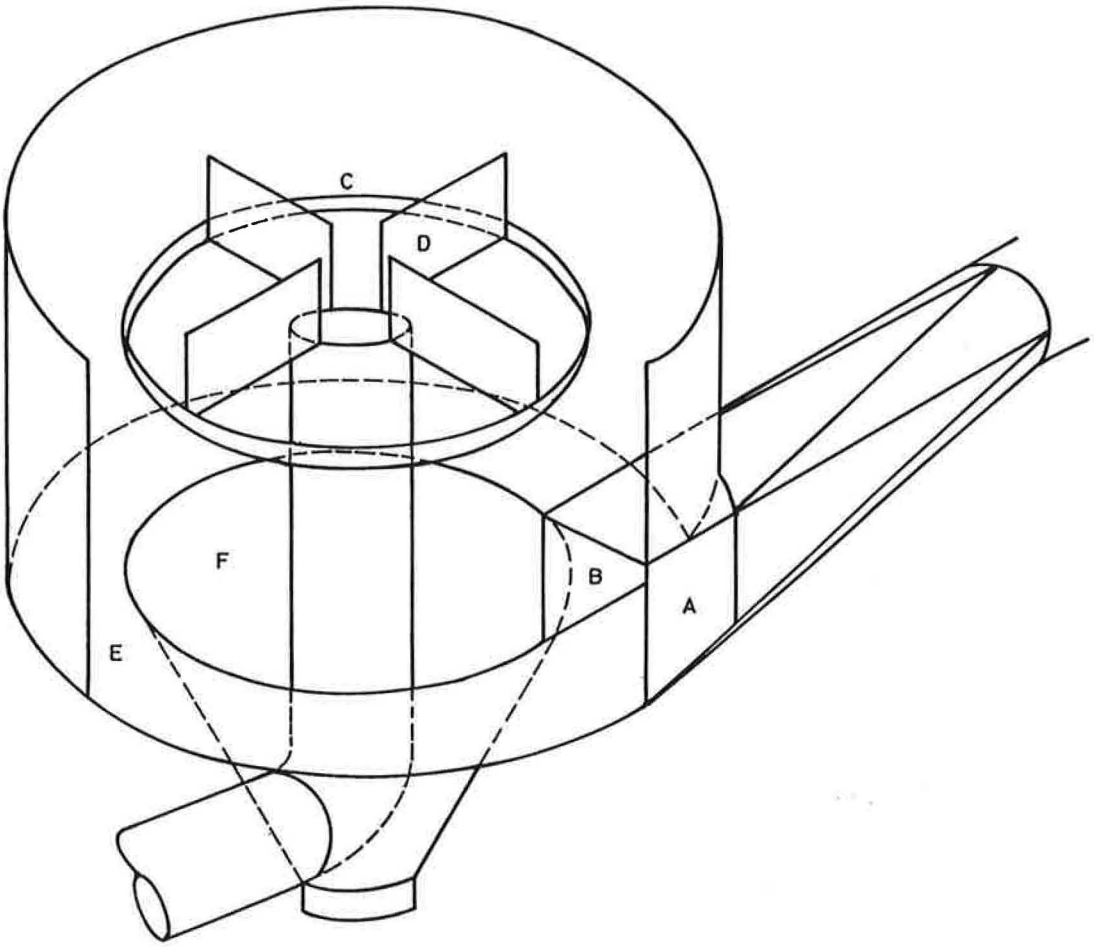

A Inlet
B Deflector
C Weir and weir plate
D Spoiler
E Floor
F Content hopper

Fig 14 Isometric view - swirl concentrator as a grit separator

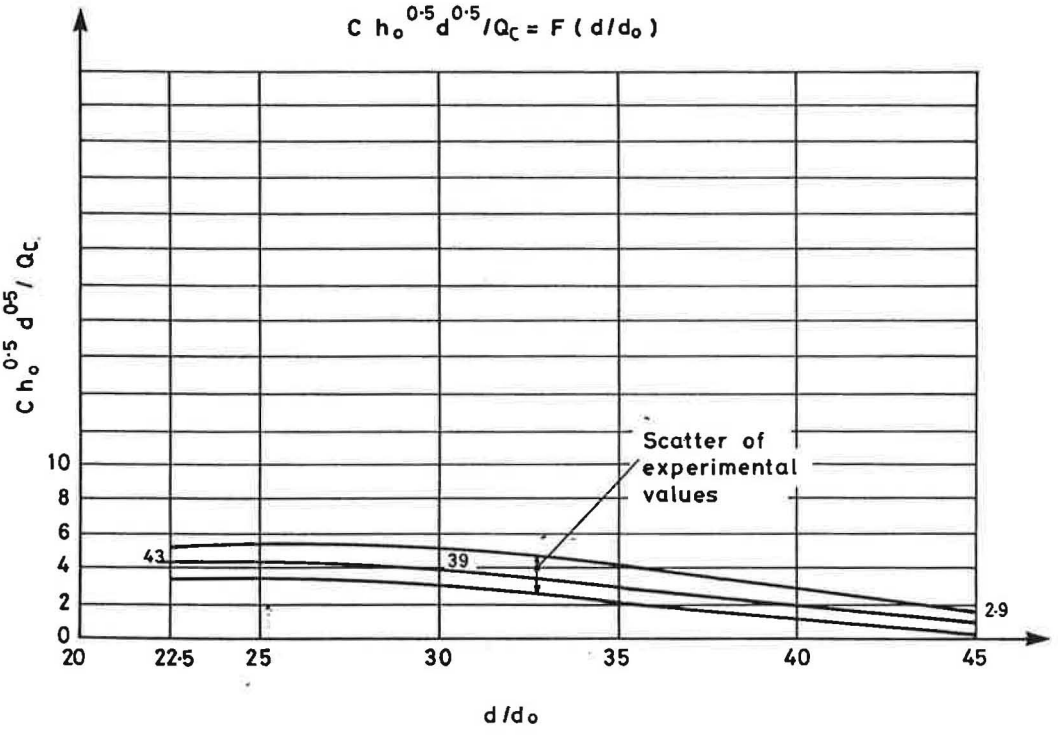

Fig 15 Plot of constant C of free vortex as a function of d/d_o

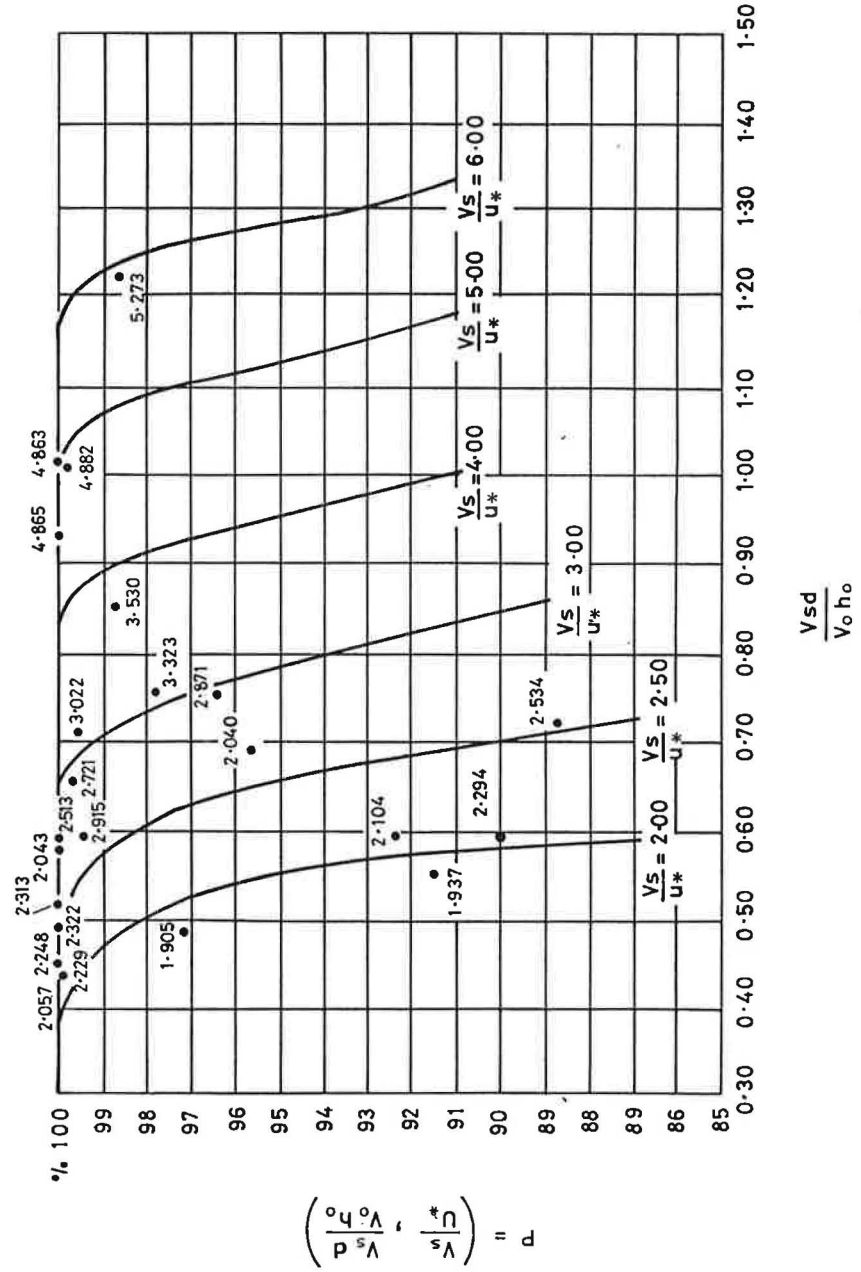

Fig 16 Sediment removal function for vortex type settling basins

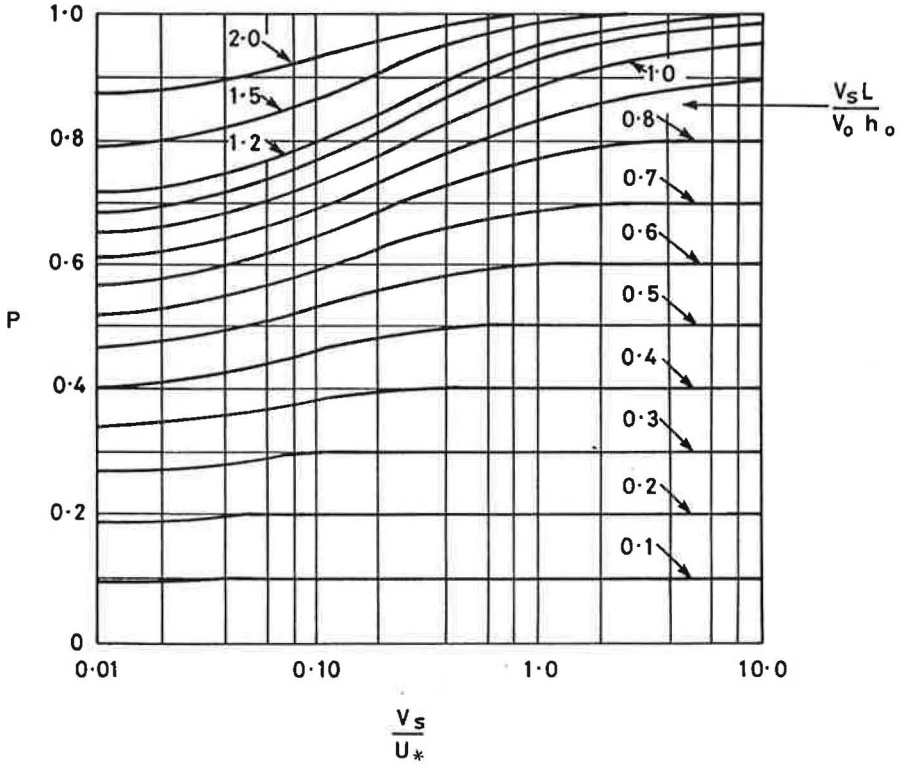

Fig 17 Sediment removal function for classical settling basin

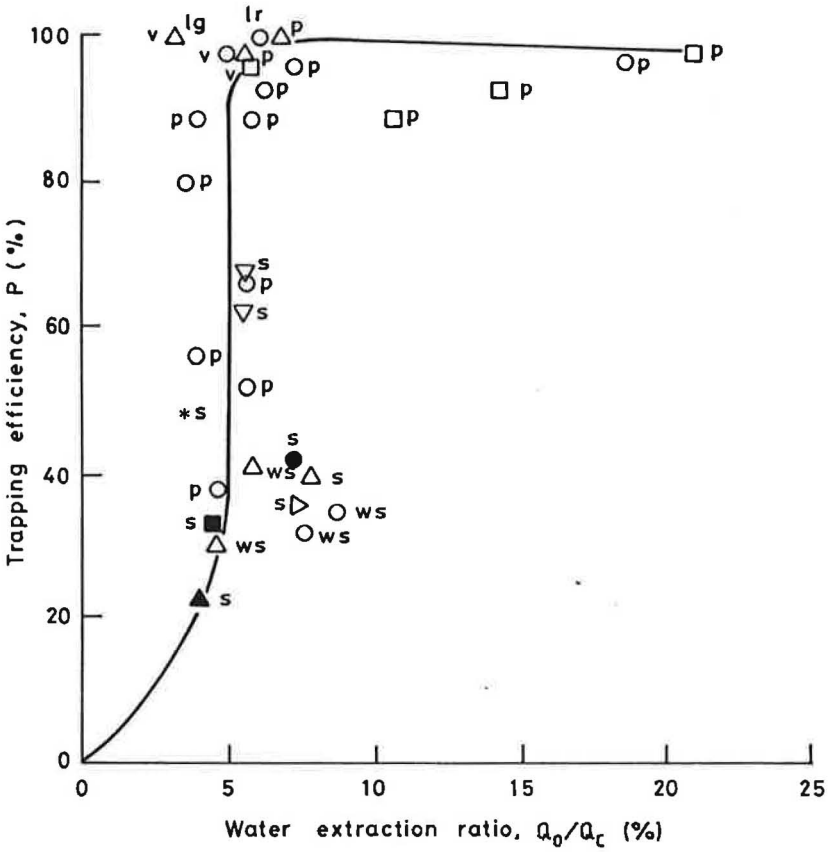

Key

d/B	d/do			
5	18 □	30 ▽	36 ○	72 △
4	24 *	60 ▷	80 ■	96 ▲
* 3	45 ●			

Curi, et al (1975a) data

Polystyrene = p
Lentil green = lg
Lentil red = lr
Volcanic tuff = v
Wood shavings = ws

IPRI data (Paul (1983))

Sand = s

Note:
All parameters are in MKS system

Fig 18 Variation of trapping efficiency with water extraction ratio

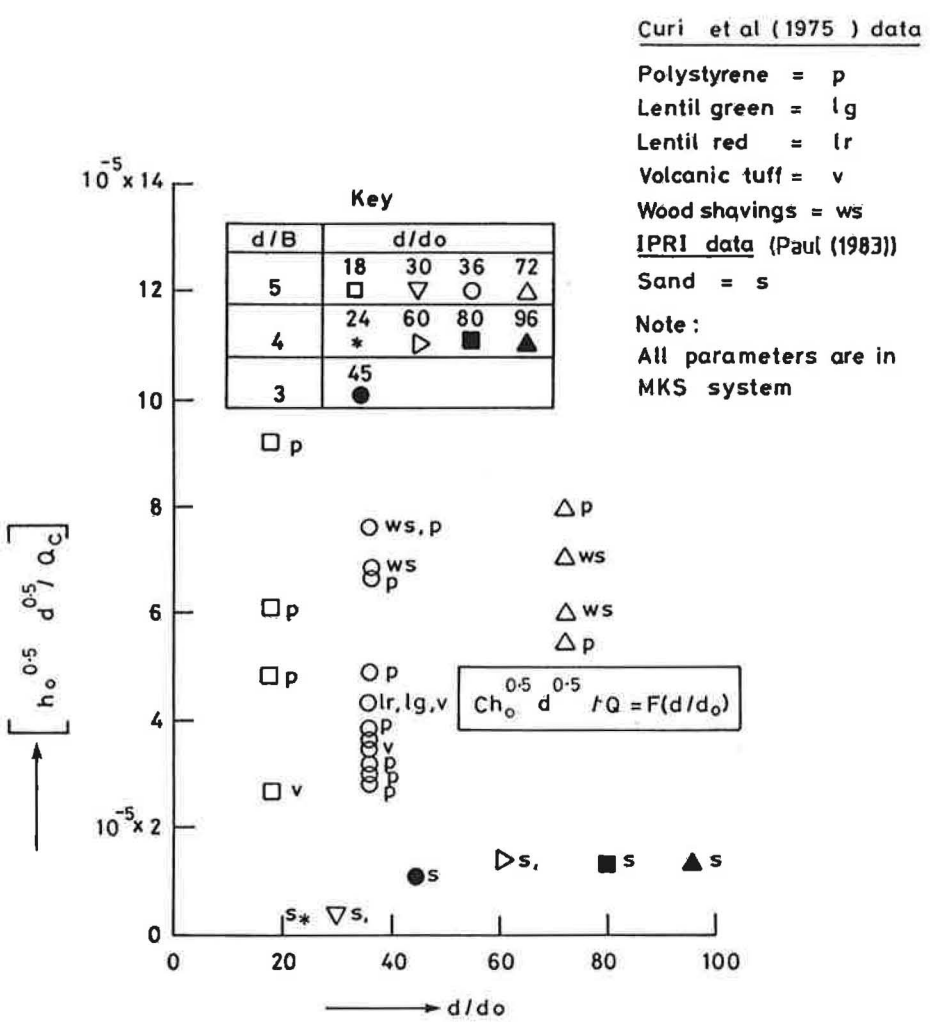

Fig 19 Evaluation of function C of the free-vortex from available data

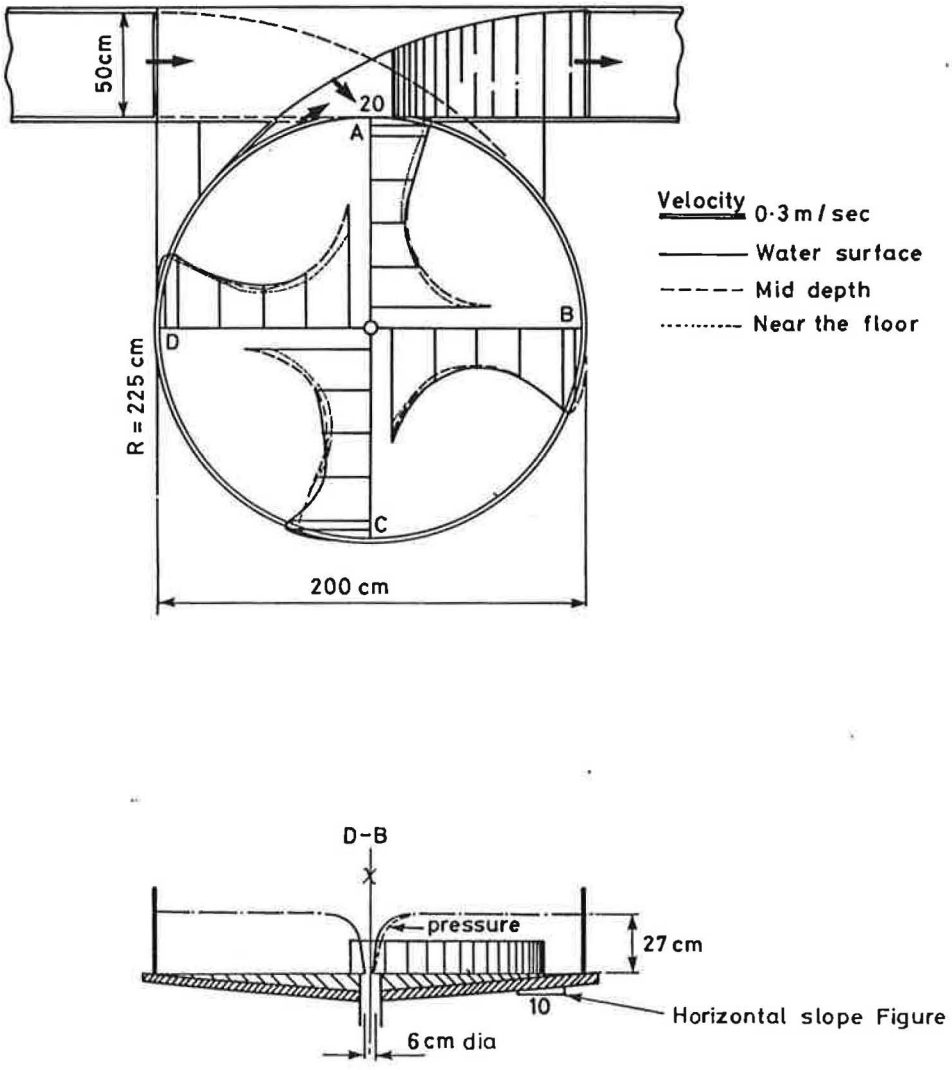

Fig 20 Typical velocity distribution, water surface and pressure profiles (tangential exit with horizontal floor variant)

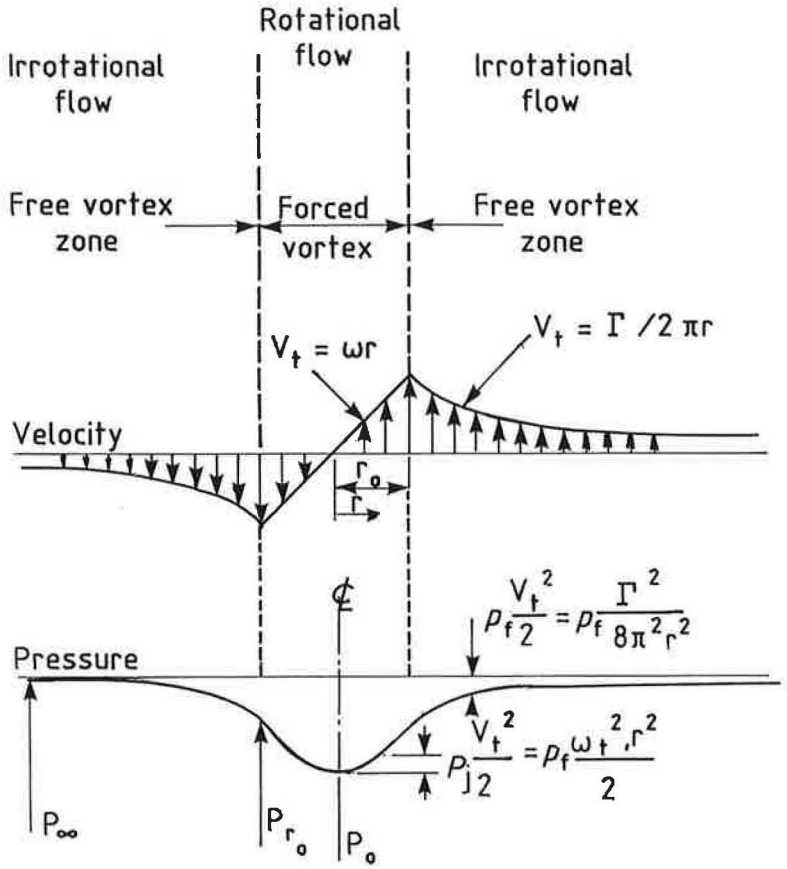

Fig 21 Velocity and pressure distribution in a two-dimensional Rankine combined vortex

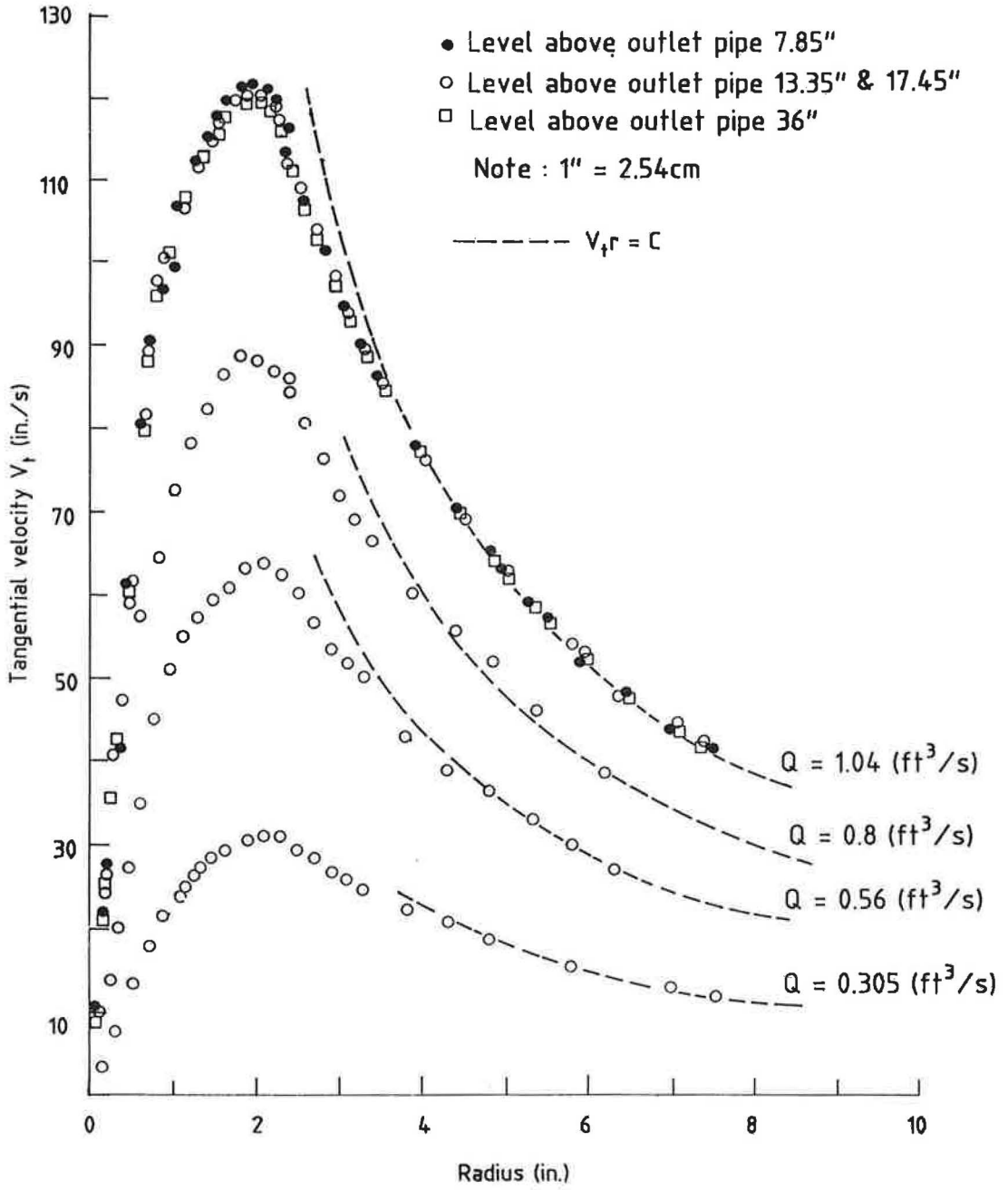

Fig 22 Distribution of tangential velocity

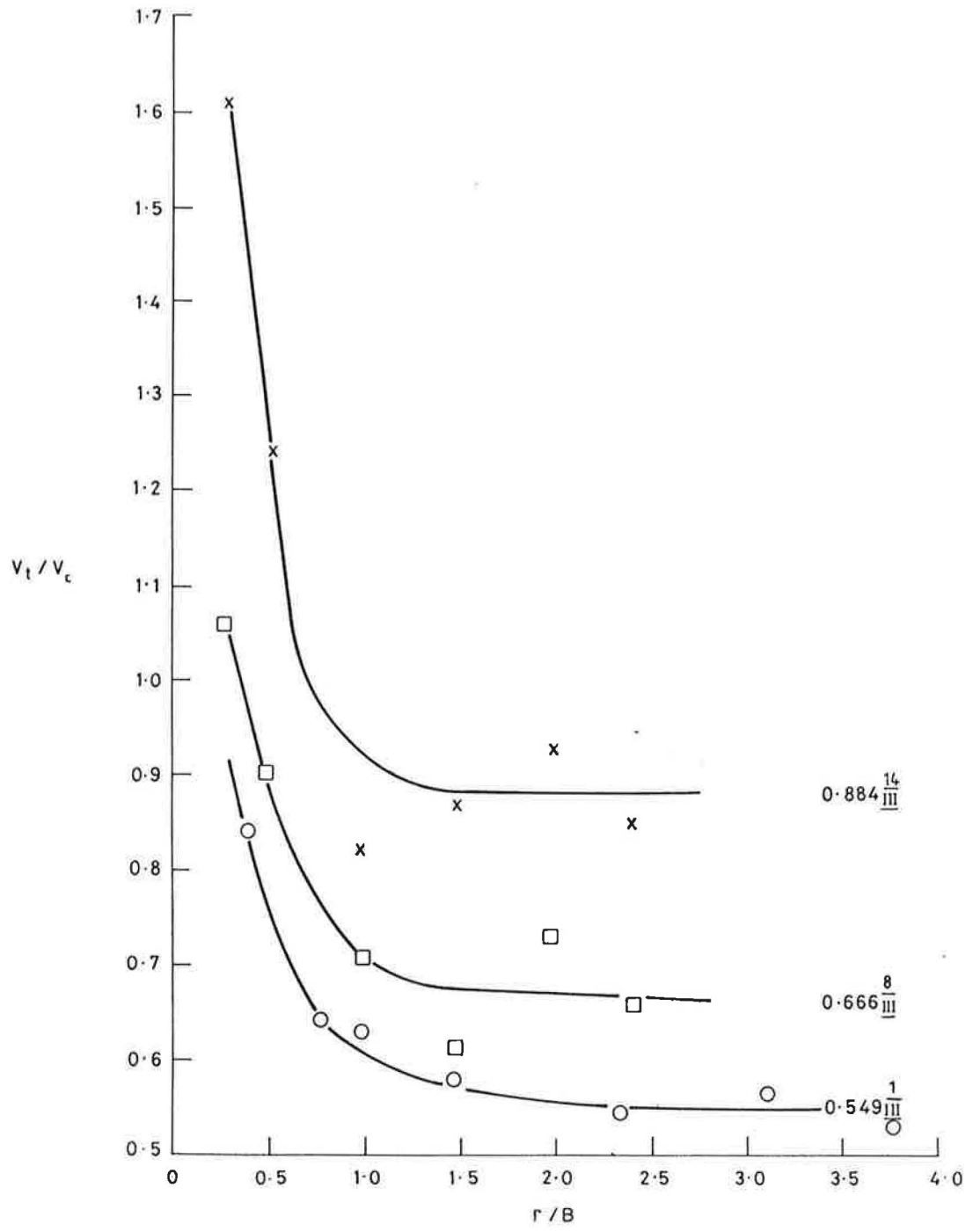

Eig 23 Distribution of tangential velocity in circulation chamber

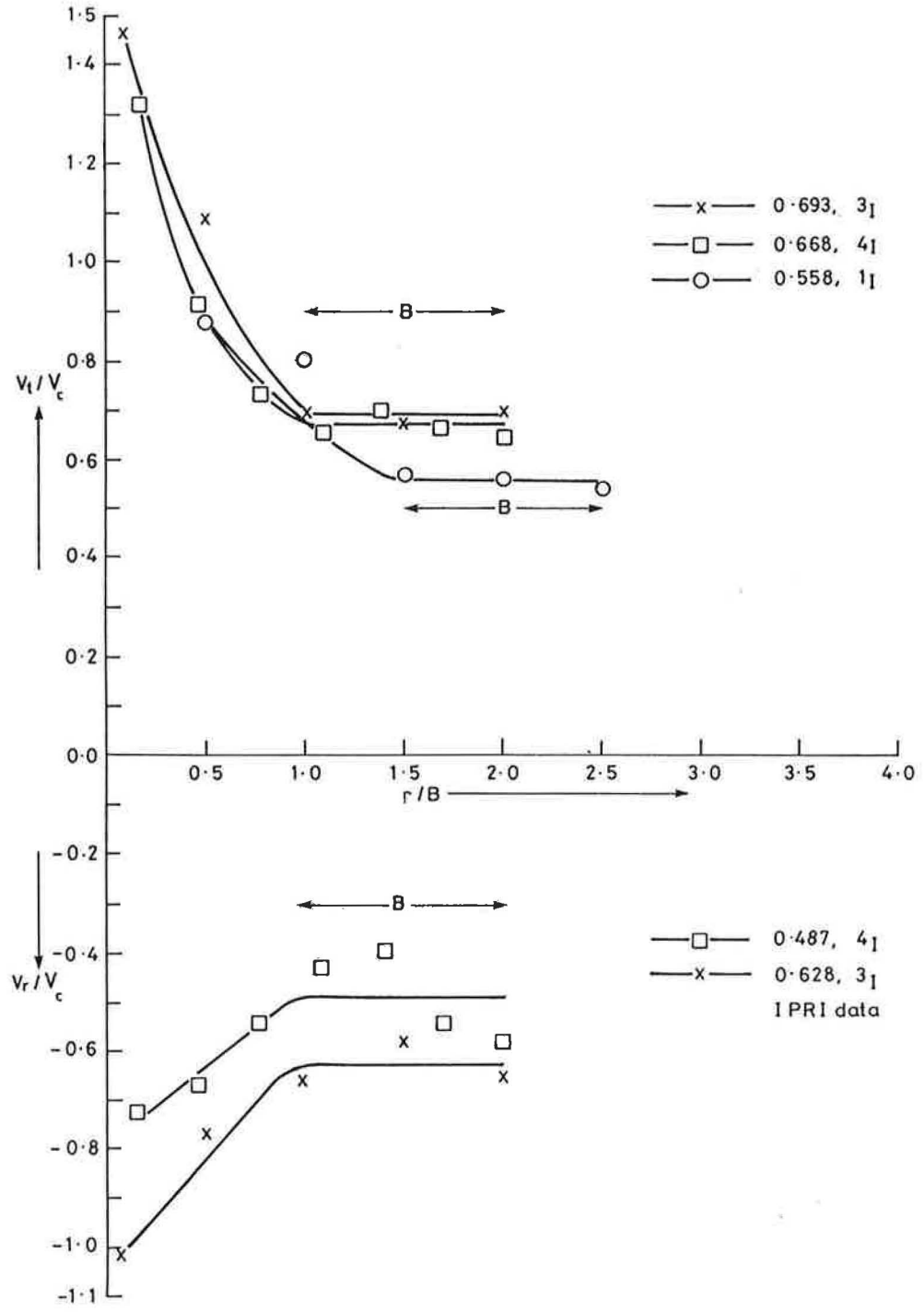

Fig 24 Distribution of tangential and radial velocities in circulation chamber

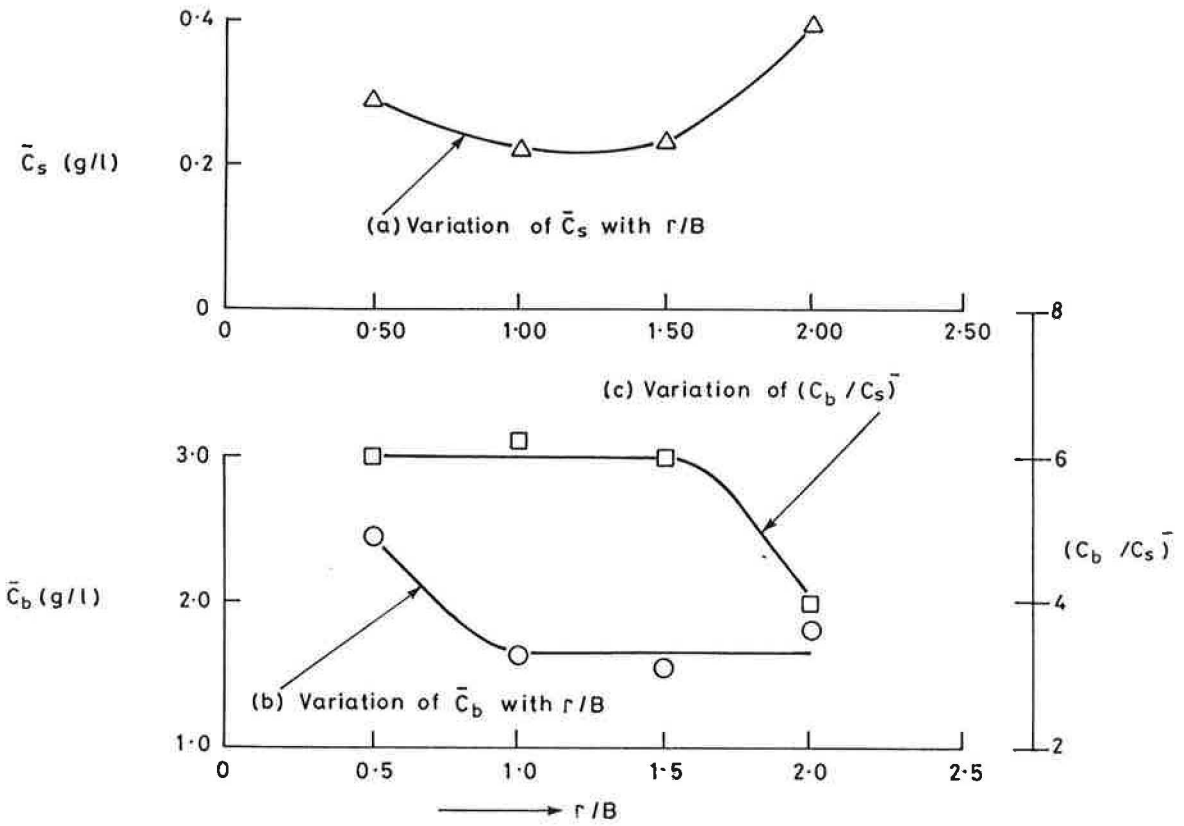

Fig 25 Distribution of sediment concentration in circulation chamber

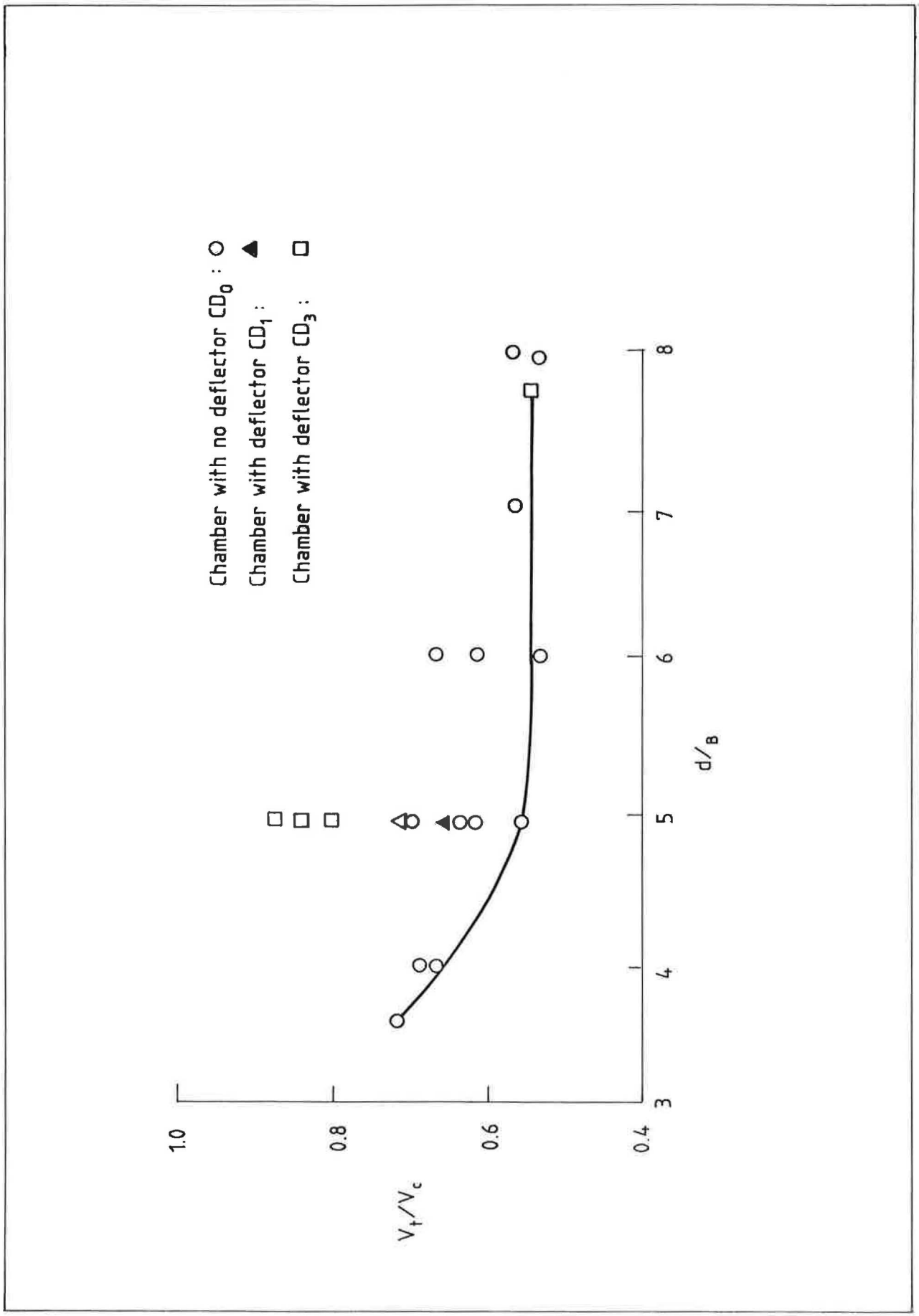

Fig 26 Effect of ratio of circulation chamber dia due to channel bed width on mean tangential velocity

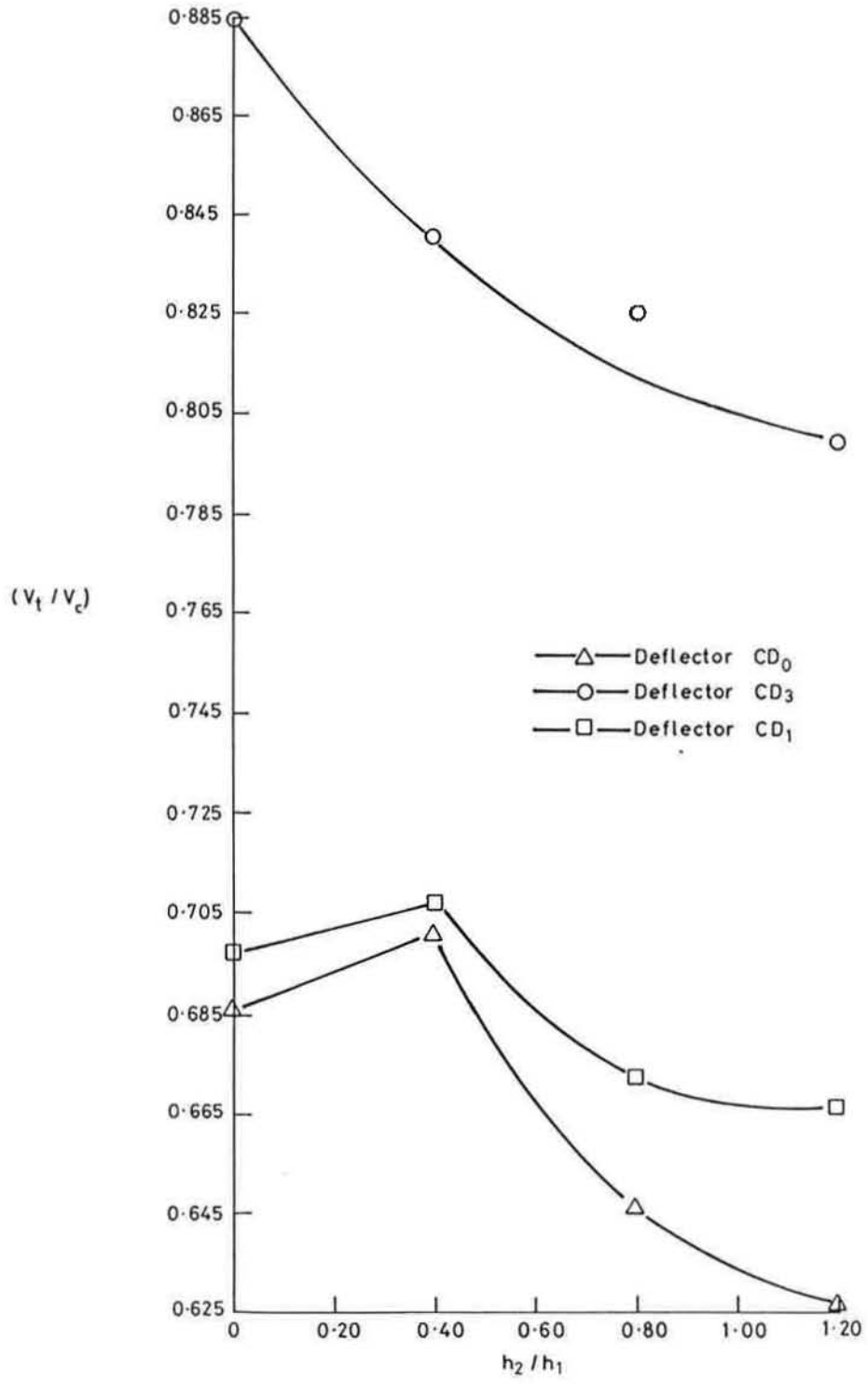

Fig 27 Effect of chamber depth on tangential velocity in constant velocity region

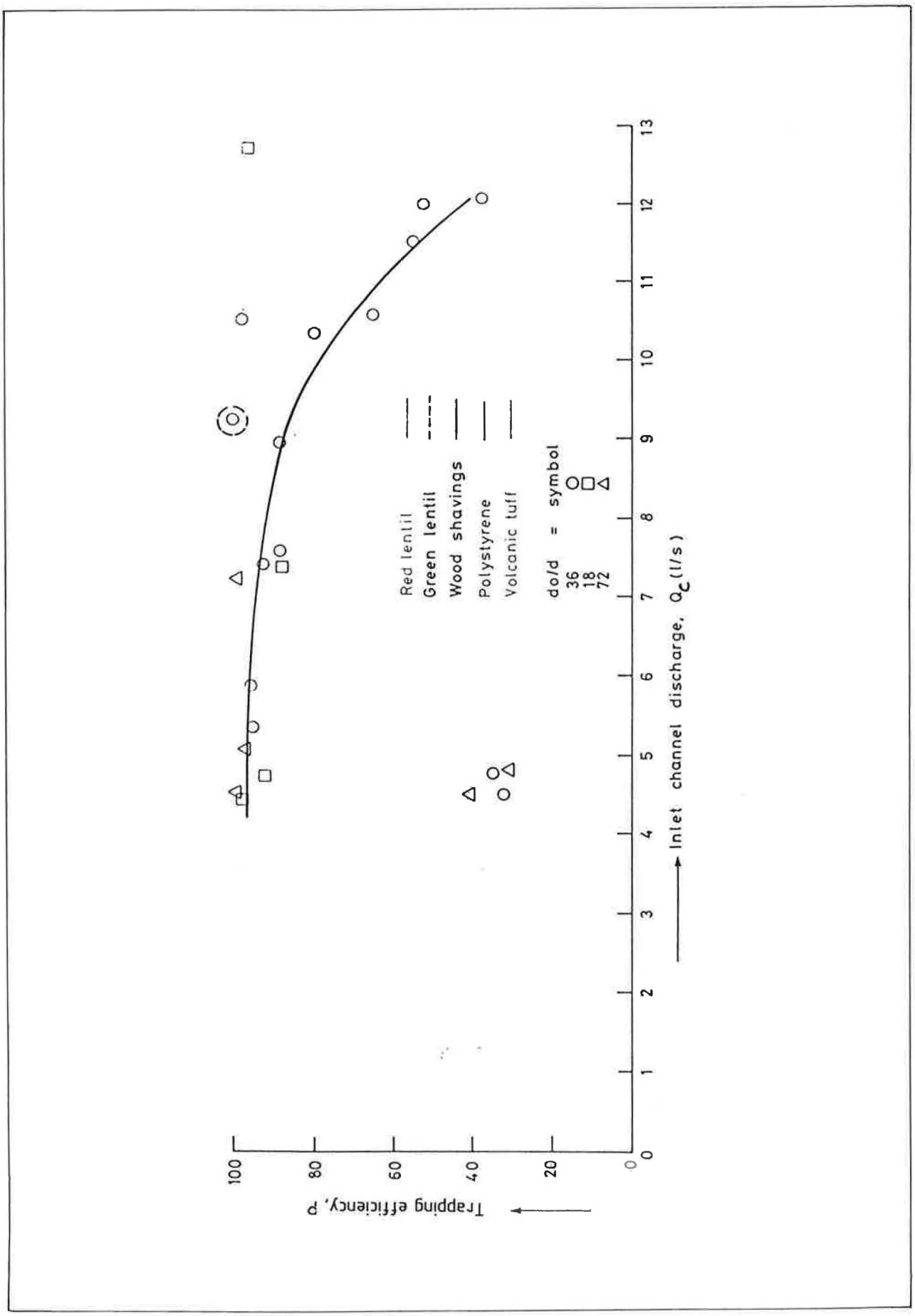

Fig 28 Effect of increased inlet channel discharge on trapping efficiency

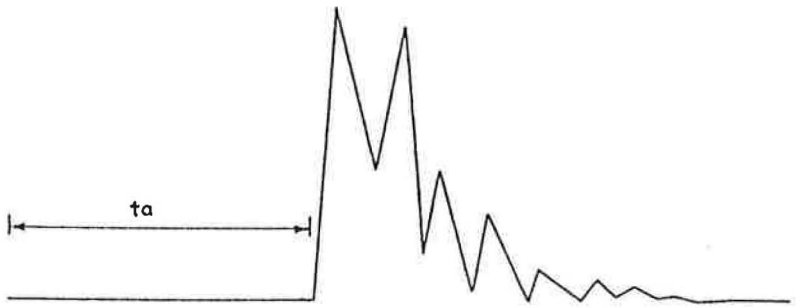

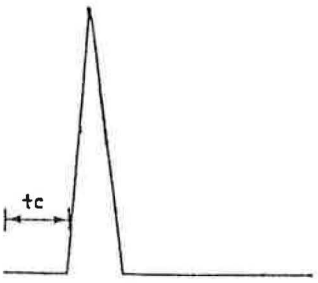

t = ta - tc

t - Detention time

ta - Time the dye takes to travel through the chamber of the colorimeter tube

tc - Time the dye takes to travel through the colorimeter tube

Fig 29 Typical U.V. oscillograph record

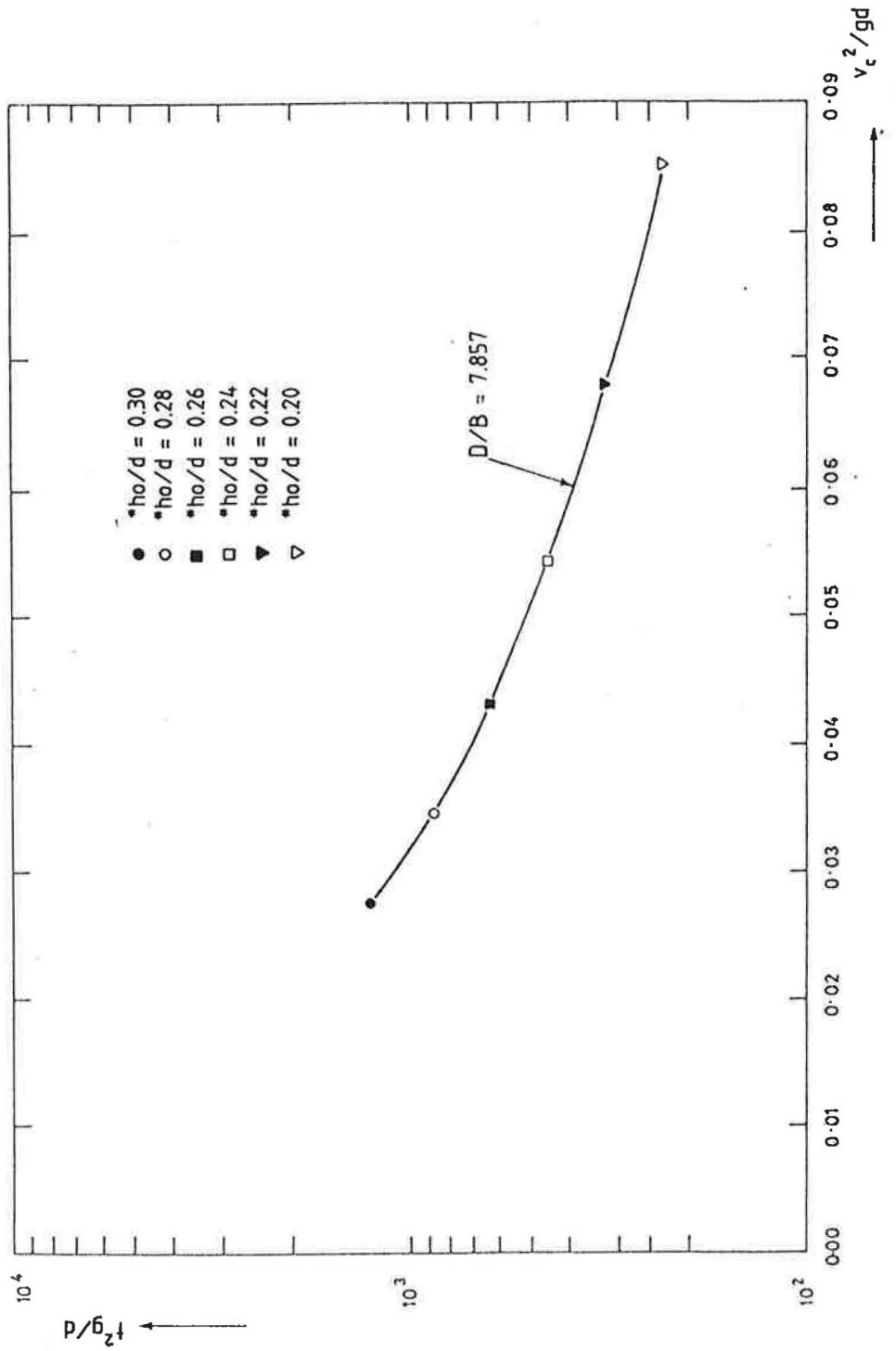

Fig 30 Effect on detention time and entry velocity of varying water levels (*ho), h_2 = 0.02m and CD_3

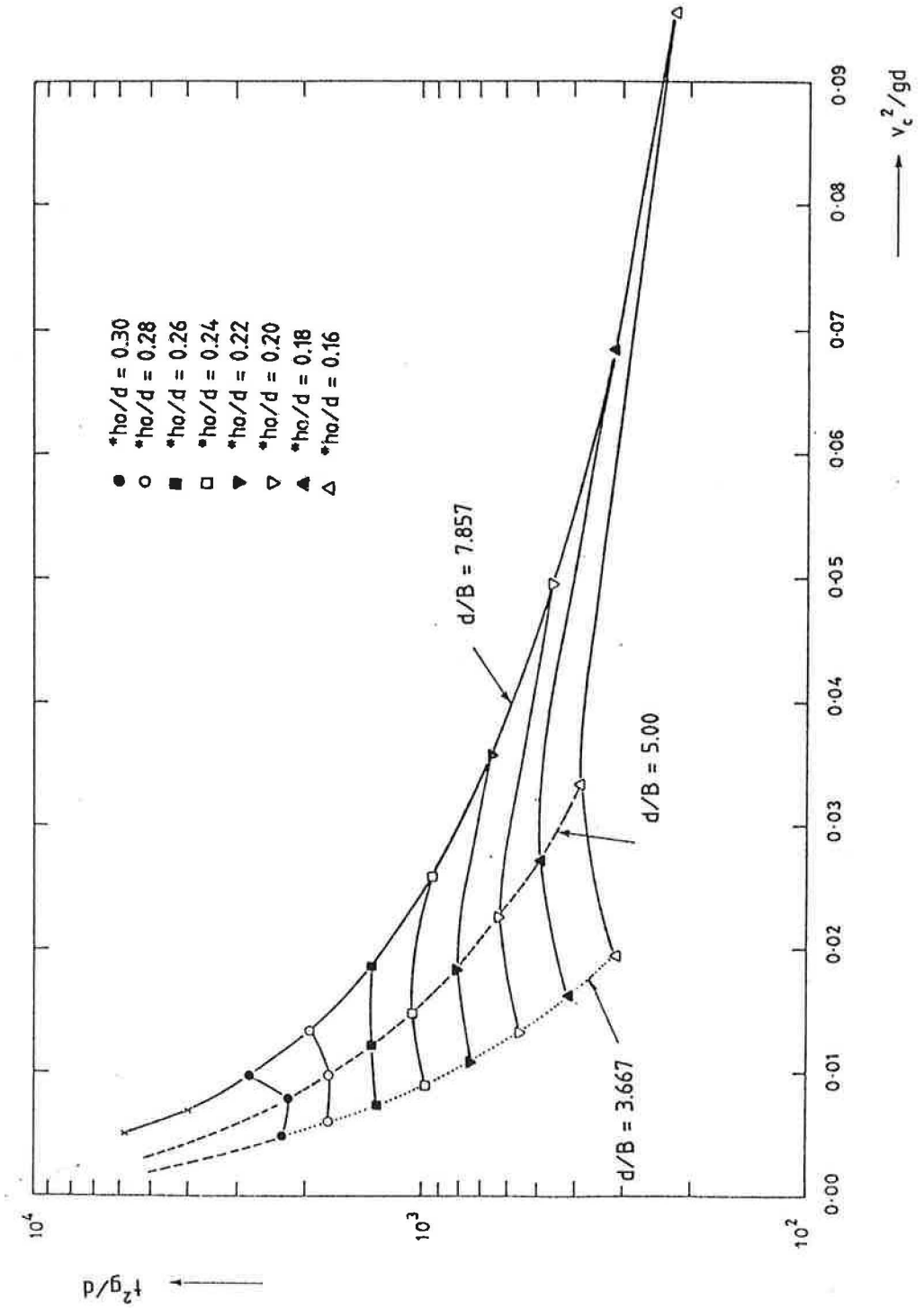

Fig 31 Variations of detention time with entry velocity for different channel widths and water levels (*ho) h_2 = 0.032m, CD_2

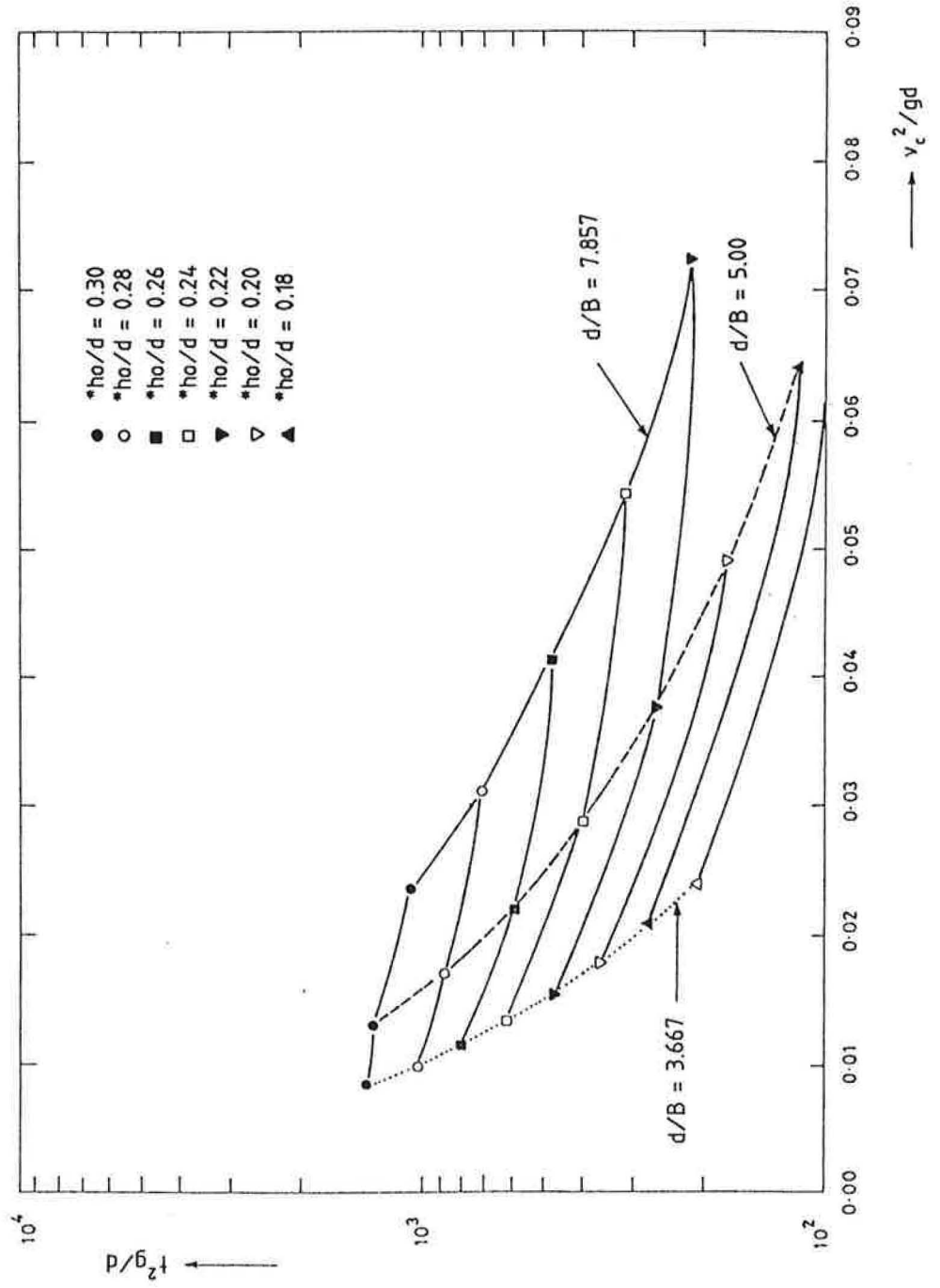

Fig 32 Variation of detention time with entry velocity for different channel widths (B) and water depths (*ho), h_2 = 0.056m, CD_2

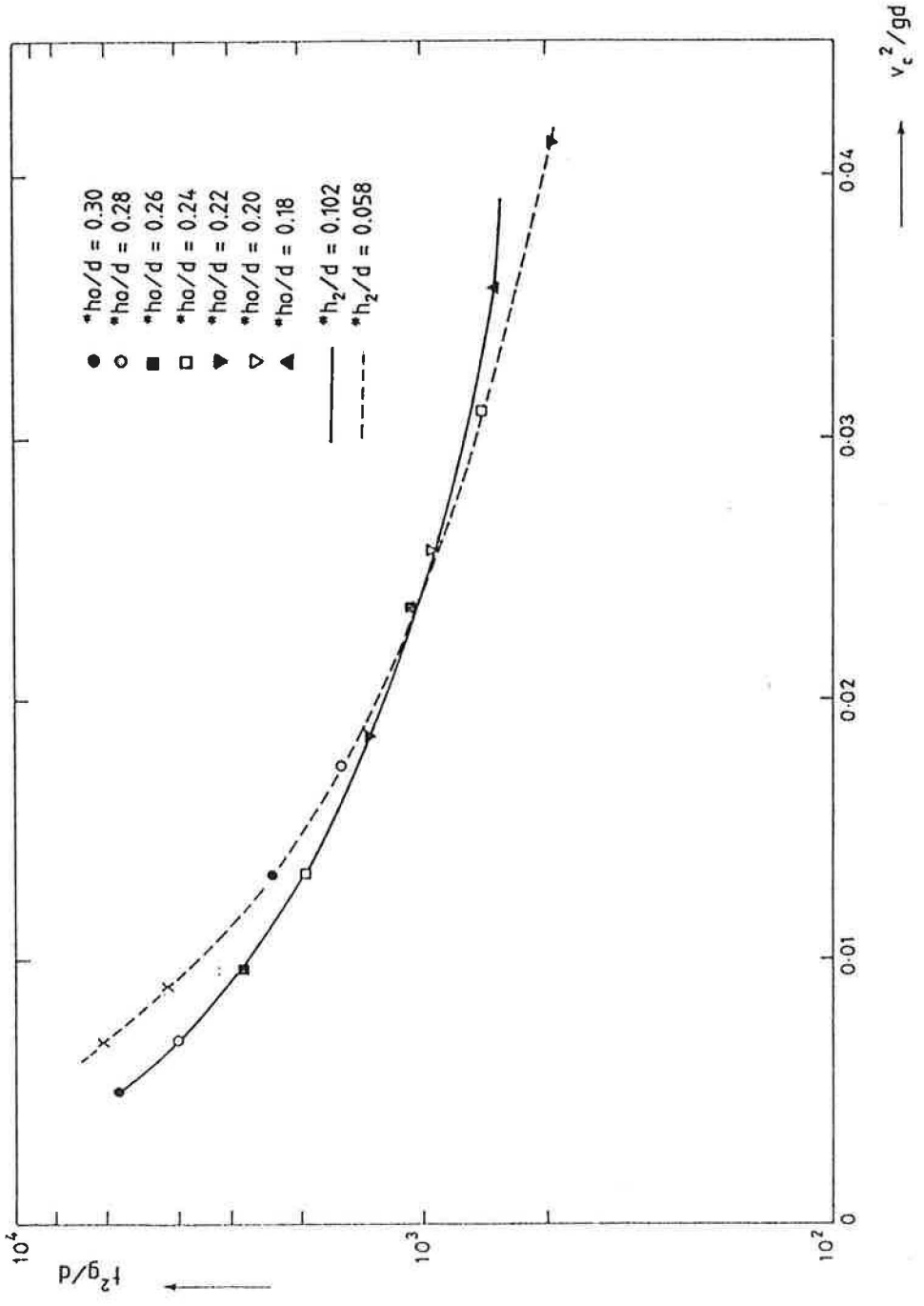

Fig 33 Variation of detention time with entry velocity for different chamber depths (h_2) and water levels (*ho)
B = 0.07m, CD_2

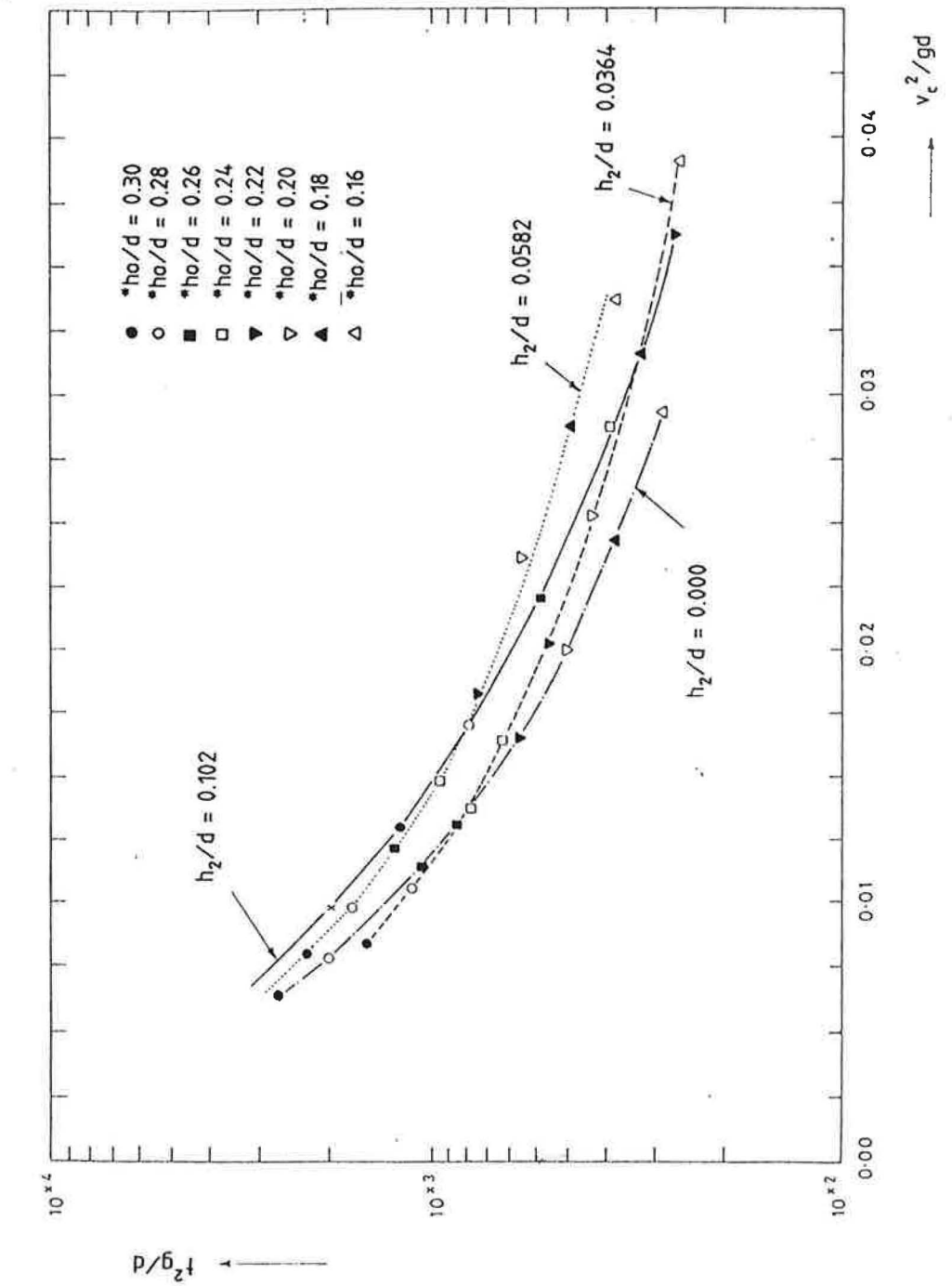

Fig 34 Variation of detention time with entry velocity for different chamber depths (h_2) and water levels (*ho), B = 0.11m, CD_2

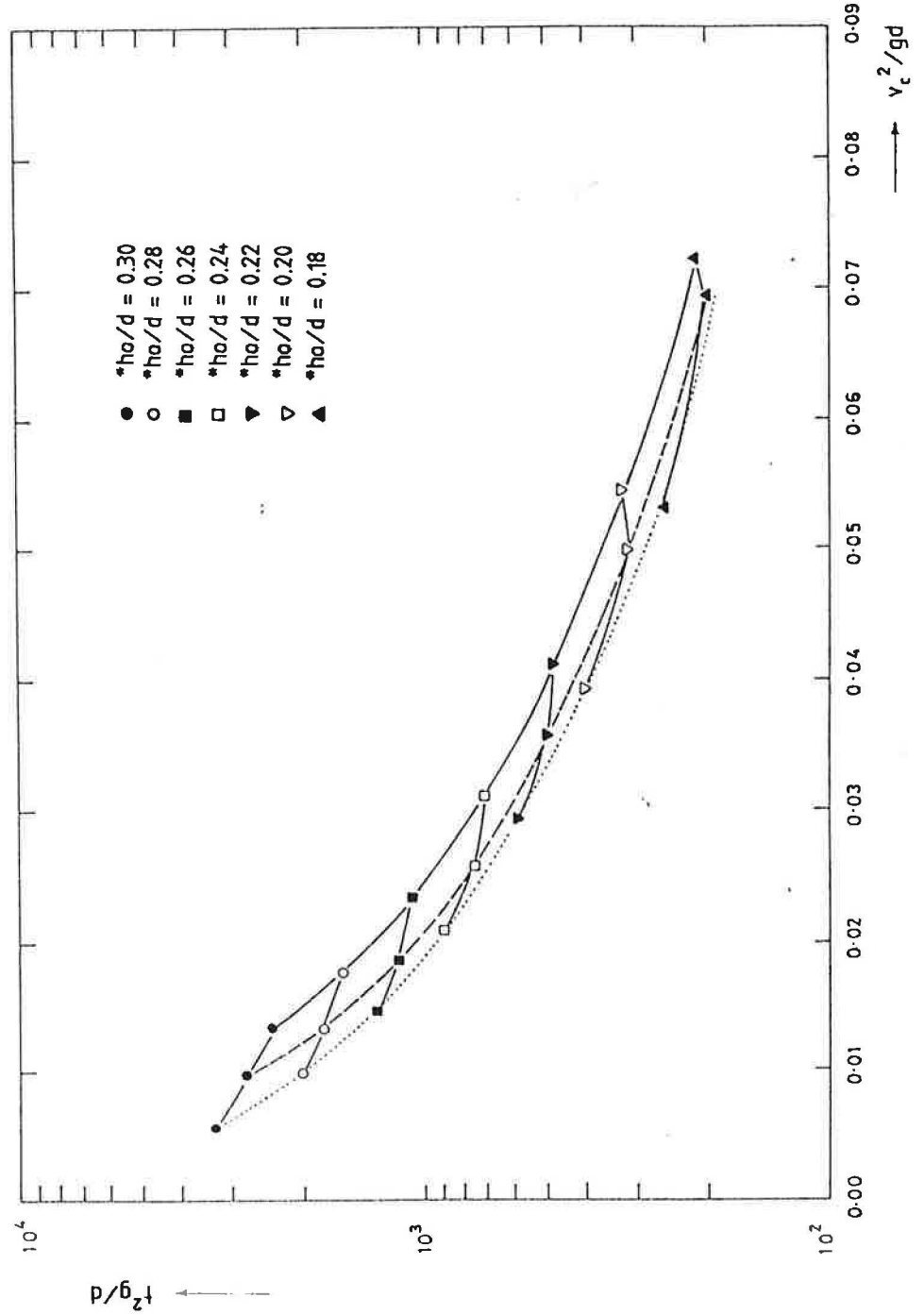

Fig 35 Variation of detention time with entry velocity for different deflector arrangements and water levels (*ho), h_2 = 0.056m, B = 0.07m

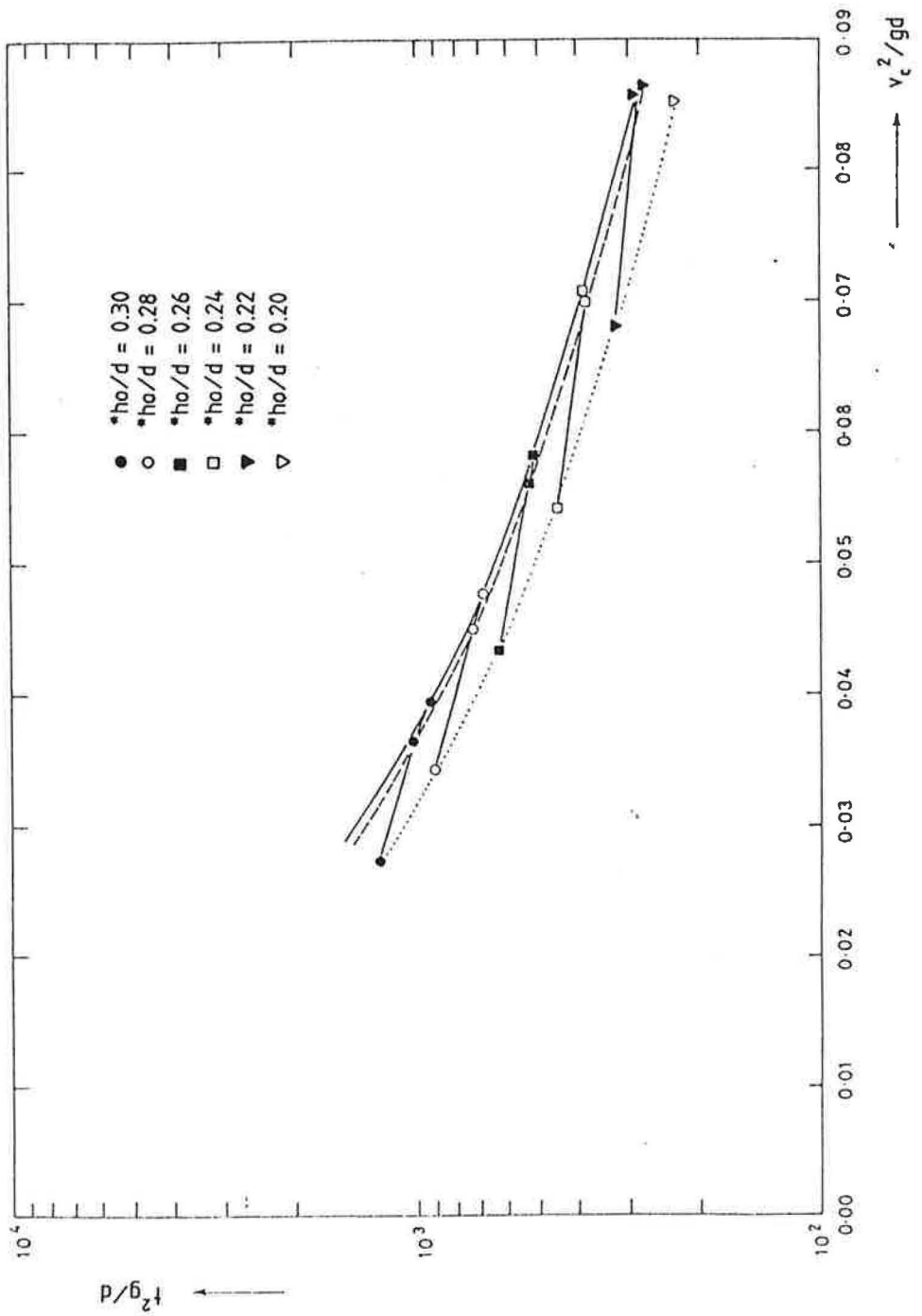

Fig 36 Variations of detention time with entry velocity for different arrangements and water levels (*ho), h_2 = 0.02m, B = 0.07m

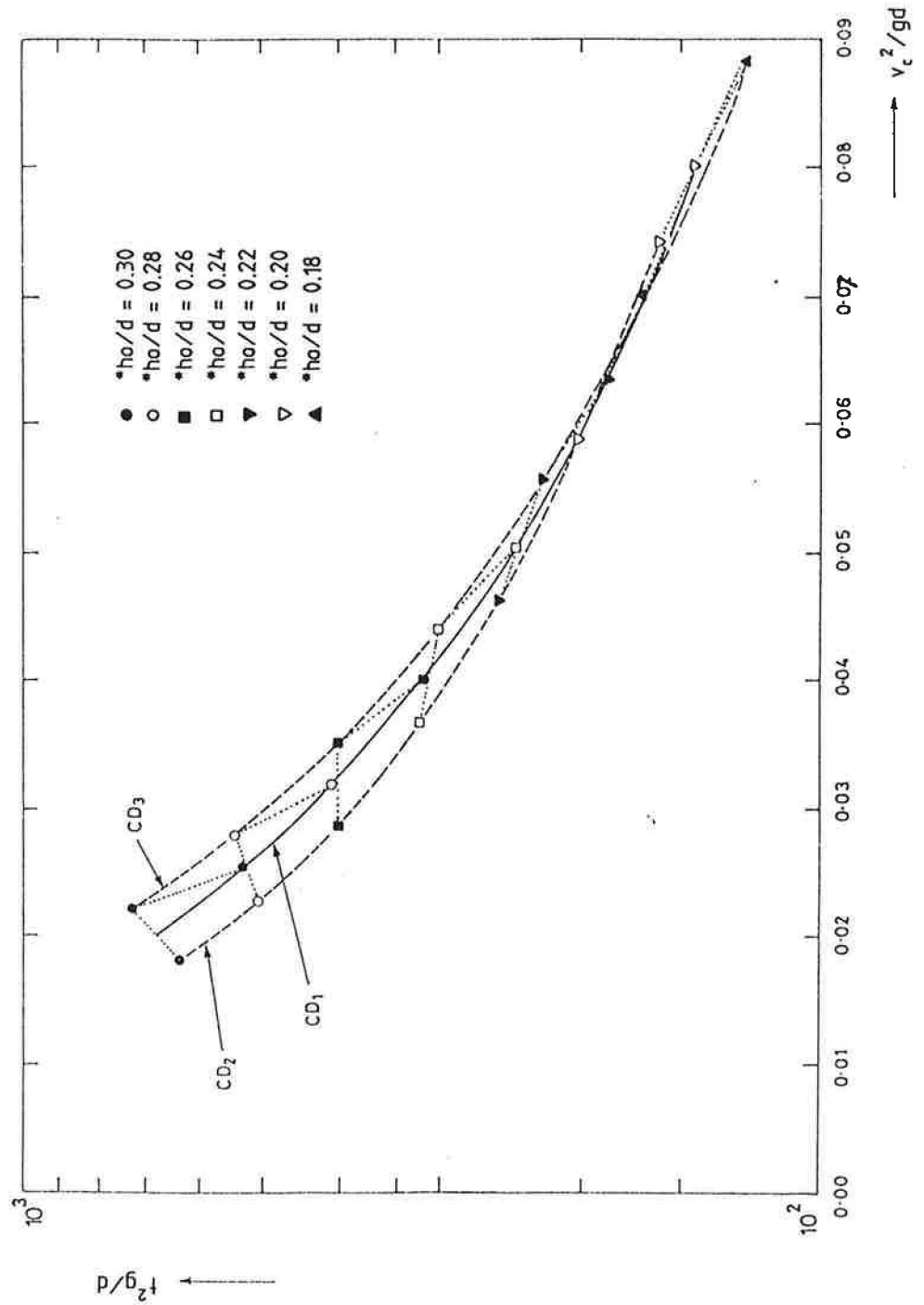

Fig 37 Variation of detention time with entry velocity for different deflector arrangements and water levels (*ho), h_2 = 0.032m, B = 0.11m

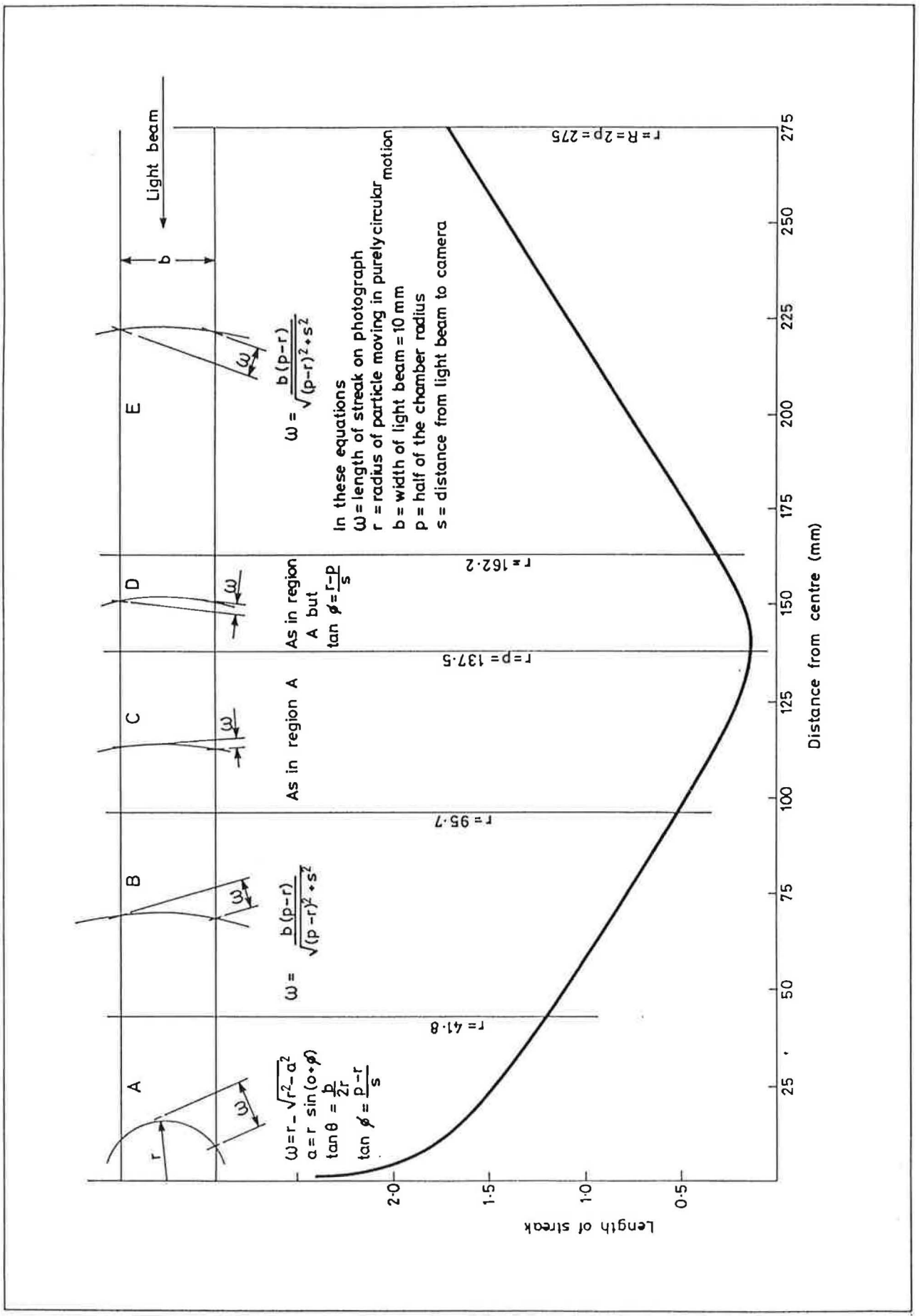

Fig 38 Horizontal length of streak produced by particle moving only in a tangential direction

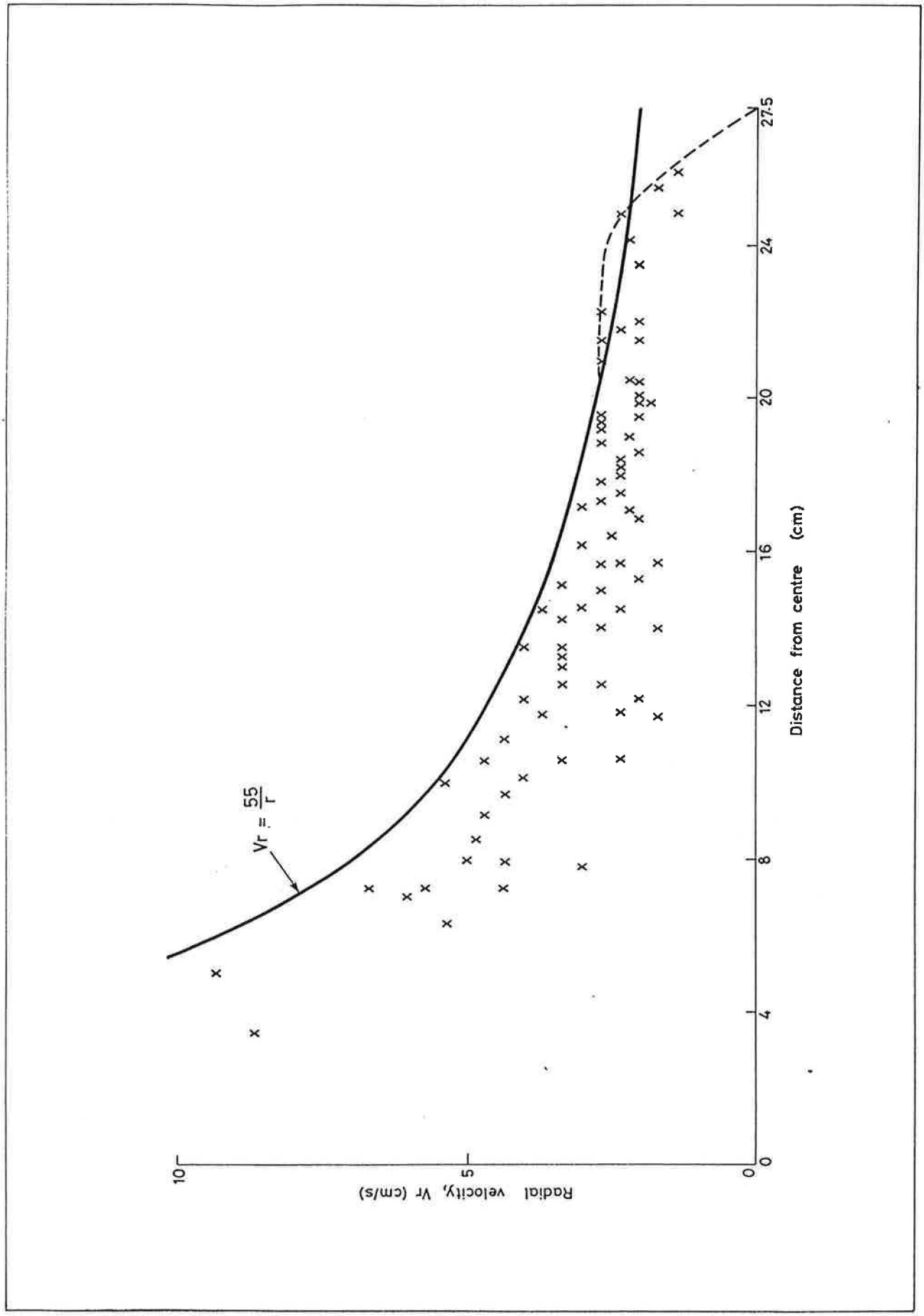

Fig 39 Radial distribution of radial velocities near the bed

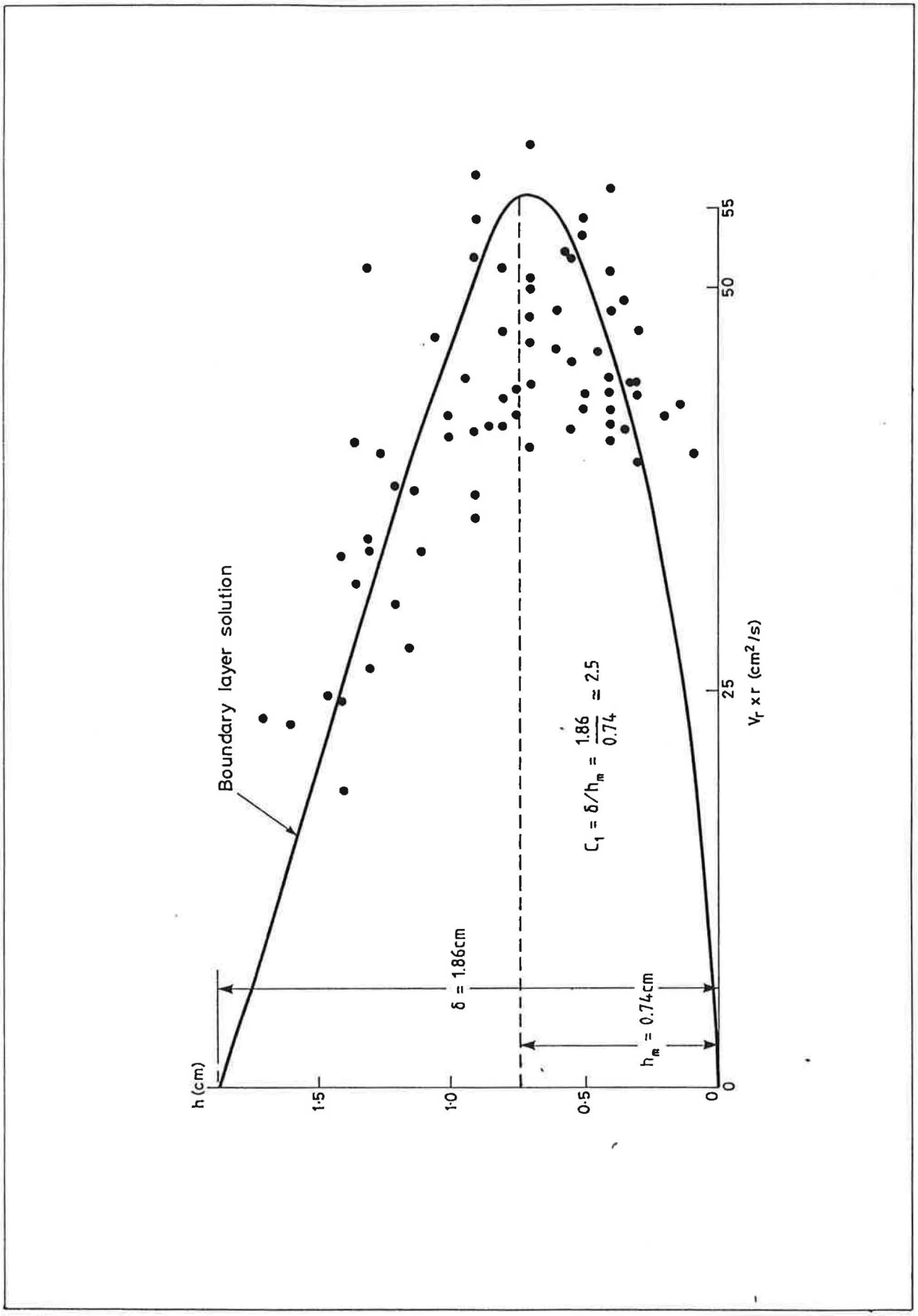

Fig 40 Vertical distribution of radial velocities

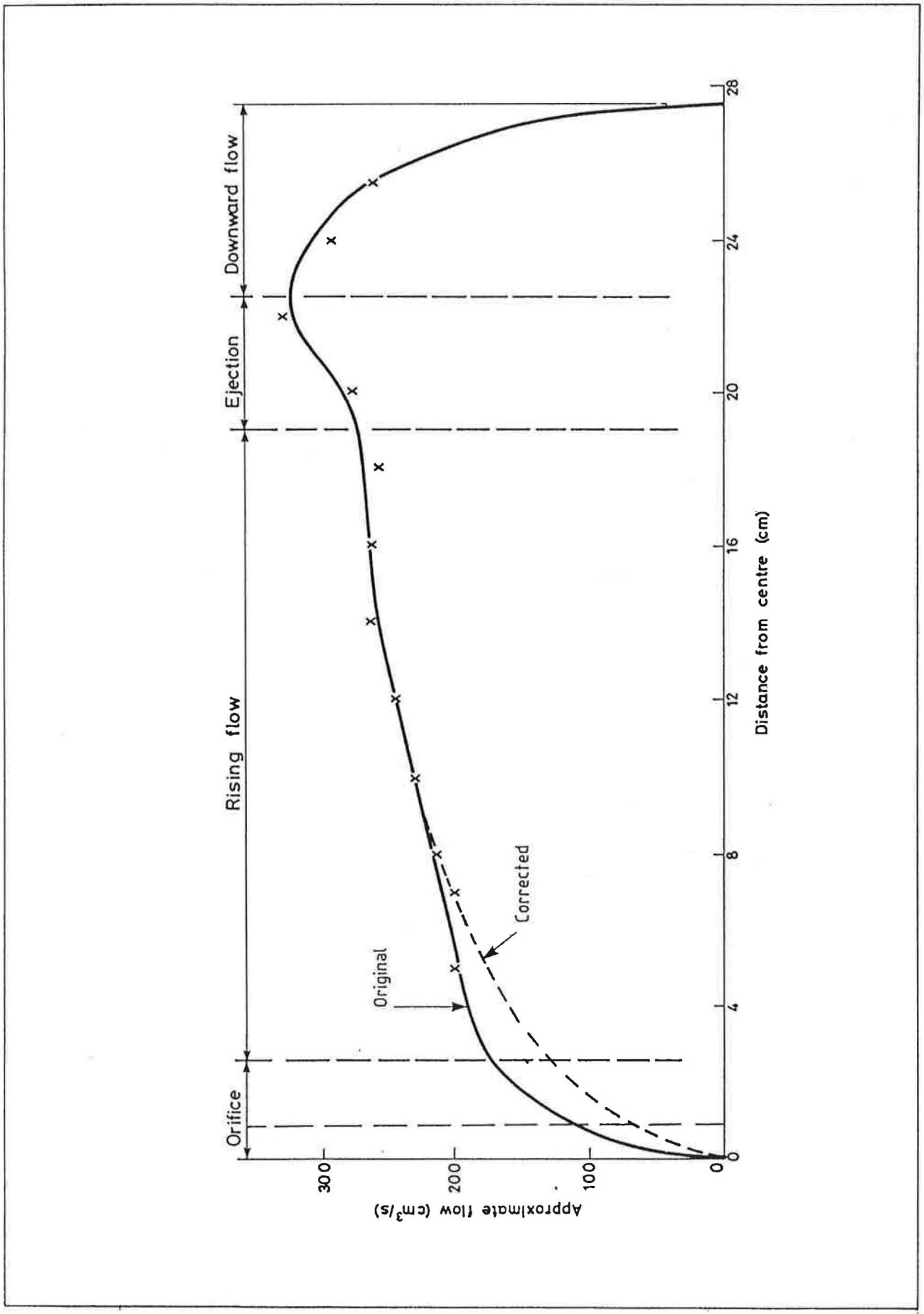

Fig 41 Approximate total near bed flow

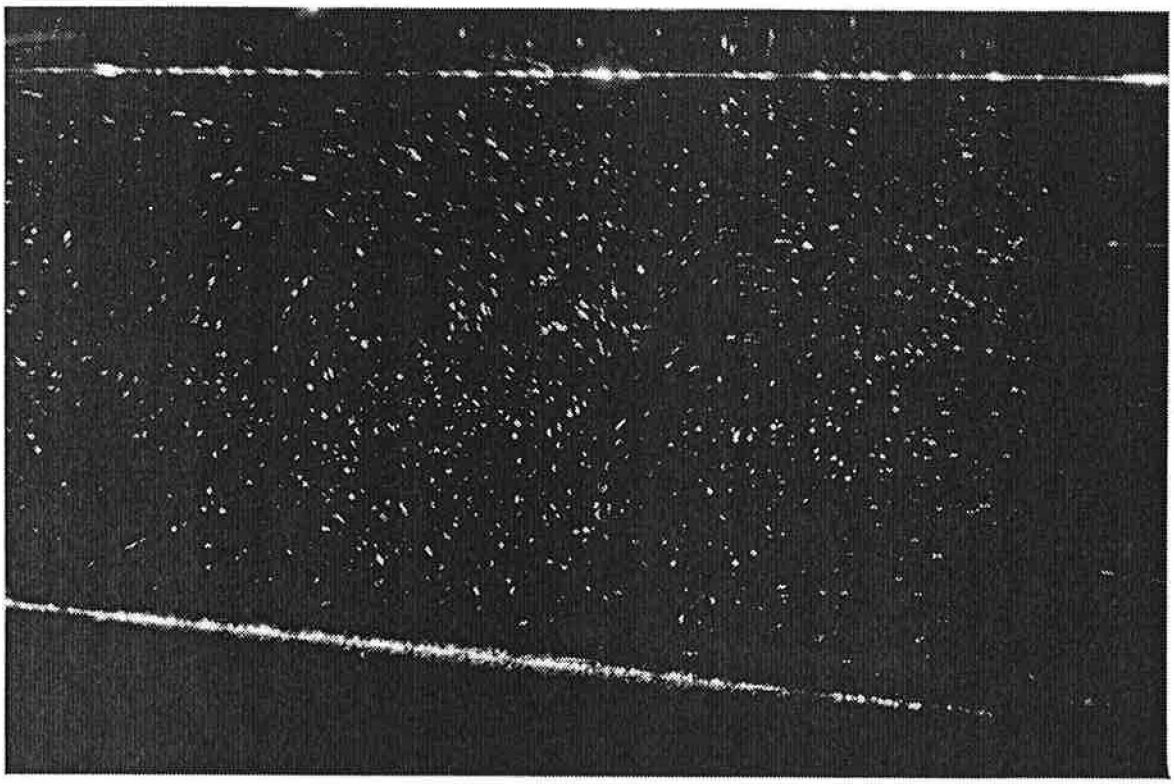

Fig 42 Showing secondary flow patterns in CCSE with inlet channel width = 15 cm and deflector CD_0

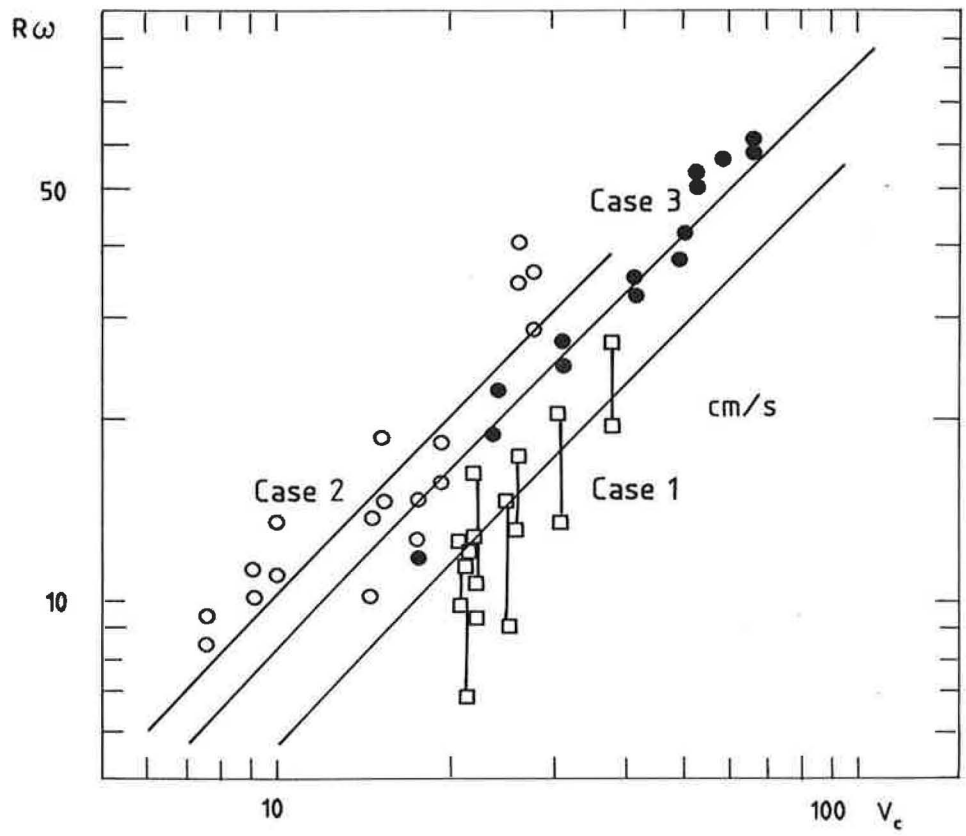

Fig 43 Relation of rotating velocity and inflow velocity

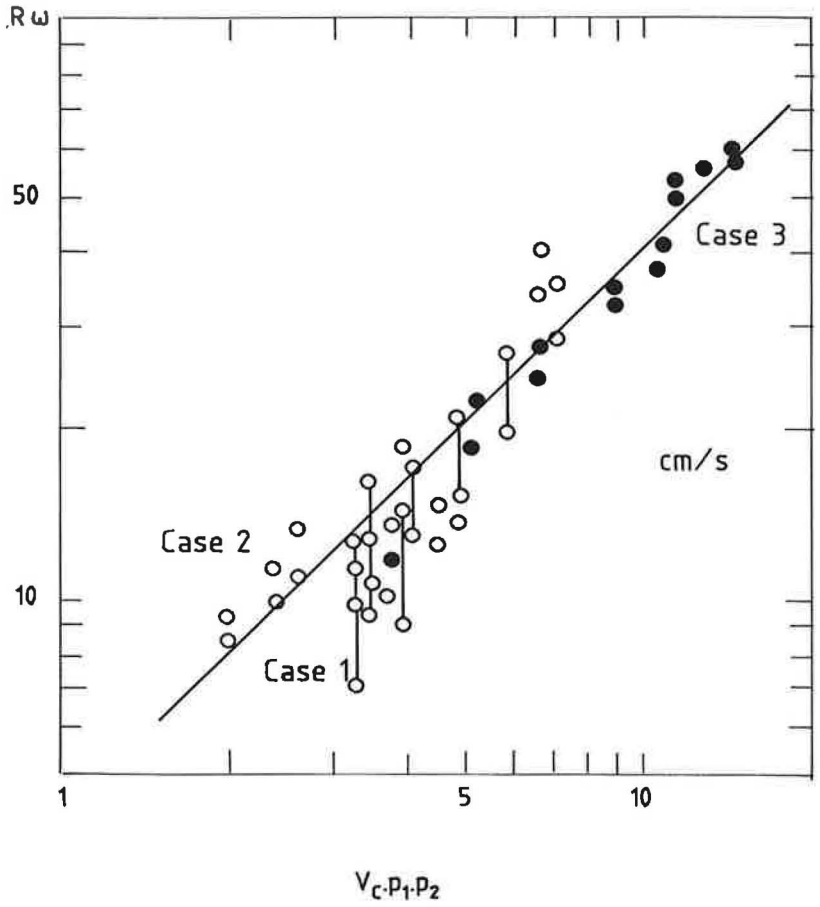

Fig 44 Relation of rotating velocity and modified inlet velocity

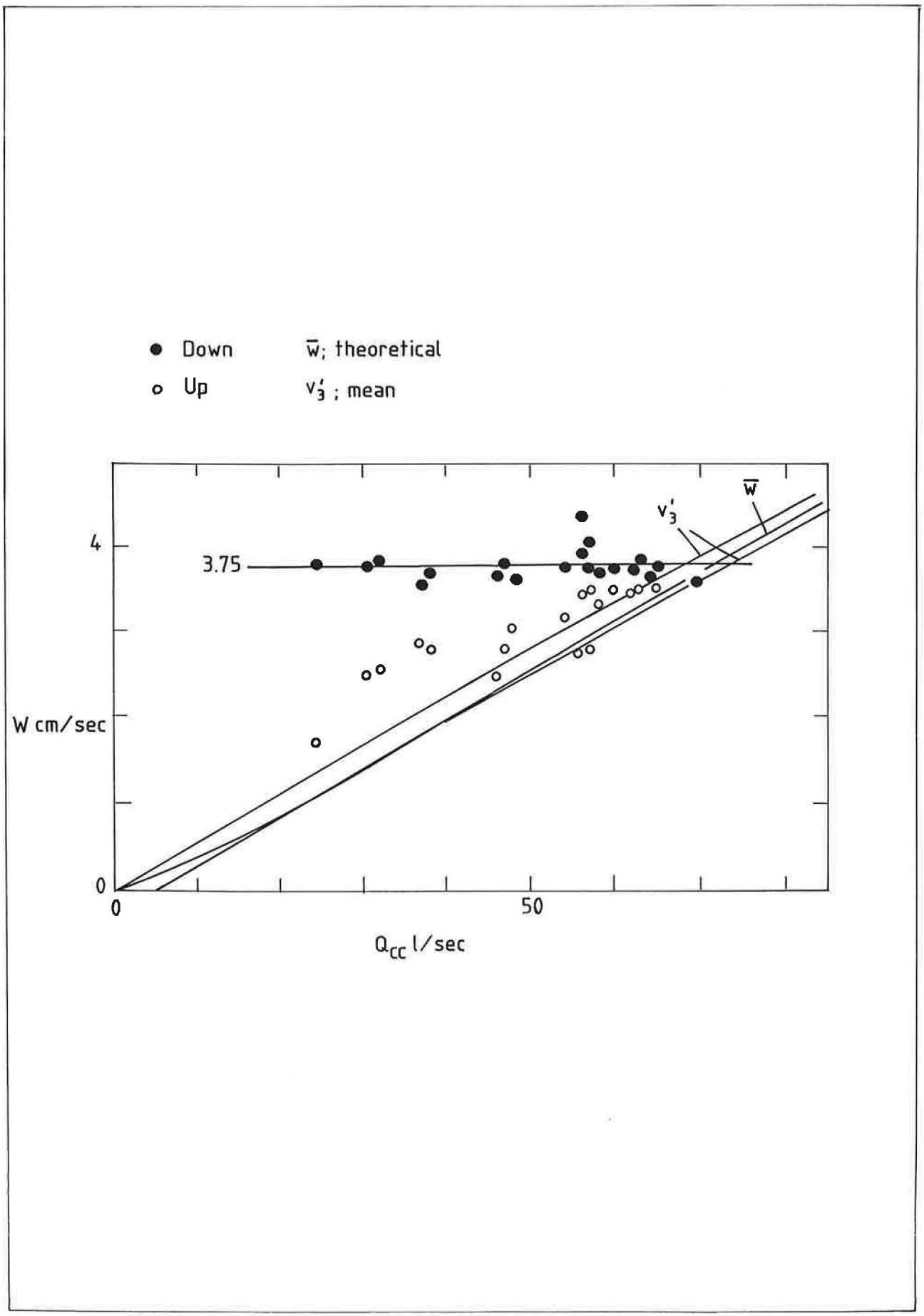

Fig 45 Relationship between upward velocity, sedimentation rate and inflow discharge

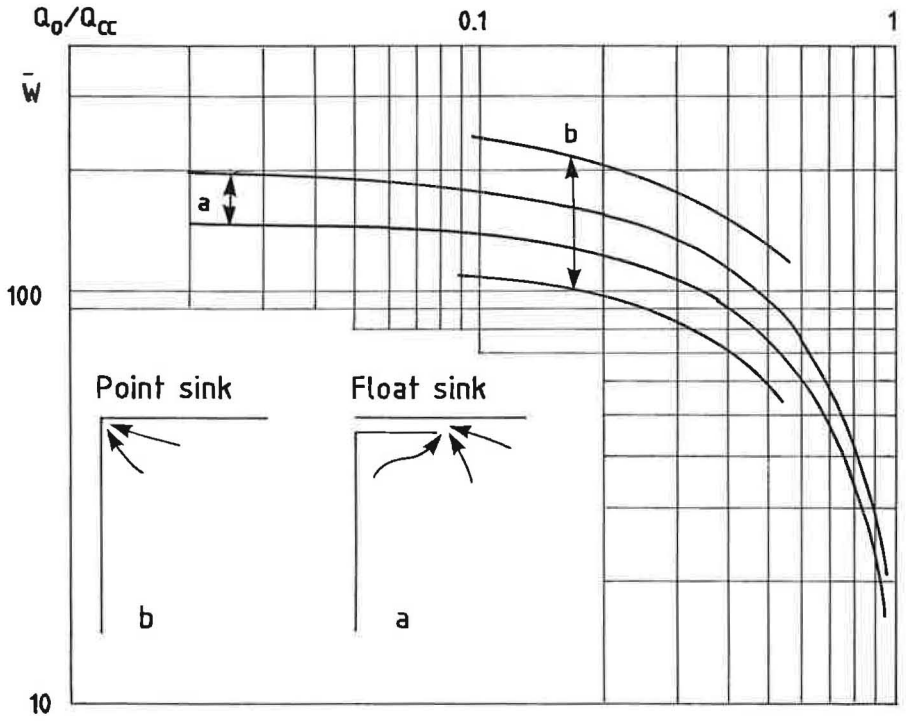

Fig 46 Upward velocity and ratio of intake discharge Q_o to inflow discharge Q_{cc}

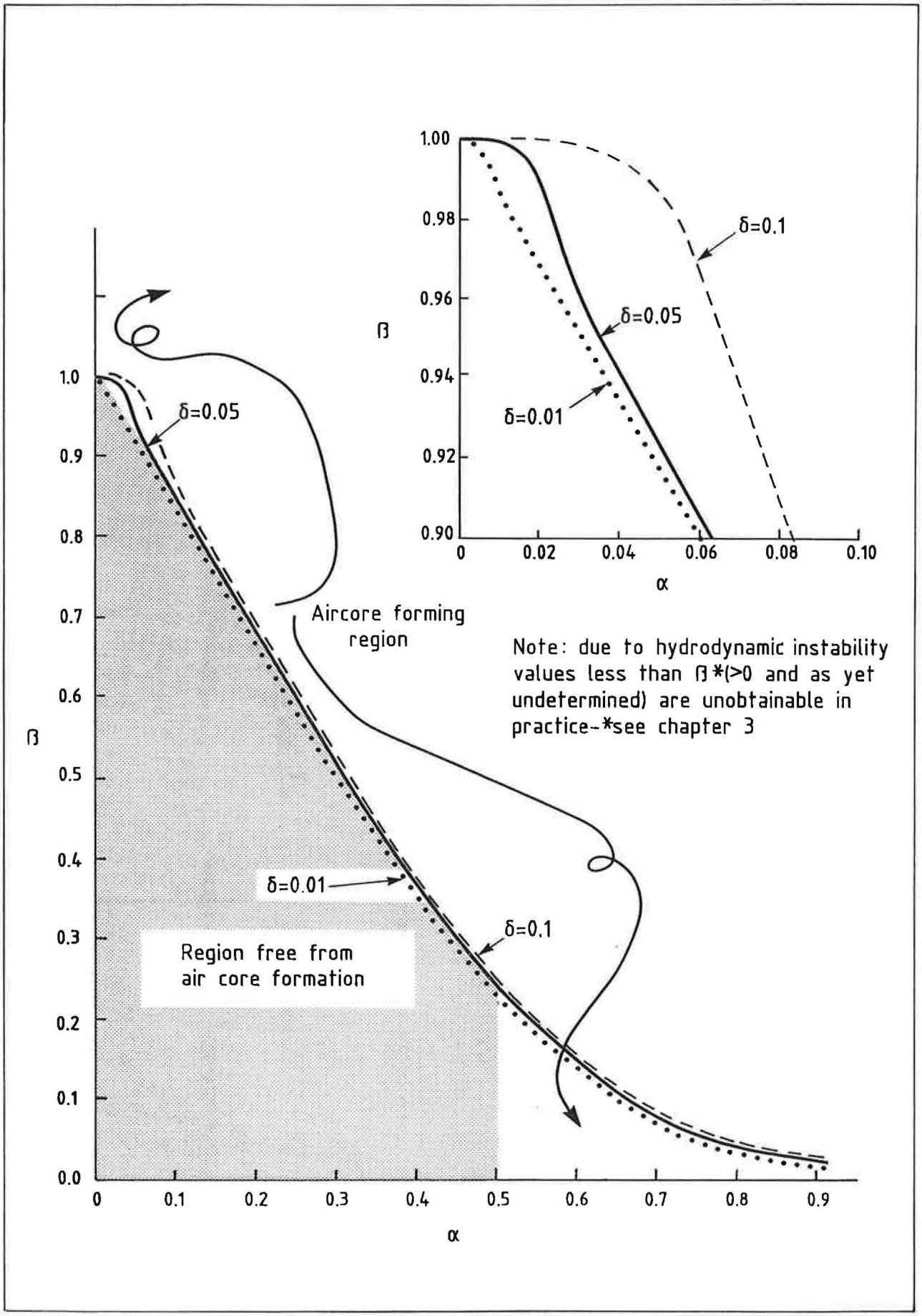

Fig 47 β Vs α for vertical gravity intakes

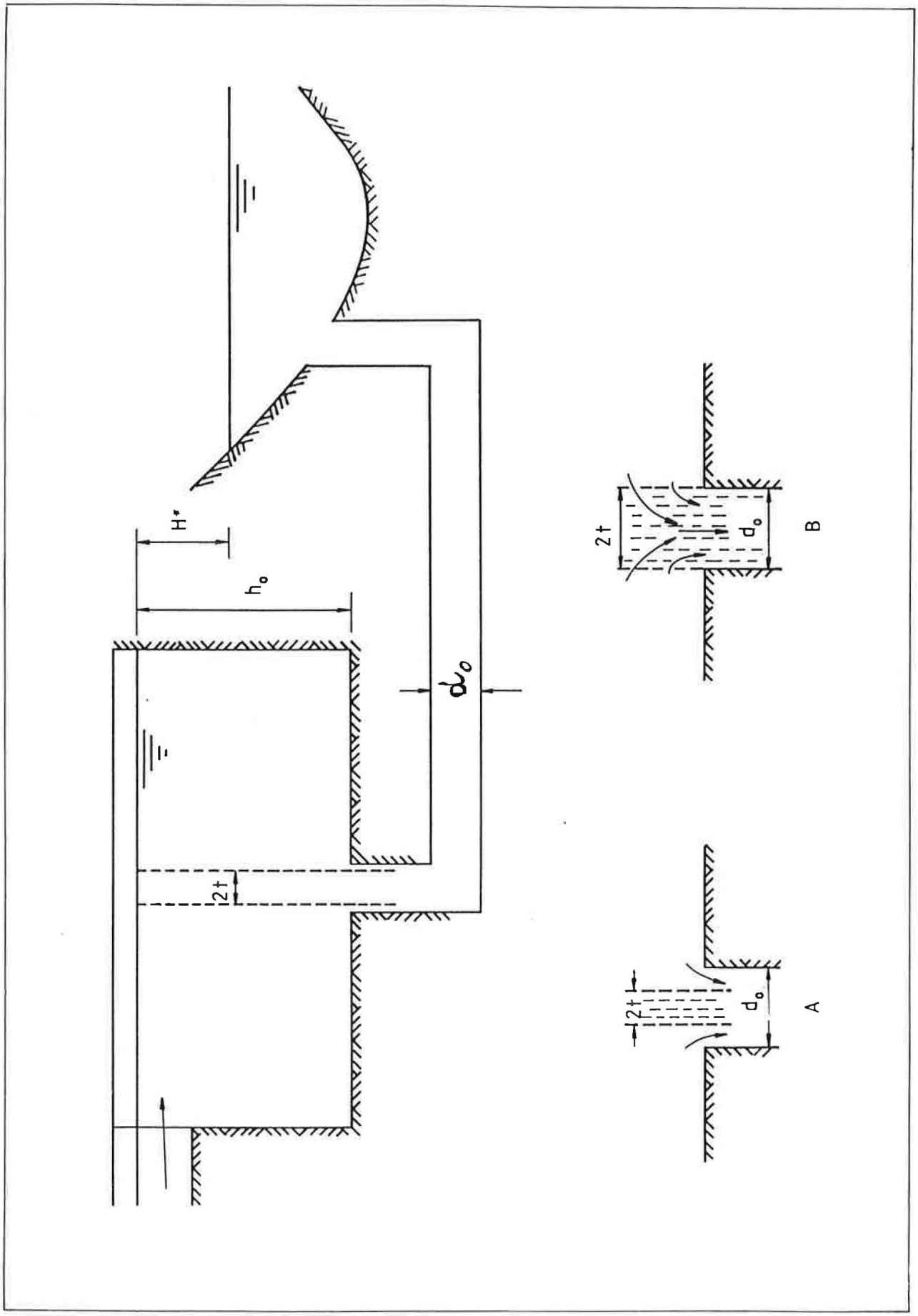

Fig 48 Typical layout of circulation chamber silt extractor

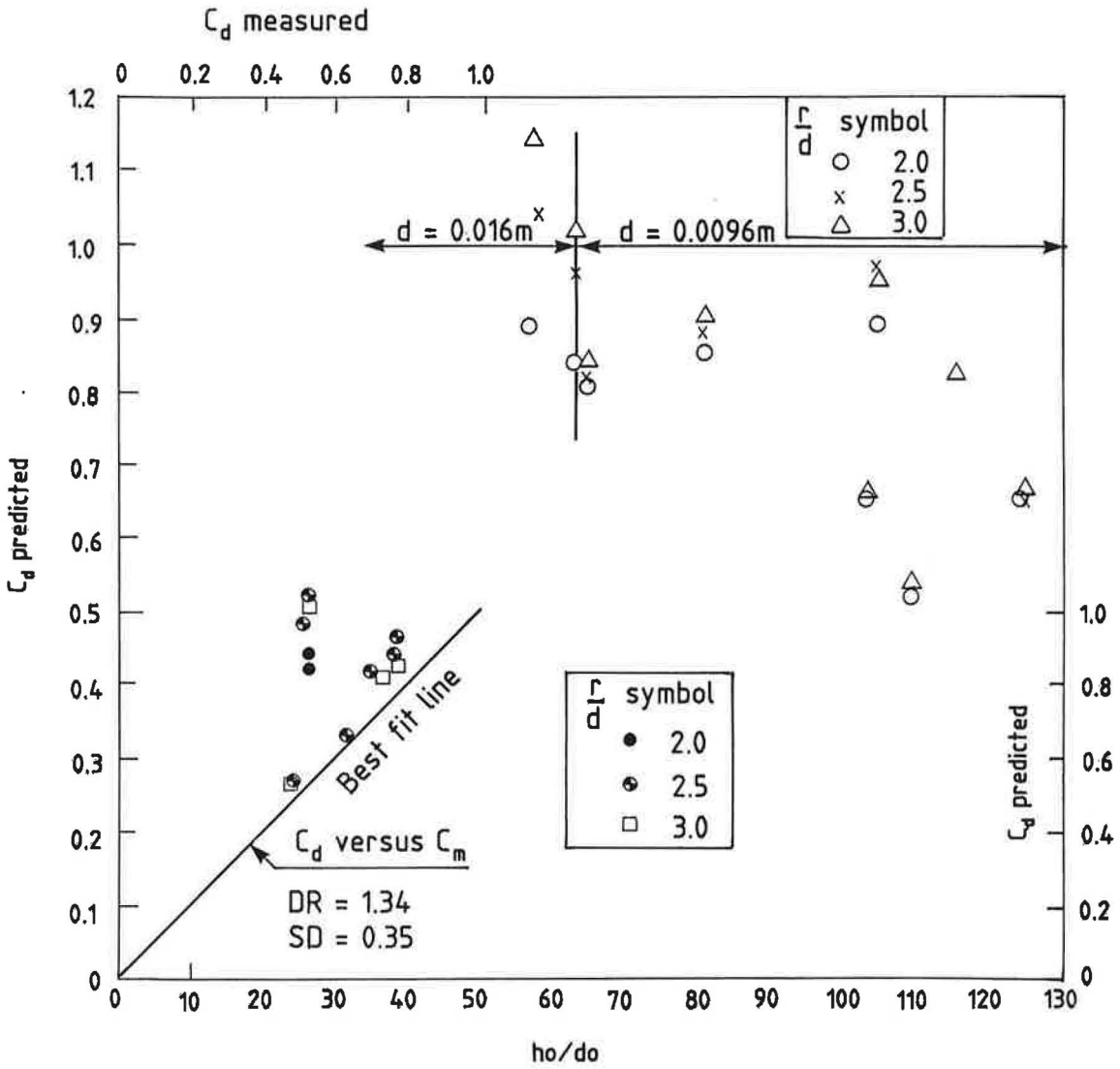

Fig 49 Variation of C_{dp} with ho/do and C_{dp} with C_{dm}

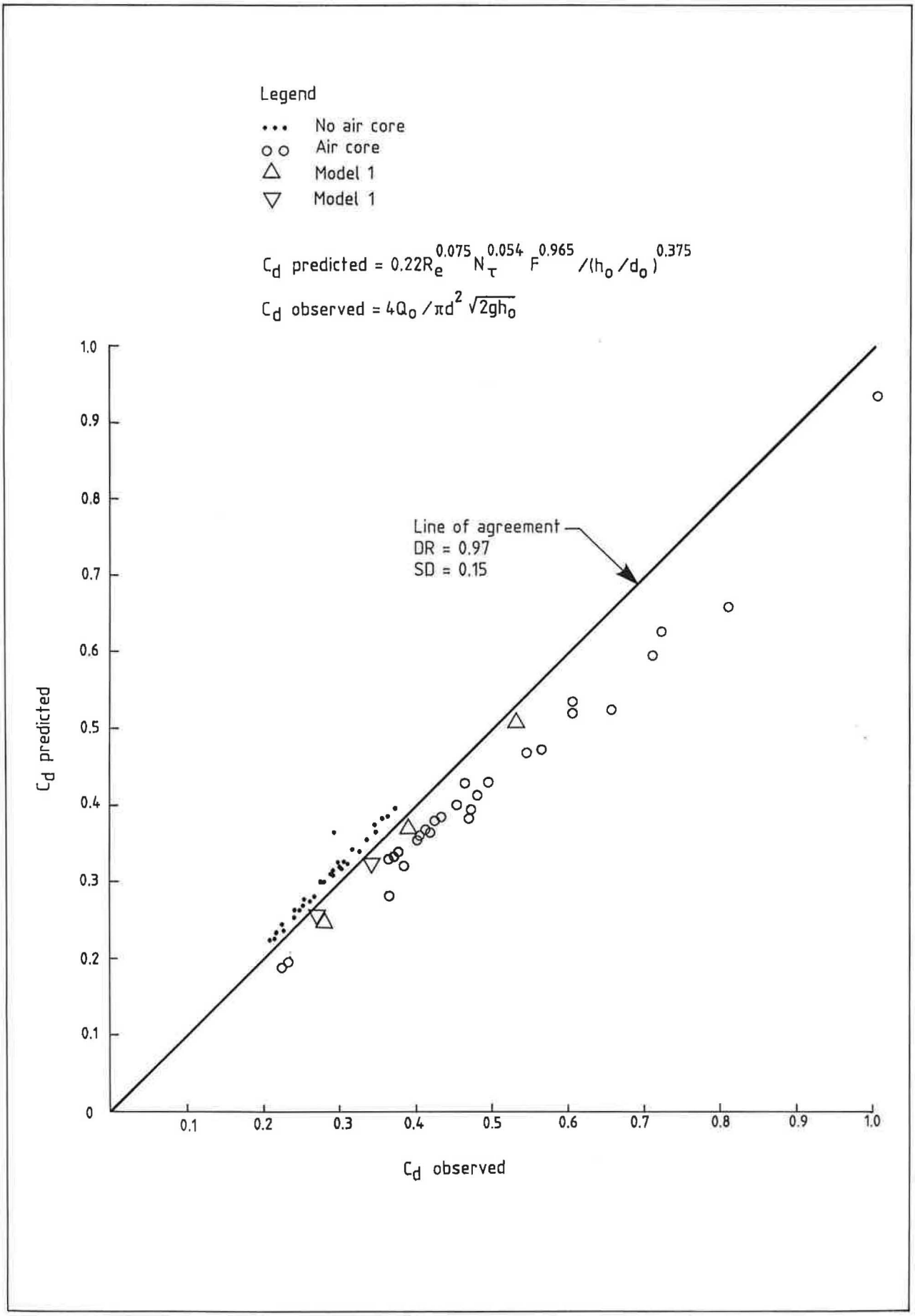

Fig 50 Comparison of discharge coefficient predicted and observed

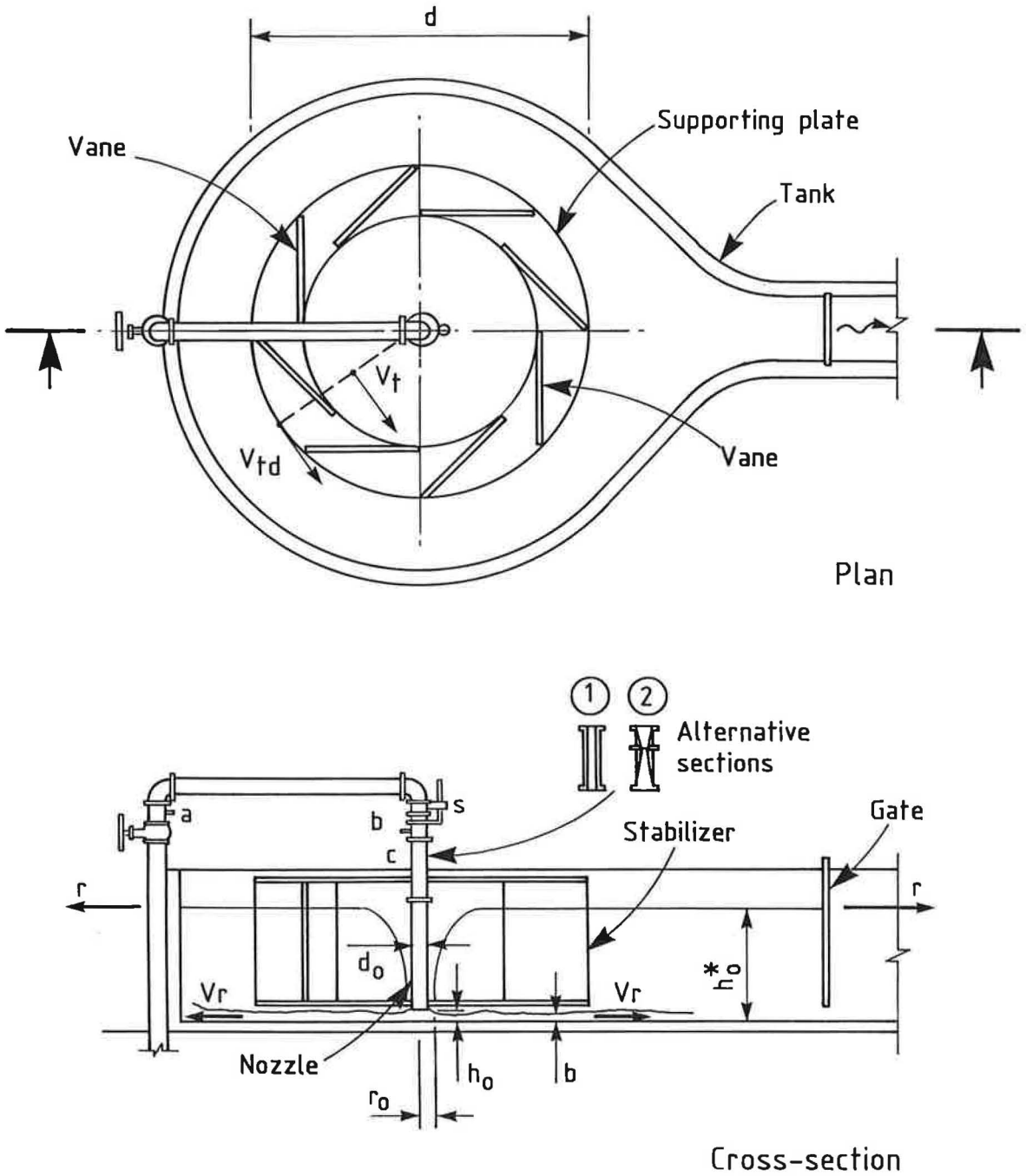

Fig 51 Vortex agitator scheme

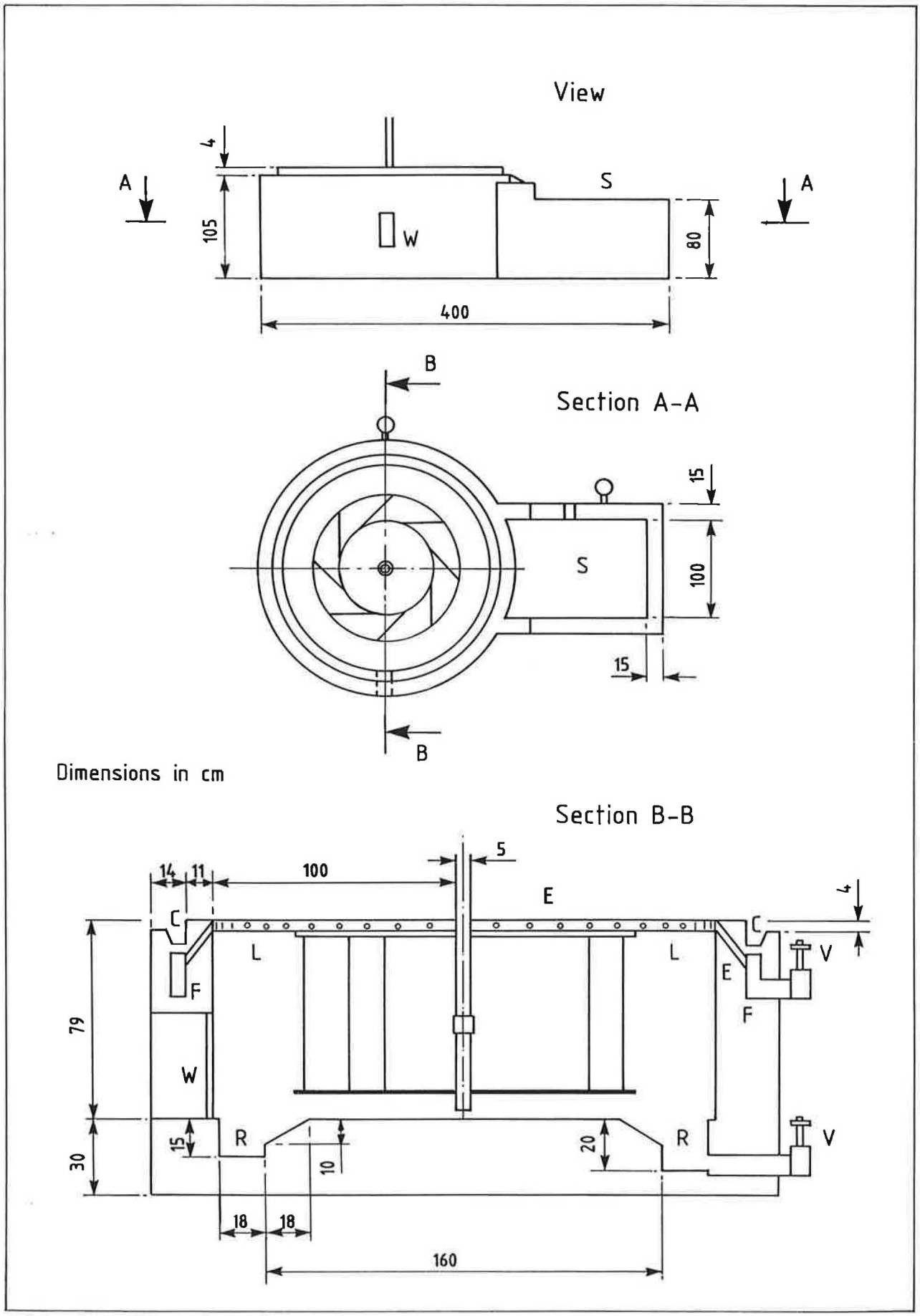

Fig 52 Scheme of the vortex device for clarifying purposes

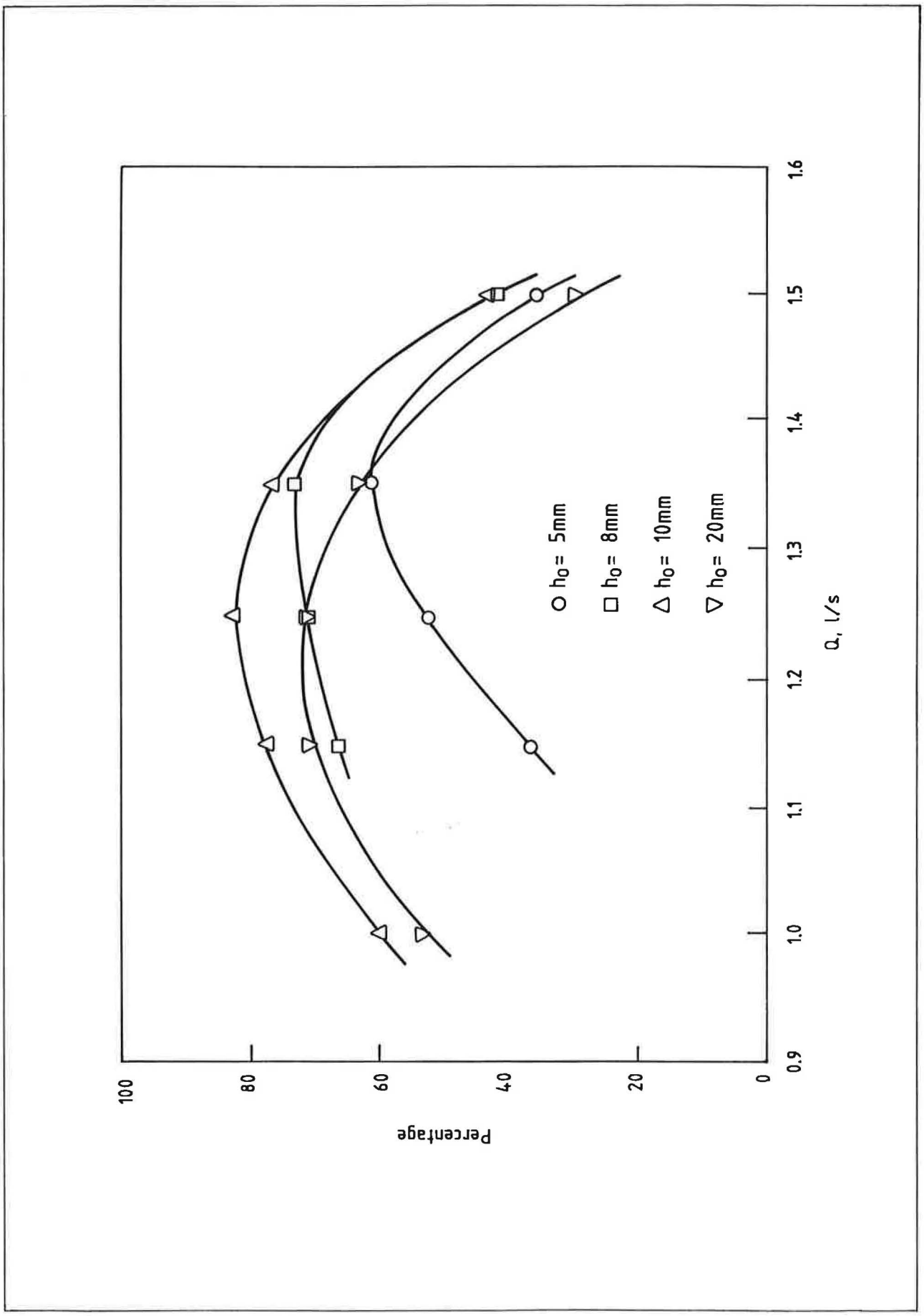

Fig 53 Settling floc percentage as a function of h and Q

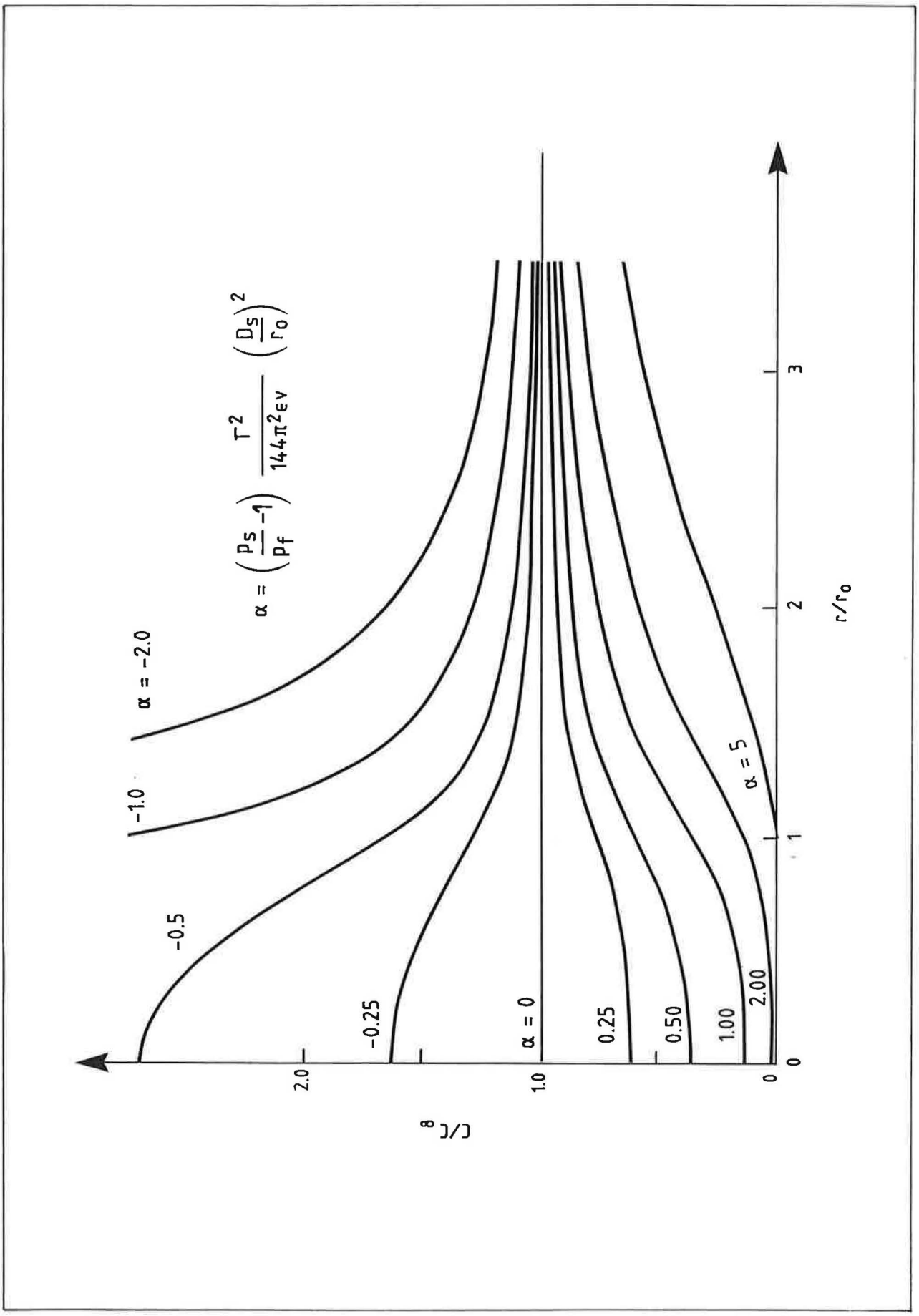

Fig 54 Steady-state concentration profile in a Rankine combined vortex

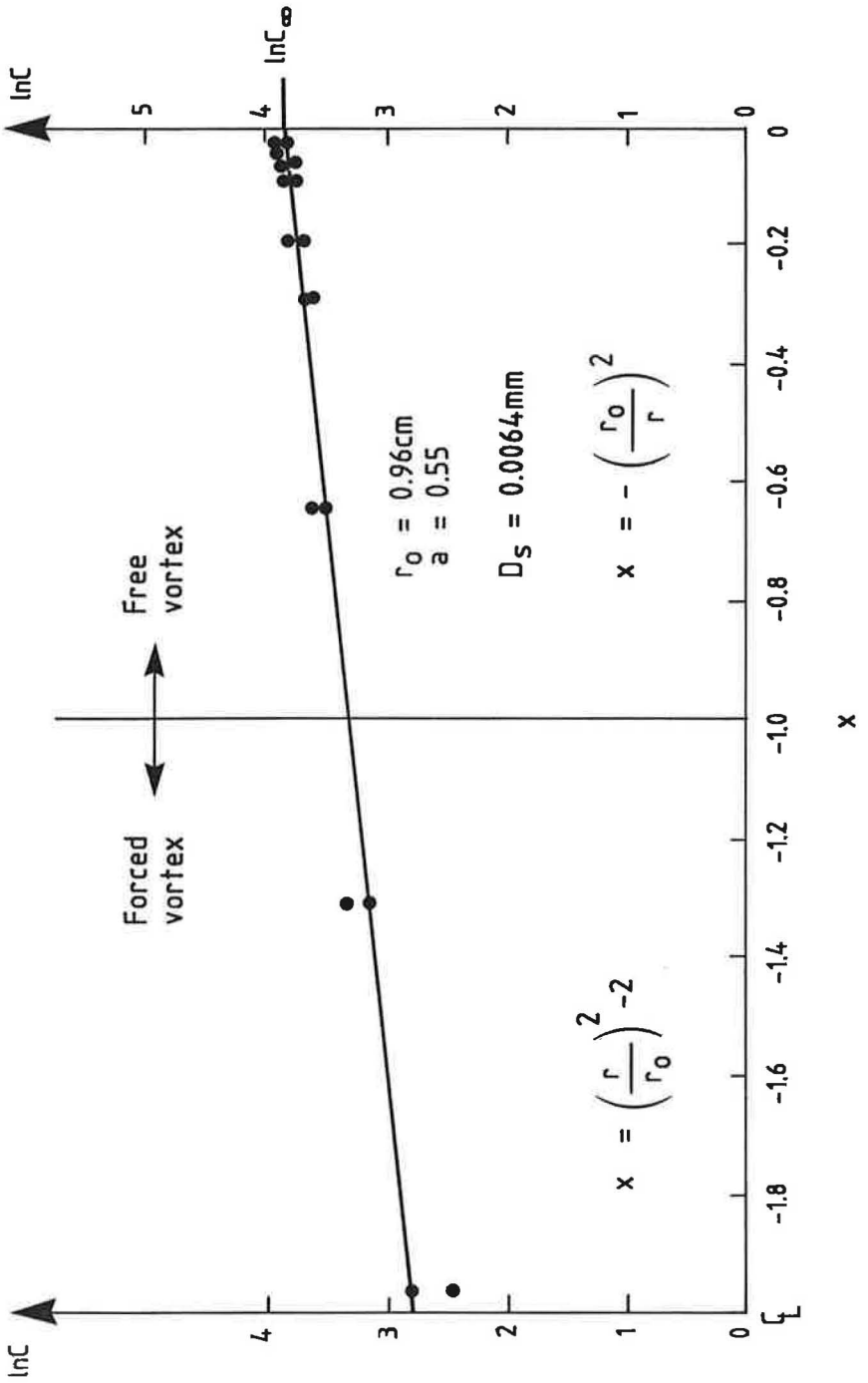

Fig 55 Linearized sediment concentration profile

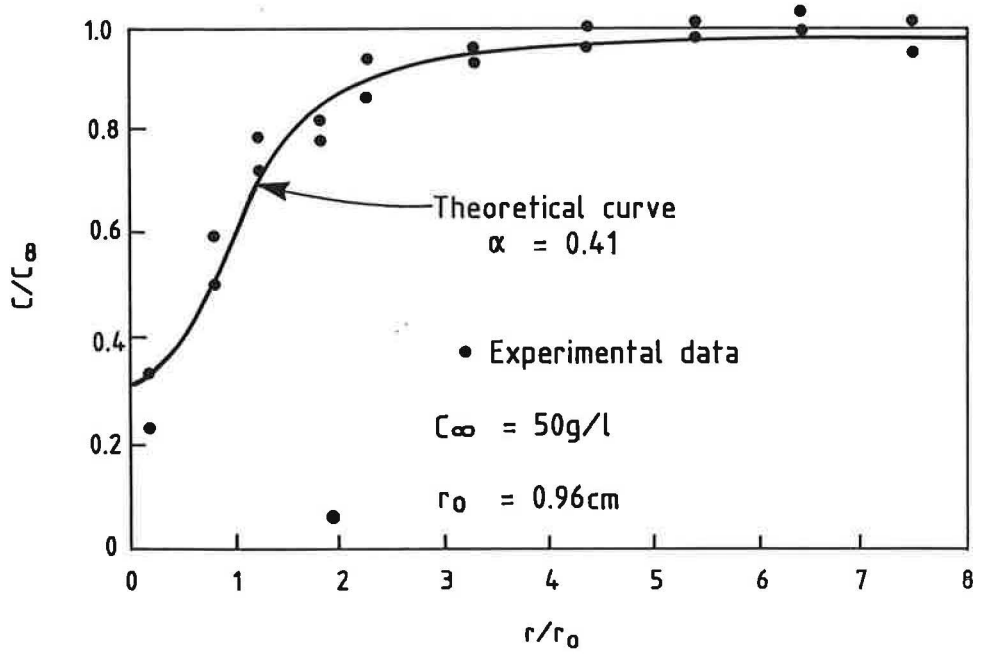

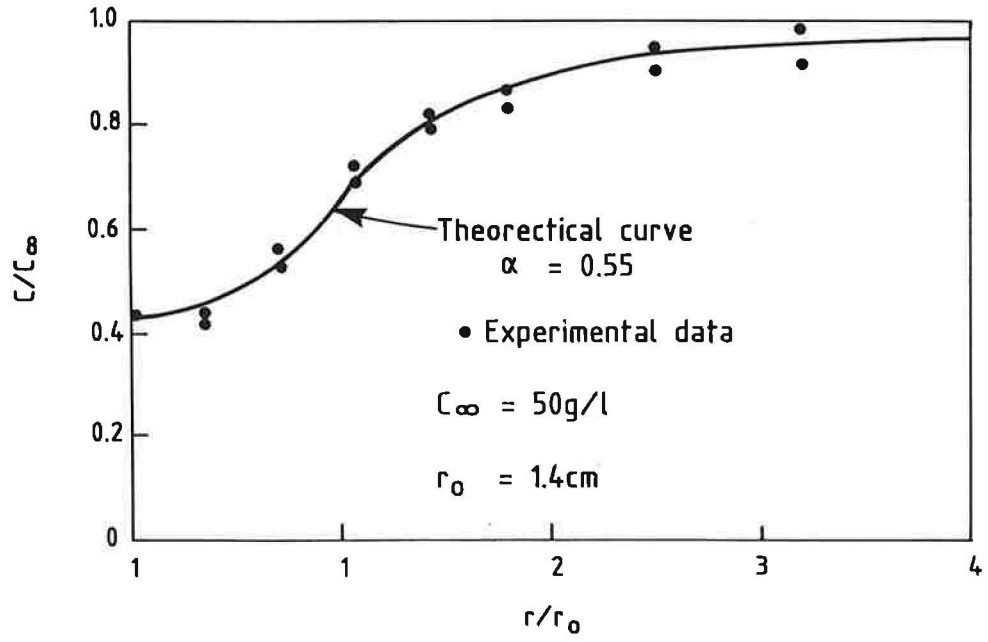

Fig 56 Sediment concentration profile

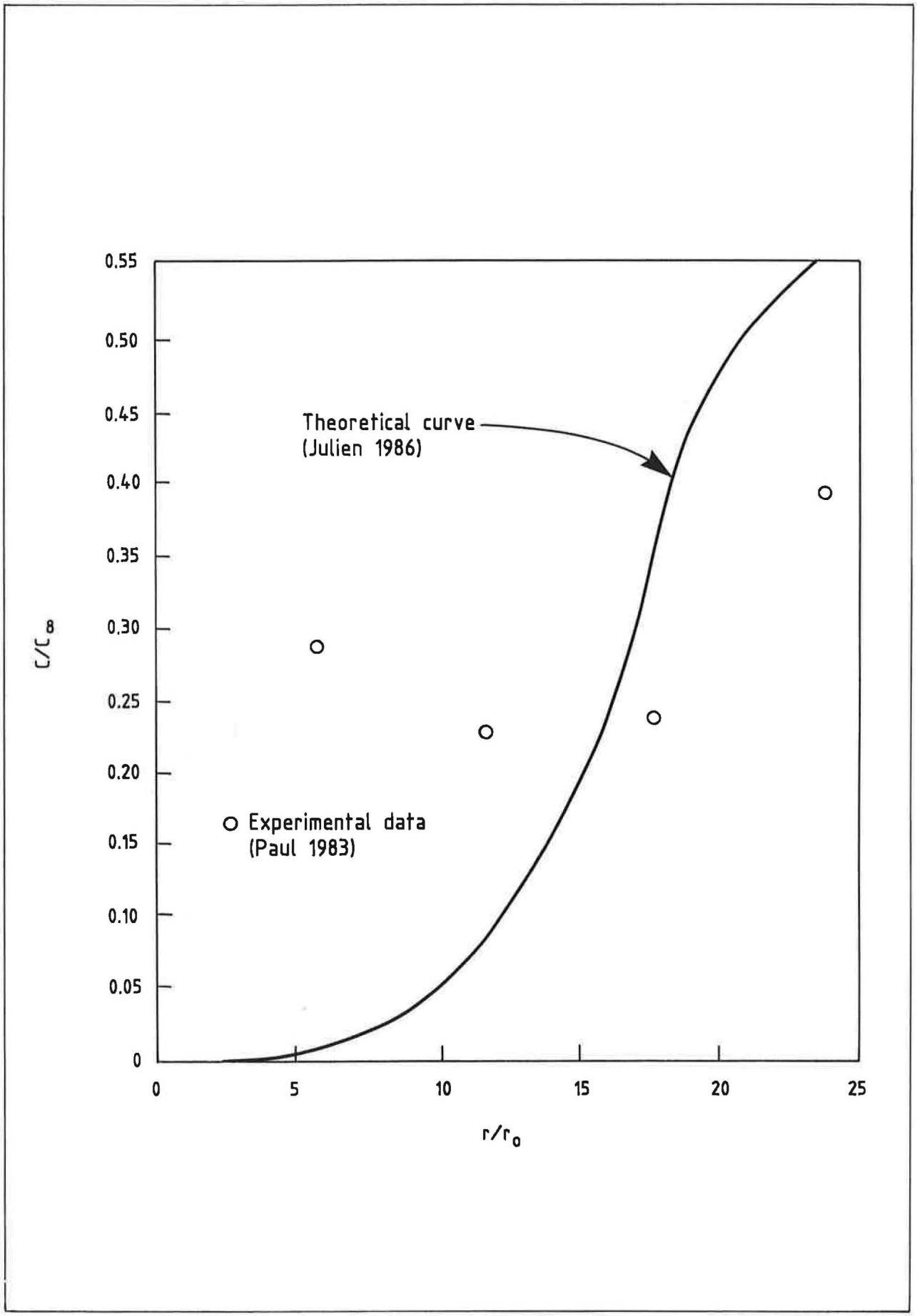

Fig 57 Sediment concentration profiles

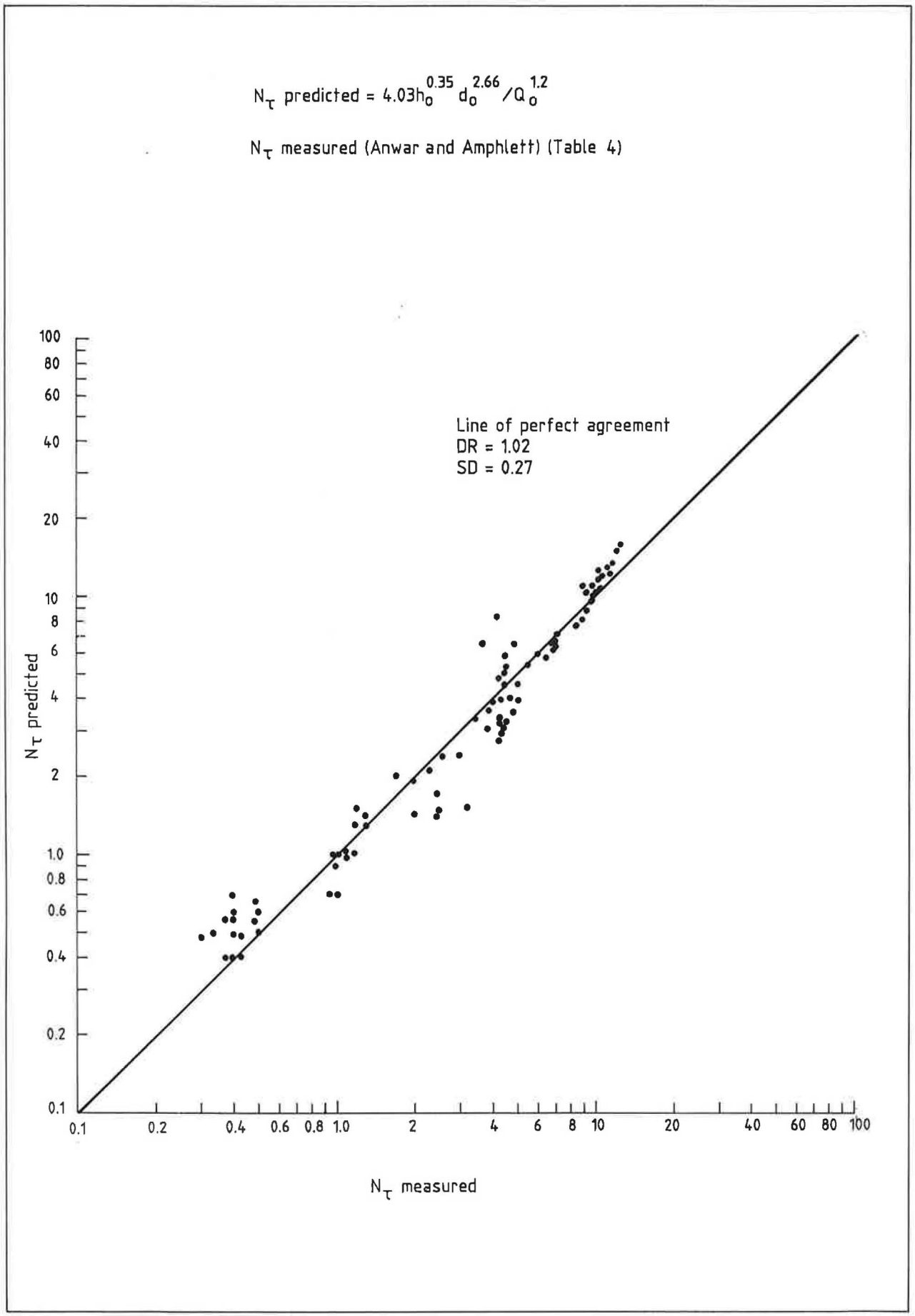

Fig 58 Comparison of circulation number N_τ ($= \tau d_o / Q_o$) predicted with measured

Size in mm	Percentage
0.037	0.40
0.074	0.59
0.089	0.93
0.105	1.23
0.147	3.34
0.177	6.51
0.297	8.20
0.42	12.42
0.50	14.53
1.00	18.75
2.00	31.41
4.75	50.40
9.50	68.34
12.70	93.67
19.05	100.00

Diameter of flushing pipe = 150mm
Discharge = 0.1606 cumec

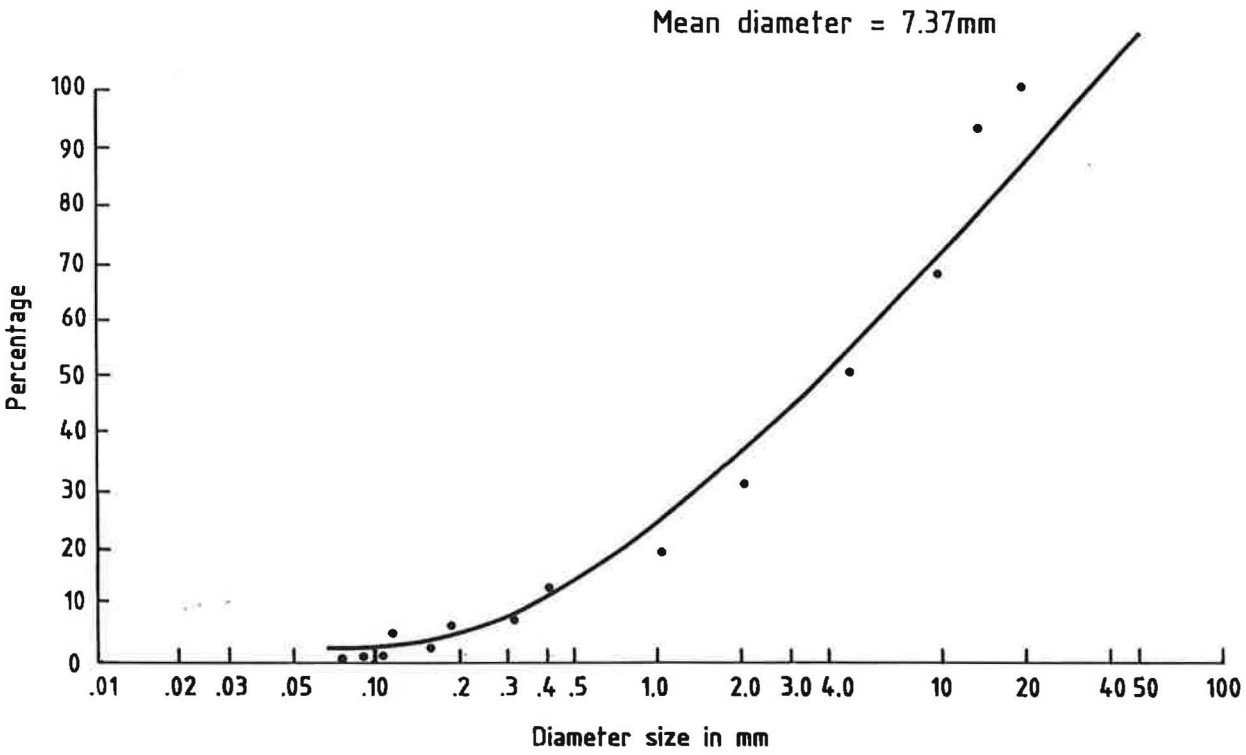

Fig 59 Showing gradation analysis of material collected in pit d/s flushing pipe

Size in mm	Percentage
0.074	1.31
0.147	5.67
0.177	16.56
0.297	23.10
0.42	30.29
0.5	39.00
1.0	56.43
2.0	78.22
4.77	89.11
9.55	100.00

Diameter of flushing pipe = 150mm
Discharge = 0.1606 cumec

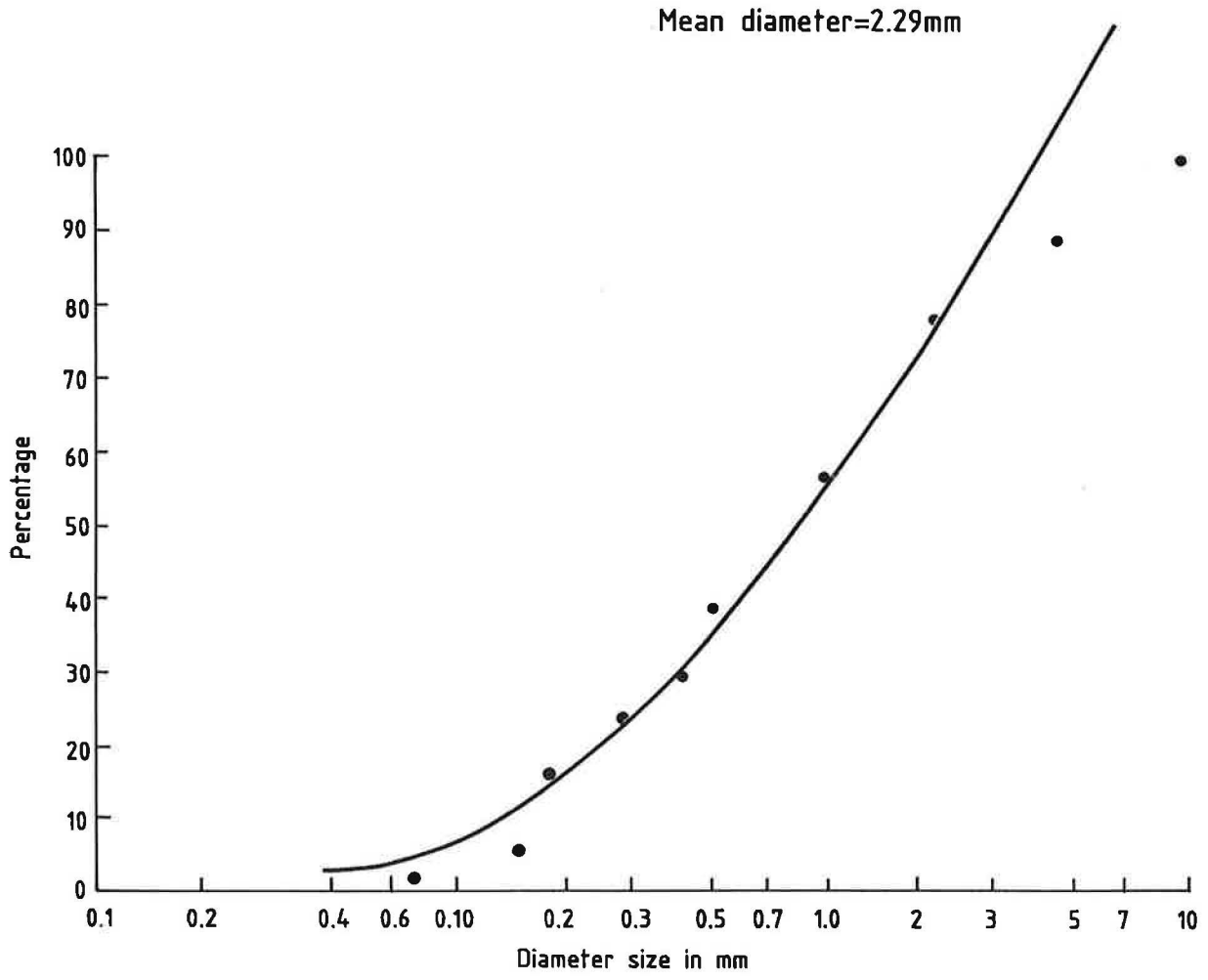

Fig 60 Showing gradation analysis of material collected in pit d/s power channel

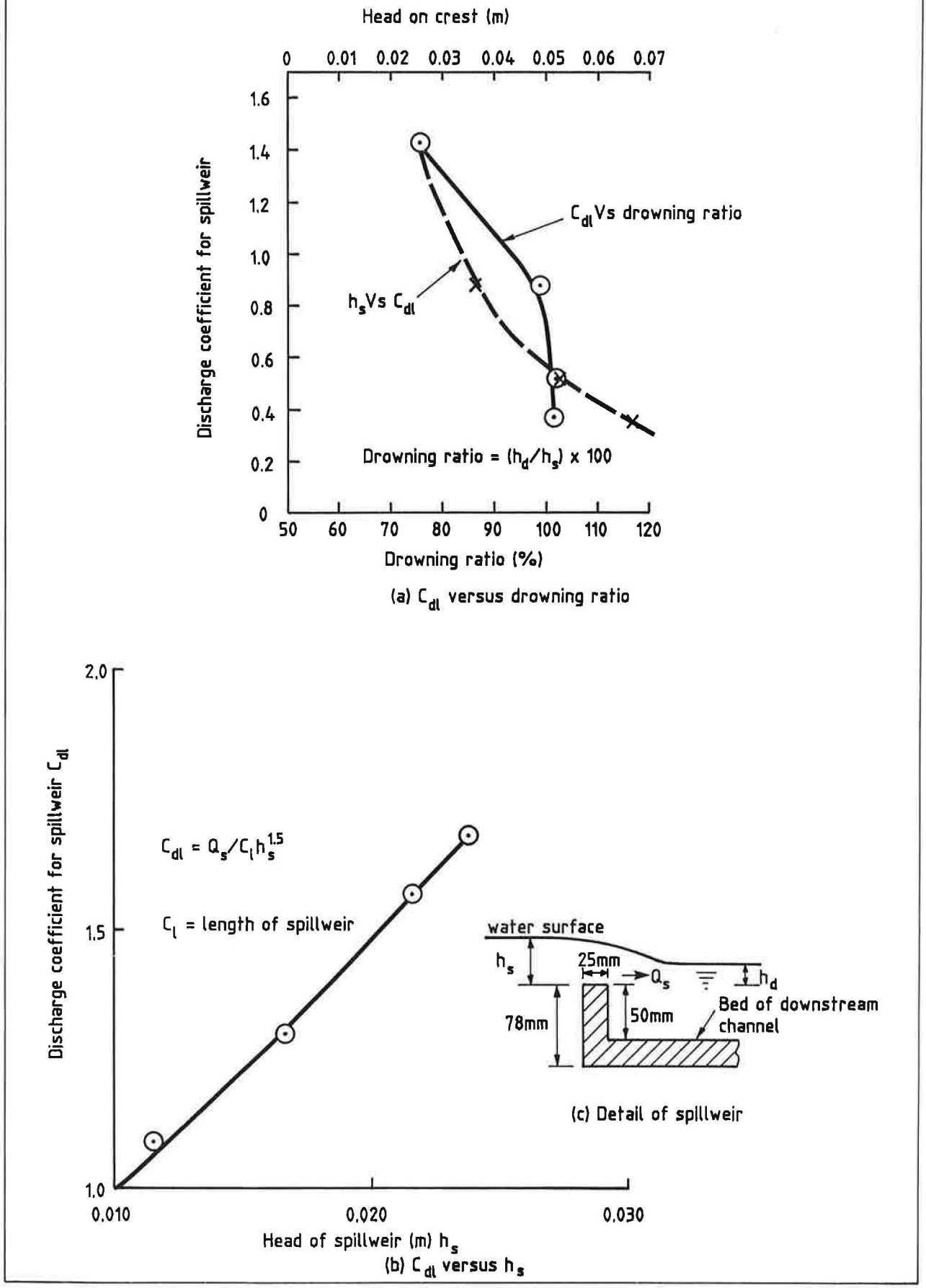

Fig 61ab&c Discharge coefficient for spillweir and diaphragm orifice

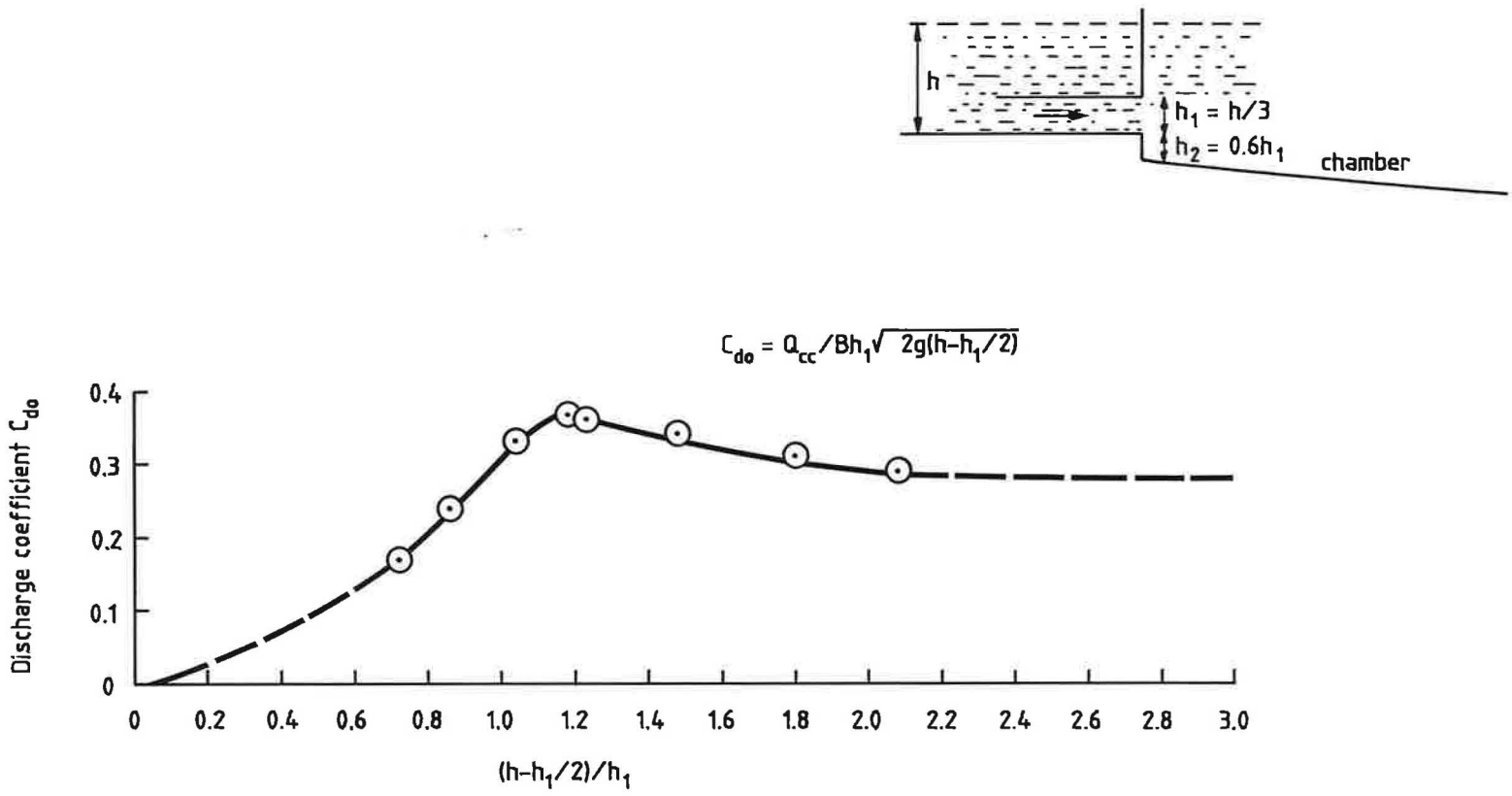

(d) Discharge coefficient for diaphragm orifice C_{do}

Fig 61d Discharge coefficient for spillweir and diaphragm orifice

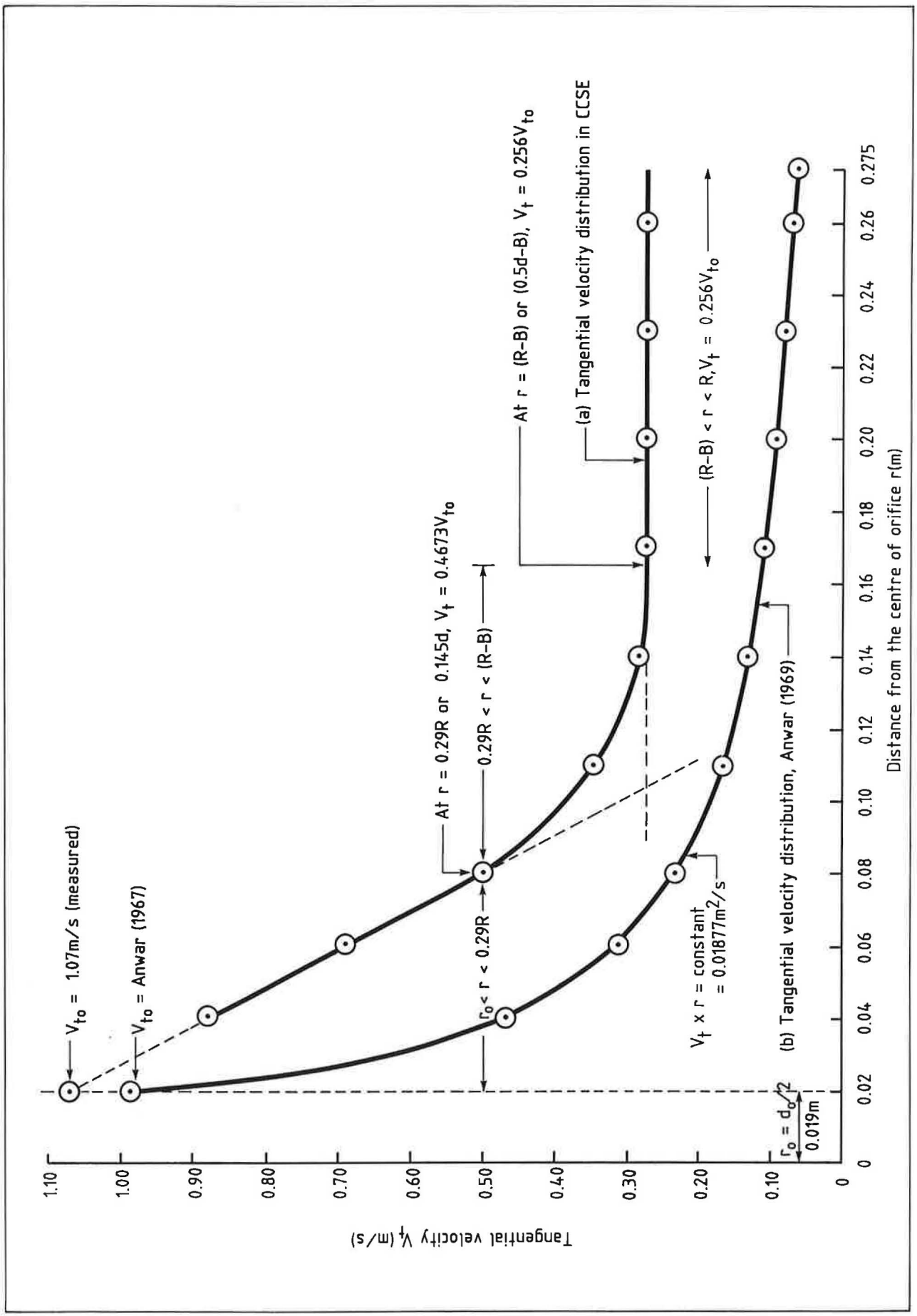

Fig 62 Tangential velocity distribution in CCSE and comparison with Anwar (1969)

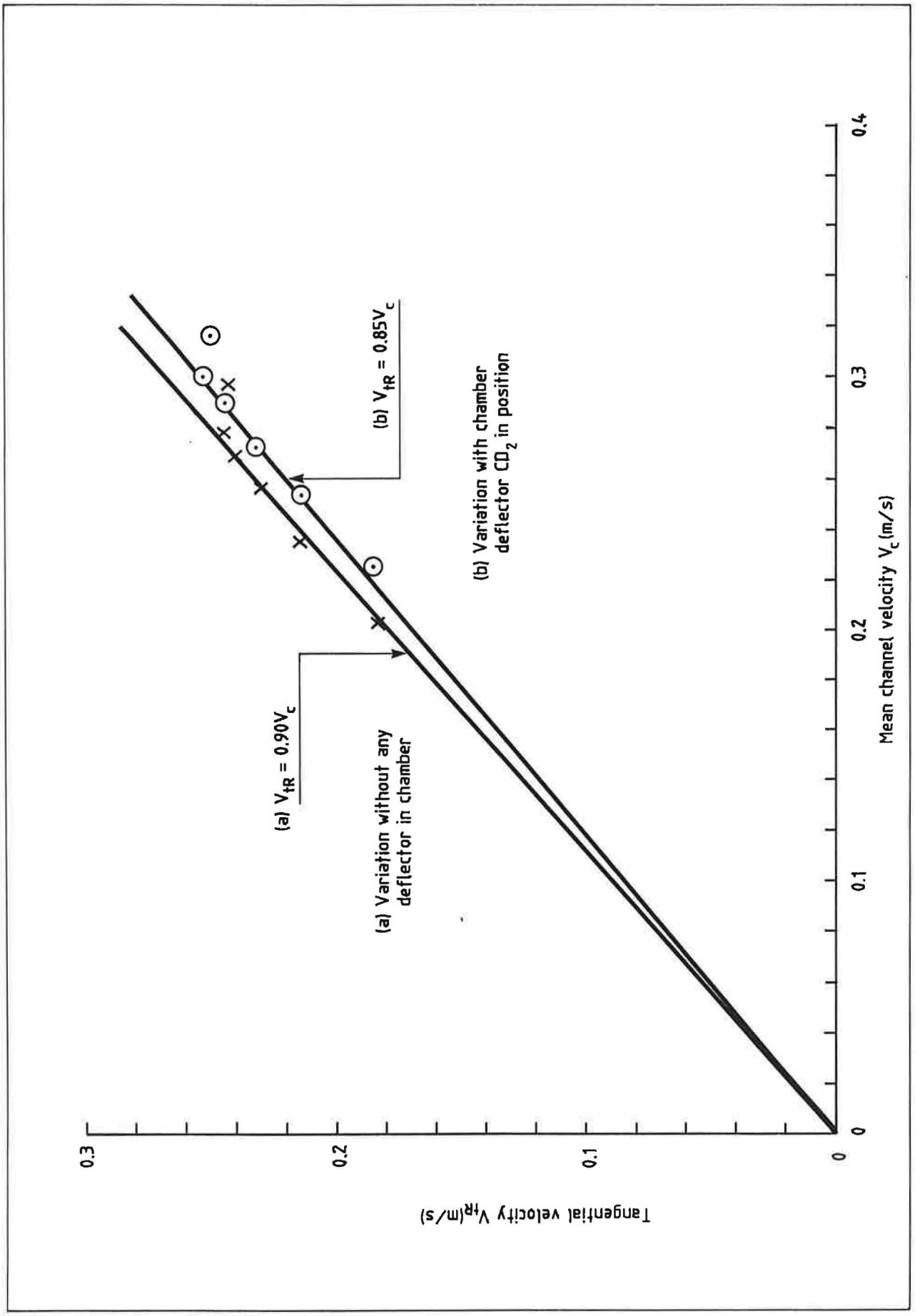

Fig 63 Variation of peripheral tangential velocity with channel velocity without and with chamber deflector CD_2

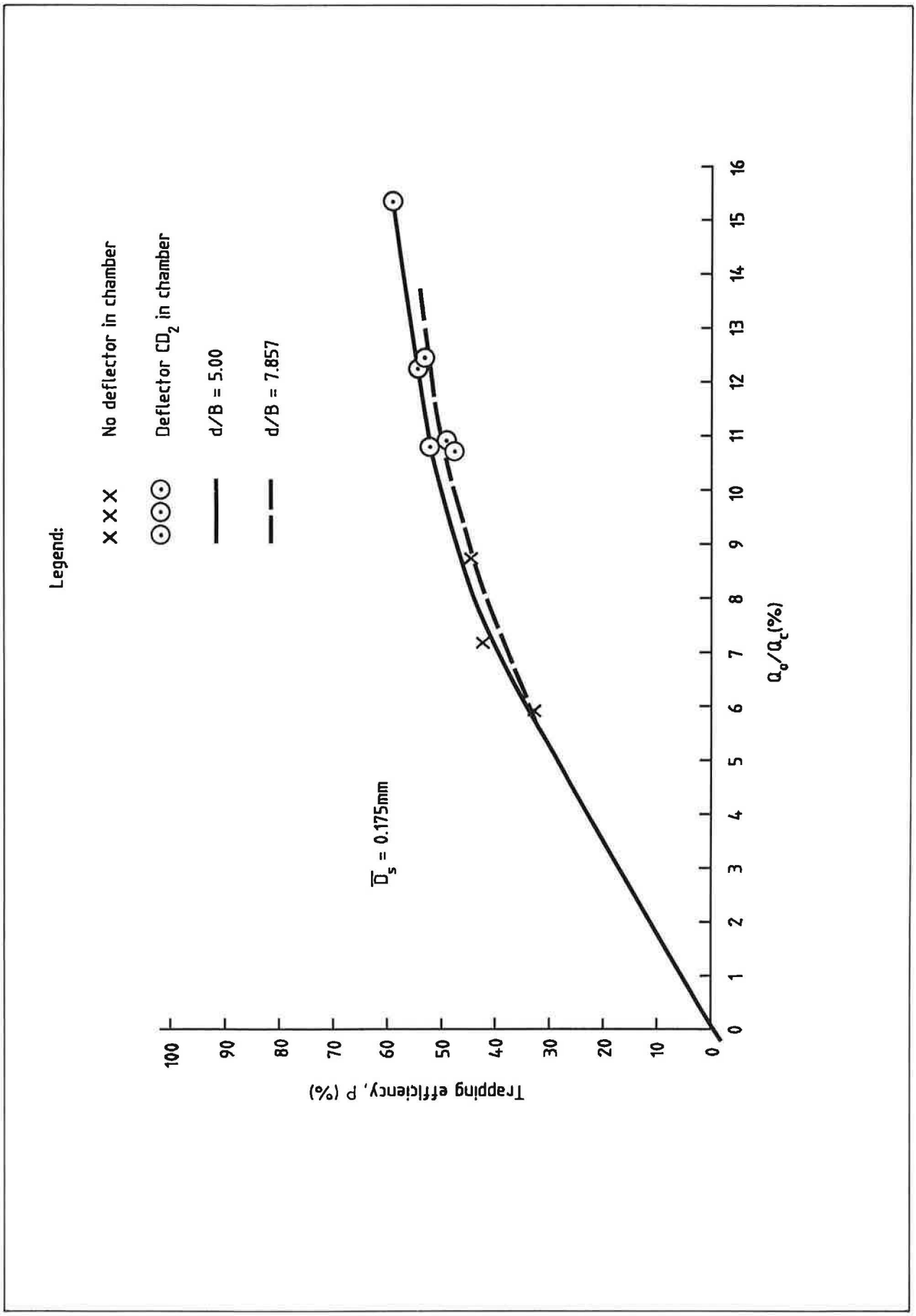

Fig 64 Effect of chamber size and chamber deflector on trapping efficiency

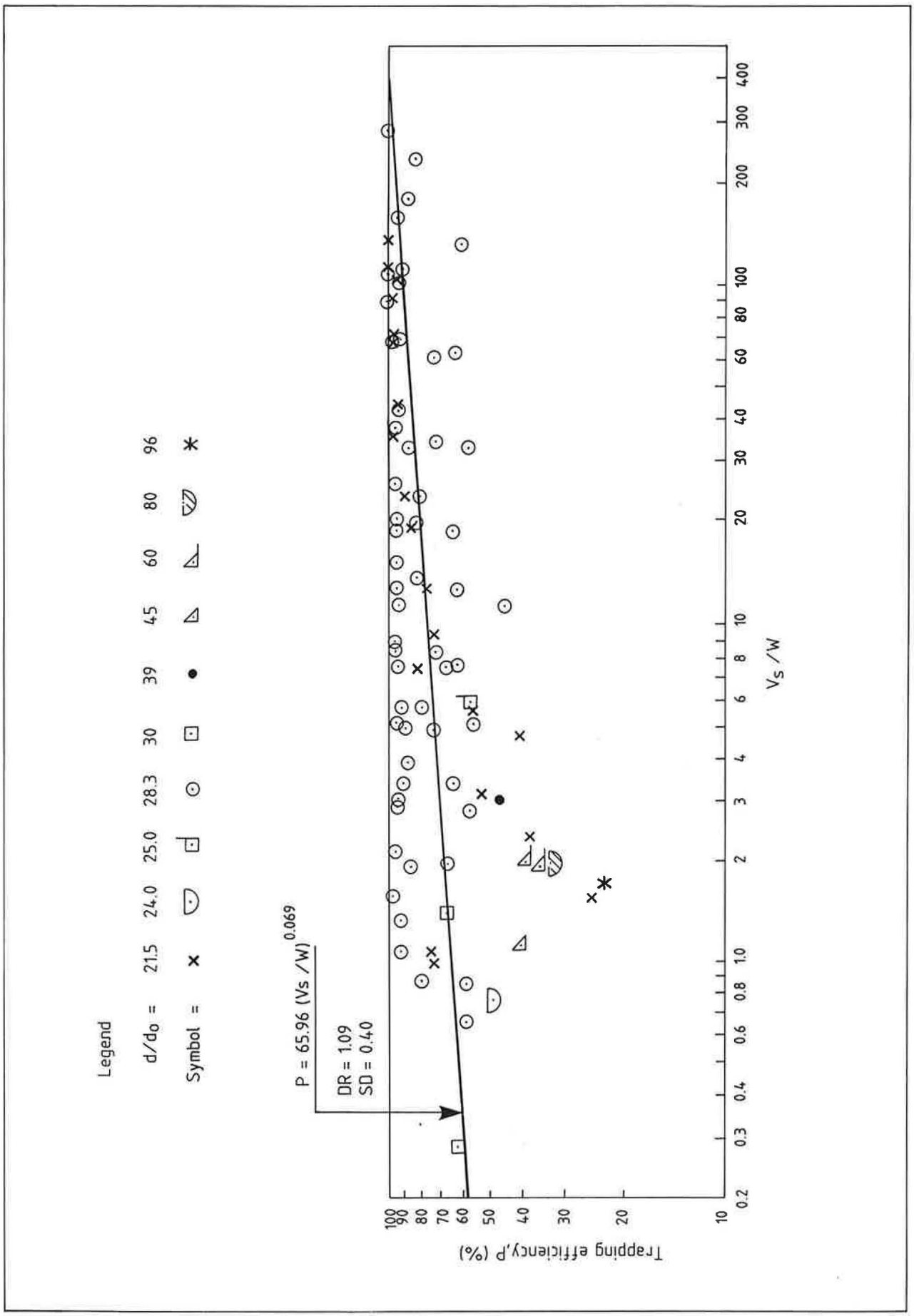

Fig 65 Variation of trapping efficiency with ratio of settling velocity to upward velocity

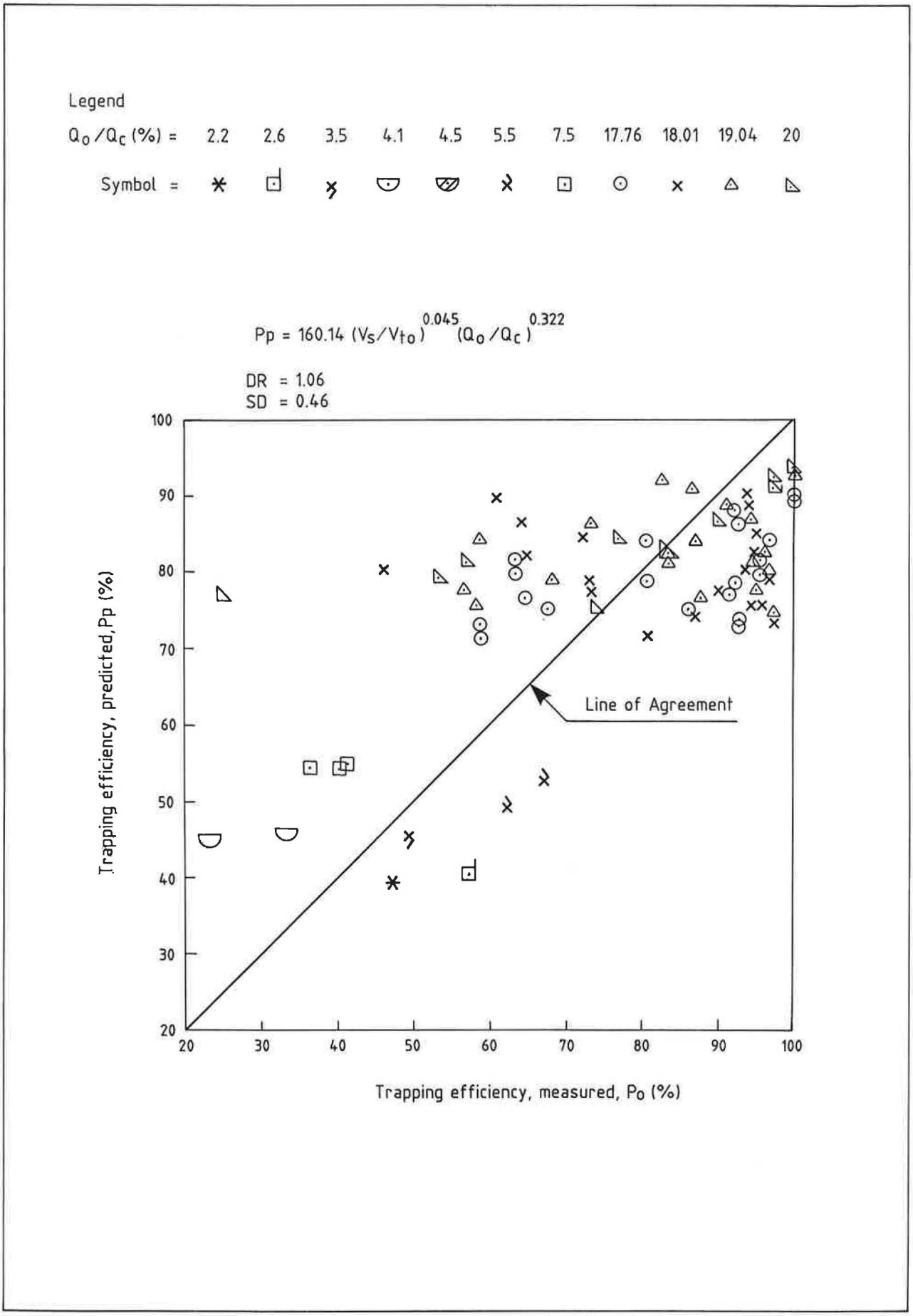

Fig 66 Comparison of trapping efficiency predictions with measurements, Equation 109

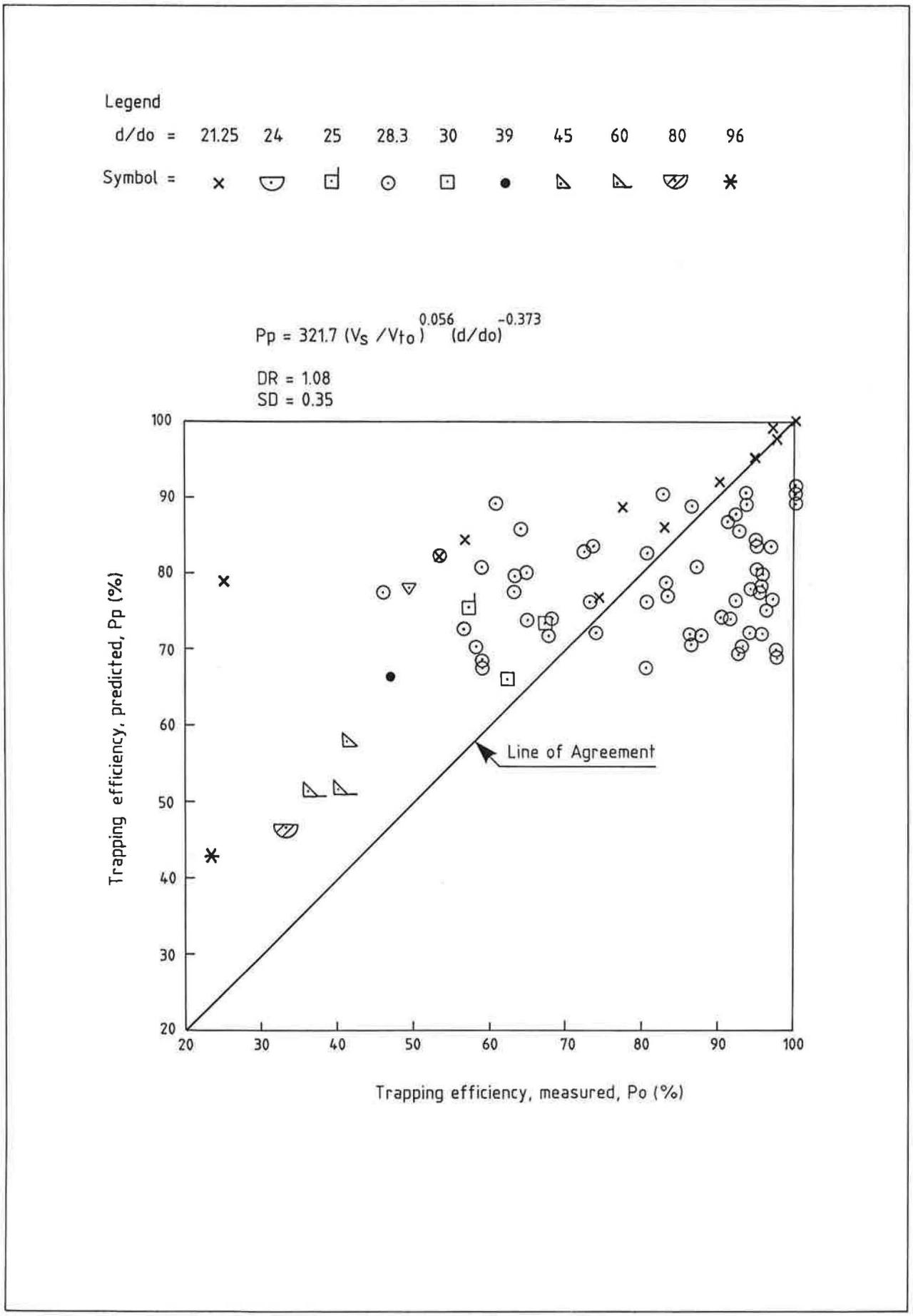

Fig 67 Comparison of trapping efficiency predictions with measurements, Equation 110

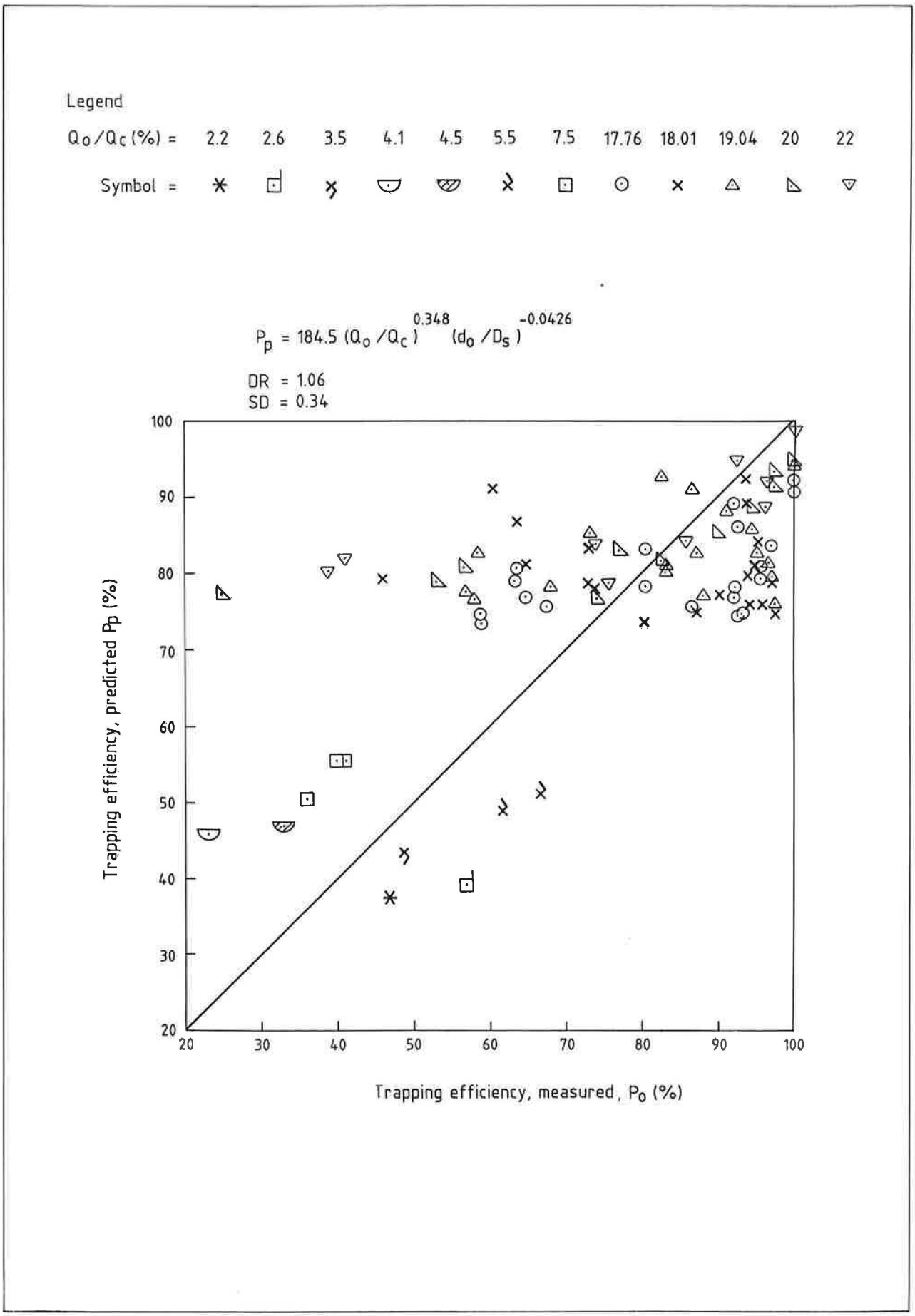

Fig 68 Comparison of trapping efficiency predictions with measurement, Equation 111

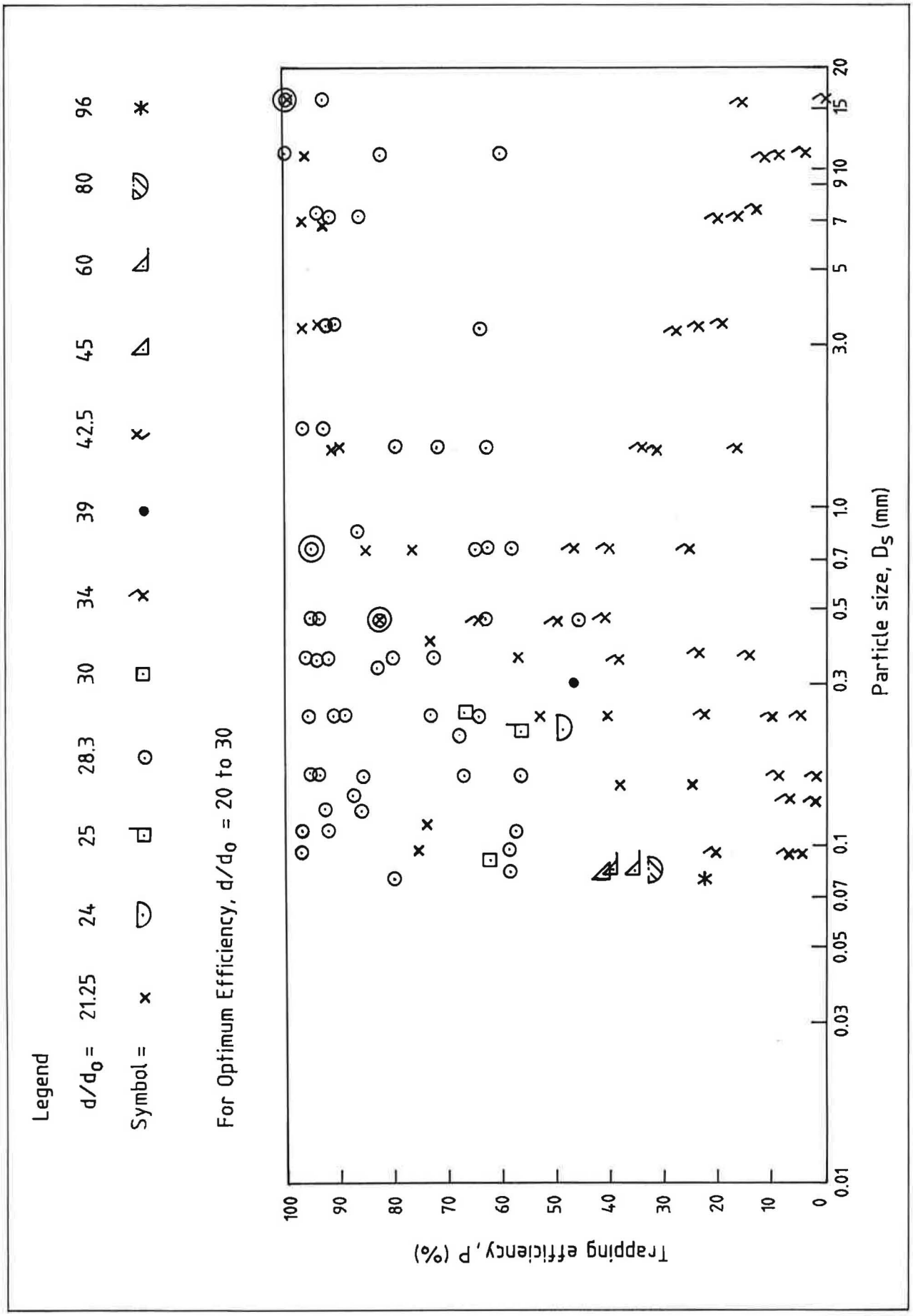

Fig 69 Limit of pipe size for optimum efficiency

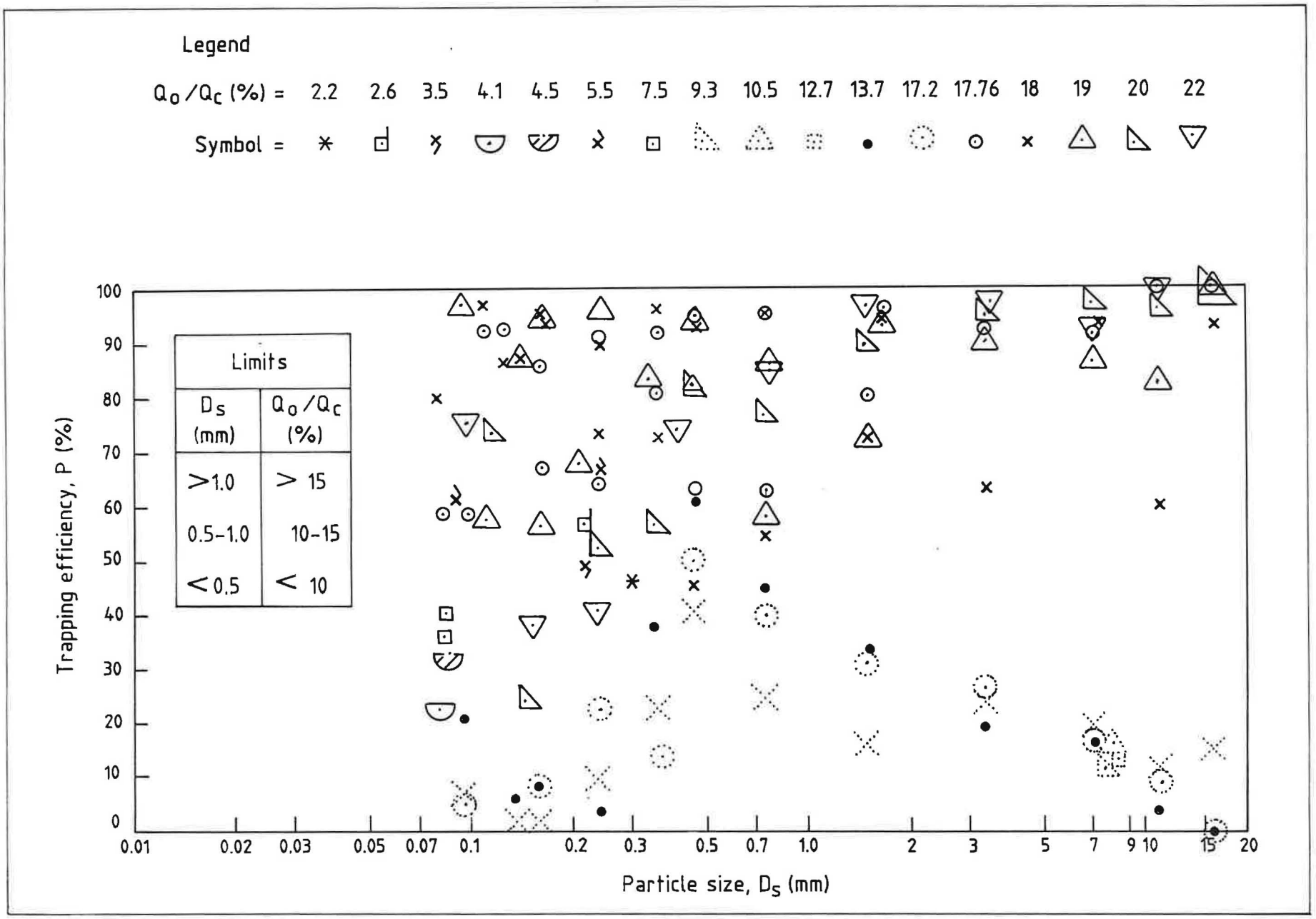

Fig 70 Limit of water abstraction for optimum efficiency

APPENDIX.

APPENDIX 'A': Analytical considerations for circulation chamber size

For an analysis of the flow field obtainable in the circulation chamber, an idealised situation is conceived. Initially viscosity and boundary friction (though important factors which cause secondary flow so crucial to the device under consideration) are ignored. The viscous effects can subsequently be incorporated through the introduction of a boundary layer.

For conceptual ease, the circualtion chamber is imagined as a relatively deep cylindrical tank and the following four characteristic flow layers identified:

Layer 1: This may be called the bottom layer, and is located in the immediate vicinity of the chamber bottom. In this layer boundary effects are more pronounced not only through viscosity but also due to the geometry of the boundary.

Layer 2: This is the region above the layer 1 but sufficiently below the inlet channel entry level.

Layer 3: This is the entry layer. In practice this will have single "tangential" entry and the flow axially asymmetric. However, this can be visualised as an entry uniformly spread round the circumference giving axially symmetric flow. The thickness of this layer will doubtless be thicker than the depth of the entry channel.

Layer 4: This is the exit layer. This region is imagined as the one in which fluid rises

vertically in a central core (with tangential velocity) and spreads radially outwards. Part of the flow in the circulation chamber will be trapped and directed out while the balance will flow back into the chamber at larger radii and mix.

For an analysis of the flow field in layer 2, the flow may be considered inviscid and irrotational. This could subsequently be used to build a boundary layer type of flow in layer 1 - the all important layer. The layers 3 and 4 are much more complex but are less important.

The momentum equations for steady, inviscid flow can be written as:

$$u\frac{\delta U}{\delta r} + \frac{v}{r}\frac{\delta u}{\delta \Theta} + w\frac{\delta u}{\delta Z} - \frac{y^2}{r} = -\frac{1}{\rho}\frac{\delta p}{\delta r} - \frac{\delta \Omega}{\delta r} \qquad (1)$$

$$u\frac{\delta v}{\delta r} + \frac{v}{r}\frac{\delta v}{\delta \Theta} + w\frac{\delta v}{\delta Z} + \frac{uv}{r} = -\frac{1}{\rho r}\frac{\delta p}{\delta \Theta} - \frac{1}{r}\frac{\delta \Omega}{\delta \Theta} \qquad (2)$$

$$u\frac{\delta \omega}{\delta r} + \frac{v}{r}\frac{\delta w}{\delta \Theta} + w\frac{\delta w}{\delta Z} = -\frac{1}{\rho}\frac{\delta \rho}{\delta Z} - \frac{\delta \Omega}{\delta Z} \qquad (3)$$

where Ω for gravity controlled flow is gZ. The equations for continuity and vorticity can be written as:

$$\text{(continuity):}\quad \frac{1}{r}\frac{\delta}{\delta r}(ur) + \frac{1}{r}\frac{\delta}{\delta \Theta}v + \frac{\delta w}{\delta z} = 0 \qquad (4)$$

Vorticity:

$$w_r = \frac{1}{r}\frac{\delta w}{\delta \Theta} - \frac{\delta v}{\delta z} \qquad (5)$$

$$w_\Theta = \frac{\delta u}{\delta z} - \frac{\delta w}{\delta r} \qquad (6)$$

and:

$$w_z = \frac{1}{r}\frac{\delta}{\delta r}(vr) - \frac{1}{r}\frac{\delta u}{\delta \Theta} \qquad (7)$$

In view of the assumption that flow in Layer 2 is irrotational and axi-symmetric, the equations (5), (6) and (7) reduce to the following:

$$\frac{\delta v}{\delta z} = 0 \qquad (8)$$

$$\frac{\delta u}{\delta z} = \frac{\delta w}{\delta r} \qquad (9)$$

$$\frac{\delta}{\delta r}(vr) = 0 \qquad (10)$$

From Equation (10), $v = C/r$ (11)

ie a free-vortex type flow.

Thus, as $r \to 0$, $v \to \infty$, and $\frac{\delta v}{\delta r} \to -\infty$ (like $\frac{1}{r^2}$)

Under these conditions of high shear, viscosity effects come into play necessitating a boundary layer type solution to be explored. Certainly the free-vortex flow breaks down resulting into rotational flow. However, another assumption is made, with some justification, that the layer is thin and can conveniently be excluded from the region of interest. From Equation 8 it is to be noted that C is a constant and not a function of Z.

Now assume that in this layer w is independent of Z. on the strength of this assumption, the continuity Equation 4 yields:

$$ur = \Pi(z) \text{ or } u = \Pi(z)/r \qquad (12)$$

Using the irrotationality condition (9),

$$\frac{\delta w}{\delta r} = \frac{dw}{dr} \text{ (because w is independent of } \Theta \text{ and z)}$$

$$= \delta u/\delta r = \frac{\Pi'(z)}{r} \text{ (using Equation 12)}$$

Hence $\Pi'(z)$ is a constant, say equal to β

or $w = \beta \ln r + \alpha$, α is a constant

$$= \beta \ln (r/R) + \alpha \qquad (13)$$

since

$$\Pi'(z) = \beta, \ \Pi = \beta (z-z_0)$$

where

Z_0 is another constant

Thus Equation 12 becomes:

$$U = \beta (z-zo)/r \qquad (14)$$

Recalling,

$$v = C/r \qquad (11)$$

$$u = b (Z-Z_0)/r \qquad (14)$$

$$w = \beta \ell n (r/R) + \alpha \qquad (13)$$

A continuity condition can now be applied on relating the quantity of fluid crossing a cylindrical surface of radius r. However, this is influenced by the inter

connections between layer 2 and the adjoining layers, and can be deferred to a subsequent stage.

Using the condition, that across a horizontal circular section of radius R at level Z, the net flow is zero, ie:

$$\int_o^R 2\pi r\, w\, dr = 0$$

$$\text{ie } \int_o^R [\beta r \ell n\, r - Br \ln R + \alpha r]\, dr = 0$$

$$\text{ie } \beta\left[\frac{R^2}{2}\ \ell n r - \frac{r^2}{4} - \frac{r^2}{2}\ell n R\right]_o^R + \alpha\left\{\frac{r^2}{2}\right\}_0^R = 0$$

$$\text{ie } \beta\left[-\frac{R^2}{4}\right] + \alpha\,\frac{R^2}{2} = 0$$

$$\text{ie } \alpha = \beta/_2 \quad [\because w = \beta \ell n(r/R) + \alpha] \qquad (13)$$

$$\text{ie } \therefore \quad = \beta\left[\ell n\left(\frac{r}{R}\right) + \tfrac{1}{2}\right] \qquad (15)$$

The point where the vertical velocity w changes sign is given by r = Ro where:

$$\ell n\ (R_o/R) = -\tfrac{1}{2}$$

$$\therefore R_0/R = 0.6065 \qquad (16)$$

This point of demarcation separting the outer and the inner region is interesting.

The outer region $R \geq r \geq R_0$ in this case has width 0.4R or 0.2 x (2R) or $^1/_5$(d). Experiments at HR and elsewhere (Ref Curi et al (1975)), Figure 26, have proved the validity of this analytical deduction that the width of the inlet channel should be $^1/_5$ the diameter of the chamber equal to five times the width of the inlet channel.